Technische Universität München

Fakultät für Medizin

Klinik und Poliklinik für Innere Medizin II

Klinikum rechts der Isar

Functions of Snail as a mediator of tumor-stroma cross signaling in pancreatic cancer

Chuan Shan

Vollständiger Abdruck der von der Fakultät für Medizin der Technischen Universität München zur Erlangung des akademischen Grades eines

Doktors der Naturwissenschaften

genehmigten Dissertation.

Vorsitzender:	Prof. Dr. Radu Roland Rad
Prüfer der Dissertation:	1. apl. Prof. Dr. Dieter Saur
	2. Prof. Angelika Schnieke, Ph.D.

Die Dissertation wurde am 22.06.2020 bei der Technischen Universität München eingereicht und durch die Fakultät für Medizin am 01.12.2020 angenommen.

Table of Contents

List of Figures

List of Tables

Abbreviations

°C	degree Celsius
A	adenine
aCGH	array comparative genomic hybridization
ACK	ammonium-chloride-potassium
ADM	acinar-to-ductal metaplasia
AF	Alexa Fluor
AFL	atypical flat lesion
APC (fluorochrome)	allophycocyanin
APC (gene)	adenomatous polyposis coli
apCAF	antigen-presenting cancer-associated fibroblast
ASI	activated stroma index
AXIN2	axis inhibition protein 2
B6	C57BL/6J
BB	Brilliant Blue
BP	band-pass
BR	broad-range
BRAF	v-raf murine sarcoma viral oncogene homolog B1
BrdU	5-Bromo-2'-deoxyuridine
BSA	bovine serum albumin
BUV	Brilliant Ultraviolet
BV	Brilliant Violet
C	cytosine
CAF	cancer-associated fibroblast
CAR-T	chimeric antigen receptor T
CCL	C-C motif chemokine ligand
Ccna	cyclin A
Ccnb	cyclin B
Ccnd	cyclin D
CCR	C-C motif chemokine receptor
CD	cluster of differentiation
CDH1	cadherin 1
CDK	cyclin-dependent kinase
CDKN2A	cyclin-dependent kinase Inhibitor 2A
cDNA	complementary deoxyribonucleic acid
ChIP	chromatin immunoprecipitation

ChIP-seq	chromatin immunoprecipitation sequencing
CK	cytokeratin
CRC	colorectal cancer
C_T	cycle threshold
CTLA-4	cytotoxic T-lymphocyte associated protein 4
CTNNB1	catenin beta 1
CXCR	C-X-C motif chemokine receptor
Cy	Cyanine
DMEM	Dulbecco's modified eagle medium
DMSO	dimethyl sulfoxide
DNA	deoxyribonucleic acid
dNTP	deoxyribonucleotide triphosphate
dsDNA	double-stranded deoxyribonucleic acid
dT	deoxythymidine
DTT	1,4-Dithiothreitol
DVL	Dishevelled
E-box	enhancer box
ECM	extracellular matrix
EDTA	ethylenediaminetetraacetic acid
EGF	epidermal growth factor
EGFP	enhanced green fluorescent protein
EGFR	epidermal growth factor receptor
ELISA	enzyme-linked immunosorbent assay
EMT	epithelial–mesenchymal transition
EpCAM	epithelial cell adhesion molecule
ER	estrogen receptor
et al.	et alii
EZH2	enhancer of zeste 2 polycomb repressive complex 2 subunit
FAP	fibroblast-activation protein α
FBS	fetal bovine serum
FBXl14	F-box and leucine-rich repeat protein 14
FBXW7	F-box and WD repeat domain containing 7
FDA	Food and Drug Administration
FDR	false discovery rate
FGF	fibroblast growth factor
FITC	fluorescein isothiocyanate
FRT	flippase recognition target
FSF	FRT-stop-FRT
Fsp1	fibroblast-specific protein 1
fwd	forward

FWER	family-wise error rate
FZD10	frizzled class receptor 10
G	guanine
G_1/S	gap 1 phase/synthesis phase
GEMM	genetically engineered mouse model
GFAP	glial fibrillary acidic protein
GM-CSF	granulocyte-macrophage colony-stimulating factor
GSEA	gene set enrichment analysis
GSK3	glycogen synthase kinase 3
GTP	guanosine-5'-triphosphate
h	hour(s)
H&E	hematoxylin and eosin
HDAC	histone deacetylase
hi	high
HNF	hepatic nuclear factor
HRP	horseradish peroxidase
IACUC	Institutional Animal Care and Use Committees
IBD	inflammatory bowel disease
iCAF	inflammatory cancer-associated fibroblast
IEC	intestinal epithelial cell
IgG	immunoglobulin G
IHC	immunohistochemistry
IL	interleukin
Il2rg	interleukin 2 receptor subunit gamma
ILK	integrin linked kinase
int	intermediate
ImmGen	Immunological Genome Project
IP	immunoprecipitation
IPMN	intraductal papillary mucinous neoplasm
ISE	intestinal stem cell
ITPN	intraductal tubular papillary neoplasm
kb	kilobase
KEGG	Kyoto Encyclopedia of Genes and Genomes
kg	kilogram
KI	knock-in
KO	knockout
KRAS	v-Ki-ras2 Kirsten rat sarcoma viral oncogene homolog
LEF-1	lymphoid enhancer-binding factor 1
lo	low
log-CPM	log counts per million

LOXL2	lysyl oxidase-like 2
loxP	locus of X-over P1
LP	longpass
LSD1	lysine-specific histone demethylase 1
LSL	LoxP-stop-LoxP
Ly6C	lymphocyte antigen 6 complex, locus C
Ly6G	lymphocyte antigen 6 complex, locus G
M1	classically activated macrophage
M2	alternatively activated macrophage
MAP2K1	dual specificity mitogen-activated protein kinase kinase 1
MAPK	mitogen-activated protein kinase
MCN	pancreatic mucinous cystic neoplasm
MDM2	mouse double minute 2 homolog
MDS	multidimensional scaling
MDSC	myeloid-derived suppressor cell
MET	mesenchymal–epithelial transition
mg	milligram
MHC-II	major histocompatibility complex class II
Min	multiple intestinal neoplasia
min	minute(s)
miRNA	micro-ribonucleic acid
mL	milliliter
mm	millimeter
mo(s)	month(s)
mRNA	messenger ribonucleic acid
MTA3	metastasis-associated protein
mTOR	mammalian target of rapamycin
mut	mutant
myCAF	myofibroblastic cancer-associated fibroblast
Myh11	myosin heavy chain 11
NB	nota bene
NES	normalized enrichment score
NF-κB	nuclear factor kappa-light-chain-enhancer of activated B cells
NK	natural killer
NKT	natural killer T
nM	nanomolar
nm	nanometer
NMF	non-negative matrix factorization
NOD	non-obese diabetic
NRAS	neuroblastoma RAS viral oncogene homolog

PAK1	p21 (RAC1) activated kinase 1
PanIN	pancreatic intraepithelial neoplasia
PBS	Dulbecco's phosphate buffered saline
PCR	polymerase chain reaction
PD-1	programmed cell death 1
PDAC	pancreatic ductal adenocarcinoma
PDGF	platelet derived growth factor
PD-L1	programmed cell death 1 ligand 1
Pdx1	pancreatic and duodenal homeobox 1
PE	phycoerythrin
PerCP	peridinin-chlorophyll-protein
pH	potential of hydrogen
PI3K	phosphoinositide 3-kinase
PIK3CA	phosphatidylinositol-4,5-bisphosphate 3-kinase catalytic subunit alpha
PIK3R1	phosphoinositide-3-kinase regulatory subunit 1
PMSF	phenylmethylsulfonyl fluoride
PRC2	polycomb repressive complex 2
Prkdc	protein kinase, DNA-activated, catalytic subunit
PRMT5	protein arginine methyltransferase 5
PSC	pancreatic stellate cell
PTEN	phosphatase and tensin homolog
Ptf1a	pancreas associated transcription factor 1a
PTHrP	parathyroid hormone related peptide
qPCR	quantitative real-time polymerase chain reaction
Rag2	recombination activating gene 2
Rb	retinoblastoma
rcf	relative centrifugal force
rec	recombination
rev	reverse
RMA	robust multiarray averaging
RNA	ribonucleic acid
RNA-seq	RNA sequencing
Rosa26	reverse oriented splice acceptor, clone 26
rpm	revolutions per minute
RT	room temperature
s	second(s)
Scid	severe combined immunodeficiency
SCRB-seq	single-cell RNA barcoding and sequencing
SEM	standard error of the mean

SHH	Sonic hedgehog
Siglec-F	sialic acid-binding immunoglobulin-like lectin F
SMAD4	mothers against decapentaplegic homolog 4
SNAG	Snail/Gfi-1
SOX9	SRY-box transcription factor 9
SPSB3	splA/ryanodine receptor domain and SOCS box containing 3
STAT3	signal transducer and activator of transcription 3
T	thymine
TAE	Tris acetate EDTA
TAM	tumor-associated macrophage
TCF4	transcription factor 4
TCR	T-cell receptor
TGF-β	transforming growth factor β
T_h	T helper
TP53	tumor protein p53
Treg	regulatory T cell
Trp53	transformation-related protein 53
US	United States of America
UV	ultraviolet
v	version
V	volt
VEGF	vascular endothelial growth factor
VISTA	V-domain Ig suppressor of T cell activation
WT	wild-type
Zeb1	zinc finger E-box binding homeobox 1
α-SMA	α-smooth muscle actin
βTrCP	β-Transducin repeat-containing proteins
µL	microliter
µm	micrometer
µM	micromolar

1 Introduction

1.1 Pancreatic cancer

1.1.1 Overview

Pancreatic cancer is the seventh leading cause of death among all cancer types worldwide (Bray et al., 2018). The incidence rate in developed countries is higher, and the death rate ranks third in the US, after lung and colorectal cancer (Siegel et al., 2019). The disease is often diagnosed at a late stage, resulting in a median overall survival time of around six months (Hang et al., 2018). Despite enormous effort to improve the treatment, the five-year survival rate of less than 9% remained virtually unchanged in the past five years (Siegel et al., 2014; Siegel et al., 2019). With progresses in the treatment of other cancer types, pancreatic cancer is projected to be the second leading cause of cancer death in the US in 2030 (Rahib et al., 2014).

1.1.2 Pancreatic ductal adenocarcinoma

Accounting for over 90% of all cases, pancreatic ductal adenocarcinoma (PDAC) is the most common type of pancreatic cancer (Feldmann and Maitra, 2008). Other types include acinar cell carcinoma, neuroendocrine tumor and cystadenocarcinoma, etc. The exact cause of PDAC is not completely known. Advanced age, smoking, alcohol consumption, dietary factors, obesity, sustained chronic pancreatitis and *Helicobacter pylori* infection have been established as risk factors (Berrington de Gonzalez et al., 2003; Everhart and Wright, 1995; Fuchs et al., 1996; Gapstur et al., 2000; McGuigan et al., 2018; Michaud et al., 2001; Stolzenberg-Solomon et al., 2005). In addition, 10% of PDAC cases are associated with familial predisposition (McGuigan et al., 2018; Tersmette et al., 2001). However, there is still no standard screening procedure for high risk population to this day.

Non-specific symptoms, early invasion into the blood vessel and rapid metastasis hold responsibility for the late diagnosis of the disease. As a result, around 85% of cases show locally advanced or metastatic tumor and are not surgically resectable (McGuigan et al., 2018). Despite the high recurrence rate, surgical resection of early stage tumors remains the only potential cure for pancreatic cancer. For patients unsuitable for surgery, gemcitabine was used as a first-line therapy, even though it provided only limited benefit in survival time (Burris et al.,

1997). Combination of gemcitabine with fluorouracil, capecitabine, oxaliplatin and cisplatin all failed to gain additional survival benefit compared to gemcitabine treatment alone (Berlin et al., 2002; Colucci et al., 2010; Herrmann et al., 2007; Louvet et al., 2005; Poplin et al., 2009). Although therapeutic antibodies have been successful in a few other cancer types, all phase III clinical trials in pancreatic cancer failed (Chames et al., 2010). Notwithstanding the huge success of immunotherapy in recent years, no immune checkpoint inhibitor has been approved for general use in pancreatic cancer. Up to now, the highest survival advantage was achieved by FOLFIRINOX (consisting of oxaliplatin, irinotecan, fluorouracil, and leucovorin) combination chemotherapy, albeit with increased toxicity (Conroy et al., 2011). Another clinical trial showed significantly improved survival using nab-paclitaxel plus gemcitabine, but increased rates of peripheral neuropathy and myelosuppression were also observed (Von Hoff et al., 2013). Currently, FOLFIRINOX and nab-paclitaxel plus gemcitabine are the first-line options for patients who are healthy enough to stand the treatment.

Although the knowledge in pancreatic cancer has expanded enormously in the past two decades, the grave situation of stagnant improvement in clinical outcome calls for more detailed mechanistic study in tumor progression, evolution and resistance.

1.1.3 Progression models and genetics

PDAC is preceded by various types of precursor lesions including pancreatic intraepithelial neoplasia (PanIN), intraductal papillary mucinous neoplasm (IPMN), pancreatic mucinous cystic neoplasm (MCN), intraductal tubular papillary neoplasm (ITPN), and the more recently described atypical flat lesion (AFL) (Aichler et al., 2012; Cooper et al., 2013; Hruban et al., 2000; Hruban et al., 2007). Among these precursor lesions, PanIN is the most common and the best characterized. These small lesions arising from pancreatic ducts are classified into three grades according to their morphology (Hruban et al., 2008). PanIN-1 lesions are mucin-producing flat lesions composed of tall columnar epithelial cells with basally located nuclei. PanIN-2 lesions are mostly papillary and have nuclear abnormality. Manifested by cribriforming, loss of nuclear polarity and budding into the lumen, PanIN-3 lesions are also called carcinoma in situ (Hruban et al., 2001). It is commonly believed that acinar-to-ductal metaplasia (ADM) is a mechanism to initiate PanIN (Kopp et al., 2012; Wei et al., 2016); indeed, PDAC originating from both acinar and ductal compartments have been described (Bailey et al., 2016; Ferreira et al., 2017).

On the molecular level, mutations of several key proteins are commonly observed in PDAC. *KRAS* (v-Ki-ras2 Kirsten rat sarcoma viral oncogene homolog) activating mutations are the most frequently found (>90%) and one of the earliest genetic alterations (Almoguera et al., 1988; Cancer Genome Atlas Research Network, 2017; Hruban et al., 2000; Morris et al., 2010). Various mutation forms exist but mutation in codon 12 is predominant as early as in PanIN-1 lesions (Kanda et al., 2012). A typical mutation substituting glycine with aspartate or valine in this codon (G12D or G12V) results in a compromised ability in GTP hydrolysis and thereby a constitutively activated KRAS signaling (Malumbres and Barbacid, 2003; Scheffzek et al., 1997). Such change in cell physiology triggers the activation of several downstream pathways including mitogen-activated protein kinase (MAPK) and phosphoinositide 3-kinase (PI3K) signaling pathways, which promotes proliferation and genomic instability and eventually leads to cancer (Choudhury et al., 1997; Hezel et al., 2006; Pages et al., 1993; Saavedra et al., 1999).

Another early event in PanIN progression is *CDKN2A* alterations, which is seen in 30% of PDAC cases (Cancer Genome Atlas Research Network, 2017; Hezel et al., 2006). A rare case in eukaryotic genome, human *CDKN2A* encodes two unrelated tumor suppressor genes $p16^{INK4A}$ and $p14^{ARF}$ by using alternative reading frames (Mao et al., 1995; Quelle et al., 1995; Stott et al., 1998). $p16^{INK4A}$ prevent S phase entry through retinoblastoma (Rb) phosphorylation inhibition (Caldas et al., 1994; Serrano et al., 1993), while $p14^{ARF}$ activates p53 by inhibiting MDM2 (Sherr, 2006; Stott et al., 1998). Mutations in tumor suppressor *TP53* occur later in PDAC progression and are found in 72% of the tumors (Cancer Genome Atlas Research Network, 2017; Morris et al., 2010). SMAD4 is a central player in transforming growth factor β (TGF-β) signaling and regulates critical cellular processes e.g. epithelial–mesenchymal transition (EMT) and DNA damage response (Bornstein et al., 2009; Mitra et al., 2013; Thuault et al., 2006; Vincent et al., 2009; Zhao et al., 2018). Its mutations therefore are implicated in tumorigenesis and metastases. Besides, aberrant Hedgehog, Notch and DNA damage repair signaling often occur in PDAC as well (Cancer Genome Atlas Research Network, 2017; Hezel et al., 2006).

1.1.4 Genetically engineered mouse models for pancreatic cancer

Genetically engineered mouse models (GEMMs) have served as powerful tools in cancer research despite the biological differences between mouse and human. Still, the modes of biological processes between mouse and human are strikingly similar, therefore mouse tumor models are developed largely based on the genetic makeup of the human disease. A classic

model for PDAC was established by expressing the constitutively active $Kras^{G12D}$ in the pancreas with *Cre/loxP* system and the pancreas-specific promoter *Pdx1* or *Ptf1a* (Hingorani et al., 2003). In this model, ubiquitous expression of $Kras^{G12D}$ is prevented by an upstream stop element flanked by two *loxP* sites (*LoxP-stop-LoxP*, *LSL*), and expression of Cre recombinase under the control of *Pdx1* or *Ptf1a* promoter enables excision of the stop element and expression of $Kras^{G12D}$ in the pancreas. These mice develop PDAC with complete penetrance via PanIN route and faithfully recapitulate the histological, molecular and clinical characteristics of human PDAC (Hingorani et al., 2003). Importantly, metastases to liver, lung and lymph nodes are also present. Additional expression of a dominant-negative oncogenic $Trp53^{R172H}$ significantly accelerates tumor progression and shortens median survival time (Hingorani et al., 2005). Precursor lesions for $Kras^{G12D}$-based tumors are mostly PanINs, but models with IPMN and MCN can be obtained by additional genetic modifications (Bardeesy et al., 2006b; Izeradjene et al., 2007; Mazur et al., 2010; Siveke et al., 2007; Taki et al., 2016). Since their creation, these autochthonous models have been fundamental to the research on tumor progression, maintenance and resistance in the presence of microenvironment as well as validation of therapeutic targets *in vivo*.

Although the understanding of PDAC has been greatly advanced with the help of GEMMs, traditional models have limitations as well. As they all depend on one recombinase, sequential genetic manipulation of tumor cells or additional control of stroma cells cannot be achieved. To better recapitulate multi-step tumorigenesis and tumor heterogeneity, which are both hallmarks of the human disease, our lab established a dual-recombinase system which combines *Cre/loxP* and *Flp/FRT* (Schonhuber et al., 2014). Similar to Cre, the Flp recombinase allows both gene expression and deletion by cutting off the upstream *FRT-stop-FRT* (*FSF*) cassette or the gene flanked by *FRT* sites. The *Pdx1-Flp;FSF-Kras$^{G12D/+}$* mice show similar PanIN progression and PDAC formation patterns as the classical *Cre/loxP*-based PDAC model with nearly identical survival time, tumor latency and metastasis rate (Schonhuber et al., 2014). Further genetic manipulation with *Cre/loxP* system enables us to achieve sequential genetic changes of tumor cells or target the microenvironment. These 'next generation' mouse models therefore better mimic human disease and can provide valuable insights in PDAC biology.

1.2 Intestinal cancer

1.2.1 Overview

In humans, intestinal cancer occurs mostly in the large intestine and very rarely in the small intestine. In the US, colorectal cancer (CRC) is the third most common cancer type and ranks second in terms of death rate (Siegel et al., 2019). While inherited predisposition is associated with 10% to 30% of the patients, sporadic somatic mutations account for 70% of all cases (Burt, 2000). Inflammatory bowel disease (IBD), overweight, smoking, low physical activity and low vegetable or fruit consumption are known risk factors for CRC (Jemal et al., 2011; Johnson et al., 2013).

Early colorectal cancers without systemic disease are primarily treated with surgery. Combinations of fluorouracil, folinic acid, irinotecan, oxaliplatin, leucovorin and cetuximab have been established as standard of care for patients with locally advanced or metastatic tumors (Bokemeyer et al., 2009; Malka et al., 2017; Van Cutsem et al., 2011). Antibodies against vascular endothelial growth factor (VEGF) and epidermal growth factor receptor (EGFR) also showed survival benefits to patients (Hurwitz et al., 2004; Lievre et al., 2006; Willett et al., 2004). With these therapeutic options available, the overall five-year survival of CRC patients in the US is 65%. However, the number for patients with distant metastasis is only 14% (Siegel et al., 2019).

1.2.2 Biology and genetics of intestinal cancer

The intestinal epithelium forms the barrier between the external environment and internal organs and is organized into crypts and villi. The multipotent intestinal stem cells (ISEs) migrate from the bottom of the crypt to the top of the villus, differentiating into enterocytes, enteroendocrine cells, goblet cells, Paneth cells, etc. (Gerbe et al., 2011; van der Flier and Clevers, 2009). The self-renewing intestinal epithelial cells (IECs) are promoted by Wnt, bone morphogenetic protein (BMP), TGF-β signaling and microenvironmental factors, and aberrant signaling inevitably leads to uncontrolled cell proliferation and cancer (De Rosa et al., 2015; Kosinski et al., 2007; Medema and Vermeulen, 2011).

Wnt/β-catenin signaling pathway is the most frequently deregulated pathway in CRC as mutations of its molecules are present in more than 90% of the cases (Cancer Genome Atlas, 2012; De Rosa et al., 2015; Fevr et al., 2007; Schneider et al., 2017). Upon stimulation, Wnt ligands bind to cell surface receptor Frizzled, which activates Dishevelled (DVL). DVL prevents

β-catenin degradation by inhibiting its phosphorylation by GSK3β/α. Accumulated β-catenin translocates into the nucleus, interacts with TCF4 or LEF-1 and activates transcription of target genes, such as c-Jun, c-Myc and cyclin D1 (Bienz and Clevers, 2000; He et al., 1998; Morin et al., 1997; Novellasdemunt et al., 2015; Salahshor and Woodgett, 2005; Shtutman et al., 1999; Tetsu and McCormick, 1999). Adenomatous polyposis coli (APC) as a negative regulator of β-catenin prevents hyperactivation of Wnt signaling (Korinek et al., 1997; Novellasdemunt et al., 2015), therefore it is not surprising that its mutations are observed in 48% of the CRC patients (Schneider et al., 2017). In fact, *APC* loss was one of the earliest known events when the genetic model for colorectal tumorigenesis was first established (Ashton-Rickardt et al., 1989; Fearon and Vogelstein, 1990; Vogelstein et al., 1988). Deletion, mutation and overexpression of other members in Wnt signaling, such as *CTNNB1*, *SOX9*, *FZD10*, *AXIN2* and *FBXW7*, are also repeatedly detected (Cancer Genome Atlas, 2012). Remarkably, deletion of c-Myc in a mouse model rescued the phenotype induced by *Apc* deletion, establishing c-Myc as a central molecule in Wnt-driven intestinal cancer (Sansom et al., 2007).

As in pancreatic cancer, MAPK and PI3K pathways are also recurrently altered in CRC. Half of the tumors bear mutually exclusive mutations in *KRAS*, *NRAS* and *BRAF*; mutations in *PIK3R1* or *PIK3CA* and deletions in *PTEN* are also present in 21% of the cases (Cancer Genome Atlas, 2012; Samuels et al., 2004). In contrast to the adenomas induced by Wnt signaling, polyps with *KRAS* or *BRAF* mutations show a serrated morphology (Jass, 2007; Makinen, 2007). In addition, aberrations in TGF-β and NF-κB signaling and DNA mismatch repair are also observed (Cancer Genome Atlas, 2012; De Rosa et al., 2015; Markowitz et al., 1995; Wei et al., 2002).

1.2.3 Genetically engineered mouse models for intestinal cancer

Since *APC* loss was established as one of the early events in human colorectal cancer, *Apc* deletion was widely used in mouse models for intestinal cancer. The earliest *Apc*-related model is the multiple intestinal neoplasia (Min) model bearing a nonsense mutation at codon 850 (Moser et al., 1993; Moser et al., 1990). These mice develop multiple adenomas, however mostly in the small intestine in contrast to the large intestine in human (Jackstadt and Sansom, 2016). Several other variants of *Apc* deletion model have also been made (Dietrich et al., 1993; Fodde et al., 1994; Pollard et al., 2009). After the application of *Cre/loxP* system, *Apc* deletion specific to IEC or ISC was achieved by the combination of Cre expressed under the *Villin-1* or *Lgr5* promoter and floxed *Apc* gene (Barker et al., 2009; Barker et al., 2007; Cheung et al.,

2010; Madison et al., 2002). These models have been used to study the intestinal tumorigenesis induced by the classical Wnt signaling pathway.

One major limitation of the *Apc* deletion models is the absence of metastasis (Jackstadt and Sansom, 2016). As *KRAS*, *BRAF*, *PTEN* and *PI3KCA* mutations are also frequently observed in human CRC, they were also used to develop intestinal cancer GEMMs. Combination of $Kras^{G12V}$ and *Apc* loss increased invasiveness, however no metastasis was reported (Sansom et al., 2006). Expression of $Kras^{G12D}$ alone induced serrated adenoma but no invasive cancer; further deletion of *Cdkn2a* led to fully invasive adenocarcinoma (Bennecke et al., 2010). Another study showed that $Kras^{G12V}$ did not induce tumor and that complete deletion of *Pten* resulted in single small intestinal adenocarcinomas, but nearly half of the mice with combination of the two possessed invasive adenocarcinomas and metastases (Davies et al., 2014). Expression of a constantly active form of PI3K produced invasive adenocarcinomas (Leystra et al., 2012), indicating that PI3K pathway is more important than Kras in intestinal tumorigenesis. $Braf^{V637E}$ mutation is the mouse ortholog to human $BRAF^{V600E}$, a mutation frequently found in human CRC (Li et al., 2006; Yuen et al., 2002). Its expression in mouse IEC led to serrated adenoma, and carcinoma was detected in 14% of the mice (Rad et al., 2013). Further $p16^{Ink4a}$ deletion or *Trp53* mutation significantly increased the number of carcinoma-bearing mice and metastasis rate (Rad et al., 2013). All these models paved the way for studying intestinal cancer development *in vivo*.

1.3 Zinc-finger transcription factor Snail

1.3.1 Snail family members

Snail family members are zinc-finger transcription factors that are crucial for biological processes involved in cell movements (Barrallo-Gimeno and Nieto, 2009; Nieto, 2002). After the identification of *snail* in *Drosophila melanogaster* in the 1980s (Grau et al., 1984; Nusslein-Volhard et al., 1984), its homologs have been reported in many species including mouse and human (Nieto, 2002; Nieto et al., 1992; Paznekas et al., 1999; Smith et al., 1992; Twigg and Wilkie, 1999). In vertebrates, Snail family mainly consists of two members: *SNAI1* (snail family transcriptional repressor 1, hereinafter referred to as *SNAIL*) and *SNAI2* (*SLUG*) (Jiang et al., 1998; Nieto, 2002; Rhim et al., 1997; Savagner et al., 1997). *Smuc*, another related gene in mouse, was reported but almost no further study ensued (Kataoka et al., 2000; Zhuge et al., 2005).

All Snail family members share a highly conserved C-terminal region with four to six C_2H_2 type zinc-fingers (Knight and Shimeld, 2001; Nieto, 2002). A classic binding motif for Snail family members is the enhancer box (E-box) consisting of CANNTG (Fuse et al., 1994; Kataoka et al., 2000; Mauhin et al., 1993). Upon binding to E-boxes, Snail is traditionally considered to be repressors for transcription (Batlle et al., 2000; Cano et al., 2000; Fujiwara et al., 1998; Fuse et al., 1994; Peinado et al., 2007). More recently, the role of Snail as a transcriptional activator has been appreciated (Guaita et al., 2002; Rembold et al., 2014; Wu et al., 2017). Apart from the zinc-fingers, Snail and Slug share a N-terminal SNAG (Snail/Gfi-1) domain containing 7–9 amino acids. The major structural differences between the two are the destruction box and the nuclear export signal domain in the central region of Snail and the less characterized SLUG domain in Slug (Peinado et al., 2007). Human and mouse Snail proteins both consist of 264 amino acids and share 87.1% identical sequence (Jiang et al., 1997; Twigg and Wilkie, 1999), making mouse an ideal organism to model Snail function in human.

1.3.2 Snail and epithelial–mesenchymal transition

The most extensively studied function of Snail is in EMT. During EMT, the epithelial cells lose cell adhesion and increase mobility by expressing EMT transcription factors (including Snail, Twist and Zeb family members) and downregulation of adhesion molecules (Kalluri and Weinberg, 2009; Nieto et al., 2016). The opposite process is named mesenchymal–epithelial transition (MET), and the coordination between the two plays important roles in both embryonic development and cancer metastasis (Pei et al., 2019; Yao et al., 2011). It should be noted that cells are not switching between epithelial and mesenchymal phenotypes, but thermodynamically stable intermediate states exist (Nieto et al., 2016; Zadran et al., 2014). Transition into an intermediate state, or a partial EMT, has been implicated in processes in development, wound healing, fibrosis and cancer (Futterman et al., 2011; Grande et al., 2015; Grigore et al., 2016; Leroy and Mostov, 2007). The critical function of Snail in EMT during embryonic development is highlighted by early Snail expression in the mesoderm (Nieto et al., 1992; Smith et al., 1992), abnormal mesodermal cells in *snail* mutant *Drosophila* (Leptin and Grunewald, 1990) and the observation that *Snail*$^{-/-}$ mice are not viable due to failure in mesoderm germ layer formation (Carver et al., 2001).

Snail is transcriptionally regulated by multiple mechanisms. TGF-β, epidermal growth factor (EGF) and fibroblast growth factor (FGF) signals induce Snail expression and EMT in a variety of experimental settings (Cheng et al., 2010; Ciruna and Rossant, 2001; Isaac et al., 2000;

Jamora et al., 2005; Lu et al., 2003; Montero et al., 2001; Spagnoli et al., 2000; Valdes et al., 2002). During mouse development, Snail is a target of parathyroid hormone related peptide (PTHrP) in parietal endoderm formation (Veltmaat et al., 2000). In human colon carcinoma cells, inhibition of integrin linked kinase (ILK) resulted in transcription repression of *SNAIL* (Tan et al., 2001). In the same SW480 cell line, NF-κB was shown to stimulate *SNAIL* transcription (Barbera et al., 2004). In a breast cancer cell line, MTA3 represses *SNAIL* transcription by directly binding to its promoter (Fujita et al., 2003). Snail also binds to its own promoter and downregulates its mRNA level, suggesting its expression is tightly controlled by a self-inhibitory feedback loop (Peiro et al., 2006).

Posttranslational modifications also play an important role in the regulation of Snail. GSK3β binds to and phosphorylates Snail at two motifs: phosphorylation of the first motif leads to export of Snail from the nucleus to the cytoplasm, and phosphorylation of the second motif targets Snail for βTrCP-mediated ubiquitylation and proteasomal degradation (Zhou et al., 2004). Another study showed that Wnt signaling inhibits phosphorylation of Snail and thereby increases its stability (Yook et al., 2005). In this way, the connection between Wnt signaling pathway and EMT is established. Since GSK3β also inhibits NF-κB, an activator of Snail transcription (Bachelder et al., 2005), Snail is negatively regulated by GSK3β through both transcriptional and posttranslational mechanisms. In addition, two other E3 ubiquitin ligases, FBXl14 and SPSB3, are also responsible for the ubiquitylation and proteasome degradation of Snail (Liu et al., 2018; Vinas-Castells et al., 2010). Phosphorylation of Snail Ser246 by PAK1, on the contrary, promotes its repressive activity (Yang et al., 2005).

The discovery of Snail as a transcriptional repressor of E-cadherin (gene name *CDH1*) was a milestone in elucidating the mechanism of EMT (Batlle et al., 2000; Cano et al., 2000). Peinado and colleagues discovered that Snail forms a repressor complex with HDAC1/HDAC2 and mSin3A to repress *CDH1* transcription (Peinado et al., 2004). The interaction between Snail and HDAC1 or HDAC2 is mediated by the SNAG domain. Results from our lab showed, however, that no interaction was found between Snail or HDAC2 to mSin3A in highly metastatic murine cell lines, arguing for a different co-repressor in the complex (von Burstin et al., 2009). At least in nasopharyngeal carcinoma cell lines, EZH2 was demonstrated to form repressor complex with HDAC1/HDAC2 and Snail (Tong et al., 2012). Another repressor complex on *CDH1* promoter is Snail/AJUBA/PRMT5. In this case, PRMT5 binds to the non-LIM region of AJUBA and its recruitment into the nucleus is facilitated by Snail and AJUBA (Hou et al., 2008). SMAD3/4, PRC2 and LSD1 were also shown to interact with Snail to repress E-cadherin

expression (Herranz et al., 2008; Lin et al., 2010; Vincent et al., 2009). Besides E-cadherin, Snail is capable of repressing the expression of other epithelial-associated genes including claudins, occludin, cytokeratin 18 (CK18), hepatic nuclear factor 4α (HNF4α) and HNF1β (Boutet et al., 2006; Cicchini et al., 2006; De Craene et al., 2005; Ikenouchi et al., 2003).

EMT is tightly regulated by miRNAs as miR-34/Snail and miR-200/Zeb1 form two negative feedback loops, (Bracken et al., 2008; Burk et al., 2008; Gregory et al., 2008; Park et al., 2008; Siemens et al., 2011), while Snail and Zeb1 also repress miR-200 and miR-34, respectively (Ahn et al., 2012; Gill et al., 2011). Apart from that, the interplay of EMT transcription factors is far from being fully understood. There are reports of a negative role of Twist on Snail expression (Forghanifard et al., 2017; Smit et al., 2009); together with the finding that Snail stabilizes Twist (Lander et al., 2013), it is speculated that Snail controls early EMT events while Twist is more important for late stage EMT. A histone-modifying enzyme lysyl oxidase-like 2 (LOXL2) interacts with Snail to impede its GSK3β-dependent degradation and modulate pericentromeric transcription for completing EMT (Millanes-Romero et al., 2013; Peinado et al., 2005). All these facts underline the highly complex regulatory mechanisms involved in EMT, and their deregulation leads to various defects and diseases.

1.3.3 Snail and cancer

The role of Snail in EMT prompted research on its involvement in cancer as EMT is long associated with invasion and metastasis. Moderate to strong Snail expression was found in 78% of PDAC samples in a study in 2007 (Hotz et al., 2007). In colorectal cancer, two studies showed 69% and 78% of cases having Snail overexpression, respectively (Palmer et al., 2004; Roy et al., 2005). In breast and ovarian cancer where Snail function has been extensively studied, its expression level negatively correlated with E-cadherin level and positively correlated with metastatic potential and poor prognosis (Blanco et al., 2002; Cheng et al., 2001; Elloul et al., 2005; Martin et al., 2005; Moody et al., 2005). Elevated Snail expression also correlated with invasiveness and metastasis in esophageal squamous cell carcinoma, colorectal adenocarcinoma and follicular thyroid tumor samples (Choi et al., 2017; Usami et al., 2008; Wu et al., 2019).

Experimentally, Snail was proven to promote invasion in several *in vitro* settings by knockdown or overexpression (Nakamura et al., 2018; Olmeda et al., 2007b; Yang et al., 2007; Yokoyama et al., 2003). Implantation of tumor cell lines (including human pancreatic cancer cell line PANC-1) in mice provided further evidence *in vivo* (Hsu et al., 2014; Jin et al., 2010; Liu et al., 2018;

Olmeda et al., 2007a; Ye et al., 2015; Yin et al., 2007; Zhang et al., 2008). However, as these experiments were carried out in immunodeficient mice and implantation models do not reproduce the entire process of tumor progression, the conclusions cannot represent what may be found in autochthonous tumor models. Indeed, Zheng and colleagues demonstrated that deletion of *Snail* or *Twist* in *Pdx1-Cre;LSL-Kras$^{G12D/+}$;Trp53$^{R172H/+}$* (KPC) mice does not change the survival time nor the metastasis rate (Zheng et al., 2015). Another study using lineage tracing in a breast cancer model showed that metastases form regardless of Fsp1 and vimentin expression (Fischer et al., 2015), and a similar conclusion was drawn with the dual-recombinase system in PDAC (Chen et al., 2018b). These publications call into question the necessity of EMT in metastasis formation. However, one should be aware that one single protein may not be sufficient to drive the entire EMT program and that functions of EMT transcription factors are not redundant (Nieto et al., 2016). In fact, deletion of Zeb1, another EMT transcription factor, reduced metastasis rate in KPC models, arguing for a prominent role of Zeb1 in EMT-dependent metastasis in PDAC (Krebs et al., 2017).

To systematically dissect the role of Snail overexpression in autochthonous PDAC models, Dr. Mariel Paul from our group generated a conditional Snail knock-in mouse line (*LSL-Rosa26$^{Snail/+}$*). This model provided the first *in vivo* evidence that Snail expression greatly accelerates PDAC progression but is not capable of increasing metastasis rate (Paul, 2013). Using another conditional Snail expressing model, Hidayatullah Munshi lab also discovered that Snail expressing mice exhibited increased number of ADM, fibrosis and mast cell infiltration (Knab et al., 2014; Shields et al., 2013). Although it was concluded that mast cells bridge the gap between Snail and inflammation in PDAC progression, they were shown to have no effect in tumor formation (Schonhuber et al., 2014).

Several studies revealed other functions of Snail in cancer. Snail has been associated with cancer stem cell features, suggesting that Snail provides a niche for proliferation and resistance (Dong et al., 2013; Hwang et al., 2011; Mani et al., 2008; Ni et al., 2016; Paul, 2013). Indeed, Snail-induced hyperproliferation and resistance to therapeutic drugs have been reported (Jamora et al., 2005; Jiang et al., 2014; Wang et al., 2017a; Yin et al., 2007; Zheng et al., 2015). The cell cycle regulation mechanism during development may be different from that in cancer, as Snail impairs cell proliferation in mouse embryos (Vega et al., 2004).

Taken together, advances in research in the past 20 years enabled us to peep into the multifaceted role of Snail in cancer. Still, how exactly Snail is involved in cancer remains largely elusive. Therefore, further investigation using *in vivo* models is urgently needed.

1.4 Tumor microenvironment

1.4.1 Composition of pancreatic tumor stroma

A special characteristic of pancreatic tumor is the high abundance of an inflammatory stroma which can take as much as 80% of the tumor mass (Erkan et al., 2012). The stromal microenvironment appears early in PDAC precursor lesions and evolves with tumor progression. Consisting of pancreatic stellate cells (PSCs), cancer-associated fibroblasts (CAFs), immune cells, endothelial cells, nerve cells and extracellular matrix (ECM), the PDAC stroma is involved in tumorigenesis, angiogenesis, resistance to therapy and metastasis (Erkan et al., 2012; Feig et al., 2012). The excessive stroma content profoundly affects vasculature in PDAC, resulting in perfusion impairment linked to poor drug delivery and hypoxia that facilitates ECM deposition and metastasis (Feig et al., 2012; Gilkes et al., 2014). This shows the potential of stroma as a promising anti-cancer therapeutic target and many relevant clinical trials are ongoing (Thomas and Radhakrishnan, 2019; Vennin et al., 2018).

PSCs were first identified in 1998 and their presence was subsequently found in PDAC stroma (Apte et al., 1998; Apte et al., 2004; Bachem et al., 1998). Upon stimulation (e.g. TGF-β, FGF, platelet derived growth factor (PDGF), fibrinogen and oxidative stress) from tumor cells and other microenvironmental factors, PSCs are activated and can sustain their activation through an autocrine periostin loop (Erkan et al., 2007; Jaster et al., 2002; Masamune et al., 2009; Masamune et al., 2008; Vogelmann et al., 2001; Yoshida et al., 2004). Quiescent PSCs are characterized by the expression of glial fibrillary acidic protein (GFAP), vimentin, desmin and nestin, while activated PSCs acquire a myofibroblast-like phenotype with additional α-smooth muscle actin (α-SMA) expression and show increased proliferation, migration and ECM production (Apte et al., 2004; Omary et al., 2007; Phillips et al., 2003). Clinically, the activated stroma index (ASI) related to α-SMA expression was proposed as an independent prognostic marker in PDAC (Erkan et al., 2008). *In vitro* experiments demonstrated the ability of activated PSCs to induce tumor cell proliferation, stemness, EMT and invasion (Froeling et al., 2011; Kikuta et al., 2010; Kiss et al., 2015; Lonardo et al., 2012; Pothula et al., 2016), and co-injection of tumor cells with PSCs in nude mice increased tumor size and metastasis (Bachem et al., 2005; Hwang et al., 2008). Activated PSCs also reduce cytotoxic T cell infiltration in PDAC (Ene-Obong et al., 2013), contributing to the immunosuppressive microenvironment to be introduced in detail in the next section.

Like PSCs, CAFs also contribute to ECM production and inflammation in PDAC. Similarly, co-injection of tumor cells with CAFs increased tumor burden and metastasis (Hwang et al., 2008;

Ligorio et al., 2019). Sonic hedgehog (SHH), a protein implicated in PDAC initiation and maintenance, promotes the differentiation and proliferation of both PSCs and myofibroblasts (Bailey et al., 2008; Thayer et al., 2003). Inhibition of Hedgehog signaling was initially demonstrated to improve drug delivery in KPC mice, consistent with the notion that stroma functions as a barrier to prevent chemotherapeutic agents from accessing the tumor (Olive et al., 2009). However, genetic deletion of *Shh* in KPC model accelerated tumor development (Rhim et al., 2014). Besides, ablation of α-SMA$^+$ myofibroblast reduced survival (Ozdemir et al., 2014). These findings sparked the debate whether stroma restrains or supports pancreatic tumor growth. Actually, the intertwined regulatory network of different stromal components means that the function of stroma cannot be generalized as a whole. For example, the CAFs seem to derive from different origins including PSCs and are phenotypically heterogeneous. Recently, three types of CAFs have been identified: (1) inflammatory CAFs (iCAFs) that express low level of α-SMA but produce interleukin-6 (IL-6) and IL-11 to stimulate the STAT3 pathway in cancer cells; (2) myofibroblastic CAFs (myCAFs) expressing α-SMA and fibroblast-activation protein α (FAP) but lacking the expression of inflammatory cytokines; (3) antigen-presenting CAFs (apCAFs) which express MHC-II and are capable of presenting antigens to T cells (Elyada et al., 2019; Ohlund et al., 2017). Their functions must be therefore individually investigated.

1.4.2 Tumor-infiltrating immune cells

The long-standing connection between pancreatitis and pancreatic cancer highlights the engagement of the immune system in pancreatic cancer development. Many studies have shown the importance of proinflammatory IL-6/STAT3 pathway in mouse models, especially in a Kras^{G12V}-based model, adult mice are refractory to PDAC formation unless challenged with chronic pancreatitis (Fukuda et al., 2011; Guerra et al., 2007; Kang et al., 2012; Lesina et al., 2011). However, mast cells, which play a major role in pancreatitis, have no effect on PDAC progression (Schonhuber et al., 2014). Indeed, the interplay between tumor-infiltrating immune cells and tumor cells as well as other stroma cells is no less complex.

In human PDAC, an immunosuppressive microenvironment is predominant (Elyada et al., 2019; Sideras et al., 2014; Wormann et al., 2014). Tumor-associated macrophages (TAMs), myeloid-derived suppressor cells (MDSCs) and regulatory T cells (Tregs) all contribute to the immunosuppression that block cytotoxic T cell function. TAM phenotype is divided into classically activated M1 and alternatively activated M2 types, and the M1 macrophages that

prevail in early tumor development gradually convert to M2 macrophages during tumor progression (Hu et al., 2015). In human PDAC, M1 macrophages is associated with longer survival while M2 macrophages have the opposite effect (Ino et al., 2013; Kurahara et al., 2011). Both tumor cells and PSCs have been shown to recruit and program TAMs (Halbrook et al., 2019; Schmid-Kotsas et al., 1999; Shi et al., 2014; Xue et al., 2015), and they in turn facilitate tumor growth by cytokine production and modulating tumor-infiltrating T cells towards a pro-tumor phenotype (Borgoni et al., 2018; Daley et al., 2017; Lesina et al., 2011; Zhu et al., 2017; Zhu et al., 2014). In addition, granulin-secreting inflammatory monocytes in the liver are crucial for metastasis formation (Nielsen et al., 2016). On the other hand, TAMs can be harnessed to turn against the tumor under special circumstances. CD40 is able to elicit anti-tumor response in PDAC that depends on macrophages instead of T cells (Beatty et al., 2011).

MDSCs phenotypically resemble neutrophils (Aarts and Kuijpers, 2018; Bronte et al., 2016) and are associated with cancer stage and poor prognosis in PDAC patients (Diaz-Montero et al., 2009; Giakoustidis et al., 2018; Nywening et al., 2018). Granulocyte-macrophage colony-stimulating factor (GM-CSF) and IL-6 produced by tumor cells are important chemoattractants for recruiting MDSCs into the tumor microenvironment (Pergamo and Miller, 2017; Pylayeva-Gupta et al., 2012), and inhibition of MDSC recruitment by GM-CSF abrogation blocked tumor development in KPC mice in a $CD8^+$ T cell-dependent manner (Bayne et al., 2012). Other studies showed that MDSCs are capable of suppressing $CD8^+$ T cell function and mediate Treg development (Huang et al., 2006; Pinton et al., 2016; Porembka et al., 2012). The number of Tregs, another major player in immune suppression, is predictive of shorter survival in PDAC patients (Ino et al., 2013; Tang et al., 2014). Tumor cells produce CCL5 to attract Tregs which express its receptor CCR5 (Tan et al., 2009; Wang et al., 2017b). Tregs have been shown to exert their function by suppressing the dendritic cell-dependent cytotoxic T cell activation (Jang et al., 2017).

Similar to macrophages, $CD4^+$ helper T cells also differentiate into two major subtypes T_h1 and T_h2. Likewise, T_h1 is a marker for prolonged survival and T_h2 is indicative of worse prognosis (De Monte et al., 2011; Nizri et al., 2018; Piro et al., 2017). Not surprisingly, there is a general shift into T_h2 phenotype in pancreatic cancer (Bellone et al., 1999; De Monte et al., 2011; Gabitass et al., 2011; Tassi et al., 2008). The function of a special T_h17 subtype defined by the production of IL-17 is under debate due to inconsistency in mouse and human data (Barilla et al., 2019; Gnerlich et al., 2010; He et al., 2011; Vizio et al., 2012).

Cytotoxic $CD8^+$ T cells play a fundamental role in eliminating tumor cells, but their cytotoxicity in tumor is largely abolished because of limited number, inhibitory signal in the microenvironment and the existence of bystanders which are specific for epitopes not related to cancer (Clark et al., 2007; Dyck and Mills, 2017; Simoni et al., 2018). The discovery of immune checkpoint molecules marked a milestone in cancer immunology research, as several checkpoint inhibitors have shown great benefit to patient survival and approved by FDA (Hargadon et al., 2018). All these approved inhibitors target PD-1/PD-L1 or CTLA-4/CD80/CD86 signaling, which inhibit T cell activation. However, no checkpoint inhibitors have been approved specifically for pancreatic cancer to date. By comparing immune infiltrates in melanoma and pancreatic cancer, Blando and colleagues identified VISTA instead of PD-1 as a potent inhibitory checkpoint for pancreatic cancer, which might explain why existing checkpoint inhibitors in the market do not work (Blando et al., 2019). Chimeric antigen receptor T (CAR-T) cell therapy is another promising remedy which engineers T cells to recognize tumor antigens. Survival benefit has been shown in KPC mice (Stromnes et al., 2015) and many clinical trials are ongoing (Ali et al., 2019).

B cells are actively involved in the adaptive immune system but have pro-tumor effect at least in part due to stimulation of tumor cell proliferation by IL-35 (Gunderson et al., 2016; Lee et al., 2016; Pylayeva-Gupta et al., 2016). High number of dendritic cells, another type of antigen-presenting cell, in the circulation is indicative of better survival (Hirooka et al., 2011; Yamamoto et al., 2012). However, a special subset of dendritic cells at secondary sites facilitates PDAC metastasis (Kenkel et al., 2017). These findings again underline the importance of studying immune cell subsets individually.

Snail has been linked with immune cells in cancer by a few studies. Kudo-Saito and colleagues showed that Snail-induced metastasis in melanoma is not only a result of increased invasion but also because of immunosuppression by Tregs (Kudo-Saito et al., 2009). In addition, Snail is shown to recruit macrophages and promote M2 polarization in independent studies (Du et al., 2010; Hsieh et al., 2018; Hsu et al., 2014; Zhang et al., 2016). In an ovarian cancer model, Snail accelerated tumor progression by upregulating the expression of CXCR2 ligands and thereby recruitment of MDSCs (Taki et al., 2018). Similar finding was made in a $Kras^{G12D}$-driven lung cancer model, and neutrophils also induced Snail expression in a feedback loop (Faget et al., 2017). Importantly, CXCR2 signaling in neutrophils/MDSCs is indeed upregulated in human PDAC and its inhibition substantially reduced metastasis, extended survival and enhanced sensitivity to anti-PD-1 therapy in KPC mice (Steele et al., 2016). Still, little is known about whether and how Snail affects other immune cells, especially in pancreatic cancer.

1.5 Aim of this work

To study the function of Snail *in vivo*, previous work in the lab generated a conditional Snail overexpressing mouse model (Paul, 2013). Surprisingly, Snail overexpression significantly accelerated tumor growth but did not increase metastasis rate. It was shown that Snail expression in the pancreas bypasses senescence and increases proliferation, however, the exact mechanism involved has not been elucidated. To this end, the binding of Snail to cell cycle gene promoters was examined by chromatin immunoprecipitation (ChIP) and analysis of publicly available ChIP-sequencing (ChIP-seq) data. Given the recent finding that *KRAS* mutant dosage and *CDKN2A* locus status determine pancreatic cancer phenotypes (Mueller et al., 2018), its relevance in Snail-expressing tumors was evaluated. To test whether Snail has similar effects in intestinal cancer, three models of intestinal cancer with additional Snail overexpression were analyzed for survival and readouts for EMT. By gene set enrichment analysis (GSEA), Snail was found to induce a proinflammatory program in the pancreas. Therefore, flow cytometry was used to assess the amount of infiltrating immune cells in PDAC. The result was further validated by deconvolution of RNA sequencing (RNA-seq) data from PDAC with bioinformatics method, which also provided the immune landscape of Snail-expressing tumors. In order to target the inflammatory microenvironment in PDAC, mature B cells, T cells and NK cells were depleted using genetic models and their effects on tumor formation were evaluated. In addition, as Snail expression in human PDAC is not confined to tumor cells, the dual-recombinase system was employed to investigate the function of Snail in stroma cells.

2 Materials and methods

2.1 Materials

2.1.1 Technical equipment

Technical equipment used in this thesis are listed in Table 2-1.

Table 2-1. List of technical equipment

Device	Source
Analytical balance A 120 S	Sartorius AG, Göttingen
Analytical balance BP 610	Sartorius AG, Göttingen
Aperio AT2 Digital Whole Slide Scanner	Leica Microsystems GmbH, Wetzlar
Autoclave 2540 EL	Tuttnauer Europe B.V., Breda, The Netherlands
AxioCam HRc	Carl Zeiss AG, Oberkochen
AxioCam MRc	Carl Zeiss AG, Oberkochen
Bag sealer Folio FS 3602	Severin Elektrogeräte GmbH, Sundern
Centrifuge Rotina 46R	Andreas Hettich GmbH & Co. KG, Tuttlingen
CO_2 incubator HERAcell®	Heraeus Holding GmbH, Hanau
CO_2 incubator MCO-5AC 17AI	Sanyo Sales & Marketing Europe GmbH, Munich
Cryostat Microm HM 560	Thermo Fisher Scientific, Inc., Waltham, MA, USA
Dewar carrying flask, type B	KGW-Isotherm, Karlsruhe
Electrophoresis power supply Power Pac 200	Bio-Rad Laboratories GmbH, Munich
Gel Doc™ XR+ system	Bio-Rad Laboratories GmbH, Munich
GentleMACS™ Dissociator	Miltenyi Biotec, Bergisch Gladbach
Glassware, Schott Duran®	Schott AG, Mainz
Heated paraffin embedding module EG1150 H	Leica Microsystems GmbH, Wetzlar
HERAsafe® biological safety cabinet	Thermo Fisher Scientific, Inc., Waltham, MA, USA
Hiseq 1500 platform	Illumina, San Diego, CA, USA
Homogenizer SilentCrusher M with tool 6F	Heidolph Instruments GmbH & Co. KG, Schwabach
Horizontal gel electrophoresis system	Biozym Scientific GmbH, Hessisch Oldenburg
Laminar flow HERAsafe	Heraeus Holding GmbH, Hanau

Device	Source
LSM 510 Laser Scanning Microscope	Carl Zeiss AG, Oberkochen
LSRFortessa™ cell analyzer	BD Biosciences, Franklin Lakes, NJ, USA
Magnetic Separation Rack 6-Tube #7017	Cell Signaling Technology, Inc., Danvers, MA, USA
Magnetic stirrer, Ikamag® RCT	IKA Werke GmbH & Co. KG, Staufen
Microcentrifuge 5415 D	Eppendorf AG, Hamburg
Microcentrifuge 5417 R	Eppendorf AG, Hamburg
Microscope Axio Imager.A1	Carl Zeiss AG, Oberkochen
Microscope Axiovert 25	Carl Zeiss AG, Oberkochen
Microscope DM LB	Leica Microsystems GmbH, Wetzlar
Microtome Microm HM355S	Thermo Fisher Scientific, Inc., Waltham, MA, USA
Microwave	Siemens AG, Munich
Mini centrifuge MCF-2360	LMS Consult GmbH & Co. KG, Brigachtal
Miseq platform	Illumina, San Diego, CA, USA
Multipette® stream	Eppendorf AG, Hamburg
Neubauer hemocytometer, improved	LO-Laboroptik GmbH, Bad Homburg
Paraffin tissue floating bath Microm SB80	Thermo Fisher Scientific, Inc., Waltham, MA, USA
pH meter 521	WTW Wissenschaftlich-Technische Werkstätten GmbH, Weilheim
Pipettes Eppendorf Reference®, Research®	Eppendorf AG, Hamburg
Pipetus®	Hirschmann Laborgeräte GmbH & Co. KG, Eberstadt
Power supplies E844, EV243	Peqlab Biotechnologie GmbH, Erlangen
Qubit® 2.0 Fluorometer	Invitrogen GmbH, Karlsruhe
Shaking Water Bath SB-12	Biozym Scientific GmbH, Hessisch Oldendorf
Spectrophotometer NanoDrop 1000	Peqlab Biotechnologie GmbH, Erlangen
StepOnePlus™ real time PCR system	Applied Biosystems, Inc., Carlsbad, CA, USA
Stereomicroscope Stemi SV 11	Carl Zeiss AG, Oberkochen
Surgical instruments	Thermo Fisher Scientific, Inc., Waltham, MA, USA
Thermo cycler T1	Biometra GmbH, Göttingen
Thermo cycler T100	Bio-Rad Laboratories GmbH, Munich
Thermo cycler Tgradient	Biometra GmbH, Göttingen
Thermo cycler T-personal	Biometra GmbH, Göttingen
Thermo cycler UNO-Thermoblock	Biometra GmbH, Göttingen
Thermomixer compact	Eppendorf AG, Hamburg

Device	Source
Tissue processor ASP300	Leica Microsystems GmbH, Wetzlar
Tumbling Table WT 17	Biometra GmbH, Göttingen
Vortex Genius 3	IKA Werke GmbH & Co. KG, Staufen
Water bath 1003	GFL Gesellschaft für Labortechnik mbH, Burgwedel

2.1.2 Disposables

Disposables are listed in Table 2-2.

Table 2-2. List of disposables

Disposable	Source
Cell culture plastics	Becton Dickinson, Franklin Lakes, NJ, USA; Greiner Bio-One GmbH, Frickenhausen; TPP Techno Plastic Products AG, Trasadingen, Switzerland
Cell scrapers	TPP Techno Plastic Products AG, Trasadingen, Switzerland
Cell strainer, 100 µm, yellow	BD Biosciences, Franklin Lakes, NJ, USA
CellTrics filter green, 30 µm	Sysmex Deutschland GmbH, Norderstedt
Combitips BioPur®	Eppendorf AG, Hamburg
Conical tubes, 15 mL	TPP Techno Plastic Products AG, Trasadingen, Switzerland
Conical tubes, 50 mL	Sarstedt AG & Co., Nümbrecht
Cover slips	Gerhard Menzel, Glasbearbeitungswerk GmbH & Co. KG, Braunschweig
Cryo embedding tubes	Carl Roth GmbH + Co. KG, Karlsruhe
CryoPure tubes	Sarstedt AG & Co., Nümbrecht
Disposable scalpels	Feather Safety Razor Co., Ltd., Osaka, Japan
GentleMACS™ C Tubes	Miltenyi Biotec, Bergisch Gladbach
Glass slides Superfrost® Plus	Gerhard Menzel, Glasbearbeitungswerk GmbH & Co. KG, Braunschweig
MicroAmp® optical 96-well reaction plate	Applied Biosystems, Inc., Carlsbad, CA, USA
Microtome blades S35 and C35	Feather Safety Razor Co., Ltd., Osaka, Japan
Pasteur pipettes	Hirschmann Laborgeräte GmbH & Co. KG, Eberstadt
PCR reaction tubes	Brand GmbH + Co. KG, Wertheim; Eppendorf AG, Hamburg
Petri dishes	Sarstedt AG & Co., Nümbrecht

Disposable	Source
Pipette tips	Sarstedt AG & Co., Nümbrecht
Reaction tubes, 0.5 mL, 1.5 mL and 2 mL	Eppendorf AG, Hamburg
Safe seal pipette tips, professional	Biozym Scientific GmbH, Hessisch Oldenburg
Safe-lock reaction tubes BioPur®	Eppendorf AG, Hamburg
Serological pipettes	Sarstedt AG & Co., Nümbrecht
Single use needles Sterican® 27 gauge	B. Braun Melsungen AG, Melsungen
Single use syringes Omnifix®	B. Braun Melsungen AG, Melsungen
Tissue embedding cassette system	Medite GmbH, Burgdorf

2.1.3 Reagents and enzymes

Reagents and enzymes used are listed in Table 2-3.

Table 2-3. List of reagents and enzymes

Reagent	Source
1 kb DNA extension ladder	Invitrogen GmbH, Karlsruhe
1,4-Dithiothreitol (DTT)	Carl Roth GmbH + Co. KG, Karlsruhe
2-Log DNA ladder (0.1–10.0 kb)	New England Biolabs GmbH, Frankfurt am Main
2-Mercaptoethanol, 98%	Sigma-Aldrich Chemie GmbH, Munich
2-Propanol (isopropanol)	Carl Roth GmbH + Co.
5-Bromo-2'-deoxyuridine (BrdU)	AppliChem GmbH, Darmstadt
Acetic acid (glacial)	Merck KGaA, Darmstadt
Agarose	Sigma-Aldrich Chemie GmbH, Munich
AluI restriction endonuclease	New England Biolabs GmbH, Frankfurt am Main
Ammonium chloride (NH_4Cl)	Sigma-Aldrich Chemie GmbH, Munich
Ammonium sulfate ($(NH_4)_2SO_4$)	Sigma-Aldrich Chemie GmbH, Munich
Antigen unmasking solution, citric acid based	Vector Laboratories, Inc., Burlingame, CA, USA
Bovine serum albumin (BSA), fraction V	Sigma-Aldrich Chemie GmbH, Munich
Bromophenol blue	Sigma-Aldrich Chemie GmbH, Munich
Buffer S, 10×	VWR International, Radnor, PA, USA
Collagenase type II	Worthington Biochemical Corporation, Lakewood, NJ, USA
cOmplete, EDTA-free, protease inhibitor cocktail Tablets	Roche Deutschland Holding GmbH, Grenzach-Wyhlen

Reagent	Source
Cresol red	Sigma-Aldrich Chemie GmbH, Munich
Dimethylsulfoxide (DMSO)	Carl Roth GmbH + Co. KG, Karlsruhe
Disodium ethylenediaminetetraacetate dihydrate ($Na_2EDTA \cdot 2H_2O$)	Sigma-Aldrich Chemie GmbH, Munich
dNTP mix, 10mM each	Fermentas GmbH, St. Leon-Rot
Dulbecco's modified eagle medium (DMEM) with L-glutamine	Invitrogen GmbH, Karlsruhe
Dulbecco's phosphate buffered saline (PBS)	Invitrogen GmbH, Karlsruhe
Dulbecco's phosphate buffered saline (PBS), powder	Biochrom AG, Berlin
Eosine	Waldeck GmbH & Co KG, Münster
Ethanol (100%)	Merck KGaA, Darmstadt
Ethanol (80%)	BrüggemannAlcohol Heilbronn GmbH, Heilbronn
Ethanol (96%, 99%)	Fischar Otto GmbH & Co. KG, Saarbrücken
Ethidium bromide	Sigma-Aldrich Chemie GmbH, Munich
Ethylenediaminetetraacetic acid (EDTA)	Invitrogen GmbH, Karlsruhe
Exonuclease I	New England Biolabs GmbH, Frankfurt am Main
Fetal bovine serum (FBS)	Biochrom AG, Berlin
Forene® isoflurane	Abbott GmbH & Co. KG, Ludwigshafen
Formaldehyde solution 37 %	Carl Roth GmbH + Co. KG, Karlsruhe
Fungizone® antimycotic	Invitrogen GmbH, Karlsruhe
Gel loading dye, blue	New England Biolabs GmbH, Frankfurt am Main
GeneRuler™ 100bp DNA ladder	Fermentas GmbH, St. Leon-Rot
Glycerol	Sigma-Aldrich Chemie GmbH, Munich
Goat serum G9023	Sigma-Aldrich Chemie GmbH, Munich
Hematoxylin	Merck KGaA, Darmstadt
HEPES Pufferan®	Carl Roth GmbH + Co. KG, Karlsruhe
HotStarTaq DNA polymerase	Qiagen GmbH, Hilden
Hydrochloric acid (HCl)	Merck KGaA, Darmstadt
Hydrogen peroxide (H_2O_2) 30%	Merck KGaA, Darmstadt
Isotonic sodium chloride (NaCl) solution	Braun Melsungen AG, Melsungen
Magnesium chloride ($MgCl_2$)	Carl Roth GmbH + Co. KG, Karlsruhe
Methanol	Merck KGaA, Darmstadt
Nonidet P-40	Roche Deutschland Holding GmbH, Grenzach-Wyhlen
Oligo(dT) Primer	Thermo Fisher Scientific, Inc., Waltham, MA, USA

Reagent	Source
Orange G	Carl Roth GmbH + Co. KG, Karlsruhe
Penicillin (10000 units/mL) / Streptomycin (10000 µg/mL) solution	Invitrogen GmbH, Karlsruhe
Pertex mounting medium	Medite GmbH, Burgdorf
PfuUltra™ high fidelity DNA polymerase	Agilent Technologies, Inc., Santa Clara, CA, USA
Phosphatase inhibitor mix I	Serva Electrophoresis GmbH, Heidelberg
Potassium bicarbonate ($KHCO_3$)	Sigma-Aldrich Chemie GmbH, Munich
Proteinase K, recombinant, PCR grade	Roche Deutschland Holding GmbH, Grenzach-Wyhlen
Q5® High-Fidelity DNA Polymerase	New England Biolabs GmbH, Frankfurt am Main
Random Primers	Thermo Fisher Scientific, Inc., Waltham, MA, USA
Recombinant human TGF-β1	PeproTech Germany, Hamburg
REDTaq® ReadyMix™ PCR reaction mix	Sigma-Aldrich Chemie GmbH, Munich
RnaseA	Fermentas GmbH, St. Leon-Rot
Roti® Histofix 4%	Carl Roth GmbH + Co. KG, Karlsruhe
Roti® Histol	Carl Roth GmbH + Co. KG, Karlsruhe
Saponin	Sigma-Aldrich Chemie GmbH, Munich
Sodium acetate buffer solution	Sigma-Aldrich Chemie GmbH, Munich
Sodium chloride (NaCl)	Merck KGaA, Darmstadt
Sodium hydroxide solution (NaOH)	Merck KGaA, Darmstadt
Sucrose	Merck KGaA, Darmstadt
SuperScript II reverse transcriptase	Thermo Fisher Scientific, Inc., Waltham, MA, USA
SYBR® green PCR master mix	Applied Biosystems, Inc., Carlsbad, CA, USA
TE buffer, pH 8.0	AppliChem GmbH, Darmstadt
Tissue-Tek® O.C.T.™ compound	Sakura Finetek Europe B.V, Alphen aan den Rijn, Netherlands
TO-PRO-3 Iodide	Thermo Fisher Scientific, Inc., Waltham, MA, USA
Tris hydrochloride	J.T.Baker® Chemicals, Phillipsburg, NJ, USA
Tris Pufferan®	Carl Roth GmbH + Co. KG, Karlsruhe
Triton® X-100	Merck KGaA, Darmstadt
Trypsin, 0.05% with 0.53 mM EDTA·4Na	Invitrogen GmbH, Karlsruhe
Tween® 20	Carl Roth GmbH + Co. KG, Karlsruhe
UltraComp eBeads Compensation Beads	Thermo Fisher Scientific, Inc., Waltham, MA, USA
Vectashield® mounting medium for immunofluorescence	Vector Laboratories, Inc., Burlingame, CA, USA

2.1.4 Solutions

Solvent for all solutions is deionized water unless otherwise stated. Solutions and their components are listed in Table 2-4.

Table 2-4. List of solutions

Solution	Component
ACK (Ammonium-Chloride-Potassium) lysis buffer	150 mM NH_4Cl 10 mM $KHCO_3$ 0.1 mM Na_2EDTA
Gitschier's buffer, 10×	670 mM Tris, pH 8.8 166 mM $(NH_4)_2SO_4$ 67 mM $MgCl_2$
Immunofluorescence blocking solution	3% BSA 1% Saponin 1% Triton® X-100 dissolved in PBS
IP buffer, pH 7.9	50 mM HEPES 150 mM NaCl 1 mM EDTA 0.5% Nonidet P-40 10% Glycerol Phosphatase inhibitor (add prior to use) Protease inhibitor (add prior to use)
Loading buffer orange G, 6×	60% Glycerol 60 mM EDTA 0.24% Orange G
PBST	0.1% Tween® 20 in PBS
Soriano lysis buffer	0.5% Triton® X-100 1% 2-Mercaptoethanol 1× Gitschier's buffer 400 µg/mL Proteinase K (add prior to use)
SucRot solution	1.5 mg/mL Cresol red 100 mM Tris, pH 9.0 30% Sucrose

Solution	Component
Tris acetate EDTA (TAE) buffer, pH 8.5, 50×	2 M Tris 50 mM EDTA 5.71% Acetic acid

2.1.5 Kits

Commercial kits used in this thesis are listed in Table 2-5.

Table 2-5. List of kits

Kit	Source
Agencourt AMPure XP Kit	Beckman Coulter GmbH, Krefeld
Ambion® WT Expression Kit	Applied Biosystems, Inc., Carlsbad, CA, USA
Avidin/biotin Blocking Kit	Vector Laboratories, Inc., Burlingame, CA, USA
DAB Peroxidase (HRP) Substrate kit	Vector Laboratories, Inc., Burlingame, CA, USA
DNeasy Blood & Tissue Kit	Qiagen GmbH, Hilden
Experion™ RNA StdSens analysis kit	Bio-Rad Laboratories GmbH, Munich
GeneChip® WT Terminal Labeling Kit	Affymetrix, Inc., Santa Clara, CA, USA
KAPA HiFi HotStart ReadyMix	Roche Deutschland Holding GmbH, Grenzach-Wyhlen
KAPA Library Quantification Kit	Roche Deutschland Holding GmbH, Grenzach-Wyhlen
Nextera XT DNA Library Prep Kit	Illumina, San Diego, CA, USA
QIAquick PCR Purification Kit	Qiagen GmbH, Hilden
QIAshredder	Qiagen GmbH, Hilden
Qubit® dsDNA BR Assay Kit	Invitrogen GmbH, Karlsruhe
RNase-free DNase Set	Qiagen GmbH, Hilden
RNeasy Mini Kit	Qiagen GmbH, Hilden
SimpleChIP® Enzymatic Chromatin IP Kit	Cell Signaling Technology, Inc., Danvers, MA, USA
TaqMan™ Reverse Transcription Reagents	Applied Biosystems, Inc., Carlsbad, CA, USA
TruSeq® Stranded mRNA Sample Preparation Kit	Illumina, San Diego, CA, USA
Tumor Dissociation Kit, mouse	Miltenyi Biotec, Bergisch Gladbach
Vectastain® Elite ABC HRP Kit	Vector Laboratories, Inc., Burlingame, CA, USA
Zombie Aqua™ Fixable Viability Kit	BioLegend, San Diego, CA, USA

2.1.6 Antibodies

Primary antibodies for immunohistochemistry (IHC) are listed in Table 2-6.

Table 2-6. List of primary antibodies for immunohistochemistry

Antibody	Source
Cytokeratin 19 (CK19), TROMA III	Developmental Studies Hybridoma Bank, Iowa City, IA, USA
E-cadherin #610181	BD Biosciences, Franklin Lakes, NJ, USA
Snail (C15D3) #3879	Cell Signaling Technology, Inc., Danvers, MA, USA

Biotinylated anti-mouse, -rabbit or -rat IgG (H+L) (Vector Laboratories, Inc., Burlingame, CA, USA) was used for signal amplification and detection in IHC.

All antibodies used in ChIP were obtained from Cell Signaling Technology, Inc., Danvers, MA, USA. Snail (C15D3, #3879) antibody was used to pull down Snail-bound chromatin fragment. Normal rabbit IgG (#2729) and histone H3 (D2B12, #4620) antibody served as negative and positive control, respectively.

Fluorochrome-conjugated antibodies for flow cytometry are listed in Table 2-7.

Table 2-7. List of antibodies for flow cytometry

Antibody	Source
AF647 anti-mouse CD326 (EpCAM)	BioLegend, San Diego, CA, USA
APC/Cy7 anti-mouse CD68	BioLegend, San Diego, CA, USA
APC/Fire 750 anti-mouse/human CD44	BioLegend, San Diego, CA, USA
BB515 anti-mouse Siglec-F	BD Biosciences, Franklin Lakes, NJ, USA
BUV395 anti-mouse CD3e	BD Biosciences, Franklin Lakes, NJ, USA
BUV395 anti-mouse NK1.1	BD Biosciences, Franklin Lakes, NJ, USA
BUV737 anti-mouse CD11c	BD Biosciences, Franklin Lakes, NJ, USA
BUV805 anti-mouse CD4	BD Biosciences, Franklin Lakes, NJ, USA
BV421 anti-mouse F4/80	BioLegend, San Diego, CA, USA
BV421 anti-mouse TCRγ/δ	BioLegend, San Diego, CA, USA
BV650 anti-mouse CD25	BioLegend, San Diego, CA, USA
BV650 anti-mouse/human CD11b	BioLegend, San Diego, CA, USA
BV785 anti-mouse CD8a	BioLegend, San Diego, CA, USA
BV785 anti-mouse Ly6C	BioLegend, San Diego, CA, USA

Antibody	Source
FITC anti-mouse CD19	BioLegend, San Diego, CA, USA
PE anti-mouse CD62L	BioLegend, San Diego, CA, USA
PE anti-mouse Ly6G	BioLegend, San Diego, CA, USA
PerCP/Cy5.5 anti-mouse CD45	BioLegend, San Diego, CA, USA
TruStain FcX (anti-mouse CD16/32)	BioLegend, San Diego, CA, USA

2.1.7 Primers

All primers were synthesized by Eurofins Genomics GmbH (Ebersberg) and diluted in molecular grade water to a concentration of 10 µM. Genotyping and recombination PCR primers are listed in Table 2-8.

Table 2-8. List of genotyping and recombination PCR primers

PCR	Name of primer	Sequence (5'–3')
Ptf1a^{Cre}	Ptf1a^{Cre} fwd	CCTCGAAGGCGTCGTTGATGGACTGCA
	Ptf1a^{Cre} WT rev	CCACGGATCACTCACAAAGCGT
	Ptf1a^{Cre} mut rev	GCCACCAGCCAGCTATCAA
LSL-Kras^{G12D}	LSL-Kras^{G12D} fwd	CACCAGCTTCGGCTTCCTATT
	LSL-Kras^{G12D} WT rev	AGCTAATGGCTCTCAAAGGAATGTA
	LSL-Kras^{G12D} mut rev	CCATGGCTTGAGTAAGTCTGC
Rosa26	LSL-Rosa26 fwd	AAAGTCGCTCTGAGTTGTTAT
	LSL-Rosa26 mut rev	GCGAAGAGTTTGTCCTCAACC
	LSL-Rosa26 WT rev	GGAGCGGGAGAAATGGATATG
LSL-Rosa26^{Snail}	LSL-Rosa26^{Snail} fwd	TGAATAGTTAATTGGAGCGGCCGCAATA
	LSL-Rosa26^{Snail} rev	ACCAGGAAGGAGCGCGGCAT
LSL-Rosa26^{Snail} recombination	LSL-Rosa26 fwd	AAAGTCGCTCTGAGTTGTTAT
	LSL-Rosa26^{Snail} rev	ACCAGGAAGGAGCGCGGCAT
Snail^{lox}	Snail^{lox} fwd	CGGGCTTAGGTGTTTTCAGA
	Snail^{lox} rev	CTTGCTTGGTACCTGCCTTC
Snail^{lox} deletion	Snail^{lox} fwd	CGGGCTTAGGTGTTTTCAGA
	Snail^{lox} del rev	TGAAAGCGGCTCTGTTCAGT
LSL-Trp53^{R172H}	LSL-Trp53^{R172H} WT fwd	AGCCTTAGACATAACACACGAACT
	LSL-Trp53^{R172H} mut fwd	GCCACCATGGCTTGAGTAA
	LSL-Trp53^{R172H} rev	CTTGGAGACATAGCCACACTG
Cdkn2a^{lox}	Cdkn2a^{lox} fwd	CCAAGTGTGCAAACCCAGGCTCC
	Cdkn2a^{lox} rev	TTGTTGGCCCAGGATGCCGACATC

PCR	Name of primer	Sequence (5'–3')
p16^{Ink4a*}	p16^{Ink4a*} fwd	GCAGTGTTGCAGTTTGAACCC
	p16^{Ink4a*} rev	TGTGGCAACTGATTCAGTTGG
Villin-Cre	Villin-Cre fwd	GTGTGGGACAGAGAACAAACC
	Villin-Cre rev	ACATCTTCAGGTTCTGCGGG
	Tcrd for (Ctrl)	CAAATGTTGCTTGTCTGGTG
	Tcrd rev (Ctrl)	GTCAGTCGAGTGCACAGTTT
APC^{lox}	APC^{lox} fwd	GATCACTCATCCGATAAGTGC
	APC^{lox} rev	TTGGTTAAGGTGGTCTTGCAG
LSL-Braf^{V637E}	LSL-Braf^{V637E} fwd	TTTATCATAGTAGGGCTTGCTGTCTTGCTT
	LSL-Braf^{V637E} WT rev	CAAATATGTTTTGAGCAAGACCTTTGTTCT
	LSL-Braf^{V637E} mut rev	CCACTGACCAGAAGGAAAGTGGT
Rag2^{-}	Rag2^{-} WT fwd	ATCAATGGTTCACCCCTTTG
	Rag2^{-} WT rev	TCATGTGAAAGCAGTTCAGGAC
	Rag2^{-} mut fwd	CAGCGCTCCTCCTGATACTC
	Rag2^{-} mut rev	CCGCCATATGCATCCAAC
Prkdc^{Scid}	Prkdc^{Scid} fwd	GGAAAAGAATTGGTATCCAC
	Prkdc^{Scid} rev	AGTTATAACAGCTGGGTTGGC
Il2rg^{-}	Il2rg^{-} fwd	GTGGGTAGCCAGCTGCTCTTCAG
	Il2rg^{-} WT rev	CCTGGAGCTGGACAACAAAT
	Il2rg^{-} mut rev	GCCAGAGGCCACTTGTGTAG
Pdx1-Flp	Pdx1-Flp fwd	AGAGAGAAAATTGAAACAAGTGCAGGT
	Pdx1-Flp rev	CGTTGTAAGGGATGATGGTGAACT
	Gabra for (Ctrl)	AACACACACTGGAGGACTGGCTAGG
	Gabra rev (Ctrl)	CAATGGTAGGCTCACTCTGGGAGATGATA
FSF-Kras^{G12D}	FSF-Kras^{G12D} fwd	CACCAGCTTCGGCTTCCTATT
	FSF-Kras^{G12D} WT rev	AGCTAATGGCTCTCAAAGGAATGTA
	FSF-Kras^{G12D} mut rev	GCGAAGAGTTTGTCCTCAACC
FSF-Kras^{G12D} recombination	FSF-Kras^{G12D} rec fwd	TGTAGCAGCTAATGGCTCTCAAA
	FSF-Kras^{G12D} rec rev	AGAATACCGCAAGGGTAGGTGTTG
LSL-Rosa26^{mT-mG}	LSL-Rosa26 fwd	AAAGTCGCTCTGAGTTGTTAT
	LSL-Rosa26 WT rev	GGAGCGGGAGAAATGGATATG
	mT-mG mut rev	GTACTTGGCATATGATACACTTGATGTAC
General Cre (for *Fsp1-Cre*)	Cre fwd	CCTGGAAAATGCTTCTGTCCG
	Cre rev	CAGGGTGTTATAAGCAATCCC
	Gabra fwd (Ctrl)	AACACACACTGGAGGACTGGCTAGG
	Gabra rev (Ctrl)	CAATGGTAGGCTCACTCTGGGAGATGATA

Quantitative real-time PCR (qPCR) primers for testing relative mRNA expression level and antibody binding to E-boxes in ChIP experiment are listed in Table 2-9 and 2-10, respectively.

Table 2-9. List of qPCR primers for expression level

Gene	Name of primer	Sequence (5'–3')
Snail	Snail fwd	GCCGGAAGCCCAACTATAGC
	Snail rev	GGTCGTAGGGCTGCTGGAA
Cdh1	Cdh1 fwd	GAGCGTGCCCCAGTATCG
	Cdh1 rev	CGTAATCGAACACCAACAGAGAGT
Ccna1	Ccna1 fwd	GCTGTCTCTTTACCCGGAGCA
	Ccna1 rev	ACGTTCACTGGCTTGTCTTCTA
Ccna2	Ccna2 fwd	CACTGACACCTCTTGACTATCC
	Ccna2 rev	CGTTCACTGGCTTGTCTTCT
Ccnb1	Ccnb1 fwd	TTGTGTGCCCAAGAAGATGCT
	Ccnb1 rev	GTACATCTCCTCATATTTGCTTGCA
Ccnb2	Ccnb2 fwd	TGAAGTCCTGGAAGTCATGC
	Ccnb2 rev	GAGGCCAGGTCTTTGATGAT
Cd44	Cd44 fwd	CACATATTGCTTCAATGCCTCAG
	Cd44 rev	CCATCACGGTTGACAATAGTTATG
Il6	Il6 fwd	CCGGAGAGGAGACTTCACAG
	Il6 rev	TCCACGATTTCCCAGAGAAC
Il2rg	Il2rg fwd	ACAGAGATCGAAGCTGGACG
	Il2rg rev	GAACCCGAAATGTGTACCGT
Snail exo	Snail exo fwd	TATTAGGTCCCTCGACCTGACGCC
	Snail exo rev	ACCAGGAAGGAGCGCGGCAT

Table 2-10. List of qPCR primers for ChIP

Gene	Name of primer	Sequence (5'–3')
Ccna1	Ccna1 E-box fwd	TTAAAGCCCATTCAGCCATTGTT
	Ccna1 E-box fwd	TGTCCCAACTTCCCGACAAAC
Ccnb1	Ccnb1 E-box fwd	CATTGCTGCCACCTGCCTTA
	Ccnb1 E-box rev	ATGCGTACTCCCCACAGTCA
Ccnb2	Ccnb2 E-box fwd	CATCGTCTCCAGGTCGTTCA
	Ccnb2 E-box rev	ATGACTCTGCTGGGGATCTGT
Ccnd1	Ccnd1 E-box fwd	AGCGTCCCTGTCTTCTTTCAA
	Ccnd1 E-box rev	GTCTGGCATCTTCGGGTGTT

Gene	Name of primer	Sequence (5'–3')
E2f2	E2f2 E-box fwd	TGCCTCAGTTTCGCCTACTG
	E2f2 E-box rev	ACAGCGATTACGACAGGAGC
E2f3	E2f3 E-box fwd	GCGCAAGTTTCGGTTTTGG
	E2f3 E-box rev	CTACACTGCTTGGTTACAGGA

Primers for testing mycoplasma contamination in cell culture are listed in Table 2-11.

Table 2-11. List of mycoplasma test primers

Primer type	Sequence (5'–3')
forward primers	CGCCTGAGTAGTACGTTCGC
	CGCCTGAGTAGTACGTACGC
	TGCCTGGGTAGTACATTCGC
	TGCCTGAGTAGTACATTCGC
	CGCCTGAGTAGTATGCTCGC
	CACCTGAGTAGTATGCTCGC
	CGCCTGGGTAGTACATTCGC
reverse primers	GCGGTGTGTACAAGACCCGA
	GCGGTGTGTACAAAACCCGA
	GCGGTGTGTACAAACCCCGA

2.1.8 Software

Software used in this thesis is listed in Table 2-12.

Table 2-12. List of software

Software	Source
Agilent Genomic Workbench 7.0	Agilent Technologies, Inc., Santa Clara, CA, USA
AxioVision 4.8	Carl Zeiss AG, Oberkochen
Excel	Microsoft Corporation, Redmond, WA, USA
FACSDiva™	BD Biosciences, Franklin Lakes, NJ, USA
FlowJo v10	FlowJo LLC, Ashland, OR, USA
GraphPad Prism 5	La Jolla, CA, USA
ImageScope v12.3	Leica Biosystems, Wetzlar
Quantity One	Bio-Rad Laboratories GmbH, Munich
R v3.1.2	R Core Team
StepOne™ v2.3	Applied Biosystems, Inc., Carlsbad, CA, USA

2.2 Methods

2.2.1 Mouse experiments

All mouse experiments were conducted in compliance with European guidelines for the care and use of laboratory animals and approved by the Institutional Animal Care and Use Committees (IACUC) of the local authorities of Technical University of Munich and the District Government of Upper Bavaria (Regierung von Oberbayern).

2.2.1.1 Mouse strains

In this study, *Cre/loxP* (Orban et al., 1992) and *Flp-FRT* (Dymecki and Tomasiewicz, 1998) recombinase systems were used to target tissue-specific genetic modifications in mice. To induce PDAC in genetically engineered mouse models, a latent $Kras^{G12D}$ allele is silenced by an upstream stop element flanked by either two *loxP* or *FRT* recombination sites, and pancreatic specific expression of $Kras^{G12D}$ is achieved by breeding with $Ptf1a^{Cre/+}$ or *Pdx1-Flp* mouse line. Additional constitutional or conditional genetic manipulation were combined with $Ptf1a^{Cre/+}$;*LSL-*$Kras^{G12D/+}$ to evaluate the functions of gene of interest in pancreatic tumor cells. Dual-recombinase system (Schonhuber et al., 2014) was used to analyze the effect of Snail expression in the stroma.

All mice were kept on a mixed *C57BL/6J;129S6/SvEv* genetic background unless otherwise stated. Experiments performed with mice backcrossed to *C57BL/6J* (B6) background were indicated, and mice with $Prkdc^{Scid/Scid}$;$Il2rg^{null}$ alleles are on a mixed *C57BL/6J;129S6/SvEv; NOD/ShiLtJ* background.

Ptfa1$^{Cre/+}$ (Nakhai et al., 2007). This knock-in mouse line was kindly provided by Dr. Hassan Nakhai (Klinikum rechts der Isar, Technical University of Munich). The mouse strain expresses Cre recombinase in exocrine and endocrine pancreas. Ptf1a expression was also observed in neural tube, cerebellum and developing neuroretina.

LSL-Kras$^{G12D/+}$ (Hingorani et al., 2003; Jackson et al., 2001). This knock-in mouse line was kindly provided by Prof. Tyler Jacks (Massachusetts Institute of Technology, Cambridge, MA, USA). In this mouse strain, a latent $Kras^{G12D}$ mutant commonly seen in human PDAC is silenced

by a stop cassette flanked by *loxP* sites (*LSL*). After Cre-mediated excision of the stop cassette, expression of $Kras^{G12D}$ mutant leads to constitutively active Kras signaling.

LSL-Rosa26$^{Snail/+}$ (Paul, 2013). This mouse line was generated by Dr. Mariel Paul in the lab of Prof. Dieter Saur (Klinikum rechts der Isar, Technical University of Munich). *loxP-stop-loxP* elements and the transcriptional region of mouse *Snail* cDNA was inserted into the ubiquitously expressed *Rosa26* locus. Cre recombinase thereby directs tissue-specific *Snail* overexpression. *LSL-Snail* is further flanked by *FRT* sites, making possible the removal of the complete knock-in sequence with Flp recombinase.

Snail$^{lox/+}$ (Murray et al., 2006). This conditional knockout mouse line was obtained from Jackson Laboratories (#010621, Bar Harbor, ME, USA). Exons 1 and 2 of the endogenous *Snail* gene are flanked by *loxP* sites and are deleted in the presence of Cre recombinase, resulting in conditional knockout of *Snail*.

Trp53$^{R172H/+}$ (Hingorani et al., 2005; Olive et al., 2004). This knock-in mouse line was kindly provided by Prof. Tyler Jacks (Massachusetts Institute of Technology, Cambridge, MA, USA). A missense mutation in codon 172 corresponding to human R175H mutation frequently found in Li–Fraumeni syndrome and spontaneous tumor patients (Liu et al., 2000) was introduced into endogenous mouse *Trp53* gene. Expression of the dominant-negative oncogenic *Trp53* mutant (de Vries et al., 2002) only in Cre-expressing cells is ensured by upstream *loxP-stop-loxP* elements.

Cdkn2a$^{lox/+}$ (Aguirre et al., 2003). This conditional knockout mouse line was kindly provided by Prof. Nabeel Berdeesy (Harvard Medical School, Boston, MA, USA). Murine *Cdkn2a* encodes both $p16^{INK4A}$ and $p19^{ARF}$ by alternative usage of the first exon and different reading frames (Krimpenfort et al., 2001). Exons 2 and 3 of *Cdkn2a* are flanked by *loxP* sites in this mouse line, allowing conditional knockout of both $p16^{INK4A}$ and $p19^{ARF}$.

p16$^{Ink4a*/+}$ (Krimpenfort et al., 2001). This knockout mouse line was kindly provided by Prof. Anton Berns (The Netherlands Cancer Institute, Amsterdam, The Netherlands). The mice bear a

nonsense mutation in *Cdkn2a* gene which leads to destabilization of $p16^{INK4A}$ mutant protein. The expression of $p19^{ARF}$ is not affected.

Villin-Cre (Madison et al., 2002). This transgenic mouse line was obtained from Jackson Laboratories (#004586, Bar Harbor, ME, USA). The mouse strain expresses Cre recombinase in intestinal epithelial cells.

APC$^{lox/+}$ (Cheung et al., 2010). This knockout mouse line was obtained from Jackson Laboratories (#009045, Bar Harbor, ME, USA). In this mouse strain, 15 exons of *Apc* gene were flanked by *loxP* sites, which permits tissue-specific deletion of APC in a Cre-dependent manner.

LSL-Braf$^{V637E/+}$ (Rad et al., 2013). This knock-in mouse line was kindly provided by Prof. Roland Rad (Klinikum rechts der Isar, Technical University of Munich). Murine *Braf^{V637E}* mutation, ortholog to human *BRAF^{V600E}* mutation frequently observed in colorectal cancer, was introduced into endogenous *Braf* locus but silenced by *loxP-stop-loxP* elements. Cre-mediated excision of the stop cassette allows expression of $Braf^{V637E}$ mutant and leads to sustained activation of Braf signaling.

Rag2$^{+/-}$ (Hao and Rajewsky, 2001). This knockout mouse line was obtained from Jackson Laboratories (#008449, Bar Harbor, ME, USA). A pan deletion of murine *Rag2* exon 3 abolishes RAG2 function, which is critical in V(D)J recombination (Oettinger et al., 1990). As a result, these mice lack mature B and T lymphocytes (Shinkai et al., 1992).

Prkdc$^{Scid/+}$ (Bosma et al., 1983). The *NOD.Cg-Prkdc^{scid} Il2rg^{tm1Wjl}/SzJ* (NSG) mice were obtained from Jackson Laboratories (#005557, Bar Harbor, ME, USA). *Prkdc$^{Scid/Scid}$* mice harbor a loss-of-function mutation which impairs V(D)J recombination (Blunt et al., 1995) and are virtually devoid of B and T lymphocytes (Bosma et al., 1983).

Il2rg$^{+/-}$ (Cao et al., 1995). The *NOD.Cg-Prkdc^{scid} Il2rg^{tm1Wjl}/SzJ* (NSG) mice were obtained from Jackson Laboratories (#005557, Bar Harbor, ME, USA). Exons 4 to 8 and part of exon 3 of murine *Il2rg* gene were deleted to generate *Il2rg* knockout mouse. These mice lack mature NK

cells and have a significant reduction in B and T lymphocytes. Since *Il2rg* is X chromosome-linked, homozygous deletion in females and hemizygous deletion in males are designated *Il2rg*^{null} in this thesis.

Pdx1-Flp (Schonhuber et al., 2014). This transgenic mouse line was generated in the lab of Prof. Dieter Saur (Klinikum rechts der Isar, Technical University of Munich). The mouse strain expresses Flp recombinase in pancreatic progenitor cells and adult pancreatic acini, ducts and islets under the control of the *Pdx1* promoter.

***FSF-Kras*$^{G12D/+}$** (Schonhuber et al., 2014). This knock-in mouse line was generated in the lab of Prof. Dieter Saur (Klinikum rechts der Isar, Technical University of Munich). A latent *Kras*^{G12D} is silenced by a stop element flanked by *FRT* sites (*FSF*), and expression of Kras^{G12D} mutant is achieved by Flp-mediated excision of the stop cassette.

Fsp1-Cre (Bhowmick et al., 2004). This Cre driver line was obtained from Jackson Laboratories (#012641, Bar Harbor, ME, USA). In this mouse strain, Cre recombinase expression is directed to Fsp1-expressing cells, which cover part of fibroblasts, macrophages and a small amount of mesenchymal tumor cells (Schuck, 2018).

***Rosa26*$^{mT-mG/+}$** (Muzumdar et al., 2007). This Cre reporter mouse line was obtained from Jackson Laboratories (#007576, Bar Harbor, ME, USA). Knocked into *Rosa26* locus under the control of the *CAG* promoter, fluorescent reporter tdTomato is flanked by two *loxP* sites, and another fluorescent reporter EGFP is present downstream the second *loxP* site. Membrane-bound tdTomato is constantly expressed in the absence of Cre, and excision of the tdTomato cassette in Cre-expressing cells leads to expression of membrane-bound EGFP.

2.2.1.2 Mouse nomenclature

For better readability of the text, abbreviations of mouse genotypes are used in the following chapters and listed in Table 2-13.

Table 2-13. Nomenclature of mouse lines

Genotype	Abbreviation
Ptf1a$^{Cre/+}$;LSL-Kras$^{G12D/+}$	*PKras*
Ptf1a$^{Cre/+}$;LSL-Kras$^{G12D/+}$;LSL-Rosa26$^{Snail/+}$	*PKras;Snail$^{KI/+}$*
Ptf1a$^{Cre/+}$;LSL-Kras$^{G12D/+}$;LSL-Rosa26$^{Snail/Snail}$	*PKras;Snail$^{KI/KI}$*
Ptf1a$^{Cre/+}$;LSL-Kras$^{G12D/+}$;Snail$^{lox/lox}$	*PKras;Snail$^{KO/KO}$*
Ptf1a$^{Cre/+}$;LSL-Kras$^{G12D/+}$;LSL-Rosa26$^{Snail/+}$;Cdkn2a$^{lox/+}$	*PKras;Snail$^{KI/+}$;Cdkn2a$^{lox/+}$*
Ptf1a$^{Cre/+}$;LSL-Kras$^{G12D/+}$;LSL-Rosa26$^{Snail/+}$;Cdkn2a$^{lox/lox}$	*PKras;Snail$^{KI/+}$;Cdkn2a$^{lox/lox}$*
Ptf1a$^{Cre/+}$;LSL-Kras$^{G12D/+}$;LSL-Rosa26$^{Snail/+}$;p16$^{Ink4a*/+}$	*PKras;Snail$^{KI/+}$;p16$^{Ink4a*/+}$*
Ptf1a$^{Cre/+}$;LSL-Kras$^{G12D/+}$;LSL-Rosa26$^{Snail/+}$;p16$^{Ink4a*/Ink4a*}$	*PKras;Snail$^{KI/+}$;p16$^{Ink4a*/*}$*
Ptf1a$^{Cre/+}$;LSL-Kras$^{G12D/+}$;LSL-Rosa26$^{Snail/+}$;Rag2$^{-/-}$	*PKras;Snail$^{KI/+}$;Rag2$^{-/-}$*
Ptf1a$^{Cre/+}$;LSL-Kras$^{G12D/+}$;Prkdc$^{Scid/Scid}$;Il2rg^{null}	*PKras;Prkdc$^{Scid/Scid}$;Il2rg^{null}*
Ptf1a$^{Cre/+}$;LSL-Kras$^{G12D/+}$;LSL-Rosa26$^{Snail/+}$;Prkdc$^{Scid/Scid}$;Il2rg^{null}	*PKras;Snail$^{KI/+}$;Prkdc$^{Scid/Scid}$;Il2rg^{null}*
Pdx1-Cre;LSL-Kras$^{G12D/+}$;Trp53$^{R172H/+}$	*KPC*
Pdx1-Cre;LSL-Braf$^{V637E/+}$	*PBraf*
Villin-Cre;Apc$^{lox/+}$	*VApc$^{\Delta IEC}$*
Villin-Cre;Apc$^{lox/+}$;LSL-Rosa26$^{Snail/+}$	*VApc$^{\Delta IEC}$;Snail$^{IEC/+}$*
Villin-Cre;LSL-Kras$^{G12D/+}$	*VKras^{IEC}*
Villin-Cre;LSL-Kras$^{G12D/+}$;LSL-Rosa26$^{Snail/+}$	*VKras^{IEC};Snail$^{IEC/+}$*
Villin-Cre;LSL-Braf$^{V637E/+}$	*VBraf^{IEC}*
Villin-Cre;LSL-Braf$^{V637E/+}$;LSL-Rosa26$^{Snail/+}$	*VBraf^{IEC};Snail$^{IEC/+}$*

2.2.1.3 Genotyping

Mice were genotyped at the age of 2–3 weeks. Each mouse was earmarked, and biological materials obtained from the earmarks were used for genotyping. Lysis and PCR are described in sections 2.2.6.1 and 2.2.6.2.

2.2.1.4 Mouse dissection

The dissection table and all dissection tools were kept as sterile as possible. Two hours before sacrifice, 5 mg/kg BrdU dissolved in sterile PBS was injected into the peritoneal cavity of the mouse for subsequent proliferation assays. The mouse was anesthetized with isoflurane,

sacrificed by cervical dislocation and fixed on the dissection table. Seventy percent ethanol was used to disinfect the surface before cutting open the abdomen. Samples of approximately 1–2 mm in diameter were taken for RNA, protein and DNA analysis. Sample for RNA was homogenized immediately in 600 µL RLT buffer with 1% 2-mercaptoethanol and sample for protein was homogenized in 600 µL IP buffer supplemented with phosphatase and protease inhibitors. Samples for RNA, protein and DNA analysis were snap frozen in liquid nitrogen and stored at -80 °C until further use. When a pancreatic tumor, metastasis or ascites was observed, relevant material was taken for isolation of primary cell lines (section 2.2.2.1).

The weight of pancreas, spleen and liver was measured. About 1/3 of the pancreatic tissue was fixed in 4% Roti® Histofix for 2 h for cryosection (section 2.2.5.1). Another 1/3 of the pancreatic tumor tissue was used for flow cytometry analysis (section 2.2.4). The rest of the pancreas and other relevant organs were fixed for at least 24 h in 4% Roti® Histofix for histological analysis (section 2.2.5.1).

2.2.2 Cell culture

All cell culture experiments were carried out in biosafety cabinets under sterile conditions. Cells were cultured in DMEM supplemented with 10% FBS and 1% penicillin-streptomycin unless otherwise stated. Cell culture incubators were kept at 37 °C with 5% CO_2 supply. In all procedures, medium was prewarmed to 37 °C and centrifugation is performed at 1000 rpm at RT for 5 min unless otherwise stated.

2.2.2.1 Isolation of primary cell lines from tumor mice

During mouse dissection, ascites was taken from the peritoneal cavity and directly cultured in medium. The medium was changed the next day and cells were kept for further culturing.

A piece of tissue from pancreatic tumor or metastasis was taken and minced with a scalpel under a biosafety cabinet. The tissue was resuspended in medium containing 1000 units type II collagenase and incubated in a 37 °C water bath overnight. The next day, the cells were centrifuged, and the pellet was resuspended in medium and transferred into a flask for further culturing.

2.2.2.2 Passaging

Cells were cultured in plastic dishes or flasks until around 80% confluency, washed with PBS, trypsinized and centrifuged. The pellet was resuspended in fresh medium and split into new dishes or flasks. The cell lines were kept in culture for maximum 20 passages and low passage cell lines were used for experiments.

2.2.2.3 Cryopreservation and thawing

Low passage cells were washed with PBS, trypsinized and centrifuged. The pellet was resuspended in ice-cold freezing medium (70% DMEM, 20% FBS and 10% DMSO) and transferred into CryoPure tubes. After frozen at -80 °C overnight, the stocks were transferred to liquid nitrogen tank for long-term storage.

To thaw a frozen cell line, cell stock from liquid nitrogen tank was incubated in a 37 °C water bath until completely thawed. Cells in freezing medium were transferred into a new tube containing fresh medium and centrifuged. After the supernatant was aspirated, the cells were cultured in fresh medium in a new flask.

2.2.2.4 Validation of cell lines

The cell lines were validated by regenotyping and mycoplasma test. Genotyping was performed as described in section 2.2.6.2. To perform mycoplasma test, cells were cultured in DMEM with 10% FBS (without penicillin-streptomycin) for at least 3 days until the medium appeared yellow. Two milliliter medium was collected and centrifuged for 2 min at 600 rcf, and the supernatant was again centrifuged for 15 min at maximum speed (about 18,000 rcf) in a table centrifuge. The supernatant was discarded, and the pellet was resuspended in 50 µL PBS and heated for 2 min at 95 °C. The resulting sample was used as template for PCR described in section 2.2.6.3. All cell lines used had the correct genotypes and were free of mycoplasma.

2.2.2.5 Documentation of cell morphology

Bright-field pictures of cell lines were documented with a camera connected to a phase-contrast microscope and Carl Zeiss AxioVision Rel. 4.8 software. Shading correction and white balance adjustment were performed before image acquisition.

2.2.2.6 TGF-β treatment

PDAC cells were cultured in FBS-free DMEM for 24 h before treated with 10 ng/mL TGF-β1 or vehicle (10 nM citric acid and 2 mg/mL BSA in H_2O) for 72 h. Cell morphology was documented as described in section 2.2.2.5.

2.2.3 Human samples

Unstained slides of human PDAC samples were obtained under the approval by the Ethics Committee of the School of Medicine of Technical University of Munich.

2.2.4 Flow cytometry

All flow cytometry experiments were performed with a BD LSRFortessa flow cytometer and BD FACSDiva software.

2.2.4.1 Titration of antibodies and Zombie Aqua

Mouse spleen was disrupted by a needle and cells were washed with PBS, filtered by a 100 µm cell strainer, centrifuged at 1500 rpm at RT for 5 min and lysed with ACK lysis buffer at RT for 5 min. The lysis was stopped by putting the sample on ice for 5 min and washed twice with PBS. Processing of PDAC sample is described in section 2.2.4.3. The cells were stained by a single antibody in a 1:2 dilution series starting from 1:20 until 1:2560. Titration range for Zombie Aqua fluorescent dye (for live/dead cell discrimination) was from 1:100 to 1:12800. The samples were analyzed by BD LSRFortessa. An optimal dilution for each antibody generating a clear positive signal with minimal background was determined.

2.2.4.2 Generating compensation matrix

Single stain controls were used to generate compensation matrix for antibody panels. Single stains for BV785 antibodies and Zombie Aqua were performed with splenocytes (see section 2.2.4.1). For antibodies of all other fluorochromes, compensation beads were used. Samples stained by optimal amount of antibody or Zombie Aqua determined by titration were analyzed by BD LSRFortessa. Optical filter configuration for the instrument is listed in Table 2-14. The compensation matrix was generated with BD FACSDiva software and manually checked in both single-stained and complete panel-stained samples.

Table 2-14. Laser and filter configuration on BD LSRFortessa

Laser (nm)	Detector	LP filter	BP filter	Fluorochrome or dye
355	A	735LP	775/50	BUV805 or BUV737
	B	450LP	515/30	
	C	–	379/28	BUV 395
405	A	750LP	780/60	BV785
	B	685LP	710/50	
	C	630LP	670/30	BV650
	D	600LP	610/20	
	E	505LP	525/50	Zombie Aqua
	F	–	450/50	BV421
488	A	685LP	710/50	PerCP/Cy5.5
	B	505LP	530/30	FITC or BB515
	C	–	488/10	SSC
561	A	750LP	780/60	
	B	685LP	710/50	
	C	600LP	610/20	
	D	570LP	586/15	PE
640	A	750LP	780/60	APC/Cy7 or APC/Fire 750
	B	690LP	730/45	
	C	–	670/14	APC

LP, longpass; BP, band-pass.

2.2.4.3 Analysis of tumor-infiltrating immune cells

PDAC sample was minced into small pieces and digested with enzymatic cocktail from mouse Tumor Dissociation Kit at 37 °C using a gentleMACS Dissociator according to manufacturer's protocol. All the following steps were carried out on ice or at 4 °C. The sample was filtered by a 70 μm cell strainer, centrifuged and washed twice with PBS containing 2% FBS. Number of live cells was determined by trypan blue staining and counting with a hemocytometer. Two million cells were resuspended in 200 μL PBS and stained with Zombie Aqua at a final concentration of 1:500 for 10 min. TruStain FcX (anti-mouse CD16/32) antibody was added with a final concentration of 1:300 to block non-specific binding to Fc receptors. The sample was equally divided into two tubes, washed with PBS containing 2% FBS, centrifuged and stained in 100 μL PBS with antibody cocktails in T cell & B cell panel (Table 2-15) or innate immune cell panel (Table 2-16) for 30 min.

Table 2-15. T cell & B cell antibody panel

Antigen	Fluorochrome	Amount of antibody in 100 µL PBS	Company	Catalogue number	Clone
CD4	BUV805	1	BD	564922	GK1.5
CD3e	BUV395	5	BD	563565	145-2C11
CD8a	BV785	1	Biolegend	100749	53-6.7
CD25	BV650	2	Biolegend	102038	PC61
TCRγ/δ	BV421	2	Biolegend	118120	GL3
CD45	PerCP/Cy5.5	1	Biolegend	147705	I3/2.3
CD19	FITC	1	Biolegend	115505	6D5
CD62L	PE	0.2	Biolegend	104407	MEL-14
CD44	APC/Fire 750	3	Biolegend	103061	IM7
EpCAM	AF647	0.5	Biolegend	118212	G8.8

Table 2-16. Innate immune cell antibody panel

Antigen	Fluorochrome	Amount of antibody in 100 µL PBS	Company	Catalogue number	Clone
CD11c	BUV737	3	BD	564986	HL3
NK1.1	BUV395	4	BD	564144	PK136
Ly6C	BV785	0.5	Biolegend	128041	HK1.4
CD11b	BV650	1	Biolegend	101239	M1/70
F4/80	BV421	3	Biolegend	123132	BM8
CD45	PerCP/Cy5.5	1	Biolegend	147705	I3/2.3
Siglec-F	BB515	1	BD	564514	E50-2440
Ly6G	PE	0.5	Biolegend	127607	1A8
CD68	APC/Cy7	5	Biolegend	137023	FA-11
EpCAM	AF647	0.5	Biolegend	118212	G8.8

The samples were then washed twice with PBS containing 2% FBS, filtered by a 30 µm CellTrics filter and analyzed by BD LSRFortessa with optical filter configuration in Table 2-14. Data were exported as flow cytometry standard (.fcs) format and analyzed with FlowJo software.

2.2.5 Histological analysis

2.2.5.1 Tissue fixation and section

Mouse tissue for paraffin section was fixed in Roti® Histofix at 4 °C for at least 24 h before washed with PBS and dehydrated in ascending ethanol concentration in tissue processor ASP300. The tissue was then embedded in paraffin and stored at RT until further use. Sections of 2.5 µm thick were cut using microtome Microm HM355S.

Tissue for cryosection was fixed in Roti® Histofix at 4 °C for 2 h. After washed three times with PBS, the tissue was dehydrated in 15% sucrose at 4 °C for 4 h and 30% sucrose at 4 °C for 8 h before embedded in Tissue-Tek® O.C.T. Compound and stored at -80 °C until further use. Sections of 20 µm thick were cut using cryotome Microm HM 560 Cryostat.

2.2.5.2 Hematoxylin and eosin (H&E) staining

Paraffin-embedded sections on glass slides were dewaxed in Roti® Histol (2 × 5 min incubation), rehydrated in descending ethanol concentration (2 × 99%, 2 × 96% and 2 × 80%, 3 min each) and washed in deionized water. The slides were stained with hematoxylin for 30 s, washed four times with water, stained with eosin for 20 s and again washed three times with water. Afterwards the sections were dehydrated in ascending ethanol concentration (2 × 80%, 2 × 96% and 2 × 99%, 30 s each) and incubated in Roti® Histol (2 × 5 min) before preserved in PERTEX® mounting medium under glass cover slips.

2.2.5.3 Immunohistochemistry

Paraffin-embedded sections were dewaxed and rehydrated as described in section 2.2.5.2. Citric acid based unmasking solution was used for antigen retrieval. Unmasking solution immersing the slides was microwaved to boiling point and then at 360 W for 15 min. The slides were left in the solution to cool at RT for 30 min and washed with water. Afterwards, they were incubated with 3% H_2O_2 for 10 min to inactivate endogenous peroxidase activity. After washed with water and PBS, the slides were blocked at RT for 1h with PBST containing 10% avidin solution and 5% serum. Then they were incubated at 4 °C overnight with PBST containing primary antibody, 10% biotin solution and 5% serum. The next day, the slides were washed three times with PBST and incubated with PBST containing biotinylated secondary antibody and

5% serum at RT for 1 h. After washing the slides again with PBST three times, VECTASTAIN® Elite® ABC HRP Kit and DAB Peroxidase (HRP) Substrate Kit were used for signal detection. The slides were counterstained with hematoxylin for 5 s, washed in water, dehydrated and mounted as described in section 2.2.5.2.

2.2.5.4 Pathological evaluation

Tumor grading and lesion counting were performed on H&E-stained sections by Dr. Katja Steiger and Dr. Moritz Jesinghaus (Institute of Pathology, Technical University of Munich). Number of adenoma and carcinoma in intestinal tumor models were evaluated from sections of intestine Swiss rolls. Representative pictures were obtained with a bright-field microscope connected to a camera or a slide scanner. All scale bars represent 50 µm.

2.2.5.5 TO-PRO-3 staining

Slides obtained from cryosection were dried at room temperature, fixed in 4% Roti® Histofix at RT for 1 min and washed with PBS. TO-PRO-3 staining was performed at a dilution of 1:1000 in immunofluorescence blocking solution at 4 °C overnight. The next day, the slides were washed twice with blocking solution and once with PBS before preserved in VECTASHIELD® mounting medium. Confocal microscopy was used to visualize the fluorescence signals.

2.2.6 Molecular biology

2.2.6.1 Lysis of tissue and cultured cells

Mouse tissue and cell line for genotyping were lysed in 50 µL Soriano lysis buffer at 55 °C for 1.5 h. Afterwards, proteinase K was inactivated at 95 °C for 15 min. The samples were briefly vortexed and centrifuged at 10,000 rpm for 10 min. Supernatant transferred to a new tube was used as DNA template for PCR and stored at -20 °C.

2.2.6.2 Genotyping and recombination PCR

Genotyping and recombination PCRs were prepared by mixing H_2O, DNA template, primers and a premix containing buffer, polymerase and dNTPs (Table 2-17 and 2-18). Standard PCR program is depicted in Table 2-19. Annealing temperature and product size for all PCR

reactions are listed in Table 2-20. PCR product was analyzed by electrophoresis (section 2.2.6.4).

Table 2-17. Composition of PCR premix

Component	Volume for one reaction
H_2O	4.375 µL
10× buffer S	2.5 µL
30% sucrose	2.5 µL
SucRot solution	2.5 µL
Taq polymerase	0.125 µL
dNTPs (10 µM each)	0.5 µL

Table 2-18. PCR reaction mix

Component	Volume for one reaction
PCR premix	12.5 µL
forward and reverse primers (10 µM each)	0.5–1.0 µL each
DNA template	1.2 µL
H_2O	top up to 25 µL

Table 2-19. Standard PCR program

Step	Temperature	Time	Cycles
Initial denaturation	95 °C	3 min	
Denaturation	95 °C	45 s	40×
Annealing	50–68 °C	60 s	
Elongation	72 °C	90 s	
Final elongation	72 °C	5 min	
Storage	25 °C	hold	

Table 2-20. Annealing temperature and product size of genotyping and recombination PCR

PCR name	Annealing temperature	Product size (bp)
Ptfa1^{Cre}	60 °C	400 (mut) / 600 (WT)
LSL-Kras^{G12D}	55 °C	170 (mut) / 270 (WT) / 300 (rec)
Rosa26	62 °C	400 (Snail) / no band (mT-mG) / 600 (WT)
LSL-Rosa26^{Snail}	68 °C	300 (mut)
Rosa26^{Snail} recombination	60 °C	800 (rec)
Snail^{lox}	64 °C	480 (mut) / 395 (WT)
Snail^{lox} deletion	60 °C	492 (del)
LSL-Trp53^{R172H}	60 °C	270 (mut) / 570 (WT) / 600 (rec)
Cdkn2a^{lox}	58 °C	180 (mut) / 140 (WT)
p16^{Ink4a*}	60 °C	600 (mut) / 500 (WT)
Villin-Cre	62 °C	1100 (mut) / 200 (WT)
APC^{lox}	62 °C	471 (mut) / 341 (WT)
LSL-Braf^{V637E}	55 °C	660 (mut) / 400 (WT)
Rag2^{-}	55 °C	195 (del) / 234 (WT)
Prkdc^{Scid}	50 °C	38, 26 (mut) / 64 (WT)^{NB}
Il2rg^{-}	60 °C	349 (del) / 269 (WT)
Pdx1-Flp	55 °C	620 (mut) / 300 (WT)
FSF-Kras^{G12D}	55 °C	351 (mut) / 270 (WT)
FSF-Kras^{G12D} recombination	60 °C	196 (rec)
Rosa26^{mT-mG}	62 °C	450 (mut) / 650 (WT)
General Cre (for *Fsp1-Cre*)	58 °C	390 (mut) / 290 (control)

NB. *Prkdc*^{Scid} PCR products were digested with 0.65 µL restriction enzyme AluI (Trevino-Villarreal et al., 2011) at 37 °C overnight before electrophoresis.

2.2.6.3 Mycoplasma test PCR

Samples for mycoplasma test were obtained as described in section 2.2.2.4. PCR was performed as Table 2-19 using 60 °C as the annealing temperature. PCR product was analyzed by electrophoresis (section 2.2.6.4). Samples negative for mycoplasma show no band, and a typical positive band appears at 500 bp.

2.2.6.4 Agarose gel electrophoresis

Typically, agarose gels are prepared at a concentration of 1.5% or 2%. AluI digested *Prkdc*^{Scid} PCR products were separated by 4% gel.

TAE buffer (diluted from 50× stock solution to 1×) containing agarose was boiled completely in a microwave oven and mixed with a magnetic stirrer until cooled down to around 60 °C. Ethidium bromide was added before the gel was poured into a chamber placed with combs. After gelling, the combs were removed.

PCR products or RNA samples were loaded into the wells and separated in 1× TAE buffer by electrophoresis at 100 V. DNA bands were visualized by UV light and documented with Gel Doc XR+ system.

2.2.6.5 Chromatin immunoprecipitation

ChIP was performed using SimpleChIP Enzymatic Chromatin IP Kit (#9003, Cell Signaling Technology). Forty million cultured tumor cells were trypsinized, centrifuged and resuspended in 20 mL medium. Then formaldehyde was added to a final concentration of 1% to fix the cells at RT for 10 min, and the reaction was stopped by adding glycine to a final concentration of 0.1 M and kept at RT for 5 min. The cells were washed twice with PBS and once with PBS with 1% PMSF, incubated in buffer A (supplemented with 0.5 mM DTT, protease inhibitor cocktail and 1% PMSF) on ice for 10 min, and then washed and resuspended in buffer B with 0.5 mM DTT. After 20 min of Micrococcal Nuclease digestion at 37 °C, the reaction was stopped by adding EDTA to a final concentration of 50 mM. The cells were then centrifuged and incubated in ChIP lysis buffer (supplemented with protease inhibitor cocktail and 1% PMSF) on ice for 10 min. Five hundred microliter of the lysate was sonicated for three cycles (30 s on and 30 s off). After centrifugation at 4 °C 10000 rpm for 10 min, the supernatant containing the chromatin was transferred into a new tube and 50 µl was kept as input for ChIP. For each precipitation, 10 µg of chromatin was used. The chromatin was precipitated at 4 °C overnight in ChIP buffer with protease inhibitor cocktail using 10 µL Snail antibody, and 1 µL rabbit IgG and H3 antibody were used as negative and positive controls, respectively. Then the precipitation was rotated with magnetic beads at 4 °C for 2 h. The beads were washed three times with ChIP buffer and once with ChIP buffer supplemented with 0.35 M NaCl by rotating at 4°C for 5 min. After the supernatant was discarded, the beads were incubated with 150 µl elution buffer at 65 °C for 30

min. The eluate and the input samples were added 6 µl 5 M NaCl and 2 µl proteinase K and incubated at 65 °C for 2 h. DNA purification was then performed using QIAquick PCR Purification Kit according to the manufacturer's protocol. Snail binding to the E-boxes in specific gene promoter regions was tested by qPCR and analyzed by percent input method.

2.2.6.6 Isolation of genomic DNA

Genomic DNA from cell lines and mouse tails was isolated using QIAGEN DNeasy Blood & Tissue Kit according to the manufacturer's protocol. DNA concentration was determined using Qubit® dsDNA BR Assay Kit and a Qubit® 2.0 Fluorometer.

2.2.6.7 Array comparative genomic hybridization (aCGH)

Agilent oligonucleotide aCGH was performed using genomic DNA according to the manufacturer's protocol in collaboration with Prof. Roland Rad's lab (Klinikum rechts der Isar, Technical University of Munich). Amplifications and deletions in PDAC cell line genome were determined by SurePrint G3 Mouse CGH 240K or customized 60K microarray. Genomic DNA from the tail of the same mouse was used as reference. Agilent Genomic Workbench version 7.0.4.0 was used for data processing. Genomic regions with relative fold change greater than 1.3 or smaller than 0.7 were considered amplification or deletion. For cell lines with *Cdkn2a*^{lox} genotype, the probe corresponding to the floxed region of *Cdkn2a* was individually assessed. Published data from 38 mouse PDAC cell lines expressing *Kras*^{G12D} (Mueller et al., 2018) were included in the analysis.

2.2.6.8 Amplicon-based deep sequencing at the *Kras* locus

Amplicon-based deep sequencing to determine *Kras*^{G12D} allele frequency in PDAC cell lines was performed in collaboration with Prof. Roland Rad's lab (Klinikum rechts der Isar, Technical University of Munich). *Kras*^{G12D} locus from cell line genomic DNA was amplified for 40 cycles using Q5® High-Fidelity DNA Polymerase and primers with Nextera adaptor overhangs. Nextera index primers were added in a second Q5 PCR step of 15 cycles. Solid-phase reversible immobilization clean-up (0.8×) was performed after each PCR step using Agencourt AMPure XP kit. qPCR and Kapa library quantification kit were used to quantify the pooled library, and 8 pM of denatured library (20% spiked PhiX DNA) was sequenced with a MiSeq system. *Kras*^{G12D}

allele frequency was calculated after reads were mapped to reference sequence. All procedures were performed according to the manufacturer's protocol.

2.2.6.9 RNA extraction and cDNA synthesis

Tissue sample for RNA extraction was homogenized as described in section 2.2.1.4. Cell lines were grown in 10 cm cell culture dishes until 60% to 80% confluency and harvested in 600 µL RLT buffer with 1% 2-mercaptoethanol. RNA extraction was performed using QIAshredder spin columns, RNeasy Mini Kit and RNase-Free DNase Set according to the manufacturer's protocols. RNA concentration was determined by NanoDrop 1000 Spectrophotometer and quality control was performed by electrophoresis (see section 2.2.6.4). Sample quality was ensured by clearly visible 28S and 18S ribosomal RNA bands.

One microgram RNA was used to generate cDNA with TaqMan reverse transcription reagents according to the manufacturer's protocol.

2.2.6.10 Quantitative real-time PCR

Relative mRNA expression level was analyzed by qPCR with $2^{-\Delta\Delta C_T}$ method (Livak and Schmittgen, 2001). In a 20 µL reaction, 10 µL SYBR Green PCR Master Mix, 2 µL 1:5 diluted cDNA sample and 100 nM of forward and reverse primers were used. The samples were tested in duplicate or triplicate in a 96-well plate using StepOnePlus real time PCR system. Housekeeping gene *Cyclophilin A* (*CypA*) was used as reference gene. Data analysis was performed with StepOne software and Excel.

qPCR primers were designed by Dr. Mariel Paul. To test primer efficiency, cDNA of various cell lines and tissue samples were mixed and diluted six times in a 1:5 serial dilution. These templates and the primers of interest were used for qPCR. Linear regression was performed with $\log_{10}$(relative cDNA amount) and respective C_T values. Primer efficiency was calculated from the resulting slope of the linear regression.

Primers with efficiency between 1.8 and 2.2 were used for experiments and $2^{-\Delta\Delta C_T}$ method calculation:

$$\Delta C_T = C_T \text{ [gene of interest]} - C_T \text{ [reference gene]}$$

$$\Delta\Delta C_T = \Delta C_T \text{ [treated sample]} - \Delta C_T \text{ [control sample]}$$

$2^{-\Delta\Delta C}{}_T$ represents relative amount of target gene.

2.2.6.11 RNA sequencing

Bulk 3′ transcript end RNA-seq (SCRB-seq) was performed in collaboration with Prof. Roland Rad's lab (Klinikum rechts der Isar, Technical University of Munich). cDNA was synthesized from extracted RNA using oligo-dT primers with sample barcodes, unique molecular identifiers and adapters. Unincorporated primers were digested with Exonuclease I after pooling all the cDNA samples. The cDNA pool was amplified with KAPA HiFi ReadyMix and tagmented. The 3′ ends were enriched using Nextera XT Kit, and the library was sequenced by paired-end sequencing on a HiSeq1500 instrument.

2.2.7 Bioinformatics analysis

All bioinformatics analyses were carried out using R version 3.1.2 (R Development Core Team, 2014) and Bioconductor version 3.0 (Gentleman et al., 2004) by Thomas Engleitner, Xiaoxiao Zhang, Fengchong Wang and Fabio Boniolo.

2.2.7.1 Multidimensional scaling plot and heatmap from RNA-seq data

RNA-seq raw data obtained from Illumina sequencer were converted from BCL files to FASTQ format using bcl2fastq Conversion Software (v2.17.1.14, Illumina). After quality control by FastQC (v0.11.5, Babraham Institute), conversion of FASTQ files to BAM files was done by FastqToSam (Picard v1.138, Broad Institute). Sample barcode and molecular barcode were extracted by TagBamWithReadSequenceExtended program, and low-quality reads were filtered out using filterBam program from Drop-seq tools (v1.12, McCarroll Lab). PolyATrimmer script from the same tool set removed poly A/T in the output BAM files, which were subsequently converted to FASTQ files by SamToFastq tool (Picard). STAR (Dobin et al., 2013) aligned the resulting reads to mouse genome (mm10). The output BAM files were sorted using SortBam (Picard), then MergeBamAlignment (Picard) merged aligned and unaligned BAM files.

TagReadWithGeneExon program (Drop-seq tools) assigned gene symbols to each record, and DigitalExpression program (Drop-seq tools) generated read count matrix using the resulting BAM files.

The differences in global gene expression pattern of *PKras* and *PKras;Snail*$^{KI/+}$ PDAC bulk tissue samples were calculated by log-CPM (log counts per million) values and visualized by multidimensional scaling (MDS) plot. Differentially expressed genes defined by adjusted p-value no larger than 0.01 and absolute fold change no smaller than 2 between *PKras* and *Pkras;Snail*$^{KI/+}$ PDAC bulk tissue samples were visualized by heatmap.

2.2.7.2 Heatmap and hierarchical clustering from microarray data

Gene expression profiling of cell lines and pancreatic tissue by microarray was performed by Dr. Mariel Paul (Paul, 2013). Microarray data were processed with the RMA method (Irizarry et al., 2003), following quantile normalization (Bolstad et al., 2003). Relative gene expression level was computed from the normalized intensity values and visualized by heatmap. Color scale represents standardized gene expression value (z-score).

Differential gene expression between mesenchymal and epithelial cell lines without Snail transgene was analyzed with Limma (Smyth, 2004). A probe set with a Benjamini–Hochberg adjusted (Benjamini and Hochberg, 1995) p-value smaller than 0.05 and an absolute fold change greater than 2 was considered differentially expressed. Annotations were downloaded from ENSEMBL (GRCm38.p3) (Cunningham et al., 2015). If multiple probe sets correspond to the same gene, the one with the maximum intensity was selected and reported. Hierarchical clustering including cell lines with and without Snail transgene was performed based on the expression level of the top 50 upregulated or downregulated genes using Ward's minimum variance method (Ward, 1963).

2.2.7.3 Gene set enrichment analysis

GSEA (Subramanian et al., 2005) was performed on RMA normalized microarray data using GSEA v3.0 jar package and MsigDB v6.2 gene sets provided by Broad Institute of the Massachusetts Institute of Technology and Harvard University. Gene sets were permuted 1000 times, enrichment statistic for scoring was set as "weighted" and genes were ranked based on

"tTest" metric. All other parameters were set as default. A gene set is considered significantly enriched if nominal p-value and q-value are both smaller than 0.05.

2.2.7.4 ChIP-seq data analysis and odds ratio permutation test

Publicly available ChIP-seq data (Ye et al., 2015) were used in this study. Snail-bound genes are defined as genes bearing sequence bound by Snail within ± 1kb from the transcription start site. Significantly enriched KEGG cell cycle genes in Snail-expressing pancreatic tissue were converted to mouse orthologs. The overlap between these two gene sets was depicted in Venn diagram.

The odds ratio of the overlap was tested by a permutation test. Snail-bound genes were replaced by the same number of genes randomly selected from the mouse genome for 10,000 times. The distribution of the odds ratios was generated and compared to the observed adds ratio.

2.2.7.5 Immuno-subtyping

Gene expression profiles of PDAC or pancreatic tissue from endpoint mice obtained by RNA-seq were deconvoluted by establishing a linear model using gene expression profiles from microarray phases 1 and 2 of the Immunological Genome Project (ImmGen) as references. Elastic net regularization implemented in glmnet R package (Friedman et al., 2010) was used to fit the model. In the linear model, fitted coefficients estimate the quantities of specific immune cell types in individual samples. Non-negative matrix factorization (NMF)(Brunet et al., 2004) was employed to perform subtyping for all samples (n = 216). The number of clusters was determined by Silhouette width and cophenetic correlation methods (Chalise and Fridley, 2017). One *PKras* sample differed from all other clusters and was excluded from subsequent analyses. Kruskal–Wallis H test was performed on estimated immune cell profiles to identify cell types with significantly different quantities between the clusters, and p-values were adjusted using false discovery rate (FDR). Estimated relative quantities of these cell types in all samples were visualized by heatmap. Color scale represents z-score.

Besides *PKras*, *PKras;Snail*$^{KI/+}$, *PKras;Snail*$^{KO/KO}$, *PKras;Prkdc*$^{Scid/Scid}$*;Il2rg*^{null} and *PKras;Snail*$^{KI/+}$*;Prkdc*$^{Scid/Scid}$*;Il2rg*^{null} samples, tumor samples from *Ptf1a*$^{Cre/+}$*;LSL-Kras*^{G12D}*;LSL-Rosa26*$^{Map2k1*,EGFP/+}$ (*PKras;Map2k1**), *Ptf1a*$^{Cre/+}$*;LSL-Kras*^{G12D}*;Map2k1*$^{lox/lox}$ (*PKras;Map2k1*$^{KO/KO}$),

PBraf with additional *Prkdc*$^{Scid/Scid}$ and *Il2rg*$^{+/-}$ alleles, *Ptf1a*$^{Cre/+}$;*LSL-Rosa26*$^{Map2k1*,EGFP/+}$ (*PMap2k1**), *Ptf1a*$^{Cre/+}$;*LSL-Rosa26*$^{Pik3ca*H1047R/+}$ or *Ptf1a*$^{Cre/+}$;*LSL-Rosa26*$^{Pik3ca*H1047R/Pik3ca*H1047R}$ (*PPik3ca*^{H1047R}), and *PPik3ca*^{H1047R} with *Map2k1*$^{lox/lox}$ (*PPik3ca*^{H1047R};*Map2k1*$^{KO/KO}$) mice generated by colleagues in the lab were also included in the analysis.

2.2.8 Additional statistical analysis

Graphical depiction and statistical analysis were performed with GraphPad Prism 5. Biological replicates were reported, and data were expressed as mean values ± SEM. Survival curves were compared by log-rank test. Tumor grading, cell morphology, *Cdkn2a* locus status and percentage of mice with carcinoma, metastasis or ascites were compared by Fisher's exact test. Relative mRNA expression level, percentage of input in ChIP, pancreas/body weight ratio, *Kras*^{G12D} allele frequency, and number of precursor lesions in the pancreas, adenomas and carcinomas in intestine, and tumor-infiltrating immune cells were compared by Student's t-test. Two-tailed tests are performed unless otherwise stated. The resulting p-values are indicated in the respective figures and significance level was set to 0.05. Bonferroni-adjusted significance level was reported if multiple statistical tests were performed on a single data set.

3 Results

3.1 Snail expression does not change PDAC grading but induces solid nested tumor growth

To investigate the function of Snail in cancer *in vivo*, our lab generated a conditional Snail overexpression allele *LSL-Rosa26*$^{Snail/+}$. Previous work by Dr. Mariel Paul demonstrated that Snail overexpression in the pancreas significantly accelerated PDAC progression but did not increase metastasis rate in liver or lung (Paul, 2013). To better characterize the tumors from *PKras;Snail*$^{KI/+}$ mice, pathological grading was performed on H&E-stained tumor sections by pathologists at the Institute of Pathology, Technical University of Munich. Analysis of *PKras*, *PKras;Snail*$^{KI/+}$ and *PKras;Snail*$^{KI/KI}$ PDACs revealed no significant difference in percentage of grade 3 (poorly differentiated) and grade 4 (undifferentiated or sarcomatoid) tumors (Figure 3-1A). CK19 IHC staining also confirmed the presence of both differentiated and undifferentiated tumor areas from all three genotypes (Figure 3-1B). These data proved that Snail expression did not change the tumor differentiation status of PDAC *in vivo*.

Interestingly, a unique feature of budding of tumor cells with solid nested growth was observed mostly in Snail-expressing tumors (Figure 3-1C and D). This feature was found in only one of the eleven tumors in the *PKras* cohort. In *PKras;Snail*$^{KI/+}$ mice, 68% of the tumors displayed such phenotype and in *PKras;Snail*$^{KI/KI}$ tumors, the percentage was as high as 93% (Figure 3-1C). These areas retained epithelial differentiation as shown by positive CK19 and E-cadherin staining (Figure 3-1D). The molecular mechanism for forming this structure needs further investigation.

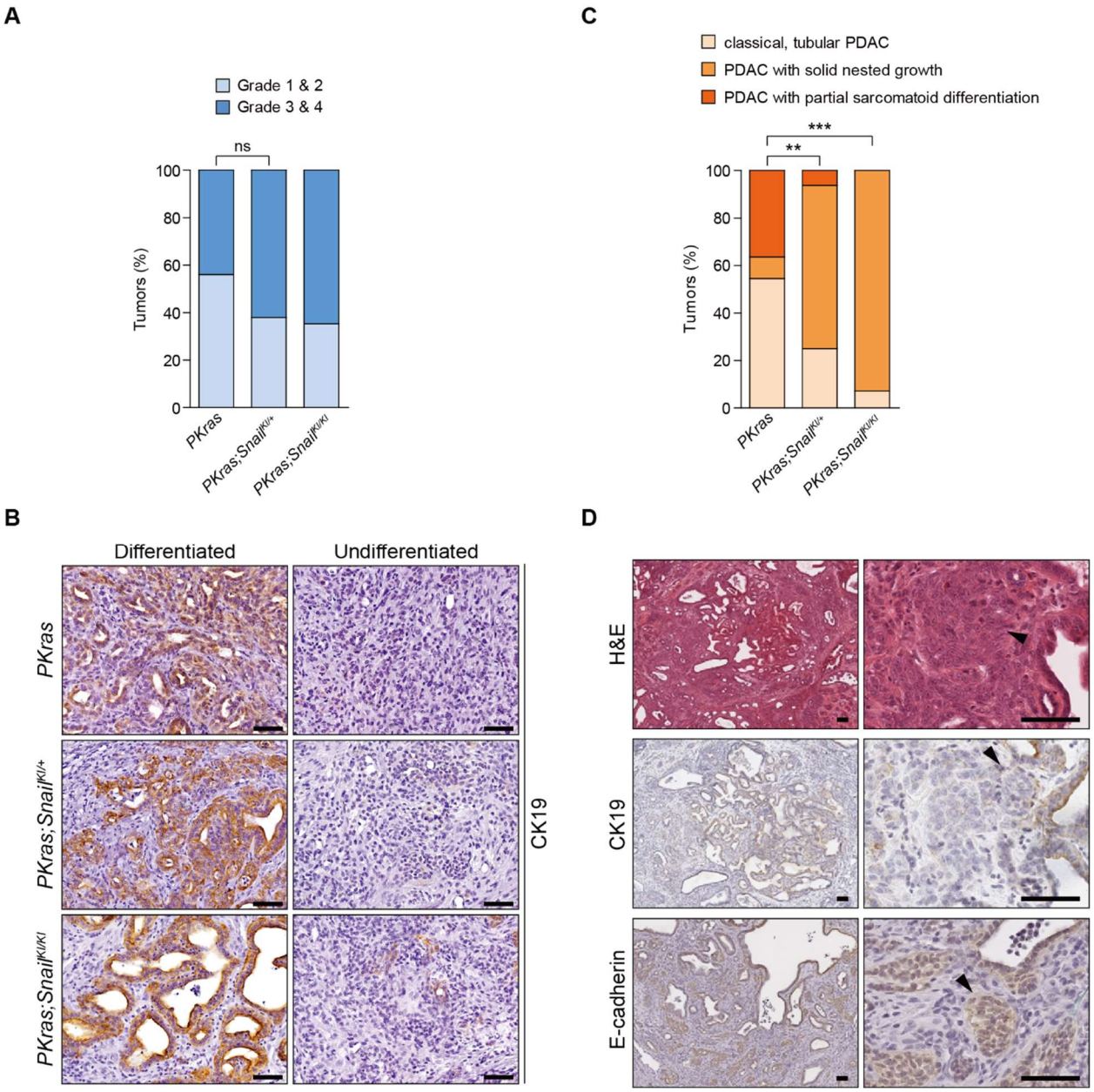

Figure 3-1. Snail does not alter PDAC differentiation *in vivo*

(A) Pathological grading of PDAC from *PKras* (n = 32), *PKras;Snail*$^{KI/+}$ (n = 21) and *PKras;Snail*$^{KI/KI}$ (n = 17) mice. ns, not significant, two-tailed Fisher's exact test.

(B) Representative CK19 IHC staining of PDAC sections from indicated genotype. Note the presence of both differentiated and undifferentiated tumor areas in all genotypes. Scale bars, 50 µm.

(C) Percentage of PDAC with classical tubular morphology, solid nested tumor cell growth and partial sarcomatoid differentiation in *PKras* (n = 11), *PKras;Snail*$^{KI/+}$ (n = 16) and *PKras;Snail*$^{KI/KI}$ (n = 14) mice. **p < 0.01, ***p < 0.001, significance level adjusted by Bonferroni correction, two-tailed Fisher's exact test.

(D) Representative images showing H&E, CK19 and E-cadherin staining in PDAC with areas of solid nested tumor cell growth (indicated by black arrows). Scale bars, 50 µm. Staining in this panel was performed by the Comparative Experimental Pathology Core Facility, Institute of Pathology, Technical University of Munich.

3.2 Snail deletion does not influence PDAC progression

Since Snail overexpression leads to accelerated PDAC development, a conditional *Snail* knockout model was crossed into the *PKras* model to evaluate the impact of *Snail* deletion in PDAC (Figure 3-2A). PCR showed complete deletion of *Snail* in *PKras;Snail*$^{KO/KO}$ tumor cells as no floxed band was visible (Figure 3-2B). Survival analysis showed that the median survival time of *PKras;Snail*$^{KO/KO}$ mice was not significantly different from that of *PKras* mice (Figure 3-2C). This finding reinforced a similar conclusion drawn from the KPC model in a previous publication (Zheng et al., 2015). Again, both differentiated and undifferentiated areas were seen in *PKras;Snail*$^{KO/KO}$ tumors (Figure 3-2D), and their grading also did not differ from that of *PKras* tumors (Figure 3-2E). Taken together, while high level of Snail expression significantly promotes PDAC progression, the existence of a basal expression level is no determining factor. Besides, Snail expression level does not have an impact on PDAC differentiation in autochthonous models.

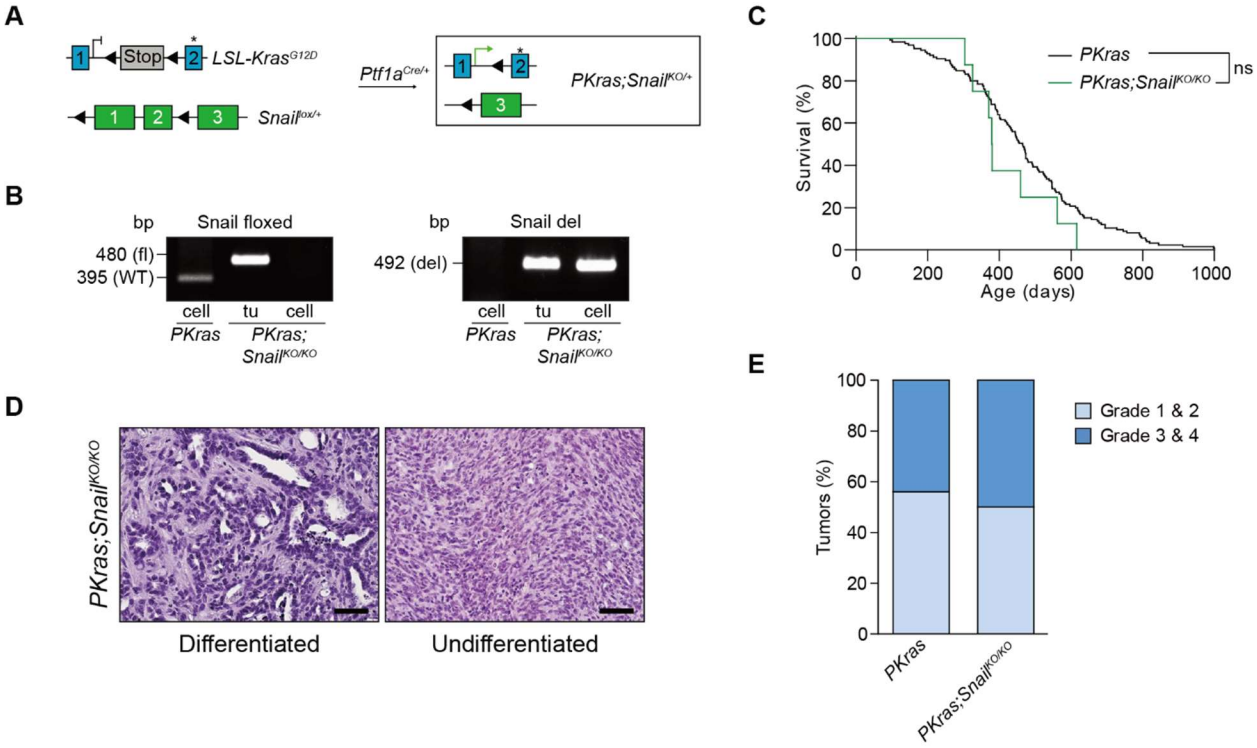

Figure 3-2. Snail deletion does not influence PDAC progression

(A) Strategy to conditionally knockout *Snail* in *Kras*^{G12D}-expressing pancreas.

(B) PCR confirms deletion of *Snail* in *PKras;Snail*$^{KO/KO}$ PDAC tumor tissue (tu) and cell line (cell). Left panel: Snail floxed allele (fl): 480 bp, Snail WT allele (WT): 395 bp, deleted Snail floxed allele: no band. Right panel: deleted Snail floxed allele (del): 492 bp, Snail floxed and WT allele: no band.

(C) Kaplan-Meier survival curves of *PKras* (n = 125, median survival 465 days) and *PKras;Snail*$^{KO/KO}$ (n = 8, median survival 380 days) mice. ns, not significant, two-tailed log-rank test.

(D) H&E staining showing the presence of both differentiated and undifferentiated area in *PKras;Snail*$^{KO/KO}$ PDAC tissue. Scale bars, 50 μm.
(E) Pathological grading of PDAC from *PKras* (n = 32) and *PKras;Snail*$^{KO/KO}$ (n = 6) mice.

3.3 Snail does not induce EMT in PDAC cell lines *in vitro*

Previous data from Dr. Mariel Paul already demonstrated that Snail-expressing epithelial tumor cell lines did not have lower *Cdh1* mRNA level and that transduction of Snail in PDAC cell lines did not downregulate E-cadherin (Paul, 2013). Analysis of cell morphology revealed no increase in the percentage of mesenchymal primary PDAC cell lines in the cohorts that have Snail overexpression (Figure 3-3A). Thus, *PKras;Snail*$^{KI/+}$ PDAC cell lines did not show higher level of EMT compared to *PKras* cell lines. *PKras;Snail*$^{KI/KI}$ cell lines, which have even higher Snail expression level, showed almost identical distribution of cell morphology as *PKras;Snail*$^{KI/+}$ cell lines (Figure 3-3A), further demonstrating that Snail expression alone did not drive EMT.

Global mRNA expression level was analyzed to prove that EMT was not induced in Snail-transgenic cell lines. Differentially expressed genes were identified between epithelial and mesenchymal cell lines without Snail overexpression regardless of *Trp53* status, and hierarchical clustering was performed using these cell lines together with Snail-expressing cell lines. Almost all Snail-expressing cell lines clustered with the epithelial cluster (Figure 3-3B), indicating that these cell lines had no EMT-related signatures.

TGF-β, a strong EMT inducer, was used to test whether Snail affects the ability to undergo EMT. PDAC cell lines from *PKras*, *PKras;Snail*$^{KI/+}$ and *PKras;Snail*$^{KO/KO}$ mice were treated with TGF-β or vehicle, and cell morphology was documented after 72 h. Compared to the vehicle, TGF-β treatment induced EMT in all genotypes as morphological changes were observed (Figure 3-3C). This finding strongly argues that EMT in PDAC cell lines is independent of Snail.

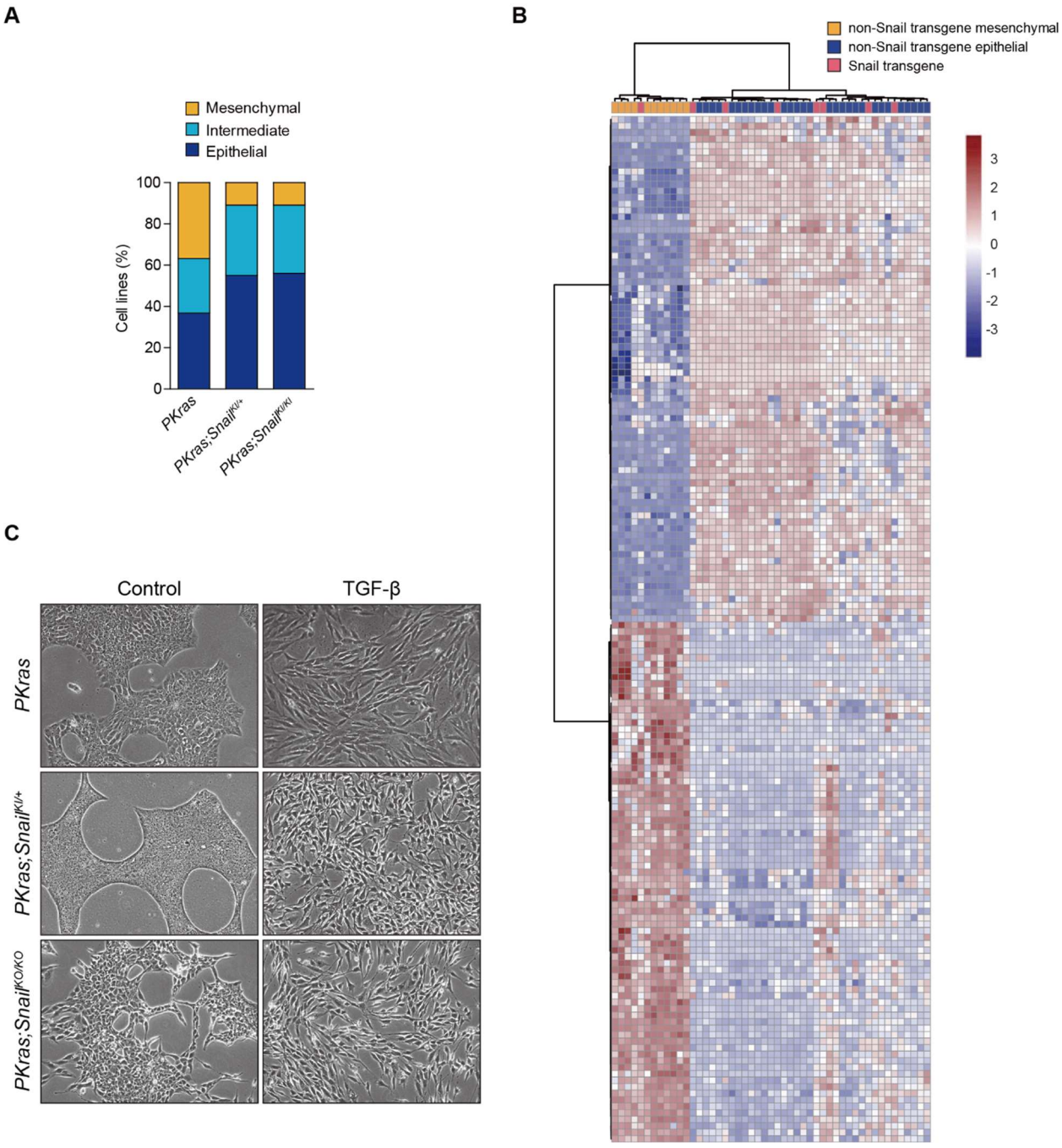

Figure 3-3. Snail does not induce EMT in PDAC cell lines *in vitro*

(A) Morphology of PDAC cell lines isolated from *PKras* (n = 38), *PKras;Snail*$^{KI/+}$ (n = 38) and *PKras;Snail*$^{KI/KI}$ (n = 9) mice.

(B) Heatmap showing hierarchical clustering of cell lines. Primary PDAC and metastasis cell lines from tumors without Snail transgene were used as reference, and top 50 up- and downregulated genes between mesenchymal and epithelial cell lines were defined. Hierarchical clustering was performed including PDAC and metastasis cell lines from tumors with Snail transgene. Color scale represents z-score.

(C) Representative pictures showing cell morphology after 72h TGF-β or vehicle treatment. Note that all cell lines undergo EMT regardless of Snail status.

3.4 Snail cooperates with complete loss of *Cdkn2a* and increased *Kras^{G12D}* dosage to promote mesenchymal phenotype

Given the long-established role of Snail in EMT in both embryonic development and cancer, it is surprising that Snail is dispensable for EMT in PDAC *in vitro* and *in vivo*. Still, a mechanistic link is missing for this unexpected finding. Recent discovery in our lab and Prof. Roland Rad's lab made a connection between EMT phenotype and *Kras^{G12D}* dosage and *Cdkn2a* locus status (Mueller et al., 2018), therefore the relevance in Snail-expressing tumors was examined. No obvious difference in *Kras^{G12D}* allele frequency was observed between *PKras* and *PKras;Snail$^{KI/+}$* cell lines (Figure 3-4A), but *PKras;Snail$^{KI/+}$* cell lines had much higher *Cdkn2a* locus integrity (Figure 3-4B). Since mesenchymal phenotype is largely driven by the combination of homozygous *Cdkn2a* loss and increased *Kras^{G12D}* gene dosage, that Snail does not drive EMT in PDAC can be explained by the retention of *Cdkn2a* in these cells. To prove that *Cdkn2a* loss is important for EMT in Snail-expressing PDAC, a *Cdkn2a* knockout allele was crossed into the models. *Kras^{G12D}* gene dosage increased as heterozygous and homozygous deletion of *Cdkn2a* was introduced into the *PKras;Snail$^{KI/+}$* model (Figure 3-4A), and *Cdkn2a* homozygous deletion significantly increased the percentage of mesenchymal cell lines and poorly differentiated or undifferentiated tumor (Figure 3-4C, D). On the contrary, its homozygous deletion in the *PKras* model did not lead to an overt mesenchymal phenotype. While all bearing increased *Kras^{G12D}* gene dosage, 88.9% of the *PKras;Snail$^{KI/+}$;Cdkn2a$^{lox/lox}$* and only 21.1% of the *PKras;Cdkn2a$^{lox/lox}$* cell lines are mesenchymal (Figure 3-4C, E). A further examination into the cell lines with homozygous *Cdkn2a* loss uncovered a link between *Kras^{G12D}* gene dosage and mesenchymal phenotype in Snail-transgenic cell lines (Figure 3-4F). These data indicate that in Snail-expressing tumors, homozygous *Cdkn2a* loss leads to increased *Kras^{G12D}* dosage; when this dosage reaches a certain threshold, the cells are likely to be converted to the mesenchymal phenotype.

As Dr. Mariel Paul analyzed the impact of mutational p16^{Ink4a} inactivation in the Snail-expressing mice (Paul, 2013), its role was also individually examined. Homozygous mutation of *p16^{Ink4a}* showed a trend of increased percentage of intermediate but not mesenchymal cell line, and its heterozygous mutation almost did not have any effect (Figure 3-4C). In addition, heterozygous and homozygous deletion of *Cdkn2a* both further contributed to Snail-accelerated PDAC progression (Figure 3-4G), while homozygous but not heterozygous *p16^{Ink4a}* loss shortened the survival time (Figure 3-4H). Hence, the function of p16^{Ink4a} in Snail-expressing tumors is still partly preserved.

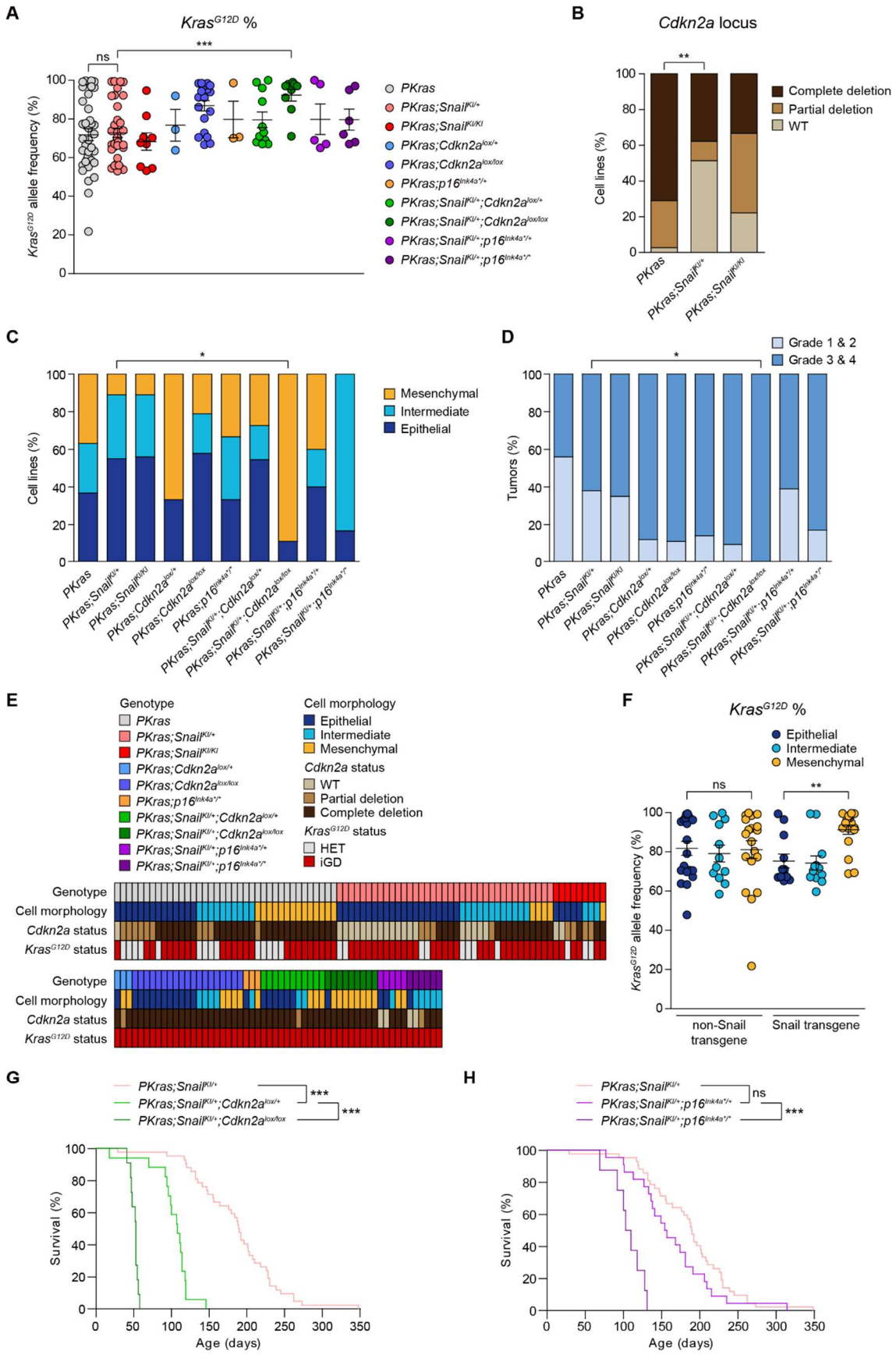
A
Kras^G12D %
ns
***
Kras^G12D allele frequency (%)
PKras
PKras;Snail^KI/+
PKras;Snail^KI/KI
PKras;Cdkn2a^lox/+
PKras;Cdkn2a^lox/lox
PKras;p16^Ink4a+/+
PKras;Snail^KI/+;Cdkn2a^lox/+
PKras;Snail^KI/+;Cdkn2a^lox/lox
PKras;Snail^KI/+;p16^Ink4a+/+
PKras;Snail^KI/+;p16^Ink4a+/+
B
Cdkn2a locus
**
Cell lines (%)
Complete deletion
Partial deletion
WT
C
*
Cell lines (%)
Mesenchymal
Intermediate
Epithelial
D
*
Tumors (%)
Grade 1 & 2
Grade 3 & 4
E
Genotype
Cell morphology
Epithelial
Intermediate
Mesenchymal
Cdkn2a status
WT
Partial deletion
Complete deletion
Kras^G12D status
HET
iGD
F
Kras^G12D %
Epithelial
Intermediate
Mesenchymal
ns
**
Kras^G12D allele frequency (%)
non-Snail transgene
Snail transgene
G
PKras;Snail^KI/+
PKras;Snail^KI/+;Cdkn2a^lox/+
PKras;Snail^KI/+;Cdkn2a^lox/lox
***
***
Survival (%)
Age (days)
H
PKras;Snail^KI/+
PKras;Snail^KI/+;p16^Ink4a+/+
PKras;Snail^KI/+;p16^Ink4a+/+
ns
***
Survival (%)
Age (days)

Figure 3-4. Snail-expressing tumor cells remain epithelial by retaining *Cdkn2a* locus

(A) *Kras*^{G12D} allele frequency in cell lines of indicated genotypes determined by amplicon-based sequencing at the *Kras* locus. Published data from 38 mouse PDAC cell lines expressing *Kras*^{G12D} (Mueller et al., 2018) were included in the *PKras* cohort. Mean ± SEM; ns, not significant, ***p < 0.001, significance level adjusted by Bonferroni correction, two-tailed Student's t-test.

(B) aCGH analysis shows *Cdkn2a* locus status in *PKras* (n = 38), *PKras;Snail*$^{KI/+}$ (n = 37) and *PKras;Snail*$^{KI/KI}$ (n = 9) PDAC cell lines. Published data from 38 mouse PDAC cell lines expressing *Kras*^{G12D} (Mueller et al., 2018) were included in the *PKras* cohort. **p < 0.01, two-tailed Fisher's exact test.

(C) Morphology of PDAC cell lines isolated from *PKras* (n = 38), *PKras;Snail*$^{KI/+}$ (n = 38), *PKras;Snail*$^{KI/KI}$ (n = 9), *PKras;Cdkn2a*$^{lox/+}$ (n = 3), *PKras;Cdkn2a*$^{lox/lox}$ (n = 19), *PKras;p16*$^{Ink4a*/+}$ (n = 3), *PKras;Snail*$^{KI/+}$*;Cdkn2a*$^{lox/+}$ (n = 11), *PKras;Snail*$^{KI/+}$*;Cdkn2a*$^{lox/lox}$ (n = 9), *PKras;Snail*$^{KI/+}$*;p16*$^{Ink4a*/+}$ (n = 5) and *PKras;Snail*$^{KI/+}$*;p16*$^{Ink4a*/*}$ (n = 6) mice. *p < 0.05, two-tailed Fisher's exact test.

(D) Pathological grading of PDAC from *PKras* (n = 32), *PKras;Snail*$^{KI/+}$ (n = 21), *PKras;Snail*$^{KI/KI}$ (n = 17), *PKras;Cdkn2a*$^{lox/+}$ (n = 8), *PKras;Cdkn2a*$^{lox/lox}$ (n = 19), *PKras;p16*$^{Ink4a*/+}$ (n = 7), *PKras;Snail*$^{KI/+}$*;Cdkn2a*$^{lox/+}$ (n = 11), *PKras;Snail*$^{KI/+}$*;Cdkn2a*$^{lox/lox}$ (n = 11), *PKras;Snail*$^{KI/+}$*;p16*$^{Ink4a*/+}$ (n = 18) and *PKras;Snail*$^{KI/+}$*;p16*$^{Ink4a*/*}$ (n = 6) mice. *p < 0.05, two-tailed Fisher's exact test.

(E) Cell morphology, *Kras*^{G12D} and *Cdkn2a* status are shown for each *PKras* (n = 38), *PKras;Snail*$^{KI/+}$ (n = 37), *PKras;Snail*$^{KI/KI}$ (n = 9), *PKras;Cdkn2a*$^{lox/+}$ (n = 3), *PKras;Cdkn2a*$^{lox/lox}$ (n = 19), *PKras;p16*$^{Ink4a*/+}$ (n = 3), *PKras;Snail*$^{KI/+}$*;Cdkn2a*$^{lox/+}$ (n = 11), *PKras;Snail*$^{KI/+}$*;Cdkn2a*$^{lox/lox}$ (n = 9), *PKras;Snail*$^{KI/+}$*;p16*$^{Ink4a*/+}$ (n = 5) and *PKras;Snail*$^{KI/+}$*;p16*$^{Ink4a*/*}$ (n = 6) PDAC cell line. Published data from 38 mouse PDAC cell lines expressing *Kras*^{G12D} (Mueller et al., 2018) were included in the *PKras* cohort. HET: heterozygous, iGD: increased gene dosage.

(F) *Kras*^{G12D} allele frequency in cell lines with complete *Cdkn2a* deletion from (E) divided into Snail transgene epithelial (n = 20), intermediate (n = 12) and mesenchymal (n = 19) and non-Snail transgene epithelial (n = 12), intermediate (n = 12) and mesenchymal (n = 18) groups. Mean ± SEM; ns, not significant, **p < 0.01, significance level adjusted by Bonferroni correction, two-tailed Student's t-test.

(G) Kaplan-Meier survival curves of *PKras;Snail*$^{KI/+}$ (n = 42, median survival 190 days), *PKras;Snail*$^{KI/+}$*;Cdkn2a*$^{lox/+}$ (n = 17, median survival 108 days) and *PKras;Snail*$^{KI/+}$*;Cdkn2a*$^{lox/lox}$ (n = 11, median survival 53 days) mice. ***p < 0.001, significance level adjusted by Bonferroni correction, two-tailed log-rank test.

(H) Kaplan-Meier survival curves of *PKras;Snail*$^{KI/+}$ (n = 42, median survival 190 days), *PKras;Snail*$^{KI/+}$*;p16*$^{Ink4a*/+}$ (n = 22, median survival 156 days) and *PKras;Snail*$^{KI/+}$*;p16*$^{Ink4a*/*}$ (n = 8, median survival 106 days) mice. ns, not significant, ***p < 0.001, significance level adjusted by Bonferroni correction, two-tailed log-rank test.

3.5 Context-specific function of Snail in intestinal tumor

The tumor-promoting function of Snail was clearly shown in PDAC *in vivo*. However, whether it has the same effect in other tumor types remained unknown. To examine the role of Snail in intestinal tumor, the *LSL-Rosa26*$^{Snail/+}$ allele was crossed into three different models: a classical Wnt-driven model induced by *Apc* loss and two serrated intestinal cancer models induced by *Kras*^{G12D} and *Braf*^{V637E} mutations.

Surprisingly, Snail expression in the *Apc*-loss model did not accelerated tumor progression; rather, *VApc*$^{\Delta IEC}$*;Snail*$^{IEC/+}$ mice had slightly longer median survival time than *VApc*$^{\Delta IEC}$ mice (Figure 3-5A, B). As a proof of concept, a marked Snail overexpression in the intestinal tumors was confirmed by qPCR (Figure 3-5C). There was no difference in the percentage of

carcinoma-bearing mice, but a tendency in lower adenoma and carcinoma numbers was observed in *VApc$^{\Delta IEC}$;Snail$^{lEC/+}$* mice (Figure 3-5D, E, F). Morphologically, *VApc$^{\Delta IEC}$;Snail$^{lEC/+}$* carcinomas resembled the classical *VApc$^{\Delta IEC}$* carcinomas (Figure 3-5G).

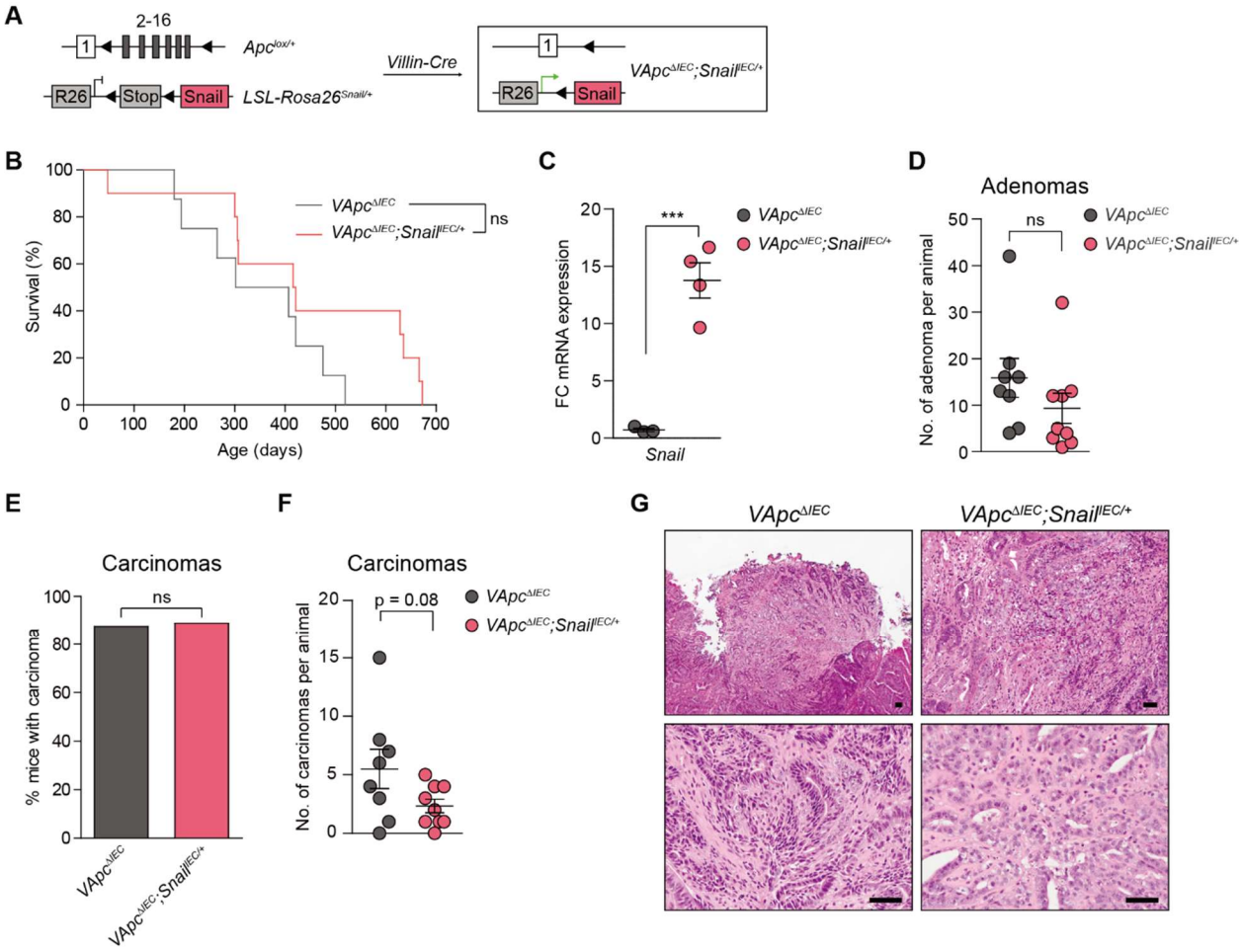

Figure 3-5. Snail does not promote intestinal cancer progression in Apc loss-of-function model

(A) Strategy to activate Snail expression in intestinal epithelium in *VApc$^{\Delta IEC}$* model.

(B) Kaplan-Meier survival curves of *VApc$^{\Delta IEC}$* (n = 8, median survival 355 days) and *VApc$^{\Delta IEC}$;Snail$^{lEC/+}$* (n = 10, median survival 418 days) mice. ns, not significant, two-tailed log-rank test.

(C) Relative *Snail* mRNA expression level normalized to *CypA* by qPCR in intestinal tumors of *VApc$^{\Delta IEC}$* (n = 3) and *VApc$^{\Delta IEC}$;Snail$^{lEC/+}$* (n = 4) mice. Mean ± SEM; ***p < 0.001, two-tailed Student's t-test. FC, fold change.

(D) Number of intestinal adenomas in *VApc$^{\Delta IEC}$* (n = 8) and *VApc$^{\Delta IEC}$;Snail$^{lEC/+}$* (n = 9) endpoint mice. Mean ± SEM; ns, not significant, two-tailed Student's t-test.

(E) Percentage of intestinal carcinoma-bearing *VApc$^{\Delta IEC}$* (n = 8) and *VApc$^{\Delta IEC}$;Snail$^{lEC/+}$* (n = 9) endpoint mice. ns, not significant, two-tailed Fisher's exact test.

(F) Number of intestinal carcinomas in *VApc$^{\Delta IEC}$* (n = 8) and *VApc$^{\Delta IEC}$;Snail$^{lEC/+}$* (n = 9) endpoint mice. Mean ± SEM; two-tailed Student's t-test.

(G) Representative pictures of *VApc$^{\Delta IEC}$* and *VApc$^{\Delta IEC}$;Snail$^{lEC/+}$* intestinal carcinomas by H&E staining. Scale bars, 50 μm.

To rule out the possibility that Snail specifically cooperates with Kras but not Wnt signaling in tumorigenesis, Snail expression was also activated in *VKras^{IEC}* model (Figure 3-6A, C). Even more unexpectedly, Snail seemed to prolong the survival of Kras^{G12D}-driven intestinal cancer model as well (Figure 3-6B). No obvious discrepancy was observed in adenoma and carcinoma count and percentage of carcinoma-bearing mice between *VKras^{IEC}* and *VKras^{IEC};Snail$^{IEC/+}$* mice (Figure 3-6D, E, F). Aberrant Snail expression also did not change the serrated tumor morphology in this model (Figure 3-6G). These data marked the striking difference between pancreatic and intestinal cancer, as the same Kras^{G12D} signaling and Snail overexpression yielded contrasting results in these two organs.

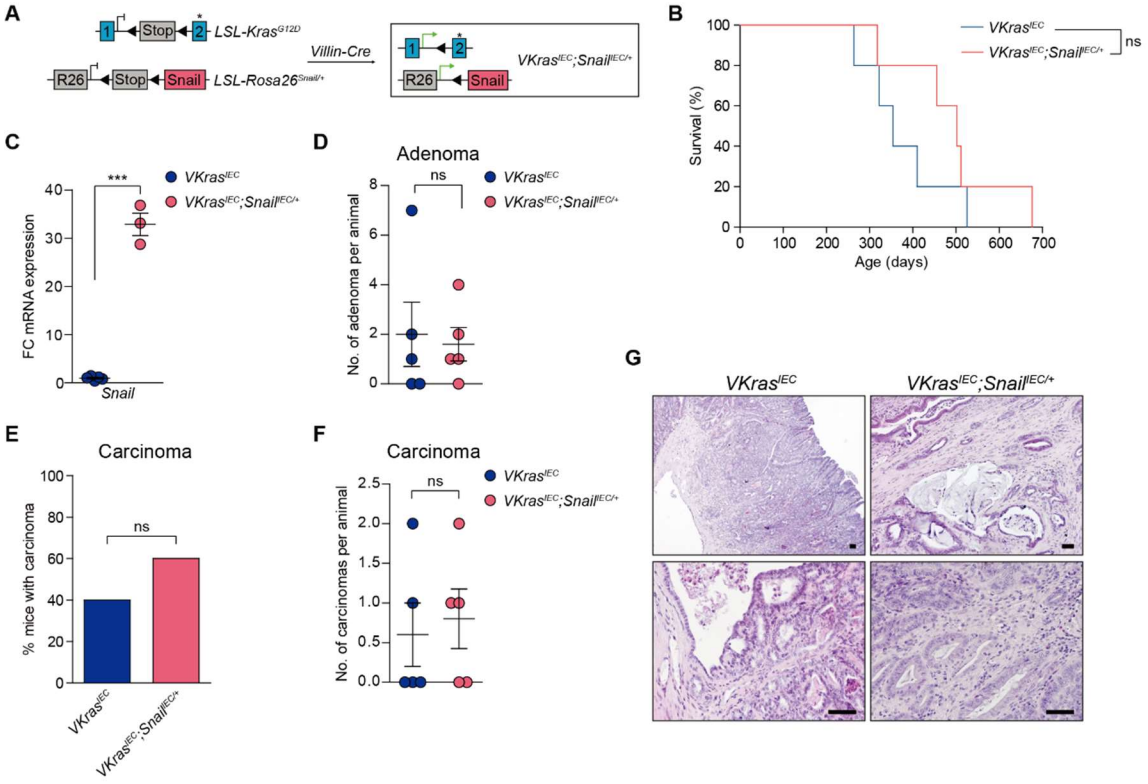

Figure 3-6. Snail does not promote intestinal cancer progression in Kras^{G12D}-driven model

(A) Strategy to activate Snail expression in intestinal epithelium in *VKras^{IEC}* model.

(B) Kaplan-Meier survival curves of *VKras^{IEC}* (n = 5, median survival 354 days) and *VKras^{IEC};Snail$^{IEC/+}$* (n = 5, median survival 502 days) mice. ns, not significant, two-tailed log-rank test.

(C) Relative *Snail* mRNA expression level normalized to *CypA* by qPCR in intestinal tumors of *VKras^{IEC}* (n = 5) and *VKras^{IEC};Snail$^{IEC/+}$* (n = 3) mice. Mean ± SEM; ***p < 0.001, two-tailed Student's t-test. FC, fold change.

(D) Number of intestinal adenomas in *VKras^{IEC}* (n = 5) and *VKras^{IEC};Snail$^{IEC/+}$* (n = 5) endpoint mice. Mean ± SEM; ns, not significant, two-tailed Student's t-test.

(E) Percentage of intestinal carcinoma-bearing *VKras^{IEC}* (n = 5) and *VKras^{IEC};Snail$^{IEC/+}$* (n = 5) endpoint mice. ns, not significant, two-tailed Fisher's exact test.

(F) Number of intestinal carcinomas in *VKras^{IEC}* (n = 5) and *VKras^{IEC};Snail$^{IEC/+}$* (n = 5) endpoint mice. Mean ± SEM; two-tailed Student's t-test.

(G) Representative pictures of *VKras*^{IEC} and *VKras*^{IEC}*;Snail*$^{IEC/+}$ intestinal carcinomas by H&E staining. Scale bars, 50 μm.

In huge contrast to Wnt- and Kras-dependent models, Snail accelerated tumor progression in Braf^{V637E}-driven intestinal cancer (Figure 3-7A, B, C). The number of adenomas per endpoint mouse was also higher in *VBraf*^{IEC}*;Snail*$^{IEC/+}$ than in *VBraf*^{IEC} mice (Figure 3-7D). Although the differences were not statistically significant, there was an increase in both the percentage of carcinoma-bearing mice and carcinoma count in the *VBraf*^{IEC}*;Snail*$^{IEC/+}$ cohort (Figure 3-7E, F). Again, Snail expression did not lead to morphological changes in tumors (Figure 3-7G). These results show that although Braf is downstream of Kras signaling, the effect of their activation can be completely different as manifested by the opposite outcome in their cooperation with Snail expression on intestinal cancer development.

Altogether, these observations demonstrate that Snail is an oncogene in Braf-driven intestinal cancer, but the role is not reproduced in intestinal tumors induced by APC loss or Kras mutation. Therefore, the need to investigate context-specific functions of pathways is demanding.

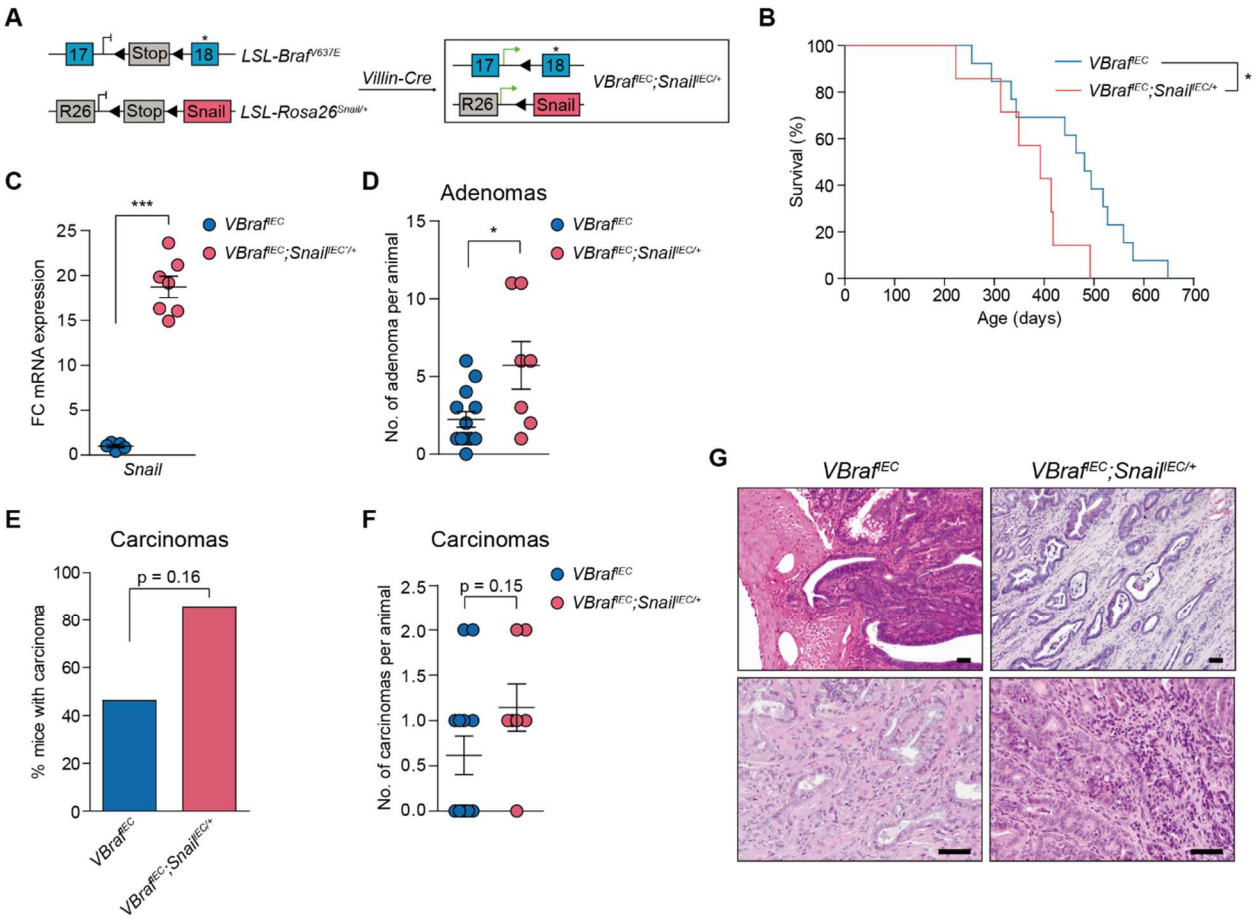

Figure 3-7. Snail accelerates intestinal cancer progression in Braf^{V637E}-dependent model

(A) Strategy to activate Snail expression in intestinal epithelium in *VBraf^{IEC}* model.

(B) Kaplan-Meier survival curves of *VBraf^{IEC}* (n = 13, median survival 481 days) and *VBraf^{IEC};Snail$^{IEC/+}$* (n = 7, median survival 392 days) mice. *p < 0.05, two-tailed log-rank test.

(C) Relative *Snail* mRNA expression level normalized to *CypA* by qPCR in intestinal tumors of *VBraf^{IEC}* (n = 5) and *VBraf^{IEC};Snail$^{IEC/+}$* (n = 7) mice. Mean ± SEM; ***p < 0.001, two-tailed Student's t-test. FC, fold change.

(D) Number of intestinal adenomas in *VBraf^{IEC}* (n = 13) and *VBraf^{IEC};Snail$^{IEC/+}$* (n = 7) endpoint mice. Mean ± SEM; *p < 0.05, two-tailed Student's t-test.

(E) Percentage of intestinal carcinoma-bearing *VBraf^{IEC}* (n = 13) and *VBraf^{IEC};Snail$^{IEC/+}$* (n = 7) endpoint mice. Two-tailed Fisher's exact test.

(F) Number of intestinal carcinomas in *VBraf^{IEC}* (n = 13) and *VBraf^{IEC};Snail$^{IEC/+}$* (n = 7) endpoint mice. Mean ± SEM; two-tailed Student's t-test.

(G) Representative pictures of *VBraf^{IEC}* and *VBraf^{IEC};Snail$^{IEC/+}$* intestinal carcinomas by H&E staining. Scale bars, 50 μm.

3.6 Snail does not induce EMT in intestinal cancer

To investigate the relationship between Snail and EMT in intestinal cancer and compare with that in pancreatic cancer, tumor grading was performed for the intestinal cancer models. In all three models, carcinomas were mostly well-differentiated with no histopathological features of

EMT regardless of Snail level (Figure 3-8A). No difference between *Cdh1* mRNA level in *VApc*$^{\Delta IEC}$ and *VApc*$^{\Delta IEC}$*;Snail*$^{IEC/+}$ tumors was observed (Figure 3-8B), and E-cadherin protein level was correspondingly unchanged (Figure 3-8E). Snail expression also did not significantly downregulate *Cdh1* mRNA expression level in colon samples in Kras- and Braf-dependent models (Figure 3-8C, D). Therefore, even though Snail had distinct effects in intestinal and pancreatic cancer, its overexpression alone was not sufficient to induce EMT in all the models examined. The compelling evidence strongly challenges the notion that Snail is a master regulator of EMT and argues for alternative mechanisms for its tumor-promoting roles.

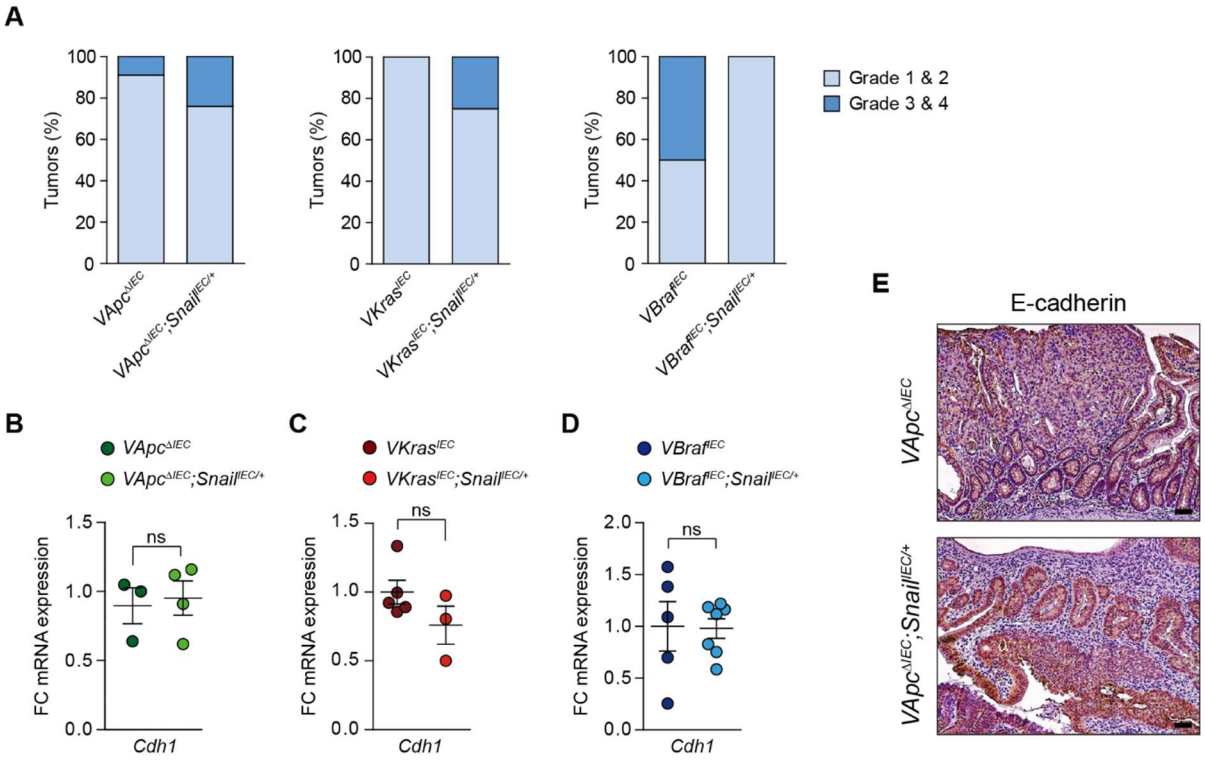

Figure 3-8. Snail does not induce EMT in intestinal cancer

(A) Pathological grading of invasive carcinomas in the intestine of *VApc*$^{\Delta IEC}$ (n = 44), *VApc*$^{\Delta IEC}$*;Snail*$^{IEC/+}$ (n = 21), *VKras*^{IEC} (n = 2), *VKras*^{IEC}*;Snail*$^{IEC/+}$ (n = 4), *VBraf*^{IEC} (n = 8) and *VBraf*^{IEC}*;Snail*$^{IEC/+}$ (n = 6) endpoint mice.
(B) Relative *Cdh1* mRNA expression level normalized to *CypA* by qPCR in intestinal tumors of *VApc*$^{\Delta IEC}$ (n = 3) and *VApc*$^{\Delta IEC}$*;Snail*$^{IEC/+}$ (n = 4) mice. Mean ± SEM; ns, not significant, two-tailed Student's t-test. FC, fold change.
(C) Relative *Cdh1* mRNA expression level normalized to *CypA* by qPCR in colon samples of *VKras*^{IEC} (n = 5) and *VKras*^{IEC}*;Snail*$^{IEC/+}$ (n = 3) mice. Mean ± SEM; ns, not significant, two-tailed Student's t-test. FC, fold change.
(D) Relative *Cdh1* mRNA expression level normalized to *CypA* by qPCR in colon samples of *VBraf*^{IEC} (n = 5) and *VBraf*^{IEC}*;Snail*$^{IEC/+}$ (n = 7) mice. Mean ± SEM; ns, not significant, two-tailed Student's t-test. FC, fold change.
(E) Representative pictures of E-cadherin IHC staining of intestinal tumors from *VApc*$^{\Delta IEC}$ and *VApc*$^{\Delta IEC}$*;Snail*$^{IEC/+}$ mice. Scale bars, 50 μm.

3.7 Snail binds to promoters of cell cycle genes and mediate their upregulation

Existing data from Dr. Mariel Paul showed clearly that Snail is a potent oncogene in pancreatic cancer, but the exact mechanisms involved remain elusive. As increased proliferation, Rb phosphorylation and E2F transcription factor activity was observed in Snail-expressing pancreas (Paul, 2013), expression of cell cycle genes was examined in collaboration with Dr. Mariel Paul. The mRNA level of *Ccna1*, *Ccna2* and *Ccnb1* was elevated with increased Snail expression level in pancreatic tissue of 1-month old mice (Figure 3-9A). Analysis of gene expression microarray data generated by Dr. Mariel Paul (Paul, 2013) also revealed a marked increase in many cell cycle genes in pancreatic tissue with aberrant Snail expression (Figure 3-9B).

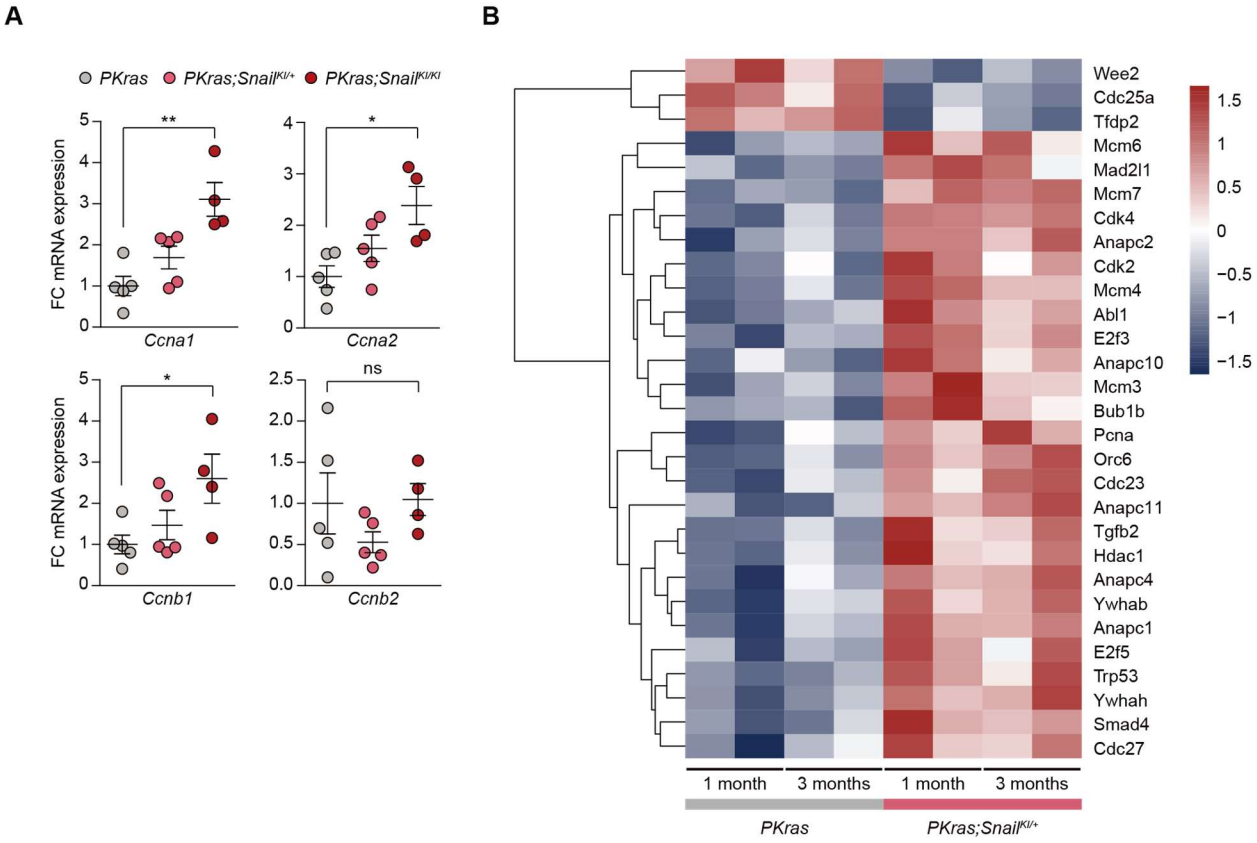

Figure 3-9. Snail expression leads to upregulation of cell cycle genes

(A) Relative mRNA expression level of *Ccna1*, *Ccna2*, *Ccnb1* and *Ccnb2* normalized to *CypA* by qPCR in pancreatic tissue of 1-month-old *PKras* (n = 5), *PKras;Snail*$^{KI/+}$ (n = 5) and *PKras;Snail*$^{KI/KI}$ (n = 4) mice. Mean ± SEM; ns, not significant, *p < 0.05, **p < 0.01, two-tailed Student's t-test. FC, fold change.

(B) Heatmap showing differentially expressed (p < 0.05 and q < 0.05) cell cycle genes in pancreatic tissue between *PKras* and *PKras;Snail*$^{KI/+}$ mice (n = 4). Color scale represents z-score.

To test whether Snail directly binds to the promoter region of cell cycle genes, publicly available ChIP-seq dataset from mouse mammary tumor cell lines (Ye et al., 2015) was analyzed. Since

GSEA showed significant enrichment in KEGG cell cycle genes in *PKras;Snail*$^{KI/+}$ pancreas (Paul, 2013), the highly enriched KEGG cell cycle genes were converted to mouse symbol and intersected with Snail-bound genes from the ChIP-seq data. Out of all enriched KEGG cell cycle genes, 89.9% were bound by Snail in their promoter region (Figure 3-10A). A permutation test demonstrated that the presence of a vast majority of enriched cell cycle genes in the Snail-bound genes was not a random event (Figure 3-10B). The binding of Snail to E-boxes in the promoter regions of *Ccnb1*, *Ccnb2*, *Ccnd1*, *E2f2* and *E2f3* was confirmed by ChIP together with Dr. Mariel Paul (Figure 3-10C). In line with the ChIP-seq dataset, binding of Snail to *Ccna1* promoter region was not detected (Figure 3-10C), although *Ccna1* mRNA expression was elevated in Snail-expressing pancreas (Figure 3-9A).

In summary, Snail directly binds to promoter regions of cell cycle genes and activates their expression, thereby driving cell cycle as a mechanism to accelerate PDAC progression.

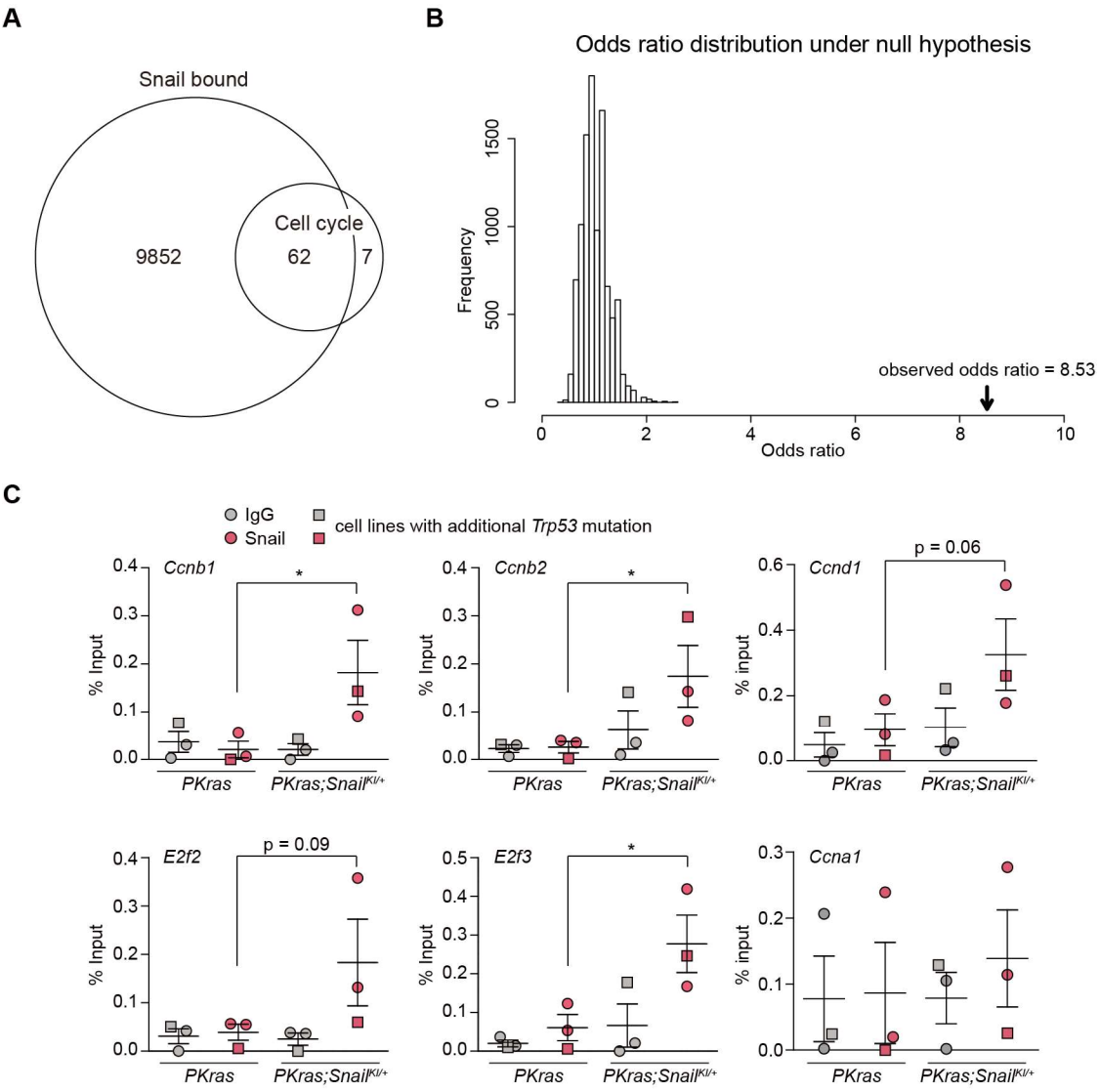

Figure 3-10. Snail binds to promoters of cell cycle genes

(A) Venn diagram showing intersection between Snail-bound genes from published ChIP-seq data (Ye et al., 2015, genes bearing sequence bound by Snail within ± 1kb from the transcription start site) and significantly enriched KEGG cell cycle genes in pancreatic tissue of 1-month-old *PKras;Snail*$^{KI/+}$ mice.

(B) Odds ratio of the intersection in (A) and odds ratio distribution generated by replacing the Snail-bound genes with 9914 random genes from the mouse genome (permuted 10,000 times).

(C) ChIP showing Snail binding to E-boxes in the promoter regions of indicated genes in PDAC cell lines. The percent input method was used, with IgG as negative control. Mean ± SEM; *p < 0.05, one-tailed Student's t-test. Note that *Ccnb1*, *Ccnb2*, *Ccnd1*, *E2f2* and *E2f3* are present in the Snail-bound cell cycle genes in (A).

3.8 Snail drives inflammation in the pancreas

Besides cell cycle, the influence of Snail on PDAC may involve other biological processes as well. GSEA revealed significant enrichment of Hallmark inflammatory response and Hallmark IL6 JAK STAT3 signaling pathways in pancreatic tissue of 1-month old *PKras;Snail*$^{KI/+}$ mice (n =

2, Figure 3-11A, B), indicating that inflammation is implicated in Snail-driven PDAC. Moreover, of the 105 significantly enriched BioCarta, KEGG and Hallmark pathways (FWER p-value < 0.05), 45 were related to inflammation and immune response (Table 3-1). Of note, the enrichment of granulocyte, monocyte, T cell receptor, B cell receptor, cytotoxic T cell and helper T cell pathways provided hints that various immune cells infiltrate early in Snail-expressing pancreas, and that PDAC formation may be accelerated by the presence of a highly immunosuppressive microenvironment. The upregulation of mRNA expression of *Cd44*, *Il6* and *Il2rg* in *PKras;Snail*$^{KI/+}$ pancreas was verified by qPCR (Figure 3-11C). CD44 is not only a marker of cancer stem cells but also an activation marker of lymphocytes (Chen et al., 2018a; Mummert et al., 2002). IL-6 is a central molecule in the proinflammatory IL-6/STAT3 signaling pathway, and IL-2R is a receptor that directs development of T cells, B cells and NK cells (Cao et al., 1995). In addition, KEGG Wnt signaling pathway was also significantly enriched in pancreatic tissue of 1-month old *PKras;Snail*$^{KI/+}$ mice (Figure 3-11D, E). Wnt signaling is critical for PDAC formation (Zhang et al., 2013), and its involvement in inflammation has also been increasingly appreciated (Li et al., 2019; Moparthi and Koch, 2019). Snail therefore creates a proinflammatory program in the pancreas, which plays an important role in pancreatic tumorigenesis (Guerra et al., 2007; Lesina et al., 2011).

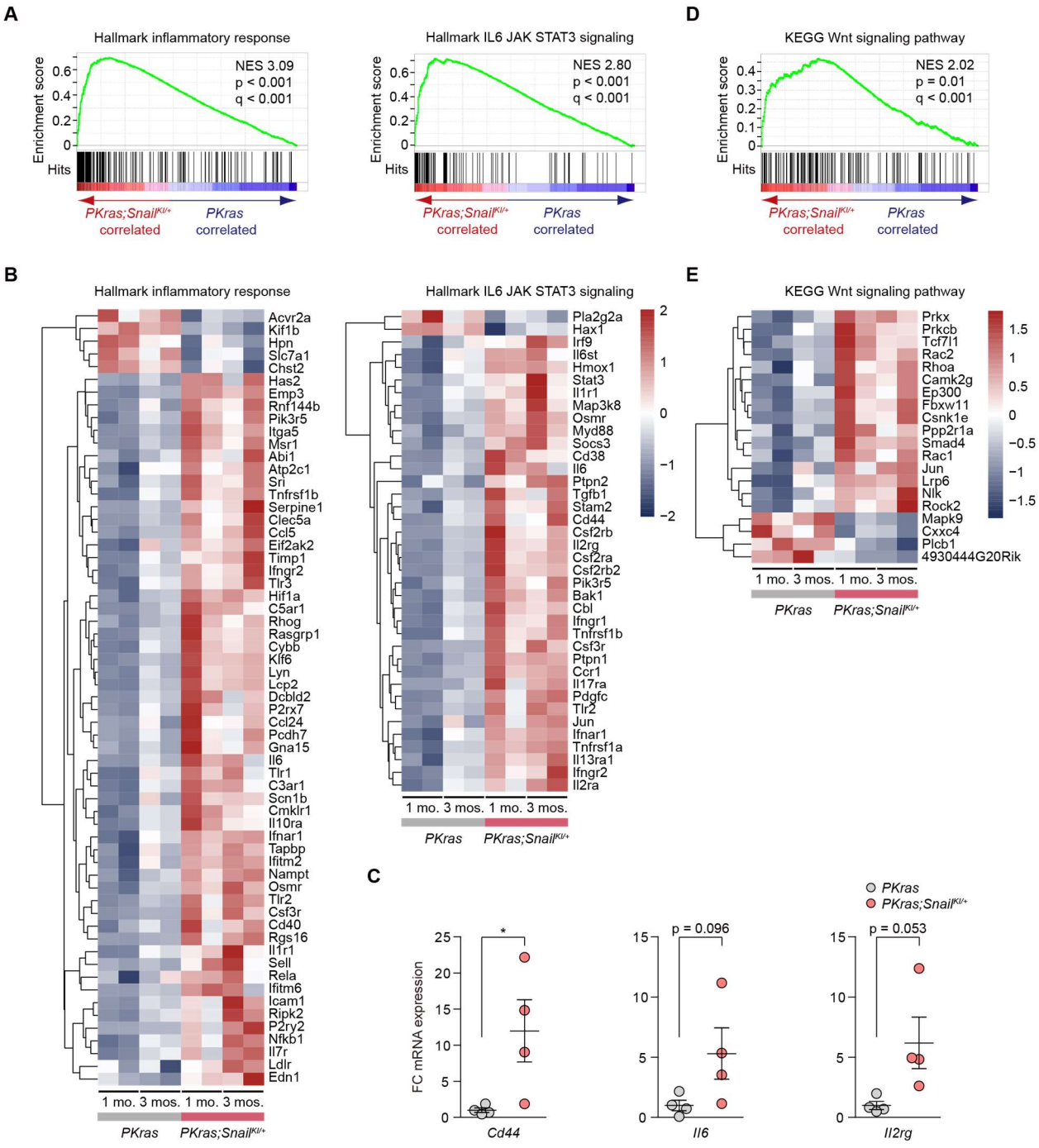

Figure 3-11. Immune-related pathways are upregulated in young Snail-expressing mice

(A) GSEA shows significant enrichment of Hallmark inflammatory response and Hallmark IL6 JAK STAT3 signaling pathways in pancreatic tissue of 1-month-old *PKras;Snail*$^{KI/+}$ mice (n = 2).

(B) Heatmap showing differentially expressed (p < 0.05 and q < 0.05) Hallmark inflammatory response and Hallmark IL6 JAK STAT3 signaling pathway genes in pancreatic tissue between *PKras* and *PKras;Snail*$^{KI/+}$ mice (n = 4). Color scale represents z-score. mo(s). month(s).

(C) Relative mRNA expression level of *Cd44*, *Il6* and *Il2rg* normalized to *CypA* in pancreatic tissue of 1-month-old mice of indicated genotypes (n = 4). Mean ± SEM; *p < 0.05, two-tailed Student's t-test. FC, fold change.

(D) GSEA shows significant enrichment of KEGG Wnt signaling pathway in pancreatic tissue of 1-month-old *PKras;Snail*$^{KI/+}$ mice (n = 2).
(E) Heatmap showing differentially expressed ($p < 0.05$ and $q < 0.05$) Wnt signaling pathway genes in pancreatic tissue between *PKras* and *PKras;Snail*$^{KI/+}$ mice (n = 4). Color scale represents z-score. mo(s). month(s).

Table 3-1. Significantly enriched BioCarta, KEGG and Hallmark pathways in Snail-expressing pancreas

Gene set	Size	NES	q-value	FWER p-value
BIOCARTA_LAIR_PATHWAY*	15	2.45	0	0
BIOCARTA_GRANULOCYTES_PATHWAY*	12	2.36	0	0
BIOCARTA_MONOCYTE_PATHWAY*	11	2.25	0	0
BIOCARTA_FCER1_PATHWAY*	35	2.23	0	0
BIOCARTA_TOLL_PATHWAY*	34	2.22	0	0
BIOCARTA_NKT_PATHWAY*	27	2.22	0	0
BIOCARTA_MAPK_PATHWAY	83	2.19	0	0
KEGG_TOLL_LIKE_RECEPTOR_SIGNALING_PATHWAY*	90	2.7	0	0
KEGG_COMPLEMENT_AND_COAGULATION_CASCADES*	59	2.65	0	0
KEGG_FOCAL_ADHESION	188	2.64	0	0
KEGG_CHEMOKINE_SIGNALING_PATHWAY*	160	2.63	0	0
KEGG_LEISHMANIA_INFECTION*	51	2.59	0	0
KEGG_APOPTOSIS	71	2.55	0	0
KEGG_FC_GAMMA_R_MEDIATED_PHAGOCYTOSIS*	86	2.54	0	0
KEGG_CYTOKINE_CYTOKINE_RECEPTOR_INTERACTION*	217	2.51	0	0
KEGG_ECM_RECEPTOR_INTERACTION	80	2.5	0	0
KEGG_B_CELL_RECEPTOR_SIGNALING_PATHWAY*	71	2.49	0	0
KEGG_HEMATOPOIETIC_CELL_LINEAGE*	65	2.46	0	0
KEGG_LEUKOCYTE_TRANSENDOTHELIAL_MIGRATION*	108	2.45	0	0
KEGG_PATHWAYS_IN_CANCER	301	2.42	0	0
KEGG_NATURAL_KILLER_CELL_MEDIATED_CYTOTOXICITY*	92	2.41	0	0
KEGG_LYSOSOME*	108	2.41	0	0
KEGG_NOD_LIKE_RECEPTOR_SIGNALING_PATHWAY*	54	2.4	0	0
KEGG_NEUROTROPHIN_SIGNALING_PATHWAY	113	2.39	0	0
KEGG_CELL_CYCLE	110	2.38	0	0
KEGG_SMALL_CELL_LUNG_CANCER	79	2.37	0	0
KEGG_REGULATION_OF_ACTIN_CYTOSKELETON	194	2.36	0	0
KEGG_CHRONIC_MYELOID_LEUKEMIA	69	2.34	0	0
KEGG_T_CELL_RECEPTOR_SIGNALING_PATHWAY*	101	2.33	0	0
KEGG_RENAL_CELL_CARCINOMA	68	2.31	0	0
KEGG_CELL_ADHESION_MOLECULES_CAMS*	105	2.31	0	0
KEGG_PATHOGENIC_ESCHERICHIA_COLI_INFECTION*	43	2.29	0	0

Gene set	Size	NES	q-value	FWER p-value
KEGG_GRAFT_VERSUS_HOST_DISEASE*	16	2.26	0	0
KEGG_COLORECTAL_CANCER	57	2.24	0	0
KEGG_PRION_DISEASES*	32	2.23	0	0
KEGG_PANCREATIC_CANCER	67	2.21	0	0
KEGG_FC_EPSILON_RI_SIGNALING_PATHWAY*	73	2.2	0	0
KEGG_AXON_GUIDANCE	126	2.2	0	0
KEGG_HYPERTROPHIC_CARDIOMYOPATHY_HCM	79	2.18	0	0
KEGG_ADHERENS_JUNCTION	68	2.17	0	0
HALLMARK_EPITHELIAL_MESENCHYMAL_TRANSITION	184	3.44	0	0
HALLMARK_INFLAMMATORY_RESPONSE*	195	3.09	0	0
HALLMARK_KRAS_SIGNALING_UP	189	3.08	0	0
HALLMARK_TNFA_SIGNALING_VIA_NFKB	192	3.04	0	0
HALLMARK_ALLOGRAFT_REJECTION*	178	2.98	0	0
HALLMARK_INTERFERON_GAMMA_RESPONSE*	183	2.97	0	0
HALLMARK_COMPLEMENT*	177	2.85	0	0
HALLMARK_IL6_JAK_STAT3_SIGNALING*	85	2.81	0	0
HALLMARK_MITOTIC_SPINDLE	181	2.75	0	0
HALLMARK_COAGULATION*	128	2.65	0	0
HALLMARK_IL2_STAT5_SIGNALING*	189	2.6	0	0
HALLMARK_APOPTOSIS	150	2.58	0	0
HALLMARK_UV_RESPONSE_DN	136	2.54	0	0
HALLMARK_APICAL_JUNCTION	184	2.53	0	0
HALLMARK_INTERFERON_ALPHA_RESPONSE*	84	2.48	0	0
HALLMARK_G2M_CHECKPOINT	181	2.47	0	0
HALLMARK_E2F_TARGETS	188	2.44	0	0
HALLMARK_HYPOXIA	186	2.37	0	0
HALLMARK_ANGIOGENESIS	34	2.37	0	0
HALLMARK_P53_PATHWAY	182	2.27	0	0
HALLMARK_TGF_BETA_SIGNALING	53	2.27	0	0
KEGG_DNA_REPLICATION	33	2.15	0	0.001
KEGG_EPITHELIAL_CELL_SIGNALING_IN_HELICOBACTER_PYLORI_INFECTION	63	2.15	0	0.001
KEGG_CYTOSOLIC_DNA_SENSING_PATHWAY*	46	2.14	0	0.001
KEGG_MAPK_SIGNALING_PATHWAY	239	2.14	0	0.001
KEGG_DILATED_CARDIOMYOPATHY	83	2.12	0	0.001
KEGG_SPLICEOSOME	98	2.11	0	0.001
HALLMARK_REACTIVE_OXIGEN_SPECIES_PATHWAY	39	2.02	0	0.001
BIOCARTA_CLASSIC_PATHWAY*	11	2.16	0	0.002
BIOCARTA_HIVNEF_PATHWAY*	52	2.16	0	0.002

Gene set	Size	NES	q-value	FWER p-value
BIOCARTA_TCR_PATHWAY*	43	2.15	0	0.002
BIOCARTA_IL1R_PATHWAY*	30	2.14	0	0.002
HALLMARK_PI3K_AKT_MTOR_SIGNALING	102	1.98	0	0.002
BIOCARTA_LYM_PATHWAY	10	2.14	0	0.003
BIOCARTA_COMP_PATHWAY*	15	2.14	0	0.003
BIOCARTA_TCYTOTOXIC_PATHWAY*	12	2.13	0	0.003
BIOCARTA_CASPASE_PATHWAY	22	2.11	0	0.004
BIOCARTA_PDGF_PATHWAY	31	2.1	0	0.005
HALLMARK_NOTCH_SIGNALING	29	1.88	0	0.005
KEGG_ARRHYTHMOGENIC_RIGHT_VENTRICULAR _CARDIOMYOPATHY_ARVC	70	2.05	0	0.006
KEGG_GLIOMA	60	2.04	0	0.008
HALLMARK_GLYCOLYSIS	181	1.86	0	0.008
KEGG_ENDOCYTOSIS	159	2.03	0	0.009
BIOCARTA_THELPER_PATHWAY*	12	2.09	0.001	0.009
KEGG_WNT_SIGNALING_PATHWAY	135	2.02	0	0.01
BIOCARTA_P53HYPOXIA_PATHWAY	20	2.05	0.002	0.018
BIOCARTA_IL10_PATHWAY*	17	2.04	0.002	0.018
HALLMARK_MTORC1_SIGNALING	184	1.79	0.001	0.02
BIOCARTA_NFKB_PATHWAY*	21	2.04	0.002	0.02
BIOCARTA_P38MAPK_PATHWAY	36	2.04	0.002	0.02
KEGG_INTESTINAL_IMMUNE_NETWORK_FOR_IGA_PRODUCTION*	30	1.99	0.001	0.022
KEGG_P53_SIGNALING_PATHWAY	58	1.98	0.001	0.024
BIOCARTA_MET_PATHWAY	36	2.02	0.002	0.025
KEGG_ERBB_SIGNALING_PATHWAY	83	1.98	0.001	0.026
BIOCARTA_TNFR1_PATHWAY	28	2.01	0.002	0.03
KEGG_PROSTATE_CANCER	80	1.97	0.001	0.031
KEGG_VEGF_SIGNALING_PATHWAY	68	1.97	0.001	0.031
HALLMARK_APICAL_SURFACE	43	1.76	0.001	0.031
BIOCARTA_BCR_PATHWAY*	32	2.01	0.002	0.031
KEGG_GAP_JUNCTION	73	1.97	0.001	0.032
BIOCARTA_EXTRINSIC_PATHWAY	13	2	0.002	0.034
KEGG_ARACHIDONIC_ACID_METABOLISM	43	1.95	0.001	0.037
HALLMARK_MYC_TARGETS_V1	179	1.73	0.002	0.039
KEGG_SYSTEMIC_LUPUS_ERYTHEMATOSUS*	67	1.94	0.001	0.044
BIOCARTA_GPCR_PATHWAY	32	1.99	0.003	0.047

NES, normalized enrichment score; FWER, family-wise error rate. Asterisks (*) mark pathways related to inflammation and immune response.

3.9 Severe combined immunodeficiency impedes Kras^{G12D}-driven PDAC progression

Since inflammation and immune network play pivotal roles in PDAC progression, they also provide potential therapeutic targets for this deadly disease. To target the inflammatory program induced by Snail, *Prkdc*$^{Scid/Scid}$ and *Il2rg*^{null} alleles from the NSG mice were crossed into the *PKras;Snail*$^{KI/+}$ model. These alleles deplete mature B cells, T cells and NK cells, resulting in a severe combined immunodeficiency phenotype. Strikingly, severe combined immunodeficiency doubled the survival time of *PKras;Snail*$^{KI/+}$ mice (Figure 3-12A). Histological analysis showed that only 2 out of 6 *PKras;Snail*$^{KI/+}$*;Prkdc*$^{Scid/Scid}$*;Il2rg*^{null} mice had invasive carcinoma, while all *PKras;Snail*$^{KI/+}$ mice included in the survival curve had full-blown PDAC (Figure 3-12B, C). There is also a tendency that endpoint *PKras;Snail*$^{KI/+}$*;Prkdc*$^{Scid/Scid}$*;Il2rg*^{null} mice has a lower pancreas/body weight ratio than *PKras;Snail*$^{KI/+}$ mice (Figure 3-12D).

To test whether the survival benefit gained by severe combined immunodeficiency is a general phenomenon in Kras^{G12D}-driven PDAC, *PKras;Prkdc*$^{Scid/Scid}$*;Il2rg*^{null} mice were also analyzed. Although they did not show longer survival time compared to *PKras* mice, they were euthanized not because of tumor but due to reduced health condition related to their compromised immunity. In fact, none of the endpoint *PKras;Prkdc*$^{Scid/Scid}$*;Il2rg*^{null} mice had invasive carcinoma (Figure 3-12B, C), and they also had a lower pancreas/body weight ratio than *PKras* mice (Figure 3-12D).

In order to assess the role of severe combined immunodeficiency in early PDAC development, pancreata from 6-month-old *PKras* and *PKras;Prkdc*$^{Scid/Scid}$*;Il2rg*^{null} mice were obtained. Already at this age, the pancreas/body weight ratio was significantly lower in the *PKras;Prkdc*$^{Scid/Scid}$*;Il2rg*^{null} group (Figure 3-12E). Analysis of precursor lesions revealed no difference in the number of ADM or PanIN, but the AFL commonly seen in *PKras* pancreas were completely absent in the *PKras;Prkdc*$^{Scid/Scid}$*;Il2rg*^{null} mice (Figure 3-12F, G, H). These data uncover a protecting role of severe combined immunodeficiency in Kras^{G12D}-driven PDAC development, possibly through a mechanism that blocks AFL formation or PanIN to PDAC progression.

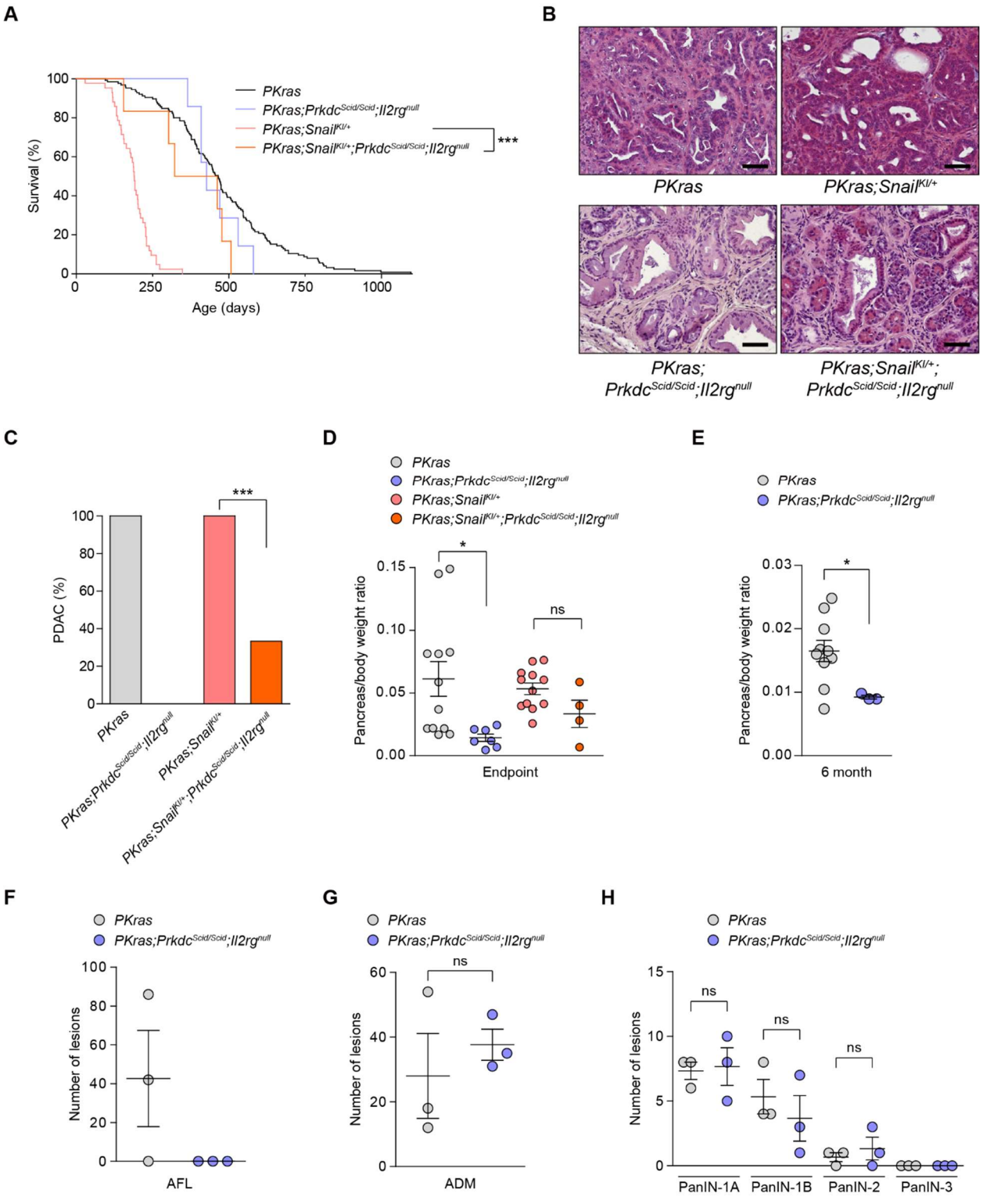

Figure 3-12. Severe combined immunodeficiency impedes Kras^{G12D}-driven PDAC progression

(A) Kaplan-Meier survival curves of *PKras* (n = 125, median survival 465 days), *PKras;Prkdc$^{Scid/Scid}$;Il2rg^{null}* (n = 7, median survival 427 days), *PKras;Snail$^{KI/+}$* (n = 42, median survival 190 days) and *PKras;Snail$^{KI/+}$;Prkdc$^{Scid/Scid}$;Il2rg^{null}* (n = 6, median survival 392 days) mice. ***p < 0.001, two-tailed log-rank test.

(B) Representative H&E stains of pancreatic tissue from endpoint mice. Scale bars, 50 μm.

(C) Percentage of PDAC-bearing *PKras* (n = 32), *PKras;Prkdc*$^{Scid/Scid}$*;Il2rg*^{null} (n = 6) , *PKras;Snail*$^{KI/+}$ (n = 21) and *PKras;Snail*$^{KI/+}$*;Prkdc*$^{Scid/Scid}$*;Il2rg*^{null} (n = 6) endpoint mice. ***p < 0.001, two-tailed Fisher's exact test.
(D) Pancreas/body weight ratio of endpoint *PKras* (n = 12), *PKras;Prkdc*$^{Scid/Scid}$*;Il2rg*^{null} (n = 7), *PKras;Snail*$^{KI/+}$ (n = 12) and *PKras;Snail*$^{KI/+}$*;Prkdc*$^{Scid/Scid}$*;Il2rg*^{null} (n = 4) mice. Mean ± SEM; *p < 0.05, ns, not significant, significance level adjusted by Bonferroni correction, two-tailed Student's t-test.
(E) Pancreas/body weight ratio of 6-month-old *PKras* (n = 10) and *PKras;Prkdc*$^{Scid/Scid}$*;Il2rg*^{null} (n = 3) mice. Mean ± SEM; *p < 0.05, two-tailed Student's t-test.
(F) Number of AFL in pancreas of 6-month-old *PKras* (n = 3) and *PKras;Prkdc*$^{Scid/Scid}$*;Il2rg*^{null} (n = 3) mice. Mean ± SEM.
(G) Number of ADM in pancreas of 6-month-old *PKras* (n = 3) and *PKras;Prkdc*$^{Scid/Scid}$*;Il2rg*^{null} (n = 3) mice. Mean ± SEM; ns, not significant, two-tailed Student's t-test.
(H) Number of PanIN of different grades in pancreas of 6-month-old *PKras* (n = 3) and *PKras;Prkdc*$^{Scid/Scid}$*;Il2rg*^{null} (n = 3) mice. Mean ± SEM; ns, not significant, two-tailed Student's t-test.

3.10 B cell and T cell depletion accelerates PDAC formation

To further evaluate the functions of B cells and T cells, *Rag2*$^{-/-}$ alleles were crossed into the *PKras;Snail*$^{KI/+}$ model. The mice were backcrossed to B6 background to exclude effects rising from different genetic backgrounds. B6 *PKras;Snail*$^{KI/+}$ mice also developed PDAC significantly faster than B6 *PKras* mice, and the survival time was almost identical to that of their counterparts on the mixed *C57BL/6J;129S6/SvEv* background (Figure 3-13A). In huge contrast to severe combined immunodeficiency, depletion of mature B cells and T cells led to even faster tumor development (Figure 3-13B). Since B cell deficiency resulted in compromised growth of pancreatic neoplasms (Pylayeva-Gupta et al., 2016), the lack of cytotoxic T cell function may explain the tumor-promoting effect of B cell and T cell depletion. Also, this effect was reversed by the added effect of severe combined immunodeficiency, which may be attributed to NK cell depletion or the mixed genetic background of the *Prkdc*$^{Scid/Scid}$*;Il2rg*^{null} model. As a proof of concept, the presence of B cells and T cells in *PKras;Snail*$^{KI/+}$*;Rag2*$^{-/-}$ PDAC was virtually lacking (Figures 3-13C and 3-16B). The very few B cells and T cells that could still be detected had similar percentages as shown by Shinkai and colleagues (Shinkai et al., 1992), which may be due to the cross-reactivity of the antibodies. There is a trend that *PKras;Snail*$^{KI/+}$*;Rag2*$^{-/-}$ mice has a lower tumor/body weight ratio compared to the *PKras;Snail*$^{KI/+}$ mice (Figure 3-13D), and morphologically, all seven *PKras;Snail*$^{KI/+}$*;Rag2*$^{-/-}$ PDACs were moderately to well-differentiated (Figure 3-13E, F), suggesting a potential role of B cells and T cells in modulating tumor differentiation. Depletion of mature B cells and T cells did not have a significant impact on metastasis or ascites formation in the *PKras;Snail*$^{KI/+}$ model (Figure 3-13G, H).

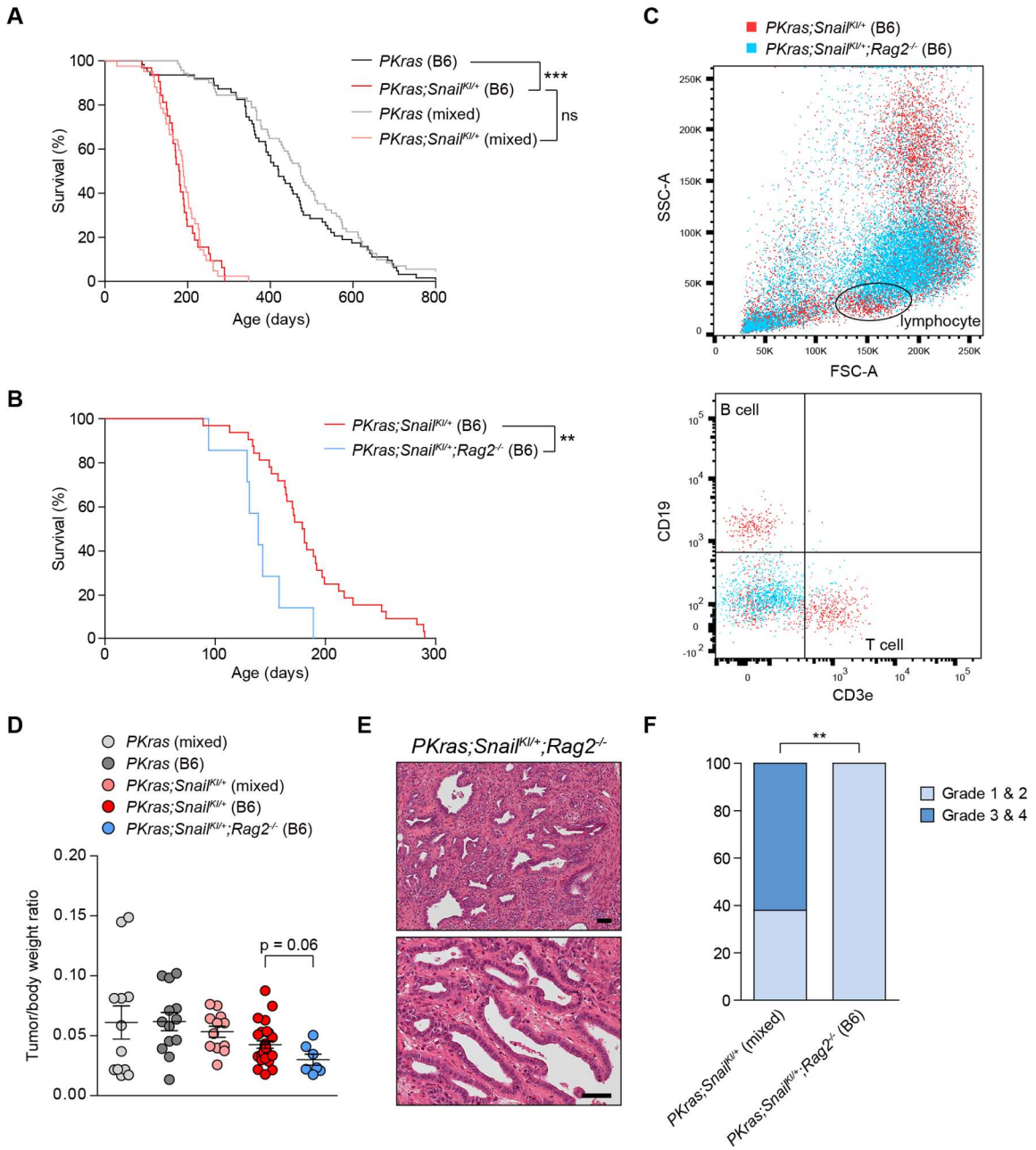
A
PKras (B6)
PKras;SnailKI/+ (B6)
PKras (mixed)
PKras;SnailKI/+ (mixed)
***
ns
Survival (%)
Age (days)
B
PKras;SnailKI/+ (B6)
PKras;SnailKI/+;Rag2-/- (B6)
**
Survival (%)
Age (days)
C
PKras;SnailKI/+ (B6)
PKras;SnailKI/+;Rag2-/- (B6)
SSC-A
FSC-A
lymphocyte
B cell
T cell
CD19
CD3e
D
PKras (mixed)
PKras (B6)
PKras;SnailKI/+ (mixed)
PKras;SnailKI/+ (B6)
PKras;SnailKI/+;Rag2-/- (B6)
Tumor/body weight ratio
p = 0.06
E
PKras;SnailKI/+;Rag2-/-
F
**
Grade 1 & 2
Grade 3 & 4
PKras;SnailKI/+ (mixed)
PKras;SnailKI/+;Rag2-/- (B6)
G
PKras (mixed)
PKras (B6)
PKras;SnailKI/+ (mixed)
PKras;SnailKI/+ (B6)
PKras;SnailKI/+;Rag2-/- (B6)
Macroscopic liver metastasis rate (%)
ns
nd
Macroscopic lung metastasis rate (%)
ns
H
PKras (mixed)
PKras (B6)
PKras;SnailKI/+ (mixed)
PKras;SnailKI/+ (B6)
PKras;SnailKI/+;Rag2-/- (B6)
% mice with ascites
ns

Figure 3-13. Depletion of B cells and T cells accelerates PDAC progression

(A) Kaplan-Meier survival curves of *PKras* (n = 71, median survival 473 days) and *PKras;Snail*$^{KI/+}$ (n = 42, median survival 190 days) mice on mixed *C57BL/6J;129S6/SvEv* background as well as *PKras* (n = 63, median survival 420 days) and *PKras;Snail*$^{KI/+}$ (n = 32, median survival 180 days) mice on *C57BL/6J* (B6) background (backcrossed at least 10 times). ns, not significant, ***p < 0.001, significance level adjusted by Bonferroni correction, two-tailed log-rank test.

(B) Kaplan-Meier survival curves of *PKras;Snail*$^{KI/+}$ (n = 32, median survival 180 days) and *PKras;Snail*$^{KI/+}$*;Rag2*$^{-/-}$ (n = 7, median survival 139 days) mice on B6 background. **p < 0.01, two-tailed log-rank test.

(C) Representative lymphocyte, B cell and T cell populations in PDAC from *PKras;Snail*$^{KI/+}$ and *PKras;Snail*$^{KI/+}$*;Rag2*$^{-/-}$ mice. The populations were pre-gated on single, live, CD45^{+} cells as shown in Figure 3-15.

(D) Tumor/body weight ratio of endpoint *PKras* (n = 12) and *PKras;Snail*$^{KI/+}$ (n = 12) mice on mixed *C57BL/6J;129S6/SvEv* background, and *PKras* (n = 13), *PKras;Snail*$^{KI/+}$ (n = 27) and *PKras;Snail*$^{KI/+}$*;Rag2*$^{-/-}$ (n = 7) mice on B6 background. Mean ± SEM; two-tailed Student's t-test.

(E) Representative pictures of *PKras;Snail*$^{KI/+}$*;Rag2*$^{-/-}$ PDACs by H&E staining. Scale bars, 50 μm.

(F) Pathological grading of PDAC from *PKras;Snail*$^{KI/+}$ (n = 21) and *PKras;Snail*$^{KI/+}$*;Rag2*$^{-/-}$ (n = 7) mice. **p < 0.01, two-tailed Fisher's exact test.

(G) Macroscopic liver (left panel) and lung (right panel) metastasis rate of endpoint *PKras* (n = 69) and *PKras;Snail*$^{KI/+}$ (n = 42) mice on mixed *C57BL/6J;129S6/SvEv* background, and *PKras* (n = 63), *PKras;Snail*$^{KI/+}$ (n = 32) and *PKras;Snail*$^{KI/+}$*;Rag2*$^{-/-}$ (n = 7) mice on B6 background. nd, not detected. ns, not significant, two-tailed Fisher's exact test.

(H) Percentage of ascites-bearing endpoint *PKras* (n = 70) and *PKras;Snail*$^{KI/+}$ (n = 42) mice on mixed *C57BL/6J;129S6/SvEv* background, and *PKras* (n = 61), *PKras;Snail*$^{KI/+}$ (n = 32) and *PKras;Snail*$^{KI/+}$*;Rag2*$^{-/-}$ (n = 7) mice on B6 background. ns, not significant, two-tailed Fisher's exact test.

3.11 Snail influences immune cell infiltration in PDAC

The ability of Snail to induce inflammation and activate immune pathways early in PDAC formation is indicative of the active participation of immune cells in Snail-promoted tumorigenesis. To examine which immune cells infiltrate mouse PDAC, two flow cytometry panels were designed (Tables 2-15 and 2-16). Antibody dilutions were determined by titration of single stains (Figure 3-14), and full stain and the gating strategies of both panels are shown in Figure 3-15. Only tumor mice backcrossed to B6 background were included in the analysis because of the stable genetic background and the reactivity of NK1.1 antibody (Carlyle et al., 2006). There was no significant difference in the percentage of live cells between the groups, although *PKras* samples tend to have higher viability (Figure 3-16A). Of all the tested immune cell populations, there was a tendency in higher amount of neutrophils/MDSCs, macrophages and dendritic cells in *PKras;Snail*$^{KI/+}$ PDACs compared to *PKras* PDACs (Figure 3-16B). Due to the long latency of autochthonous PDAC, only two *PKras* tumors were analyzed. Nevertheless, the result suggests that Snail promotes an immunosuppressive microenvironment by recruiting MDSCs and TAMs, thereby accelerating PDAC progression.

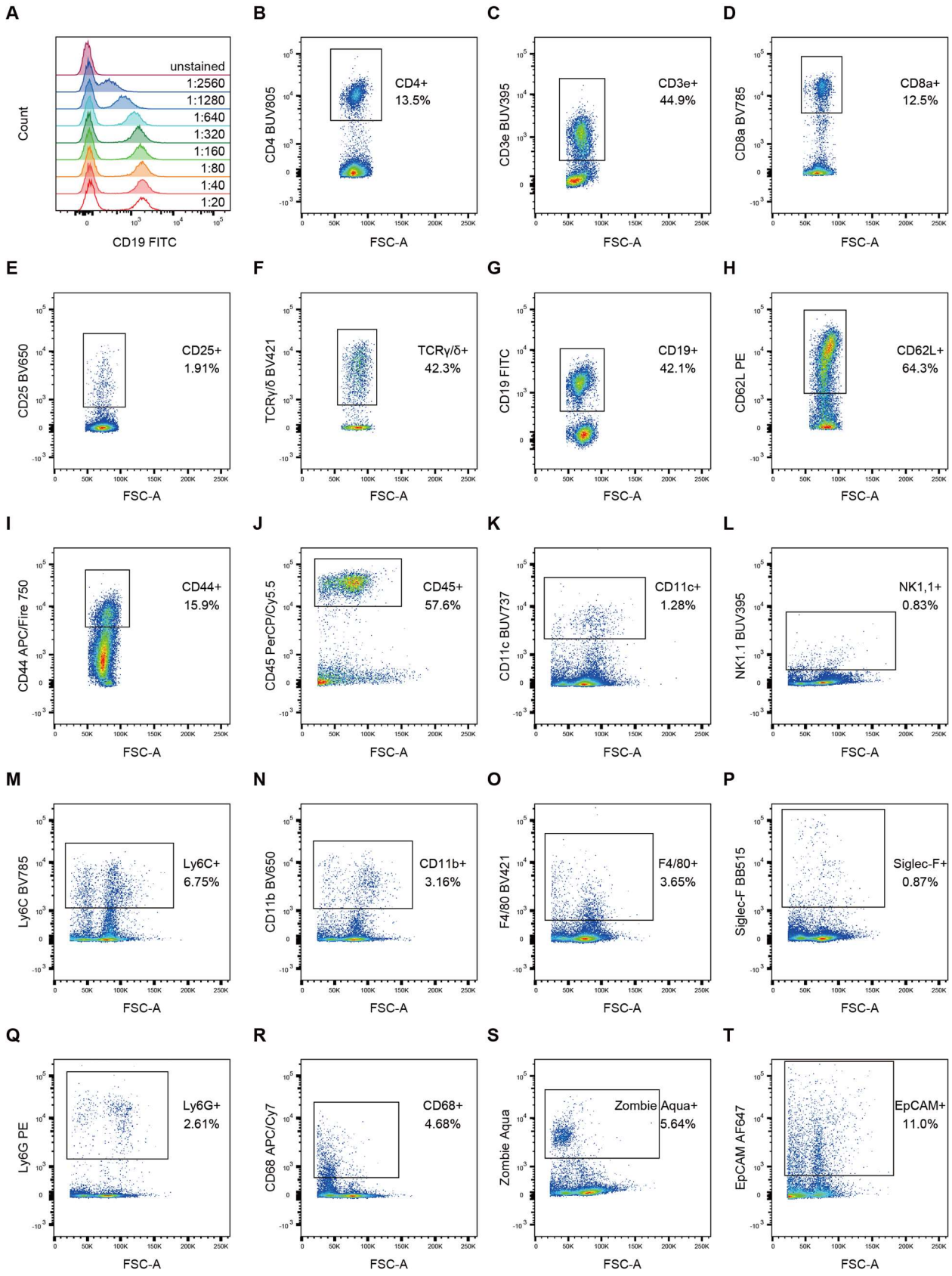
A
Count
unstained
1:2560
1:1280
1:640
1:320
1:160
1:80
1:40
1:20
CD19 FITC
B
CD4 BUV805
CD4+
13.5%
FSC-A
C
CD3e BUV395
CD3e+
44.9%
FSC-A
D
CD8a BV785
CD8a+
12.5%
FSC-A
E
CD25 BV650
CD25+
1.91%
FSC-A
F
TCRγ/δ BV421
TCRγ/δ+
42.3%
FSC-A
G
CD19 FITC
CD19+
42.1%
FSC-A
H
CD62L PE
CD62L+
64.3%
FSC-A
I
CD44 APC/Fire 750
CD44+
15.9%
FSC-A
J
CD45 PerCP/Cy5.5
CD45+
57.6%
FSC-A
K
CD11c BUV737
CD11c+
1.28%
FSC-A
L
NK1.1 BUV395
NK1,1+
0.83%
FSC-A
M
Ly6C BV785
Ly6C+
6.75%
FSC-A
N
CD11b BV650
CD11b+
3.16%
FSC-A
O
F4/80 BV421
F4/80+
3.65%
FSC-A
P
Siglec-F BB515
Siglec-F+
0.87%
FSC-A
Q
Ly6G PE
Ly6G+
2.61%
FSC-A
R
CD68 APC/Cy7
CD68+
4.68%
FSC-A
S
Zombie Aqua
Zombie Aqua+
5.64%
FSC-A
T
EpCAM AF647
EpCAM+
11.0%
FSC-A

Figure 3-14. Single stain and titration of flow cytometry antibodies and Zombie Aqua

(A) Example of antibody titration. The cells were stained by CD19 FITC antibody in a 1:2 dilution series starting from 1:20 until 1:2560. Histogram overlay shows the decrease of fluorescence intensity in the serial dilution. An ideal dilution was between 1:80 and 1:160 as no obvious decrease of fluorescence intensity was observed within this range yet. Dilutions for other antibodies were determined in the same way. Titration range for Zombie Aqua was from 1:100 to 1:12800.

(B-S) Splenocytes were stained by antibodies or Zombie Aqua in the following dilution: (B) CD4 BUV805, 1:160; (C) CD3e BUV395, 1:20; (D) CD8a BV785, 1:160; (E) CD25 BV650, 1:80; (F) TCRγ/δ BV421, 1:80; (G) CD19 FITC, 1:160; (H) CD62L PE, 1:640; (I) CD44 APC/Fire 750, 1:40; (J) CD45 PerCP/Cy5.5, 1:160; (K) CD11c BUV737, 1:40; (L) NK1.1 BUV395, 1:40; (M) Ly6C BV785, 1:320; (N) CD11b BV650, 1:160; (O) F4/80 BV421, 1:40; (P) Siglec-F BB515, 1:160; (Q) Ly6G PE, 1:320; (R) CD68 APC/Cy7, 1:20; (S) Zombie Aqua, 1:640. The cells have been gated by single cell gates and panels B-I were further gated by the lymphocyte gate as in Figure 3-15A. These panels show positive single stains and the next dilutions resulted in decrease of fluorescence intensity. The numbers next to the gates show the percentages of cells with positive staining.

(T) PDAC cells were stained by EpCAM AF647 antibody in 1:320 dilution. The cells have been gated by single cell gates as in Figure 3-15A. The next dilution resulted in decrease of fluorescence intensity. The number next to the gate shows the percentage of cells with positive staining.

Figure 3-15. Gating strategy for flow cytometry analysis of tumor-infiltrating immune cells (next page)

(A) Gating strategy for T cell & B cell panel. Single cell events were gated based on forward scatter (FSC) area (A), height (H) and width (W). Zombie Aqua$^-$ events were considered live cells. Among the single live cells, CD45$^-$EpCAM$^+$ were epithelial cells and CD45$^+$EpCAM$^-$ were leukocytes. From the leukocyte gates, lymphocytes were gated based on forward scatter (FSC) and side scatter (SSC). Then CD19$^+$CD3e$^-$ defined B cells and CD19$^-$CD3e$^+$ defined T cells. In the T cell population, γδ T cells were TCRγ/δ$^+$. Helper T cells were CD4$^+$CD8a$^-$ and cytotoxic T cells were CD4$^-$CD8a$^+$. For helper T cells and cytotoxic T cells, CD44$^+$CD62L$^+$ and CD44$^+$CD62L$^-$ reflected central memory and effector memory status, respectively. Tregs were defined as CD4$^+$CD8a$^-$CD25$^+$ T cells.

(B) Gating strategy for innate immune cell panel. Among the CD45$^+$EpCAM$^-$ leukocytes gated as in panel A, neutrophils/MDSCs were defined as CD11b^{hi}Ly6G^{hi}. Eosinophils were gated as Siglec-F^{hi}SSC^{hi} from the non-neutrophil/MDSC population, and CD11c$^+$F4/80$^-$ cells from the non-eosinophil population were defined as dendritic cells. CD11b^{hi}F4/80$^+$ cells were macrophages, which were divided into inflammatory and patrolling states based on Ly6C level. NK cells were designated as CD11c$^-$F4/80$^-$NK1.1$^+$.

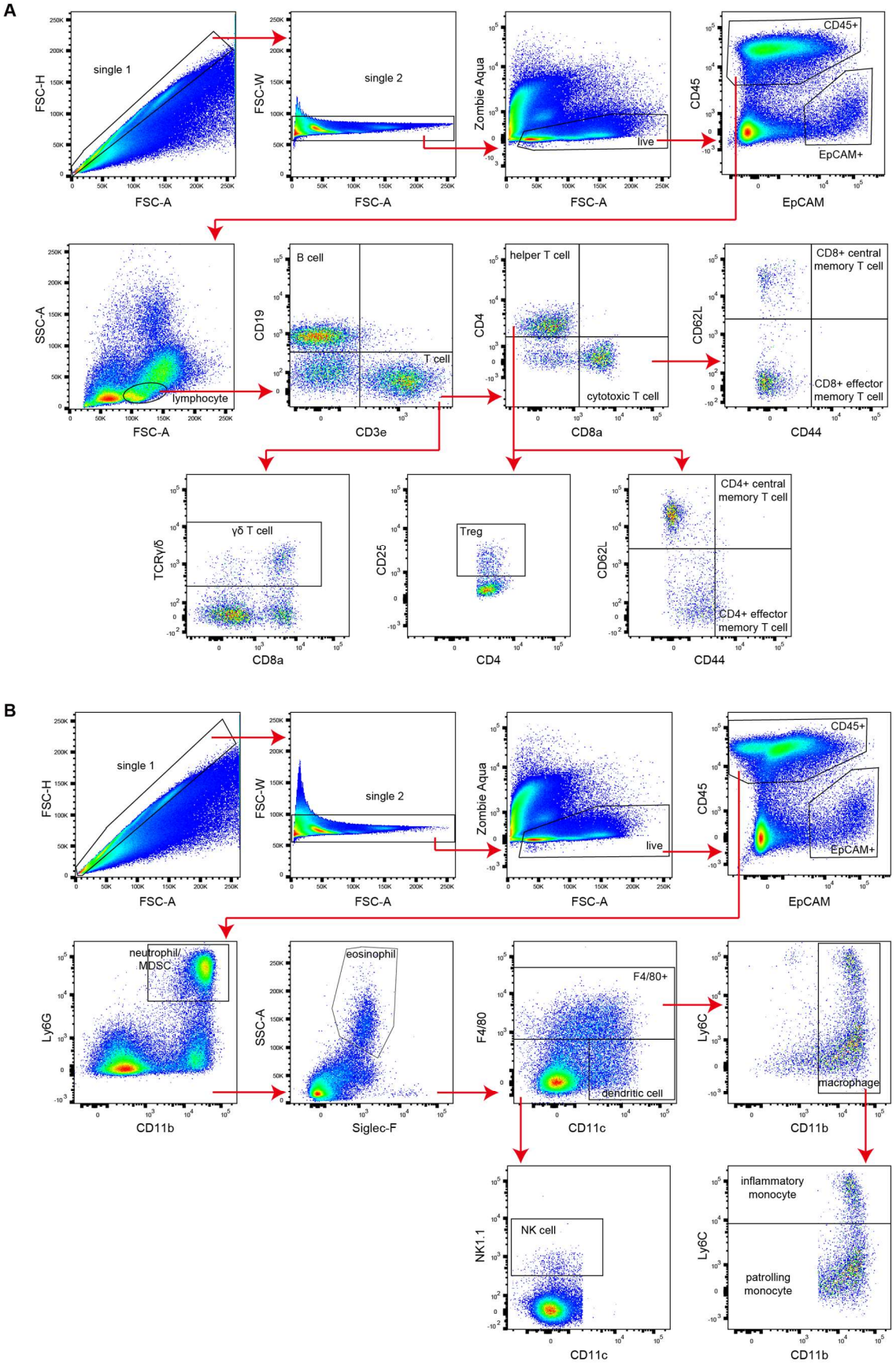
A
single 1
FSC-H
FSC-A
single 2
FSC-W
FSC-A
Zombie Aqua
live
FSC-A
CD45+
EpCAM+
CD45
EpCAM
SSC-A
lymphocyte
FSC-A
B cell
T cell
CD19
CD3e
helper T cell
cytotoxic T cell
CD4
CD8a
CD8+ central memory T cell
CD8+ effector memory T cell
CD62L
CD44
γδ T cell
TCRγ/δ
CD8a
Treg
CD25
CD4
CD4+ central memory T cell
CD4+ effector memory T cell
CD62L
CD44
B
single 1
FSC-H
FSC-A
single 2
FSC-W
FSC-A
Zombie Aqua
live
FSC-A
CD45+
EpCAM+
CD45
EpCAM
neutrophil/ MDSC
Ly6G
CD11b
eosinophil
SSC-A
Siglec-F
F4/80+
dendritic cell
F4/80
CD11c
macrophage
Ly6C
CD11b
NK cell
NK1.1
CD11c
inflammatory monocyte
patrolling monocyte
Ly6C
CD11b

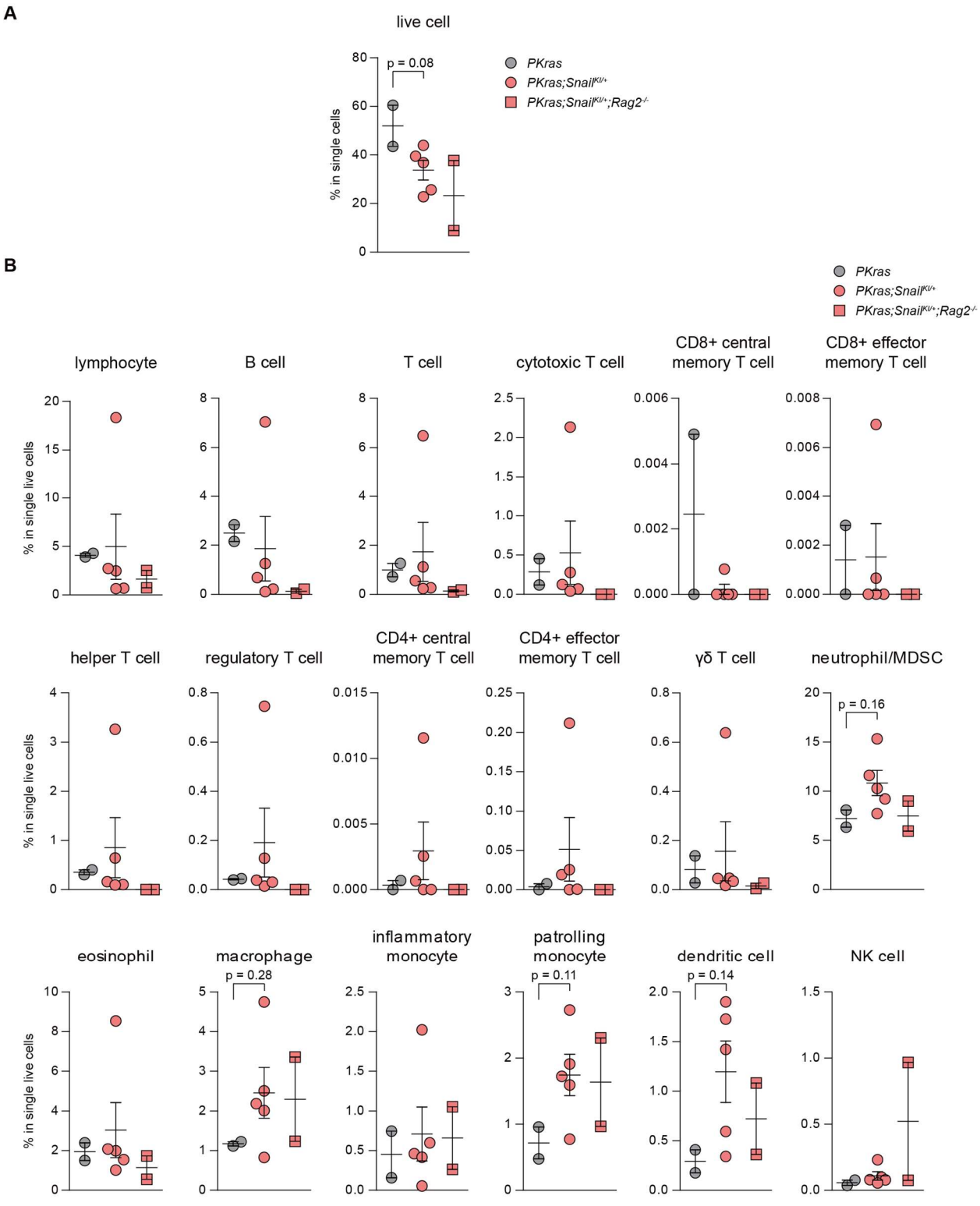

Figure 3-16. Flow cytometry analysis of tumor-infiltrating immune cells

(A) PDACs from *PKras* (n = 2), *PKras;Snail*$^{KI/+}$ (n = 5) and *PKras;Snail*$^{KI/+}$*;Rag2*$^{-/-}$ (n = 2) mice were minced, digested with enzymatic cocktail, washed and stained by the two antibody panels. For each PDAC, one million viable cells were stained by each antibody panel before analyzed by flow cytometry. The percentage of live cells in the single cell

population as gated in Figure 3-15 is shown. PDACs were verified on H&E-stained sections. Mean ± SEM; two-tailed Student's t-test.
(B) Immune cell populations were gated as in Figure 3-15, and percentages of indicated cell types in the single live cell population in *PKras* (n = 2), *PKras;Snail*$^{KI/+}$ (n = 5) and *PKras;Snail*$^{KI/+}$*;Rag2*$^{-/-}$ (n = 2) PDACs are shown. Mean ± SEM; two-tailed Student's t-test.

PDACs are characterized by molecular and cellular heterogeneity even when they are driven by the same oncogene Kras. This was shown by global gene expression analysis by RNA-seq of bulk tumor samples, where *PKras* samples scattered on the MDS plot. On the contrary, *PKras;Snail*$^{KI/+}$ tumors clustered together with few exceptions (Figure 3-17A), indicating that Snail drives global gene expression of PDAC into a uniform direction. Indeed, heatmap visualization of differentially expressed genes between *PKras* and *PKras;Snail*$^{KI/+}$ bulk PDACs showed similar gene expression pattern in *PKras;Snail*$^{KI/+}$ samples and visible subgroups in the *PKras* group (Figure 3-17B).

Bioinformatics methods allow *in silico* estimation of cell type abundances from bulk tumor data. Deconvolution of bulk tumor RNA-seq data were carried out by a bioinformatician using transcriptomics data available from ImmGen as references, and six clusters were identified by immuno-subtyping 215 samples collected in the lab (Figure 3-17C). Notably, *PKras* tumors were present in all the clusters, and all but one *PKras;Snail*$^{KI/+}$ samples clustered in C3 and C4 clusters. Thus, Snail also has a strong influence on PDAC microenvironment. Compared to other clusters, C3 and C4 have tumors with higher numbers of infiltrating immune cell types. C4 is characterized by the presence of seven macrophage or monocyte subsets and three dendritic cell subsets; other highly abundant cell types in C4 include T cell, memory B cell, eosinophil and innate lymphoid cell subsets. Similarly, C3 has infiltration of macrophage and dendritic cell subsets, while subsets of cytotoxic T cell, mast cell, NK cell, NKT cell and γδ T cell are also present. These data support the finding that Snail recruits macrophages and dendritic cells into PDAC microenvironment. However, MDSC/neutrophil infiltration is a feature of C1 cluster, which has only one *PKras;Snail*$^{KI/+}$ sample and otherwise comprises mostly oncogenic Braf- and PI3K-driven tumors. C1 also has signatures of macrophage, monocyte and T cell subsets. In contrast, C2 tumors have infiltration of B cell, endothelial cell, medullary epithelial cell, fibroblast and mast cell subsets. C5 cluster, consisting of only MAP2K1-driven tumors and two *PKras* tumors, has the least number of immune cell signatures, with only lymphatic endothelial cells and bone marrow common dendritic cell progenitors significantly present. C6 is characterized by one dendritic cell, one NK cell and three T cell subsets (Table 3-2).

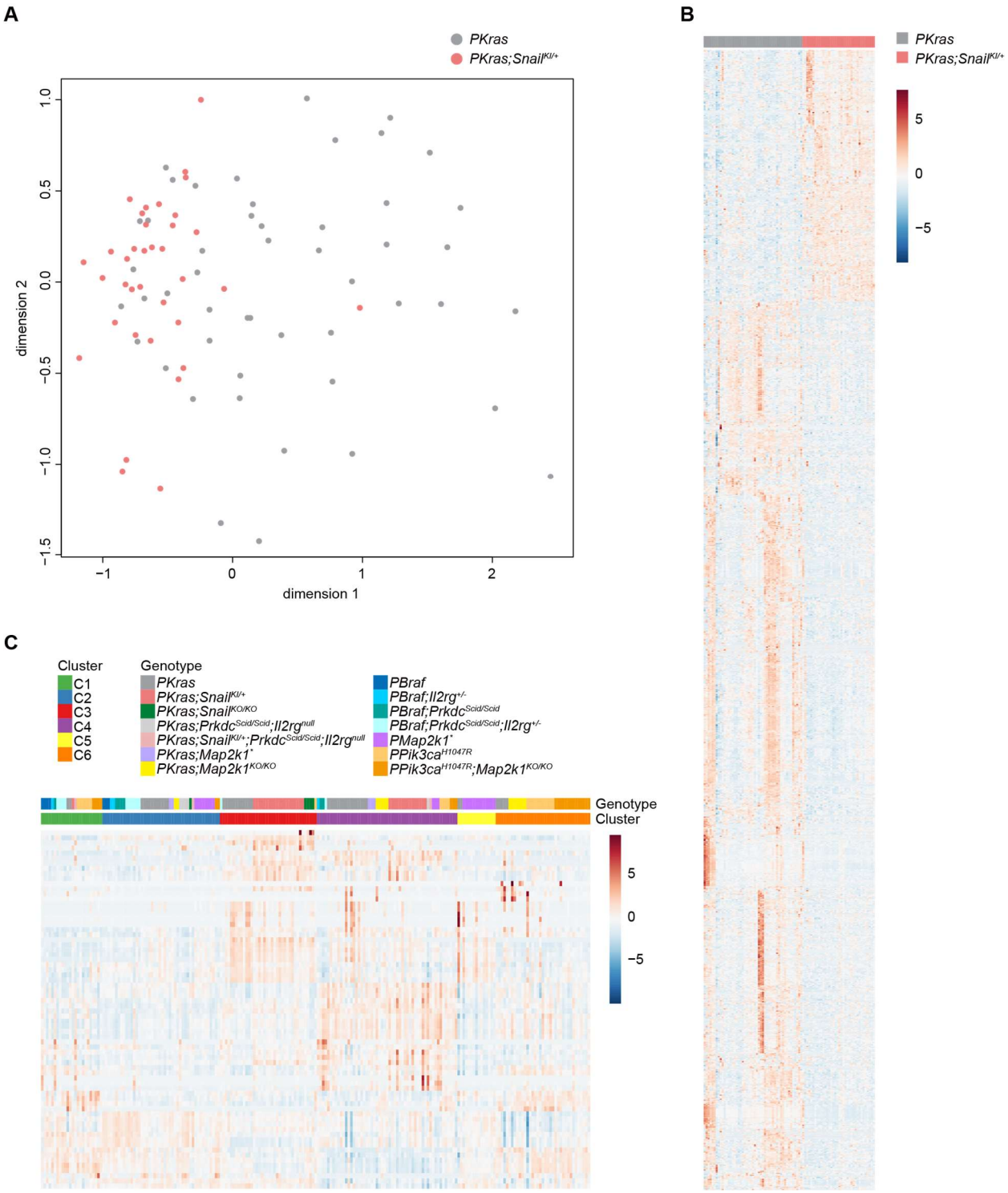

Figure 3-17. Snail drives immune landscape in PDAC

(A) MDS plot of *PKras* (n = 49) and *PKras;Snail*$^{KI/+}$ (n = 36) PDACs. The differences of bulk tumor samples in global gene expression pattern obtained by RNA-seq were calculated by log-CPM (log counts per million) values and visualized. Note that *PKras;Snail*$^{KI/+}$ PDACs cluster together while *PKras* PDACs scatter on the plot.
(B) Heatmap showing top differentially expressed genes (adjusted p-value ≤ 0.01 and abs($\log_2$FC) ≥ 1) between *PKras* (n = 49) and *PKras;Snail*$^{KI/+}$ (n = 36) PDACs. Color scale represents z-score.

(C) Immuno-subtyping of mouse PDAC. Gene expression profiles of mouse tumor tissue by RNA-seq were deconvoluted using cell type-specific gene expression profiles from ImmGen as references. Subtyping was performed by non-negative matrix factorization (NMF) and Silhouette width and cophenetic correlation methods determined the number of clusters. Cell types with significantly different quantities between the clusters were identified by Kruskal–Wallis H test with FDR adjustment and are presented in rows. Top color bars indicate genotypes and clusters of the samples. Color scale represents z-score. The total 215 samples include PDAC or pancreatic tissue from endpoint mice of the following genotypes: *PKras* (n = 48), *PKras;Snail*$^{KI/+}$ (n = 36), *PKras;Snail*$^{KO/KO}$ (n = 5), *PKras;Prkdc*$^{Scid/Scid}$*;Il2rg*^{null} (n = 5), *PKras;Snail*$^{KI/+}$*;Prkdc*$^{Scid/Scid}$*;Il2rg*^{null} (n = 3), *Ptf1a*$^{Cre/+}$*;LSL-Kras*^{G12D}*;LSL-Rosa26*$^{Map2k1*,EGFP/+}$ (*PKras;Map2k1**, n = 5), *Ptf1a*$^{Cre/+}$*;LSL-Kras*^{G12D}*;Map2k1*$^{lox/lox}$ (*PKras;Map2k1*$^{KO/KO}$, n = 14), *PBraf* (n = 7), *PBraf;Il2rg*$^{+/-}$ (n = 4), *PBraf;Prkdc*$^{Scid/Scid}$ (n = 7), *PBraf;Prkdc*$^{Scid/Scid}$*;Il2rg*$^{+/-}$ (n = 12), *Ptf1a*$^{Cre/+}$*;LSL-Rosa26*$^{Map2k1*,EGFP/+}$ (*PMap2k1**, n = 24), *Ptf1a*$^{Cre/+}$*;LSL-Rosa26*$^{Pik3ca*H1047R/+}$ or *Ptf1a*$^{Cre/+}$*;LSL-Rosa26*$^{Pik3ca*H1047R/Pik3ca*H1047R}$ (*PPik3ca*^{H1047R}, n = 22) and *PPik3ca*^{H1047R} with *Map2k1*$^{lox/lox}$ (*PPik3ca*^{H1047R}*;Map2k1*$^{KO/KO}$, n = 23).

Table 3-2. Significantly more abundant ImmGen cell types in different immune clusters

Phenotype marker	Cell type	Max in cluster	Adjusted p-value
CD11b$^+$Ly6G$^+$	MDSC/neutrophil	C1	6.29E-06
B220$^-$CD115$^+$CD43$^+$Ly6C$^+$MHC-II^{int}	monocyte	C1	0.0020223
c-Kit^{hi}Flt3$^+$MCSFR$^+$Sca-1$^-$	granulocyte-monocyte progenitor	C1	0.0005562
CD45.2$^+$CD8$^+$	cytotoxic T cell	C1	2.21E-06
CD45$^+$CD64$^+$F4/80^{hi}MerTK$^+$PI$^-$	macrophage	C1	1.73E-07
CD45$^+$CD64$^+$F4/80^{hi}MerTK$^+$	macrophage	C1	6.29E-06
CD45$^+$CD64$^+$F4/80^{lo}MerTK$^+$	macrophage	C1	9.54E-05
CD11a$^+$CD44$^+$CD49D$^+$CD4$^+$	effector T cell	C1	6.29E-06
CD19$^+$CD21/CD35$^+$CD23$^+$CD45R$^+$	follicular B cell	C2	6.44E-07
CD31$^+$GP38$^-$	endothelial cell	C2	6.44E-07
CD45$^-$EpCAM$^+$Ly-51$^-$MHC-II^{hi}	medullary epithelial cell	C2	2.20E-06
CD45$^-$MTS15$^+$PDGFRα$^+$	fibroblast	C2	3.70E-08
CD140a$^+$GP38$^+$	fibroblast	C2	8.48E-05
Mast$^+$	mast cell	C2	3.70E-08
CD4$^+$CD8$^+$FSC^{lo}TCR$^-$	double-positive thymocyte	C3	1.96E-10
CD8$^+$	cytotoxic T cell	C3	6.19E-07
CD11b$^+$CD4$^-$CD8a$^-$	myeloid progenitor	C3	2.26E-16
CD103$^+$CD11b$^-$CD11c$^+$Langerin$^+$MHC-II^{hi}	dendritic cell	C3	9.59E-13
α-GalCer$^+$CD1d-tet$^+$CD4$^-$TCRβ$^+$	NKT cell	C3	3.36E-10
α-GalCer$^+$CD1d-tet$^+$CD3e$^+$CD44$^+$NK1.1$^+$	NKT cell	C3	2.47E-09
CD44^{lo}CD8a$^+$CD8b$^-$TCRγ/δ$^+$Vg5$^-$	γδ T cell	C3	5.38E-05
Ly49H$^+$NK1.1$^+$	NK cell	C3	1.10E-06
CD34$^-$c-Kit$^+$FcgR$^-$Lin$^-$Sca-1$^-$	megakaryocyte-erythroid progenitor	C3	5.50E-12
CD34$^+$c-Kit$^+$Flk-2$^+$Lin$^-$Sca-1$^+$	multi-potent progenitor	C3	8.40E-15
AA4.1$^+$CD117$^+$CD19$^-$CD24$^-$CD43$^+$CD45R$^-$IgM$^-$IL7R$^-$	multi-lymphoid progenitor	C3	1.27E-08

Phenotype marker	Cell type	Max in cluster	Adjusted p-value
CD103$^-$CD11b$^+$CD11c$^+$CD24$^-$MHC-II$^+$	macrophage	C3	7.29E-10
CD24^{hi}TCRδ$^+$Vg5$^+$	γδ T cell	C3	9.12E-11
CD115$^+$Ly6C$^+$MHC-II$^+$	monocyte	C3	5.50E-12
CD117$^+$CD11b/c-CD19$^-$CD45$^+$CD4$^-$CD8$^-$FCER1A$^+$	mast cell	C3	7.06E-09
CD8$^-$	non-cytotoxic T cell	C4	2.55E-11
CD11b$^-$CD11c$^+$CD4$^-$CD8a$^-$	dendritic cell	C4	0.0002177
CD11b^{lo}CD11c$^-$F4/80^{hi}	red pulp macrophage	C4	3.75E-09
CD115$^+$CD11c$^+$F4/80^{lo}MHC-II$^+$Siglec-F$^-$	macrophage	C4	1.66E-05
CD25^{hi}CD28$^-$CD44$^-$Lin$^-$	DN3a thymocyte	C4	4.74E-10
CD25^{hi}CD28$^+$CD44$^-$Lin$^-$	DN3b thymocyte	C4	2.86E-12
CD25^{int}CD44$^+$c-Kit$^+$Lin$^-$	DN1-DN2 transitional thymocyte	C4	2.58E-12
CD25$^-$CD28$^+$CD44$^-$Lin$^-$	DN4 thymocyte	C4	7.29E-13
AA4.1$^-$CD19$^+$CD23$^-$CD43$^+$CD45R$^+$CD5$^+$IgM$^+$	B cell	C4	9.40E-17
CD103$^-$CD11b$^+$CD11c^{hi}CD45$^+$F4/80$^+$Gr-1$^-$MHC-II$^+$	macrophage	C4	7.83E-12
CD103$^-$CD11b$^+$CD11c^{hi}CD45$^+$F4/80$^+$MHC-II$^+$	macrophage	C4	3.03E-16
CD103$^-$CD11b$^+$CD11c$^+$CD24$^+$MHC-II$^+$	dendritic cell	C4	3.97E-13
CD11b$^+$CD11c^{lo}CD45$^+$Gr-1$^-$MHC-II$^+$	macrophage	C4	1.30E-09
CD11b$^+$CD169$^+$F4/80$^+$	macrophage	C4	1.06E-05
CD11b$^+$CD11c$^{int/lo}$CD64$^+$Ly6C$^+$MHC-II$^+$	monocyte	C4	4.19E-11
AA4.1$^-$CD19$^+$CD23$^+$CD24$^+$IgD$^-$IgM$^-$Igκ$^+$Igλ$^+$	memory B cell	C4	3.70E-09
CD11b$^+$CD11c$^+$CD45$^+$MHC-II^{hi}	dendritic cell	C4	4.77E-09
CD11b$^+$Siglec-F$^+$	eosinophil	C4	2.73E-15
CD4$^+$CD69$^-$CD8$^+$	double-positive thymocyte	C4	2.54E-07
CD127$^+$CD45$^+$NK1.1$^+$NKp46$^+$RORγT$^-$	innate lymphoid cell	C4	1.05E-13
CD44$^-$CD4$^+$	naive helper T cell	C4	8.99E-12
CD45.1$^-$CD45.2$^+$CD8$^+$	cytotoxic T cell	C4	3.42E-14
CD31$^+$GP38$^+$	endothelial cell	C5	0.0016001
c-Kit^{lo}Flt3$^+$MCSFR$^+$Sca-1$^-$	common dendritic cell progenitor	C5	0.0033171
CD44^{lo}CD4$^+$CD8$^-$GFP$^-$	naive helper T cell	C6	6.36E-07
CD25^{int}CD28$^+$CD44$^-$Lin$^-$	DN3-DN4 transitional thymocyte	C6	3.33E-08
CD11b$^+$CD11c^{hi}CD169$^+$	dendritic cell	C6	9.78E-13
CD24^{hi}TCRδ$^+$VG2$^+$	γδ T cell	C6	7.44E-05
CD19$^-$CD3$^-$CD45$^+$DX5$^+$NK1.1$^+$NKp46$^+$TRAIL$^-$	NK cell	C6	2.03E-05

ImmGen cell types that are estimated to be significantly more abundant in one cluster compared to the others are shown. Adjusted p-values were obtained by Kruskal–Wallis H test with FDR adjustment. hi, high; int, intermediate; lo, low; max, maximum.

To sum up, Snail defines immune landscape in PDAC and accelerates tumor progression possibly by recruiting MDSCs and TAMs to its microenvironment.

3.12 Role of Snail expression in PDAC stroma

IHC staining on human PDAC sections showed that Snail is not only expressed in tumor cells but also in stroma cells (Figure 3-18A). Therefore, Snail expression in the stroma could also have an impact on tumor progression. To evaluate such impact *in vivo*, the dual-recombinase system was used to activate Snail expression in the stroma compartment (Figure 3-18B). *Pdx1-Flp;FSF-Kras*$^{G12D/+}$ was used to induce autochthonous PDAC, and *Fsp1-Cre* was employed to target Snail expression in fibroblasts and macrophages (Schuck, 2018). Although *Fsp1-Cre* was also found to target a small amount of mesenchymal tumor cells (Chen et al., 2018b; Schuck, 2018), Snail expression in the tumor cells can be avoided because the Snail knock-in construct is flanked by two *FRT* sites and therefore deleted in all tumor cells originated from Flp-positive lineage. In addition, a double-fluorescent reporter mT-mG was used to distinguish Cre-expressing cells from other cells.

As expected, the *Pdx1-Flp;FSF-Kras*$^{G12D/+}$*;Fsp1-Cre;LSL-Rosa26*$^{Snail/mT-mG}$ mice developed full-blown PDACs, which are morphologically similar to those developed from the *Pdx1-Flp;FSF-Kras*$^{G12D/+}$ model (Figure 3-18C). Confocal microscopy showed successful recombination of mT-mG reporter in the tumor, notably in stroma cells rather than tumor cells (Figure 3-18D). Snail expression in *Pdx1-Flp;FSF-Kras*$^{G12D/+}$*;Fsp1-Cre;LSL-Rosa26*$^{Snail/mT-mG}$ tumors was also higher than tumors without Snail transgene (Figure 3-18E). Since Snail expression may not be a consequence of targeted expression in the Fsp1-positive lineage but a result of EMT, qPCR primers targeting only the Snail transgene were designed. Indeed, Snail transgene expression was observed in *Pdx1-Flp;FSF-Kras*$^{G12D/+}$*;Fsp1-Cre;LSL-Rosa26*$^{Snail/mT-mG}$ PDACs but undetectable in *Pdx1-Flp;FSF-Kras*$^{G12D/+}$*;Fsp1-Cre;LSL-Rosa26*$^{mT-mG/mT-mG}$ tumors (Figure 3-18E). However, *Pdx1-Flp;FSF-Kras*$^{G12D/+}$*;Fsp1-Cre;LSL-Rosa26*$^{Snail/mT-mG}$ mice had a median survival time of 492 days, which was close to 478 days of the *Pdx1-Flp;FSF-Kras*$^{G12D/+}$ mice (Figure 3-18F). The tumor-promoting effect of Snail therefore confines to tumor cells rather than Fsp1-positive stroma cells.

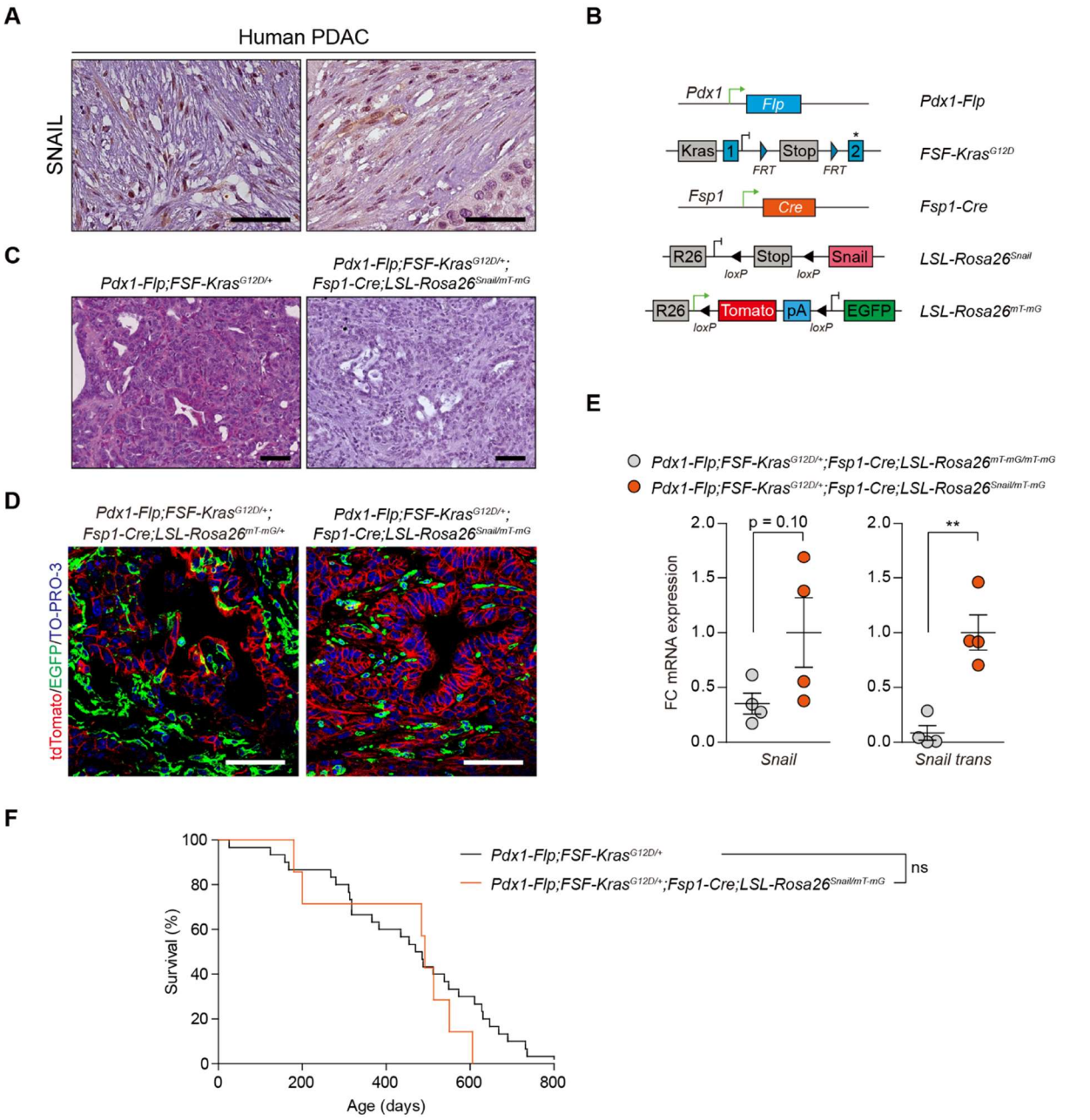

Figure 3-18. Snail expression by *Fsp1-Cre* has no effect on PDAC progression

(A) SNAIL IHC staining of human PDAC samples. Scale bars, 50 μm.

(B) Strategy to overexpress Snail with *Fsp1-Cre* in dual-recombinase PDAC model.

(C) Representative pictures of *Pdx1-Flp;FSF-Kras*$^{G12D/+}$ and *Pdx1-Flp;FSF-Kras*$^{G12D/+}$*;Fsp1-Cre;LSL-Rosa26*$^{Snail/mT-mG}$ PDACs by H&E staining. Scale bars, 50 μm.

(D) Representative confocal microscopic images of PDACs from mice of indicated genotypes. Scale bars, 50 μm.

(E) Relative *Snail* total and transgene (trans) mRNA expression level normalized to *CypA* by qPCR in PDAC tissue from mice of indicated genotypes (n = 4). Mean ± SEM; **p < 0.01, two-tailed Student's t-test. FC, fold change.

(F) Kaplan-Meier survival curves of *Pdx1-Flp;FSF-Kras*$^{G12D/+}$ (n = 30, median survival 478 days) and *Pdx1-Flp;FSF-Kras*$^{G12D/+}$*;Fsp1-Cre;LSL-Rosa26*$^{Snail/mT-mG}$ (n = 7, median survival 492 days) mice. ns, not significant, two-tailed log-rank test.

4 Discussion

The understanding of PDAC has been greatly advanced with the help of GEMMs. Nevertheless, the complex underlying molecular mechanism of tumor development and the tangled network of tumor-stroma interaction remain elusive, and the knowledge of both is critical for developing novel therapeutic approaches. Particularly, that every cancer is biologically unique calls for investigations into the effects of different driver oncogenes, which form the basis of personalized medicine. Besides, the importance of tissue specificity in tumorigenesis has been increasingly appreciated (Schneider et al., 2017).

In this study, EMT-independent functions of transcription factor Snail in PDAC was shown. Snail directly binds to promoter regions of cell cycle genes and thereby drives proliferation. Snail expression in PDAC also defines immune landscape in the microenvironment, and its recruitment of TAMs and MDSCs is likely to contribute to accelerated tumor progression. Despite being an oncogene when expressed in PDAC tumor cells, Snail does not have a strong impact in the stroma cells. Surprisingly, Snail expression in three different intestinal cancer models yielded mixed results, which highlights again the context-dependent roles of oncogenes.

4.1 Snail and EMT in pancreatic cancer

Snail has been long known as an inducer of EMT in embryonic development and cancer (Nieto et al., 2016; Thiery et al., 2009). Previous publication from the lab showed increased Snail level in an *in vivo* selection model of metastatic cancer cell line (von Burstin et al., 2009). However, the first autochthonous PDAC GEMM expressing Snail generated in the lab demonstrated that Snail accelerated tumor progression in an EMT-independent manner (Paul, 2013). Other studies in recent years also challenge the notion that EMT is required for cancer metastasis (Chen et al., 2018b; Fischer et al., 2015; Zheng et al., 2015).

Supplementing the findings by Dr. Mariel Paul, Snail expression does not lead to overt increase in tumor grading and percentage of mesenchymal cell lines. Importantly, global gene expression profiling clusters more Snail-expressing cell lines to the epithelial cluster. These findings greatly differ from previous publications showing correlation between Snail and metastasis rate in implantation models (Hsu et al., 2014; Jin et al., 2010; Liu et al., 2018; Olmeda et al., 2007a; Ye et al., 2015; Yin et al., 2007; Zhang et al., 2008). The usage of immunodeficient mice in these

studies may explain the contrasting results in the autochthonous model, as certain immune cells have metastasis-inhibiting roles (Blomberg et al., 2018; Gonzalez et al., 2018). Snail deletion also does not change tumor differentiation, and that the survival time remains unchanged is the same as in KPC model (Zheng et al., 2015). Fendrich and colleagues used the same conditional Snail knockout model but claimed to observe delayed initiation and progression of PanINs (Fendrich et al., 2018). However, the percentage of PanINs including normal ducts instead of absolute number of lesions was reported in the study, making it difficult to interpret the data. Moreover, the authors did not show comparison of survival curves. Data in this thesis also demonstrate EMT induction by TGF-β *in vitro* in both Snail-expressing and knockout cell lines, providing strong evidence that Snail is dispensable for EMT in PDAC. As a reverse correlation of Snail and E-cadherin was found across several tumor types (Batlle et al., 2000; Blanco et al., 2002), that Snail expression alone does not repress E-cadherin in PDAC (Paul, 2013) indicates that Snail expression in human disease is a result of rather than a cause for EMT. The mechanisms involved in E-cadherin repression in different organs and pathological conditions can also be different. This is supported by the absence of interaction between Snail and mSin3A in murine PDAC cell line (von Burstin et al., 2009), which was initially found in HEK 293T cells (Peinado et al., 2004). Therefore, additional mechanism in the Snail regulatory network is worth investigating.

Consistent with the finding by Dr. Mariel Paul (Paul, 2013), *Cdkn2a* locus integrity is far better preserved in Snail-expressing PDAC cell lines. A recent study made interesting links between $Kras^{G12D}$ dosage, *Cdkn2a* status and PDAC phenotypes, including cell morphology, histological grade and metastatic potential (Mueller et al., 2018). Fitting the data to the model proposed in the publication, that Snail expression does not induce EMT and metastasis can be further explained by the presence of *Cdkn2a* locus. Indeed, additional *Cdkn2a* deletion in $PKras;Snail^{KI/+}$ model leads to increased $Kras^{G12D}$ dosage, tumor grading and percentage of mesenchymal cell lines. Despite better-preserved gene locus and increased mRNA expression level, $p16^{INK4A}$ has impaired tumor suppressor function in Snail-expressing model. However, its function is not completely lost as its homozygous deletion leads to reduced survival time. Whether $p16^{INK4A}$ or $p19^{ARF}$ plays a more important role and how exactly they influence EMT in cooperation with mutant Kras remain unclear. In addition, the determination of tumor cell phenotype cannot be oversimplified to a genetic model since TGF-β treatment is able to induce EMT. Microenvironmental and epigenetic factors must be therefore also taken into consideration.

4.2 Context-dependent functions of Snail in cancer

Researchers have been increasingly aware of the tissue-specific mechanism of tumorigenesis (Schneider et al., 2017). The differences between pancreatic cancer and intestinal cancer development have been clearly demonstrated in this thesis, as Snail fuels Kras-dependent PDAC development, while the same genetic model has no, if not protective, effect in intestinal cancer. In the classical *Apc* deletion model, Snail also fails to promote cancer development. Interestingly, Snail accelerates tumor progression in another Braf-driven intestinal cancer model with serrated morphology.

One explanation for these results is the different driver oncogenes or tumor suppressor genes in different cancer types. KRAS is the leading oncogene in human PDAC (Cancer Genome Atlas Research Network, 2017; Schneider et al., 2017), while APC loss is one of the earliest and the most frequently found oncogenic event in CRC patients (Ashton-Rickardt et al., 1989; Schneider et al., 2017; Vogelstein et al., 1988). The first GEMMs for these cancers are also based on mimicking these driver genetic alterations (Hingorani et al., 2003; Moser et al., 1990). Although KRAS mutations are also common in CRC cases (Schneider et al., 2017), activating Kras mutation alone in IEC seldom allows progression into carcinoma (Bennecke et al., 2010; Davies et al., 2014). In this thesis, it is also shown that APC deletion in IEC results in much more carcinomas than Kras mutation, reaffirming the dominant role of Wnt signaling in intestinal cancer. In adult pancreas, Wnt signaling is kept low since its hyperactivation impairs pancreas formation and redirects cell fate towards intestinal differentiation (Munoz-Bravo et al., 2016; Sharon et al., 2019). However, canonical Wnt signaling is a prerequisite for $Kras^{G12D}$-dependent pancreatic carcinogenesis (Zhang et al., 2013). Therefore, it is likely to play a role in Snail-accelerated PDAC development since KEGG Wnt signaling pathway is significantly enriched in 1-month-old *PKras;Snail*$^{KI/+}$ pancreas. On the contrary, Wnt signaling is the driving force of constant self-renewal of the intestinal crypts (Pinto et al., 2003; Schepers and Clevers, 2012) and is constantly activated in the *VApc*$^{\Delta IEC}$ model, so Snail expression may have no additive effect in this regard. In addition, Snail and Wnt signaling also both promote cancer stem cell features in CRC (Fan et al., 2012; Hwang et al., 2011; Vermeulen et al., 2010).

Why Snail expression and Kras mutation in the intestine fail to recapitulate the aggressive phenotype in pancreatic cancer should have other explanations because Wnt signaling activation is not required for $Kras^{G12D}$-initiated serrated tumor (Bennecke et al., 2010). It is also puzzling that a different effect is observed in the $Braf^{V637E}$ model, as Wnt signaling induction is

substantial for Braf^{V637E}-driven tumors (Rad et al., 2013). Mutually exclusive mutations of *KRAS*, *NRAS* and *BRAF* in half of the CRC cases suggests that they share common mechanisms in tumorigenesis (Cancer Genome Atlas, 2012), but very little is known about how they differ from each other. One difference is that resistance to MEK1/2 inhibitor driven by BRAF^{V600E} but not KRAS^{G13D} amplification can be reversed by drug withdrawal (Sale et al., 2019). Besides, intestinal tumors with *KRAS* mutation are usually microsatellite stable, while *BRAF* mutant tumors typically have higher microsatellite instability (Rad et al., 2013). In microsatellite instable colon cancer cells, EMT is impaired (Pino et al., 2010). If Snail had the ability to induce EMT in intestinal cancer, shortened survival time of *VBraf^{IEC};Snail$^{IEC/+}$* mice could have been explained. However, Snail does not downregulate E-cadherin expression in any of the three models, and its aberrant expression also does not significantly increase tumor grading. Therefore, as in pancreatic cancer, Snail alone is incapable of inducing EMT in intestinal cancer. In this case, acceleration of Braf-induced intestinal tumor by Snail cannot be attributed to EMT. It will be interesting if Snail is involved in other Kras downstream pathways like PI3K pathway in intestinal cancer, which may serve as a mechanism to reverse its cooperative effect with Braf signaling.

Hence, there are similarities of Snail functions in pancreatic and intestinal cancer, however its cooperation with driver oncogenes can be substantially different in these two cancer types. It is not surprising if Snail has distinct functions in other organs, which must be assessed in a case-specific manner. To explore the possibility of targeting Snail in human CRC, exquisite experiments should be designed to mechanistically probe its roles in both classical and serrated intestinal tumors.

4.3 Cell cycle induction by Snail in pancreatic cancer

EMT-independent roles of Snail were relatively less known in the literature. Since Snail promotes locally advanced tumor rather than metastasis in the autochthonous PDAC model, noncanonical functions supporting cancer cell growth instead of plasticity are involved. Previous data in the lab showed that Snail overcomes senescence and increases proliferation (Paul, 2013). In this thesis, the mechanism of Snail-induced proliferation is explored.

As discussed in section 4.1, Snail-expressing PDAC cells have impaired p16^{INK4A} functions. In cell cycle, the tumor suppressor p16^{INK4A} guards the G_1/S entry by inhibiting the interaction between CDK4 or CDK6 with cyclin D. Non-functional p16^{INK4A} facilitates Rb phosphorylation mediated by CDK4/6-cyclin D complexes, which in turn leads to the translocation of E2F transcription factors into the nucleus and the expression of target cell cycle genes (Bardeesy et

al., 2006a; Harbour and Dean, 2000). In line with this finding, cyclin A1, A2 and B1 show gradient increase with Snail expression level in pancreatic tissue of 1-month-old mice, and the expression levels of many cell cycle genes are significantly upregulated in Snail-expressing pancreas. Publicly available ChIP-seq dataset from mouse mammary tumor cells (Ye et al., 2015) makes it possible to identify direct Snail target genes, which contain a large proportion of cell cycle genes. Of these, *Ccnb1*, *Ccnb2*, *Ccnd1*, *E2f2* and *E2f3* are verified by ChIP. Although cyclin A expression is upregulated, it is not a transcriptional target of Snail but E2F transcription factors (Yam et al., 2002). Snail thus promotes cell cycle by both impairing $p16^{INK4A}$ functions and direct transcriptional activation of cell cycle genes.

The involvement of Snail in proliferation was reported a few times, even in breast cancer where its association with EMT has been extensively studied. Ye and colleagues not only provided the ChIP-seq dataset but also linked Snail to the phenotype of basal-like breast cancer (Ye et al., 2015), a subtype known to have the highest proliferation rate and poor prognosis (Livasy et al., 2006). In breast cancer patients, Snail is associated with higher grade and proliferation rate (Lundgren et al., 2009). Mechanistically, Snail bypasses the anti-proliferative effects by wild-type p53, and the deacetylation and proteasomal degradation of p53 facilitated by Snail/HDAC1/p53 complex is essential for neoplastic epithelial cell growth (Ni et al., 2016). Genetic ablation of Snail resulted in impaired proliferative response in intestinal epithelium regeneration (Horvay et al., 2015), and Snail-mediated mitigation of the anti-proliferative effect by mTOR kinase inhibitors was observed in several human colorectal and breast cancer cell lines (Wang et al., 2017a). In pancreatic cancer, contradictory data exist. Zheng and colleagues reported increased proliferation in tumor areas but no survival change following Snail knockout in KPC model (Zheng et al., 2015). Data from this thesis also show that Snail knockout does not affect median survival time, but increase in proliferation in Snail-expressing precursor lesions is obvious (Paul, 2013). It should be noted that models with excess or insufficient amount of endogenous protein may not lead to the same conclusion, and the differences between tumor and its precursor lesions further complicate the interpretation of data.

Although Snail promotes proliferation in both breast and pancreatic cancer, distinct mechanisms are employed. Ni and colleagues showed that high Snail expression marks worse prognosis for patients with wild-type but not mutant p53 (Ni et al., 2016), a finding contradicting Dr. Mariel Paul's data that Snail accelerates PDAC progression in both p53 wild-type and mutant models (Paul, 2013). Besides, expression level of p53 is not reduced in Snail-expressing pancreas, and bypass of senescence is achieved in a p53-independent manner. Still, Snail-p53 interaction

inhibitor GN25 led to decreased proliferation in human PDAC cells and tumor growth inhibition in a xenograft model (Fendrich et al., 2018), indicating multiple mechanisms involved in Snail-induced proliferation in PDAC. Whether Snail also impairs $p16^{INK4A}$ function in breast cancer remains to be explored. Importantly, screening with human open reading frame libraries identified Snail as a pancreas-specific proliferation driver (Sack et al., 2018). Therefore, even when the same effect is observed in different tissue types, the cause can still be fundamentally different.

4.4 Snail and tumor-infiltrating immune cells

Immune cells obviously play important roles in PDAC promoted by Snail. At an early timepoint, Snail-expressing pancreas show enrichment of several key pathways related to inflammation and immune response, many of them having higher normalized enrichment score than cell cycle pathways. As high expression level of IL-6/STAT3 pathway components is observed, rapid PanIN progression and early tumor onset are at least in part attributed to Snail-driven inflammation. It should be noted that at the age of one month, pancreata from *PKras;Snail*$^{KI/+}$ mice have more and higher grade PanINs than those from *PKras* mice. However, it is difficult to compare pancreatic tissue with similar number of lesions from models with different survival times in a timepoint experiment. A better comparison will be analyzing positivity of certain markers adjacent to the same grade of lesions on IHC staining slides. Such method allows spatial analysis and visualizes immune cells surrounding or proteins secreted by neoplastic lesions, although it does not provide the sensitivity or quantitative power in qPCR or ELISA.

The pivotal role of inflammation in PDAC development makes it a promising target. While depletion of mast cells does not delay tumor progression (Schonhuber et al., 2014), severe combined immunodeficiency gains great survival benefit for *PKras;Snail*$^{KI/+}$ mice. The delayed tumor onset is not confined to *PKras;Snail*$^{KI/+}$ but also *PKras* mice. However, the survival time of *PKras* mice does not improve, likely due to their inability to combat infection. Thus, the specific immune cell population causing the effect must be discovered before the concept can be translated into clinical application. The model used in this study lacks mature B cells, T cells and NK cells due to *Prkdc*$^{Scid/Scid}$ and *Il2rg*^{null} alleles. Strikingly, depletion of B cells and T cells in *PKras;Snail*$^{KI/+}$ mice on B6 background leads to shortened survival. In the literature, B cells are known to have pro-tumor effect (Gunderson et al., 2016; Lee et al., 2016; Pylayeva-Gupta et al., 2016). Different T cell subpopulations have different prognostic values (De Monte et al., 2011; Ino et al., 2013; Nizri et al., 2018; Piro et al., 2017; Tang et al., 2014), but high level of total T

cell infiltration is associated with longer survival (Carstens et al., 2017). Since cytotoxic T cells exert the main intrinsic anti-tumor function, T cell depletion overruns the protective effect of B cell depletion. As a result, the survival time is shortened. In the case of severe combined immunodeficiency, the effect of B cell and T cell depletion is reversed by defects in NK cell functions or the mixed genetic background of the model. It is interesting to see that 6-month-old *PKras* and *PKras;Prkdc*$^{Scid/Scid}$*;Il2rg*^{null} mice do not differ in ADM and PanIN numbers, but the latter display no AFL formation. Since little is known about AFL, it is essential to study the mechanism governing the rise of this type of lesion to explain the phenotype. The genetic background can be a critical factor for tumor susceptibility, and severe combined immunodeficiency leads to reduced survival time of *PBraf* mice (unpublished observation of the lab). This not only provides evidence for the differences between tumors driven by different oncogenes but also argues for their dependence on the genetic background. Therapeutic options should also be stratified accordingly.

Flow cytometry is a golden method to analyze multiple immune cell populations from the same sample. To perform immunophenotyping in PDAC, two flow cytometry panels targeting several general immune cell populations were designed, validated and used in this study. In PDAC, Snail has a clear tendency to attract neutrophils/MDSCs, macrophages and dendritic cells, suggesting a highly immunosuppressive microenvironment.

Several publications have linked Snail to TAM recruitment and M2 polarization. Du and colleagues reported a lack of EMT but recruitment of macrophages and granulocytes in Snail-expressing epidermal keratinocytes. More interestingly, the induction of IL-6/STAT3 pathway and increased proliferation were observed in their model (Du et al., 2010). In human head and neck cancer cells, acetylation of Snail activates expression of CCL2 and CCL5, which promote the recruitment of TAMs (Hsu et al., 2014). Later, the same group showed with the same cell line that Snail induces miR-21 expression, and miR-21-abundant tumor-derived exosomes promote M2 polarization of TAMs (Hsieh et al., 2018). In this head and neck cancer model and a breast cancer model, CCR2–CCL2 axis is responsible for attracting macrophages to the tumor site (Hsu et al., 2014; Qian et al., 2011). Correspondingly, Snail-expressing pancreas also has a boost in CCR2 level in 1-month-old mice. Besides, CCR2-independent *in situ* expansion of tissue macrophages has been reported in PDAC, colon adenoma and mammary tumor (Soncin et al., 2018; Tymoszuk et al., 2014; Zhu et al., 2017). These tissue-resident macrophages promote proliferation and PDAC progression (Zhu et al., 2017). Whether Snail contributes to such mechanism is worth investigating.

Upregulation of IL-6 could attract MDSCs to the Snail-expressing pancreas as well (Bunt et al., 2007). In addition, neutrophil/MDSC recruitment by Snail via CXCR2/CXCL2 axis in ovarian and lung cancers seems to be mirrored in PDAC (Faget et al., 2017; Taki et al., 2018). Conventional dendritic cells are antigen-presenting cells to boost immune response, but regulatory dendritic cells can exhibit immunosuppressive phenotype (Shurin et al., 2013). How Snail affects dendritic cell infiltration remains unclear.

Though a relatively cheap and easy technique, flow cytometry is limited by the choice of fluorescent channels. As a result, the two panels used in this study are still far from exhausting the common immunophenotyping markers, making it impossible to analyze a lot of immune cell subsets which represent more specific functions than general populations. For example, M1 and M2 macrophages, which predict opposite clinical outcome, are not distinguished in the panel. Methods of much higher throughput, such as single-cell RNA sequencing and mass cytometry, are preferred for future studies.

Although single-cell RNA sequencing data are not commonly available, computational deconvolution methods are able to resolve bulk tumor RNA-seq data and calculate the relative amount of specific cell types using existing transcriptomic data as reference (Finotello and Trajanoski, 2018). In recent years, many methods applied to both human and mouse datasets have emerged (Bindea et al., 2013; Charoentong et al., 2017; Chen et al., 2017; Chen et al., 2018c; Newman et al., 2015; Newman et al., 2019; Thorsson et al., 2018; Wang et al., 2019). ImmGen provides expression profiles of 258 mouse cell populations in two phases of microarray experiments. Other RNA-seq datasets are also available, but the specific purposes for some datasets and inconsistencies in sequencing format make it difficult to combine them. Therefore, the microarray datasets, which contain data of the widest range of cell types in a consistent manner, were employed to deconvolute mouse bulk tumor data. Subtyping reveals homogeneous immune signatures in *PKras;Snail*$^{KI/+}$ tumors, while *PKras* tumors show great heterogeneity and are scattered into all six subtypes. This indicates again that Kras as the driver oncogene gives rise to diverged roads to PDAC and calls for comparison between the subtypes instead of simply between *PKras;Snail*$^{KI/+}$ and *PKras* tumors. Therefore, flow cytometry data will be more meaningful when the immune subtype of the *PKras* samples are known. Nevertheless, in consistency with the flow cytometry data, C3 and C4 clusters, which contain almost all *PKras;Snail*$^{KI/+}$ PDACs, are high in numbers of macrophage and dendritic cell subsets. But why neutrophils/MDSCs are highly present in C1 cannot be explained. One should be cautious that the ImmGen datasets contain much more subpopulations than the flow cytometry experiment,

so the findings should be carefully validated. Another limitation is that cells used to generate ImmGen data are typically from lymphoid tissues. It is quite likely that many will change expression profile when migrating into another organ under pathological conditions. Since a study has shown the advantage of tissue-specific signatures (Chen et al., 2019), it will be ideal to generate PDAC immune cell expression data as references for deconvolution.

In humans, a large-scale study of more than 10,000 tumors across 33 cancer types identified six immune subtypes (Thorsson et al., 2018). Most of the pancreatic cancers belong to the inflammatory subtype and show high leukocyte fraction. To this day, immuno-subtyping for human pancreatic cancer is lacking. In a recent review, Karamitopoulou summarized three immunophenotypes of pancreatic cancer, namely immune escape, immune rich and immune exhausted phenotypes, and connected them with genetic alterations and clinicopathologic characteristics (Karamitopoulou, 2019). Data from this thesis also show that immune subtypes are driven by genetics. Deep characterization of how oncogenes shape the immune landscape using GEMMs and validation in patient samples are likely to provide new solutions in personalized medicine.

4.5 Snail expression in tumor stroma

It is no surprise to find Snail expression in the stroma since it is an EMT marker. In colorectal cancer and pharyngeal squamous cell carcinoma, Snail expression in the stroma is linked to worse prognosis (Franci et al., 2009; Jouppila-Matto et al., 2011). Co-culture experiments demonstrated that Snail in fibroblasts promotes survival, proliferation and invasion of pancreatic cancer cells (Richards et al., 2017; Stanisavljevic et al., 2015). Moreover, Snail is also involved in activation of PSCs (Tian et al., 2016). However, compelling *in vivo* evidence that stromal Snail affects PDAC progression was lacking. The advent of dual-recombinase system made it possible to interrogate such functions in autochthonous models. Contrary to the findings mentioned above, expression of Snail in Fsp1-positive lineage, which includes part of the fibroblasts and macrophages (Schuck, 2018), does not change the median survival time. Since Snail has been shown to induce M2 polarization of macrophages (Zhang et al., 2016), either this is not the case or such change fails to have lasting impact during PDAC progression. Admittedly, *Fsp1-Cre* does not target all the fibroblasts or macrophages; still, a large number of stroma cells have Cre expression. Another limitation of the model is that once a cell expresses Cre, Snail is constantly expressed even if Fsp1 expression is shut down later. To specifically target tumor stroma cells, tamoxifen-inducible CreER recombinases are preferred. The effect of

Snail expression driven by several CreER lines in PDAC progression is being investigated in the lab.

4.6 Outlook

This thesis addresses the functions of Snail in pancreatic and intestinal cancer and showed its tissue-specific roles in tumor development. Special focuses of this work are EMT, cell cycle and tumor-stroma interaction, and some open questions remain for each aspect. Understanding why Snail does not downregulate E-cadherin is essential for targeting cell plasticity in cancer therapy. The regulation of co-repressors of Snail and their interaction should be studied. Especially, elucidating how $p16^{INK4A}$ and $p19^{ARF}$ are involved will provide new knowledge to the EMT field. Given the context-dependent nature of cellular processes, it is important to see if Snail binding sites in PDAC and mammary tumor cells are similar. Therefore, ChIP-seq in PDAC cells should be performed. To set Snail as the only variable in cell culture assays, cell lines with tamoxifen-inducible Snail knock-in or knockout alleles using dual-recombinase system are desired. These cell lines will be powerful tools to perform the above-mentioned experiments with clean controls.

In PDAC, Snail is a potent oncogene that shapes the immune landscape in tumor microenvironment. Flow cytometry and RNA-seq with computational method were used to analyze tumor-infiltrating immune cells. Multicolor immunofluorescence staining should be used to further validate these results as well as to visualize the spatial relationship of tumor cells and immune cells. Particularly, this technique will be useful to study how immune cell populations evolve with tumor progression. Single-cell RNA sequencing and mass cytometry can be used to analyze many more subpopulations at the same time. It is also critical to understand which chemoattractants from Snail-expressing tumor cells recruit macrophages, neutrophils/MDSCs and dendritic cells. For this purpose, secretome of Snail-expressing cell lines or organoids should be analyzed by mass spectrometry, and functional validation using co-culture systems should be performed. This study has expanded the knowledge of tumor-stroma interaction, and subsequent projects will provide valuable insights into novel therapeutic approaches to pancreatic cancer.

5 Summary

Transcription factor Snail is a prominent epithelial–mesenchymal transition (EMT) marker and is expressed in many cancer types. To study Snail function *in vivo*, a conditional overexpressing mouse model was generated in the lab. Previous data showed Snail expression in $Kras^{G12D}$-driven pancreatic ductal adenocarcinoma (PDAC) mouse model accelerated tumor progression, but surprisingly did not induce overt EMT. Proliferation was induced in Snail-expressing pancreas, but the mechanism was unknown. How Snail promotes PDAC formation through tumor-stroma interaction raised many interesting questions as well. Whether Snail has the same effect in intestinal cancer was also not clear.

In this thesis, how Snail promotes PDAC and its role in intestinal cancer was investigated using autochthonous mouse models. Snail-expressing PDAC cells did not convert to mesenchymal phenotype at least in part due to *Cdkn2a* locus retention. In pancreas, Snail led to higher expression of many cell cycle genes, and Snail binding to promoters of cell cycle genes was confirmed by analyzing publicly available chromatin immunoprecipitation (ChIP) sequencing dataset and ChIP using PDAC cell lines. In addition, gene set enrichment analysis (GSEA) showed an inflammatory microenvironment in Snail-expressing pancreas. To target inflammation, alleles responsible for severe combined immunodeficiency were introduced into the model and significantly delayed tumor onset. Interestingly, depletion of only B cells and T cells led to shorter survival time. Analysis of tumor-infiltrating immune cells revealed abundant macrophages, myeloid-derived suppressor cells (MDSCs) and dendritic cells in Snail-expressing PDAC. Snail therefore promotes PDAC by activating cell cycle, inducing inflammation and creating an immunosuppressive microenvironment. As Snail expression was also found in PDAC stroma, dual-recombinase system developed in the lab was used to target Snail expression in fibroblasts and macrophages, which had no impact on survival.

The Snail conditional expression allele was crossed into three different models to evaluate its impact on intestinal cancer. Snail accelerated $Braf^{V637E}$-dependent intestinal tumor but failed to have the same effect in models driven by $Kras^{G12D}$ mutation or APC deletion.

This work provides valuable insights into the context-dependent function of Snail in pancreatic and intestinal cancer *in vivo*. The knowledge of PDAC tumor-stroma interaction driven by Snail will create opportunities for new therapeutic strategies for this deadly disease.

Acknowledgement

I would like to express my thanks to everyone who has helped me during the time I worked on this doctoral thesis project.

First of all, I thank my supervisor Prof. Dr. Dieter Saur for giving me the opportunity to work on this project in his lab and all his support and supervision over these years. I am grateful to Prof. Angelika Schnieke and Dr. Günter Schneider for their excellent scientific input as supervisory committee members.

I especially thank Dr. Mariel Paul for generating the Snail-expressing mouse line and her data, which laid the groundwork for this project. Many thanks go to Thomas Engleitner, Xiaoxiao Zhang, Fengchong Wang and Fabio Boniolo for bioinformatics analysis, Dr. Katja Steiger, Dr. Moritz Jesinghaus and Olga Seelbach for pathological analysis, and Prof. Roland Rad's lab—especially Sebastian Müller and Dr. Rupert Öllinger—for performing aCGH and sequencing. Their diligent work created valuable data for this project.

I am also grateful to Dr. Jan Sodenkamp, Dr. Selina Keppler, Dr. Bastian Höchst and Markus Utzt for their help in flow cytometry, and the animal caretakers who took nice care of the mice. I sincerely thank Dr. Markus Tschurtschenthaler, Dr. Christian Veltkamp, Dr. Kathleen Schuck and Dr. Ankit Sinha for the fruitful discussion and all members of the Saur, Schneider, Rad and Reichert labs for the great work environment.

I would like to thank the Bayer Science & Education Foundation for awarding me the Otto Bayer Scholarship. It was a great financial help at the beginning of my thesis project.

Finally, I would like to express my deepest gratitude to my family and friends. From the bottom of my heart, I want to thank my wife Shan Huang—this thesis would not have been possible without her continuous support, encouragement and understanding.

References

Aarts, C. E. M., and Kuijpers, T. W. (2018). Neutrophils as myeloid-derived suppressor cells. Eur J Clin Invest *48 Suppl 2*, e12989.

Aguirre, A. J., Bardeesy, N., Sinha, M., Lopez, L., Tuveson, D. A., Horner, J., Redston, M. S., and DePinho, R. A. (2003). Activated Kras and Ink4a/Arf deficiency cooperate to produce metastatic pancreatic ductal adenocarcinoma. Genes Dev *17*, 3112-3126.

Ahn, Y. H., Gibbons, D. L., Chakravarti, D., Creighton, C. J., Rizvi, Z. H., Adams, H. P., Pertsemlidis, A., Gregory, P. A., Wright, J. A., Goodall, G. J.*, et al.* (2012). ZEB1 drives prometastatic actin cytoskeletal remodeling by downregulating miR-34a expression. J Clin Invest *122*, 3170-3183.

Aichler, M., Seiler, C., Tost, M., Siveke, J., Mazur, P. K., Da Silva-Buttkus, P., Bartsch, D. K., Langer, P., Chiblak, S., Durr, A.*, et al.* (2012). Origin of pancreatic ductal adenocarcinoma from atypical flat lesions: a comparative study in transgenic mice and human tissues. J Pathol *226*, 723-734.

Ali, A. I., Oliver, A. J., Samiei, T., Chan, J. D., Kershaw, M. H., and Slaney, C. Y. (2019). Genetic Redirection of T Cells for the Treatment of Pancreatic Cancer. Front Oncol *9*, 56.

Almoguera, C., Shibata, D., Forrester, K., Martin, J., Arnheim, N., and Perucho, M. (1988). Most human carcinomas of the exocrine pancreas contain mutant c-K-ras genes. Cell *53*, 549-554.

Apte, M. V., Haber, P. S., Applegate, T. L., Norton, I. D., McCaughan, G. W., Korsten, M. A., Pirola, R. C., and Wilson, J. S. (1998). Periacinar stellate shaped cells in rat pancreas: identification, isolation, and culture. Gut *43*, 128-133.

Apte, M. V., Park, S., Phillips, P. A., Santucci, N., Goldstein, D., Kumar, R. K., Ramm, G. A., Buchler, M., Friess, H., McCarroll, J. A.*, et al.* (2004). Desmoplastic reaction in pancreatic cancer: role of pancreatic stellate cells. Pancreas *29*, 179-187.

Ashton-Rickardt, P. G., Dunlop, M. G., Nakamura, Y., Morris, R. G., Purdie, C. A., Steel, C. M., Evans, H. J., Bird, C. C., and Wyllie, A. H. (1989). High frequency of APC loss in sporadic colorectal carcinoma due to breaks clustered in 5q21-22. Oncogene *4*, 1169-1174.

Bachelder, R. E., Yoon, S. O., Franci, C., de Herreros, A. G., and Mercurio, A. M. (2005). Glycogen synthase kinase-3 is an endogenous inhibitor of Snail transcription: implications for the epithelial-mesenchymal transition. J Cell Biol *168*, 29-33.

Bachem, M. G., Schneider, E., Gross, H., Weidenbach, H., Schmid, R. M., Menke, A., Siech, M., Beger, H., Grunert, A., and Adler, G. (1998). Identification, culture, and characterization of pancreatic stellate cells in rats and humans. Gastroenterology *115*, 421-432.

Bachem, M. G., Schunemann, M., Ramadani, M., Siech, M., Beger, H., Buck, A., Zhou, S., Schmid-Kotsas, A., and Adler, G. (2005). Pancreatic carcinoma cells induce fibrosis by stimulating proliferation and matrix synthesis of stellate cells. Gastroenterology *128*, 907-921.

Bailey, J. M., Hendley, A. M., Lafaro, K. J., Pruski, M. A., Jones, N. C., Alsina, J., Younes, M., Maitra, A., McAllister, F., Iacobuzio-Donahue, C. A., and Leach, S. D. (2016). p53 mutations cooperate with oncogenic Kras to promote adenocarcinoma from pancreatic ductal cells. Oncogene *35*, 4282-4288.

Bailey, J. M., Swanson, B. J., Hamada, T., Eggers, J. P., Singh, P. K., Caffery, T., Ouellette, M. M., and Hollingsworth, M. A. (2008). Sonic hedgehog promotes desmoplasia in pancreatic cancer. Clin Cancer Res *14*, 5995-6004.

Barbera, M. J., Puig, I., Dominguez, D., Julien-Grille, S., Guaita-Esteruelas, S., Peiro, S., Baulida, J., Franci, C., Dedhar, S., Larue, L., and Garcia de Herreros, A. (2004). Regulation of Snail transcription during epithelial to mesenchymal transition of tumor cells. Oncogene *23*, 7345-7354.

Bardeesy, N., Aguirre, A. J., Chu, G. C., Cheng, K. H., Lopez, L. V., Hezel, A. F., Feng, B., Brennan, C., Weissleder, R., Mahmood, U.*, et al.* (2006a). Both p16(Ink4a) and the p19(Arf)-p53 pathway constrain progression of pancreatic adenocarcinoma in the mouse. Proc Natl Acad Sci U S A *103*, 5947-5952.

Bardeesy, N., Cheng, K. H., Berger, J. H., Chu, G. C., Pahler, J., Olson, P., Hezel, A. F., Horner, J., Lauwers, G. Y., Hanahan, D., and DePinho, R. A. (2006b). Smad4 is dispensable for normal pancreas development yet critical in progression and tumor biology of pancreas cancer. Genes Dev *20*, 3130-3146.

Barilla, R. M., Diskin, B., Caso, R. C., Lee, K. B., Mohan, N., Buttar, C., Adam, S., Sekendiz, Z., Wang, J., Salas, R. D.*, et al.* (2019). Specialized dendritic cells induce tumor-promoting IL-10(+)IL-17(+) FoxP3(neg) regulatory CD4(+) T cells in pancreatic carcinoma. Nat Commun *10*, 1424.

Barker, N., Ridgway, R. A., van Es, J. H., van de Wetering, M., Begthel, H., van den Born, M., Danenberg, E., Clarke, A. R., Sansom, O. J., and Clevers, H. (2009). Crypt stem cells as the cells-of-origin of intestinal cancer. Nature *457*, 608-611.

Barker, N., van Es, J. H., Kuipers, J., Kujala, P., van den Born, M., Cozijnsen, M., Haegebarth, A., Korving, J., Begthel, H., Peters, P. J., and Clevers, H. (2007). Identification of stem cells in small intestine and colon by marker gene Lgr5. Nature *449*, 1003-1007.

Barrallo-Gimeno, A., and Nieto, M. A. (2009). Evolutionary history of the Snail/Scratch superfamily. Trends Genet *25*, 248-252.

Batlle, E., Sancho, E., Franci, C., Dominguez, D., Monfar, M., Baulida, J., and Garcia De Herreros, A. (2000). The transcription factor snail is a repressor of E-cadherin gene expression in epithelial tumour cells. Nat Cell Biol *2*, 84-89.

Bayne, L. J., Beatty, G. L., Jhala, N., Clark, C. E., Rhim, A. D., Stanger, B. Z., and Vonderheide, R. H. (2012). Tumor-derived granulocyte-macrophage colony-stimulating factor regulates myeloid inflammation and T cell immunity in pancreatic cancer. Cancer Cell *21*, 822-835.

Beatty, G. L., Chiorean, E. G., Fishman, M. P., Saboury, B., Teitelbaum, U. R., Sun, W., Huhn, R. D., Song, W., Li, D., Sharp, L. L.*, et al.* (2011). CD40 agonists alter tumor stroma and show efficacy against pancreatic carcinoma in mice and humans. Science *331*, 1612-1616.

Bellone, G., Turletti, A., Artusio, E., Mareschi, K., Carbone, A., Tibaudi, D., Robecchi, A., Emanuelli, G., and Rodeck, U. (1999). Tumor-associated transforming growth factor-beta and interleukin-10 contribute to a systemic Th2 immune phenotype in pancreatic carcinoma patients. Am J Pathol *155*, 537-547.

Benjamini, Y., and Hochberg, Y. (1995). Controlling the false discovery rate: A practical and powerful approach to multiple testing. Journal of the Royal Statistical Society *57*, 289-300.

Bennecke, M., Kriegl, L., Bajbouj, M., Retzlaff, K., Robine, S., Jung, A., Arkan, M. C., Kirchner, T., and Greten, F. R. (2010). Ink4a/Arf and oncogene-induced senescence prevent tumor progression during alternative colorectal tumorigenesis. Cancer Cell *18*, 135-146.

Berlin, J. D., Catalano, P., Thomas, J. P., Kugler, J. W., Haller, D. G., and Benson, A. B., 3rd (2002). Phase III study of gemcitabine in combination with fluorouracil versus gemcitabine alone in patients with advanced pancreatic carcinoma: Eastern Cooperative Oncology Group Trial E2297. J Clin Oncol *20*, 3270-3275.

Berrington de Gonzalez, A., Sweetland, S., and Spencer, E. (2003). A meta-analysis of obesity and the risk of pancreatic cancer. Br J Cancer *89*, 519-523.

Bhowmick, N. A., Chytil, A., Plieth, D., Gorska, A. E., Dumont, N., Shappell, S., Washington, M. K., Neilson, E. G., and Moses, H. L. (2004). TGF-beta signaling in fibroblasts modulates the oncogenic potential of adjacent epithelia. Science *303*, 848-851.

Bienz, M., and Clevers, H. (2000). Linking colorectal cancer to Wnt signaling. Cell *103*, 311-320.

Bindea, G., Mlecnik, B., Tosolini, M., Kirilovsky, A., Waldner, M., Obenauf, A. C., Angell, H., Fredriksen, T., Lafontaine, L., Berger, A.*, et al.* (2013). Spatiotemporal dynamics of intratumoral immune cells reveal the immune landscape in human cancer. Immunity *39*, 782-795.

Blanco, M. J., Moreno-Bueno, G., Sarrio, D., Locascio, A., Cano, A., Palacios, J., and Nieto, M. A. (2002). Correlation of Snail expression with histological grade and lymph node status in breast carcinomas. Oncogene *21*, 3241-3246.

Blando, J., Sharma, A., Higa, M. G., Zhao, H., Vence, L., Yadav, S. S., Kim, J., Sepulveda, A. M., Sharp, M., Maitra, A.*, et al.* (2019). Comparison of immune infiltrates in melanoma and pancreatic cancer highlights VISTA as a potential target in pancreatic cancer. Proc Natl Acad Sci U S A *116*, 1692-1697.

Blomberg, O. S., Spagnuolo, L., and de Visser, K. E. (2018). Immune regulation of metastasis: mechanistic insights and therapeutic opportunities. Dis Model Mech *11*.

Blunt, T., Finnie, N. J., Taccioli, G. E., Smith, G. C., Demengeot, J., Gottlieb, T. M., Mizuta, R., Varghese, A. J., Alt, F. W., Jeggo, P. A., and Jackson, S. P. (1995). Defective DNA-dependent protein kinase activity is linked to V(D)J recombination and DNA repair defects associated with the murine scid mutation. Cell *80*, 813-823.

Bokemeyer, C., Bondarenko, I., Makhson, A., Hartmann, J. T., Aparicio, J., de Braud, F., Donea, S., Ludwig, H., Schuch, G., Stroh, C.*, et al.* (2009). Fluorouracil, leucovorin, and oxaliplatin with and without cetuximab in the first-line treatment of metastatic colorectal cancer. J Clin Oncol *27*, 663-671.

Bolstad, B. M., Irizarry, R. A., Astrand, M., and Speed, T. P. (2003). A comparison of normalization methods for high density oligonucleotide array data based on variance and bias. Bioinformatics *19*, 185-193.

Borgoni, S., Iannello, A., Cutrupi, S., Allavena, P., D'Incalci, M., Novelli, F., and Cappello, P. (2018). Depletion of tumor-associated macrophages switches the epigenetic profile of pancreatic cancer infiltrating T cells and restores their anti-tumor phenotype. Oncoimmunology *7*, e1393596.

Bornstein, S., White, R., Malkoski, S., Oka, M., Han, G., Cleaver, T., Reh, D., Andersen, P., Gross, N., Olson, S.*, et al.* (2009). Smad4 loss in mice causes spontaneous head and neck cancer with increased genomic instability and inflammation. J Clin Invest *119*, 3408-3419.

Bosma, G. C., Custer, R. P., and Bosma, M. J. (1983). A severe combined immunodeficiency mutation in the mouse. Nature *301*, 527-530.

Boutet, A., De Frutos, C. A., Maxwell, P. H., Mayol, M. J., Romero, J., and Nieto, M. A. (2006). Snail activation disrupts tissue homeostasis and induces fibrosis in the adult kidney. EMBO J *25*, 5603-5613.

Bracken, C. P., Gregory, P. A., Kolesnikoff, N., Bert, A. G., Wang, J., Shannon, M. F., and Goodall, G. J. (2008). A double-negative feedback loop between ZEB1-SIP1 and the microRNA-200 family regulates epithelial-mesenchymal transition. Cancer Res *68*, 7846-7854.

Bray, F., Ferlay, J., Soerjomataram, I., Siegel, R. L., Torre, L. A., and Jemal, A. (2018). Global cancer statistics 2018: GLOBOCAN estimates of incidence and mortality worldwide for 36 cancers in 185 countries. CA Cancer J Clin *68*, 394-424.

Bronte, V., Brandau, S., Chen, S. H., Colombo, M. P., Frey, A. B., Greten, T. F., Mandruzzato, S., Murray, P. J., Ochoa, A., Ostrand-Rosenberg, S.*, et al.* (2016). Recommendations for myeloid-derived suppressor cell nomenclature and characterization standards. Nat Commun *7*, 12150.

Brunet, J. P., Tamayo, P., Golub, T. R., and Mesirov, J. P. (2004). Metagenes and molecular pattern discovery using matrix factorization. Proc Natl Acad Sci U S A *101*, 4164-4169.

Bunt, S. K., Yang, L., Sinha, P., Clements, V. K., Leips, J., and Ostrand-Rosenberg, S. (2007). Reduced inflammation in the tumor microenvironment delays the accumulation of myeloid-derived suppressor cells and limits tumor progression. Cancer Res *67*, 10019-10026.

Burk, U., Schubert, J., Wellner, U., Schmalhofer, O., Vincan, E., Spaderna, S., and Brabletz, T. (2008). A reciprocal repression between ZEB1 and members of the miR-200 family promotes EMT and invasion in cancer cells. EMBO Rep *9*, 582-589.

Burris, H. A., 3rd, Moore, M. J., Andersen, J., Green, M. R., Rothenberg, M. L., Modiano, M. R., Cripps, M. C., Portenoy, R. K., Storniolo, A. M., Tarassoff, P.*, et al.* (1997). Improvements in survival and clinical benefit with gemcitabine as first-line therapy for patients with advanced pancreas cancer: a randomized trial. J Clin Oncol *15*, 2403-2413.

Burt, R. W. (2000). Colon cancer screening. Gastroenterology *119*, 837-853.

Caldas, C., Hahn, S. A., da Costa, L. T., Redston, M. S., Schutte, M., Seymour, A. B., Weinstein, C. L., Hruban, R. H., Yeo, C. J., and Kern, S. E. (1994). Frequent somatic mutations and homozygous deletions of the p16 (MTS1) gene in pancreatic adenocarcinoma. Nat Genet *8*, 27-32.

Cancer Genome Atlas, N. (2012). Comprehensive molecular characterization of human colon and rectal cancer. Nature *487*, 330-337.

Cancer Genome Atlas Research Network (2017). Integrated Genomic Characterization of Pancreatic Ductal Adenocarcinoma. Cancer Cell *32*, 185-203 e113.

Cano, A., Perez-Moreno, M. A., Rodrigo, I., Locascio, A., Blanco, M. J., del Barrio, M. G., Portillo, F., and Nieto, M. A. (2000). The transcription factor snail controls epithelial-mesenchymal transitions by repressing E-cadherin expression. Nat Cell Biol *2*, 76-83.

Cao, X., Shores, E. W., Hu-Li, J., Anver, M. R., Kelsall, B. L., Russell, S. M., Drago, J., Noguchi, M., Grinberg, A., Bloom, E. T., and et al. (1995). Defective lymphoid development in mice lacking expression of the common cytokine receptor gamma chain. Immunity *2*, 223-238.

Carlyle, J. R., Mesci, A., Ljutic, B., Belanger, S., Tai, L. H., Rousselle, E., Troke, A. D., Proteau, M. F., and Makrigiannis, A. P. (2006). Molecular and genetic basis for strain-dependent NK1.1 alloreactivity of mouse NK cells. J Immunol *176*, 7511-7524.

Carstens, J. L., Correa de Sampaio, P., Yang, D., Barua, S., Wang, H., Rao, A., Allison, J. P., LeBleu, V. S., and Kalluri, R. (2017). Spatial computation of intratumoral T cells correlates with survival of patients with pancreatic cancer. Nat Commun *8*, 15095.

Carver, E. A., Jiang, R., Lan, Y., Oram, K. F., and Gridley, T. (2001). The mouse snail gene encodes a key regulator of the epithelial-mesenchymal transition. Mol Cell Biol *21*, 8184-8188.

Chalise, P., and Fridley, B. L. (2017). Integrative clustering of multi-level 'omic data based on non-negative matrix factorization algorithm. PLoS One *12*, e0176278.

Chames, P., Kerfelec, B., and Baty, D. (2010). Therapeutic antibodies for the treatment of pancreatic cancer. ScientificWorldJournal *10*, 1107-1120.

Charoentong, P., Finotello, F., Angelova, M., Mayer, C., Efremova, M., Rieder, D., Hackl, H., and Trajanoski, Z. (2017). Pan-cancer Immunogenomic Analyses Reveal Genotype-Immunophenotype Relationships and Predictors of Response to Checkpoint Blockade. Cell Rep *18*, 248-262.

Chen, C., Zhao, S., Karnad, A., and Freeman, J. W. (2018a). The biology and role of CD44 in cancer progression: therapeutic implications. J Hematol Oncol *11*, 64.

Chen, Y., LeBleu, V. S., Carstens, J. L., Sugimoto, H., Zheng, X., Malasi, S., Saur, D., and Kalluri, R. (2018b). Dual reporter genetic mouse models of pancreatic cancer identify an epithelial-to-mesenchymal transition-independent metastasis program. EMBO Mol Med *10*.

Chen, Z., Huang, A., Sun, J., Jiang, T., Qin, F. X., and Wu, A. (2017). Inference of immune cell composition on the expression profiles of mouse tissue. Sci Rep *7*, 40508.

Chen, Z., Ji, C., Shen, Q., Liu, W., Qin, F. X., and Wu, A. (2019). Tissue-specific deconvolution of immune cell composition by integrating bulk and single-cell transcriptomes. Bioinformatics.

Chen, Z., Quan, L., Huang, A., Zhao, Q., Yuan, Y., Yuan, X., Shen, Q., Shang, J., Ben, Y., Qin, F. X., and Wu, A. (2018c). seq-ImmuCC: Cell-Centric View of Tissue Transcriptome Measuring Cellular Compositions of Immune Microenvironment From Mouse RNA-Seq Data. Front Immunol *9*, 1286.

Cheng, C. W., Wu, P. E., Yu, J. C., Huang, C. S., Yue, C. T., Wu, C. W., and Shen, C. Y. (2001). Mechanisms of inactivation of E-cadherin in breast carcinoma: modification of the two-hit hypothesis of tumor suppressor gene. Oncogene *20*, 3814-3823.

Cheng, J. C., Klausen, C., and Leung, P. C. (2010). Hydrogen peroxide mediates EGF-induced down-regulation of E-cadherin expression via p38 MAPK and snail in human ovarian cancer cells. Mol Endocrinol *24*, 1569-1580.

Cheung, A. F., Carter, A. M., Kostova, K. K., Woodruff, J. F., Crowley, D., Bronson, R. T., Haigis, K. M., and Jacks, T. (2010). Complete deletion of Apc results in severe polyposis in mice. Oncogene *29*, 1857-1864.

Choi, J. E., Bae, J. S., Kang, M. J., Chung, M. J., Jang, K. Y., Park, H. S., and Moon, W. S. (2017). Expression of epithelial-mesenchymal transition and cancer stem cell markers in colorectal adenocarcinoma: Clinicopathological significance. Oncol Rep *38*, 1695-1705.

Choudhury, G. G., Karamitsos, C., Hernandez, J., Gentilini, A., Bardgette, J., and Abboud, H. E. (1997). PI-3-kinase and MAPK regulate mesangial cell proliferation and migration in response to PDGF. Am J Physiol *273*, F931-938.

Cicchini, C., Filippini, D., Coen, S., Marchetti, A., Cavallari, C., Laudadio, I., Spagnoli, F. M., Alonzi, T., and Tripodi, M. (2006). Snail controls differentiation of hepatocytes by repressing HNF4alpha expression. J Cell Physiol *209*, 230-238.

Ciruna, B., and Rossant, J. (2001). FGF signaling regulates mesoderm cell fate specification and morphogenetic movement at the primitive streak. Dev Cell *1*, 37-49.

Clark, C. E., Hingorani, S. R., Mick, R., Combs, C., Tuveson, D. A., and Vonderheide, R. H. (2007). Dynamics of the immune reaction to pancreatic cancer from inception to invasion. Cancer Res *67*, 9518-9527.

Colucci, G., Labianca, R., Di Costanzo, F., Gebbia, V., Carteni, G., Massidda, B., Dapretto, E., Manzione, L., Piazza, E., Sannicolo, M.*, et al.* (2010). Randomized phase III trial of gemcitabine plus cisplatin compared with single-agent gemcitabine as first-line treatment of patients with advanced pancreatic cancer: the GIP-1 study. J Clin Oncol *28*, 1645-1651.

Conroy, T., Desseigne, F., Ychou, M., Bouche, O., Guimbaud, R., Becouarn, Y., Adenis, A., Raoul, J. L., Gourgou-Bourgade, S., de la Fouchardiere, C*., et al.* (2011). FOLFIRINOX versus gemcitabine for metastatic pancreatic cancer. N Engl J Med *364*, 1817-1825.

Cooper, C. L., O'Toole, S. A., and Kench, J. G. (2013). Classification, morphology and molecular pathology of premalignant lesions of the pancreas. Pathology *45*, 286-304.

Cunningham, F., Amode, M. R., Barrell, D., Beal, K., Billis, K., Brent, S., Carvalho-Silva, D., Clapham, P., Coates, G., Fitzgerald, S*., et al.* (2015). Ensembl 2015. Nucleic Acids Res *43*, D662-669.

Daley, D., Mani, V. R., Mohan, N., Akkad, N., Pandian, G., Savadkar, S., Lee, K. B., Torres-Hernandez, A., Aykut, B., Diskin, B*., et al.* (2017). NLRP3 signaling drives macrophage-induced adaptive immune suppression in pancreatic carcinoma. J Exp Med *214*, 1711-1724.

Davies, E. J., Marsh Durban, V., Meniel, V., Williams, G. T., and Clarke, A. R. (2014). PTEN loss and KRAS activation leads to the formation of serrated adenomas and metastatic carcinoma in the mouse intestine. J Pathol *233*, 27-38.

De Craene, B., Gilbert, B., Stove, C., Bruyneel, E., van Roy, F., and Berx, G. (2005). The transcription factor snail induces tumor cell invasion through modulation of the epithelial cell differentiation program. Cancer Res *65*, 6237-6244.

De Monte, L., Reni, M., Tassi, E., Clavenna, D., Papa, I., Recalde, H., Braga, M., Di Carlo, V., Doglioni, C., and Protti, M. P. (2011). Intratumor T helper type 2 cell infiltrate correlates with cancer-associated fibroblast thymic stromal lymphopoietin production and reduced survival in pancreatic cancer. J Exp Med *208*, 469-478.

De Rosa, M., Pace, U., Rega, D., Costabile, V., Duraturo, F., Izzo, P., and Delrio, P. (2015). Genetics, diagnosis and management of colorectal cancer (Review). Oncol Rep *34*, 1087-1096.

de Vries, A., Flores, E. R., Miranda, B., Hsieh, H. M., van Oostrom, C. T., Sage, J., and Jacks, T. (2002). Targeted point mutations of p53 lead to dominant-negative inhibition of wild-type p53 function. Proc Natl Acad Sci U S A *99*, 2948-2953.

Diaz-Montero, C. M., Salem, M. L., Nishimura, M. I., Garrett-Mayer, E., Cole, D. J., and Montero, A. J. (2009). Increased circulating myeloid-derived suppressor cells correlate with clinical cancer stage, metastatic tumor burden, and doxorubicin-cyclophosphamide chemotherapy. Cancer Immunol Immunother *58*, 49-59.

Dietrich, W. F., Lander, E. S., Smith, J. S., Moser, A. R., Gould, K. A., Luongo, C., Borenstein, N., and Dove, W. (1993). Genetic identification of Mom-1, a major modifier locus affecting Min-induced intestinal neoplasia in the mouse. Cell *75*, 631-639.

Dobin, A., Davis, C. A., Schlesinger, F., Drenkow, J., Zaleski, C., Jha, S., Batut, P., Chaisson, M., and Gingeras, T. R. (2013). STAR: ultrafast universal RNA-seq aligner. Bioinformatics *29*, 15-21.

Dong, C., Yuan, T., Wu, Y., Wang, Y., Fan, T. W., Miriyala, S., Lin, Y., Yao, J., Shi, J., Kang, T*., et al.* (2013). Loss of FBP1 by Snail-mediated repression provides metabolic advantages in basal-like breast cancer. Cancer Cell *23*, 316-331.

Du, F., Nakamura, Y., Tan, T. L., Lee, P., Lee, R., Yu, B., and Jamora, C. (2010). Expression of snail in epidermal keratinocytes promotes cutaneous inflammation and hyperplasia conducive to tumor formation. Cancer research *70*, 10080-10089.

Dyck, L., and Mills, K. H. G. (2017). Immune checkpoints and their inhibition in cancer and infectious diseases. Eur J Immunol *47*, 765-779.

Dymecki, S. M., and Tomasiewicz, H. (1998). Using Flp-recombinase to characterize expansion of Wnt1-expressing neural progenitors in the mouse. Dev Biol *201*, 57-65.

Elloul, S., Elstrand, M. B., Nesland, J. M., Trope, C. G., Kvalheim, G., Goldberg, I., Reich, R., and Davidson, B. (2005). Snail, Slug, and Smad-interacting protein 1 as novel parameters of disease aggressiveness in metastatic ovarian and breast carcinoma. Cancer *103*, 1631-1643.

Elyada, E., Bolisetty, M., Laise, P., Flynn, W. F., Courtois, E. T., Burkhart, R. A., Teinor, J. A., Belleau, P., Biffi, G., Lucito, M. S.*, et al.* (2019). Cross-Species Single-Cell Analysis of Pancreatic Ductal Adenocarcinoma Reveals Antigen-Presenting Cancer-Associated Fibroblasts. Cancer Discov *9*, 1102-1123.

Ene-Obong, A., Clear, A. J., Watt, J., Wang, J., Fatah, R., Riches, J. C., Marshall, J. F., Chin-Aleong, J., Chelala, C., Gribben, J. G.*, et al.* (2013). Activated pancreatic stellate cells sequester CD8+ T cells to reduce their infiltration of the juxtatumoral compartment of pancreatic ductal adenocarcinoma. Gastroenterology *145*, 1121-1132.

Erkan, M., Hausmann, S., Michalski, C. W., Fingerle, A. A., Dobritz, M., Kleeff, J., and Friess, H. (2012). The role of stroma in pancreatic cancer: diagnostic and therapeutic implications. Nat Rev Gastroenterol Hepatol *9*, 454-467.

Erkan, M., Kleeff, J., Gorbachevski, A., Reiser, C., Mitkus, T., Esposito, I., Giese, T., Buchler, M. W., Giese, N. A., and Friess, H. (2007). Periostin creates a tumor-supportive microenvironment in the pancreas by sustaining fibrogenic stellate cell activity. Gastroenterology *132*, 1447-1464.

Erkan, M., Michalski, C. W., Rieder, S., Reiser-Erkan, C., Abiatari, I., Kolb, A., Giese, N. A., Esposito, I., Friess, H., and Kleeff, J. (2008). The activated stroma index is a novel and independent prognostic marker in pancreatic ductal adenocarcinoma. Clin Gastroenterol Hepatol *6*, 1155-1161.

Everhart, J., and Wright, D. (1995). Diabetes mellitus as a risk factor for pancreatic cancer. A meta-analysis. JAMA *273*, 1605-1609.

Faget, J., Groeneveld, S., Boivin, G., Sankar, M., Zangger, N., Garcia, M., Guex, N., Zlobec, I., Steiner, L., Piersigilli, A.*, et al.* (2017). Neutrophils and Snail Orchestrate the Establishment of a Pro-tumor Microenvironment in Lung Cancer. Cell Rep *21*, 3190-3204.

Fan, F., Samuel, S., Evans, K. W., Lu, J., Xia, L., Zhou, Y., Sceusi, E., Tozzi, F., Ye, X. C., Mani, S. A., and Ellis, L. M. (2012). Overexpression of snail induces epithelial-mesenchymal transition and a cancer stem cell-like phenotype in human colorectal cancer cells. Cancer Med *1*, 5-16.

Fearon, E. R., and Vogelstein, B. (1990). A genetic model for colorectal tumorigenesis. Cell *61*, 759-767.

Feig, C., Gopinathan, A., Neesse, A., Chan, D. S., Cook, N., and Tuveson, D. A. (2012). The pancreas cancer microenvironment. Clin Cancer Res *18*, 4266-4276.

Feldmann, G., and Maitra, A. (2008). Molecular genetics of pancreatic ductal adenocarcinomas and recent implications for translational efforts. J Mol Diagn *10*, 111-122.

Fendrich, V., Jendryschek, F., Beeck, S., Albers, M., Lauth, M., Esni, F., Heeger, K., Dengler, J., Slater, E. P., Holler, J. P. N.*, et al.* (2018). Genetic and pharmacologic abrogation of Snail1

inhibits acinar-to-ductal metaplasia in precursor lesions of pancreatic ductal adenocarcinoma and pancreatic injury. Oncogene *37*, 1845-1856.

Ferreira, R. M. M., Sancho, R., Messal, H. A., Nye, E., Spencer-Dene, B., Stone, R. K., Stamp, G., Rosewell, I., Quaglia, A., and Behrens, A. (2017). Duct- and Acinar-Derived Pancreatic Ductal Adenocarcinomas Show Distinct Tumor Progression and Marker Expression. Cell Rep *21*, 966-978.

Fevr, T., Robine, S., Louvard, D., and Huelsken, J. (2007). Wnt/beta-catenin is essential for intestinal homeostasis and maintenance of intestinal stem cells. Mol Cell Biol *27*, 7551-7559.

Finotello, F., and Trajanoski, Z. (2018). Quantifying tumor-infiltrating immune cells from transcriptomics data. Cancer Immunol Immunother *67*, 1031-1040.

Fischer, K. R., Durrans, A., Lee, S., Sheng, J., Li, F., Wong, S. T., Choi, H., El Rayes, T., Ryu, S., Troeger, J.*, et al.* (2015). Epithelial-to-mesenchymal transition is not required for lung metastasis but contributes to chemoresistance. Nature *527*, 472-476.

Fodde, R., Edelmann, W., Yang, K., van Leeuwen, C., Carlson, C., Renault, B., Breukel, C., Alt, E., Lipkin, M., Khan, P. M., and et al. (1994). A targeted chain-termination mutation in the mouse Apc gene results in multiple intestinal tumors. Proc Natl Acad Sci U S A *91*, 8969-8973.

Forghanifard, M. M., Ardalan Khales, S., Farshchian, M., Rad, A., Homayouni-Tabrizi, M., and Abbaszadegan, M. R. (2017). Negative Regulatory Role of TWIST1 on SNAIL Gene Expression. Pathol Oncol Res *23*, 85-90.

Franci, C., Gallen, M., Alameda, F., Baro, T., Iglesias, M., Virtanen, I., and Garcia de Herreros, A. (2009). Snail1 protein in the stroma as a new putative prognosis marker for colon tumours. PLoS One *4*, e5595.

Friedman, J., Hastie, T., and Tibshirani, R. (2010). Regularization Paths for Generalized Linear Models via Coordinate Descent. J Stat Softw *33*, 1-22.

Froeling, F. E., Feig, C., Chelala, C., Dobson, R., Mein, C. E., Tuveson, D. A., Clevers, H., Hart, I. R., and Kocher, H. M. (2011). Retinoic acid-induced pancreatic stellate cell quiescence reduces paracrine Wnt-beta-catenin signaling to slow tumor progression. Gastroenterology *141*, 1486-1497, 1497 e1481-1414.

Fuchs, C. S., Colditz, G. A., Stampfer, M. J., Giovannucci, E. L., Hunter, D. J., Rimm, E. B., Willett, W. C., and Speizer, F. E. (1996). A prospective study of cigarette smoking and the risk of pancreatic cancer. Arch Intern Med *156*, 2255-2260.

Fujita, N., Jaye, D. L., Kajita, M., Geigerman, C., Moreno, C. S., and Wade, P. A. (2003). MTA3, a Mi-2/NuRD complex subunit, regulates an invasive growth pathway in breast cancer. Cell *113*, 207-219.

Fujiwara, S., Corbo, J. C., and Levine, M. (1998). The snail repressor establishes a muscle/notochord boundary in the Ciona embryo. Development *125*, 2511-2520.

Fukuda, A., Wang, S. C., Morris, J. P. t., Folias, A. E., Liou, A., Kim, G. E., Akira, S., Boucher, K. M., Firpo, M. A., Mulvihill, S. J., and Hebrok, M. (2011). Stat3 and MMP7 contribute to pancreatic ductal adenocarcinoma initiation and progression. Cancer Cell *19*, 441-455.

Fuse, N., Hirose, S., and Hayashi, S. (1994). Diploidy of Drosophila imaginal cells is maintained by a transcriptional repressor encoded by escargot. Genes Dev *8*, 2270-2281.

Futterman, M. A., Garcia, A. J., and Zamir, E. A. (2011). Evidence for partial epithelial-to-mesenchymal transition (pEMT) and recruitment of motile blastoderm edge cells during avian epiboly. Dev Dyn *240*, 1502-1511.

Gabitass, R. F., Annels, N. E., Stocken, D. D., Pandha, H. A., and Middleton, G. W. (2011). Elevated myeloid-derived suppressor cells in pancreatic, esophageal and gastric cancer are an independent prognostic factor and are associated with significant elevation of the Th2 cytokine interleukin-13. Cancer Immunol Immunother *60*, 1419-1430.

Gapstur, S. M., Gann, P. H., Lowe, W., Liu, K., Colangelo, L., and Dyer, A. (2000). Abnormal glucose metabolism and pancreatic cancer mortality. JAMA *283*, 2552-2558.

Gentleman, R. C., Carey, V. J., Bates, D. M., Bolstad, B., Dettling, M., Dudoit, S., Ellis, B., Gautier, L., Ge, Y., Gentry, J.*, et al.* (2004). Bioconductor: open software development for computational biology and bioinformatics. Genome Biol *5*, R80.

Gerbe, F., van Es, J. H., Makrini, L., Brulin, B., Mellitzer, G., Robine, S., Romagnolo, B., Shroyer, N. F., Bourgaux, J. F., Pignodel, C.*, et al.* (2011). Distinct ATOH1 and Neurog3 requirements define tuft cells as a new secretory cell type in the intestinal epithelium. J Cell Biol *192*, 767-780.

Giakoustidis, A., Neofytou, K., Costa Neves, M., Giakoustidis, D., Louri, E., Cunningham, D., and Mudan, S. (2018). Identifying the role of neutrophil-to-lymphocyte ratio and platelets-to-lymphocyte ratio as prognostic markers in patients undergoing resection of pancreatic ductal adenocarcinoma. Ann Hepatobiliary Pancreat Surg *22*, 197-207.

Gilkes, D. M., Semenza, G. L., and Wirtz, D. (2014). Hypoxia and the extracellular matrix: drivers of tumour metastasis. Nat Rev Cancer *14*, 430-439.

Gill, J. G., Langer, E. M., Lindsley, R. C., Cai, M., Murphy, T. L., Kyba, M., and Murphy, K. M. (2011). Snail and the microRNA-200 family act in opposition to regulate epithelial-to-mesenchymal transition and germ layer fate restriction in differentiating ESCs. Stem Cells *29*, 764-776.

Gnerlich, J. L., Mitchem, J. B., Weir, J. S., Sankpal, N. V., Kashiwagi, H., Belt, B. A., Porembka, M. R., Herndon, J. M., Eberlein, T. J., Goedegebuure, P., and Linehan, D. C. (2010). Induction of Th17 cells in the tumor microenvironment improves survival in a murine model of pancreatic cancer. J Immunol *185*, 4063-4071.

Gonzalez, H., Hagerling, C., and Werb, Z. (2018). Roles of the immune system in cancer: from tumor initiation to metastatic progression. Genes Dev *32*, 1267-1284.

Grande, M. T., Sanchez-Laorden, B., Lopez-Blau, C., De Frutos, C. A., Boutet, A., Arevalo, M., Rowe, R. G., Weiss, S. J., Lopez-Novoa, J. M., and Nieto, M. A. (2015). Snail1-induced partial epithelial-to-mesenchymal transition drives renal fibrosis in mice and can be targeted to reverse established disease. Nat Med *21*, 989-997.

Grau, Y., Carteret, C., and Simpson, P. (1984). Mutations and Chromosomal Rearrangements Affecting the Expression of Snail, a Gene Involved in Embryonic Patterning in DROSOPHILA MELANOGASTER. Genetics *108*, 347-360.

Gregory, P. A., Bert, A. G., Paterson, E. L., Barry, S. C., Tsykin, A., Farshid, G., Vadas, M. A., Khew-Goodall, Y., and Goodall, G. J. (2008). The miR-200 family and miR-205 regulate epithelial to mesenchymal transition by targeting ZEB1 and SIP1. Nat Cell Biol *10*, 593-601.

Grigore, A. D., Jolly, M. K., Jia, D., Farach-Carson, M. C., and Levine, H. (2016). Tumor Budding: The Name is EMT. Partial EMT. J Clin Med *5*.

Guaita, S., Puig, I., Franci, C., Garrido, M., Dominguez, D., Batlle, E., Sancho, E., Dedhar, S., De Herreros, A. G., and Baulida, J. (2002). Snail induction of epithelial to mesenchymal transition in tumor cells is accompanied by MUC1 repression and ZEB1 expression. J Biol Chem *277*, 39209-39216.

Guerra, C., Schuhmacher, A. J., Canamero, M., Grippo, P. J., Verdaguer, L., Perez-Gallego, L., Dubus, P., Sandgren, E. P., and Barbacid, M. (2007). Chronic pancreatitis is essential for induction of pancreatic ductal adenocarcinoma by K-Ras oncogenes in adult mice. Cancer Cell *11*, 291-302.

Gunderson, A. J., Kaneda, M. M., Tsujikawa, T., Nguyen, A. V., Affara, N. I., Ruffell, B., Gorjestani, S., Liudahl, S. M., Truitt, M., Olson, P.*, et al.* (2016). Bruton Tyrosine Kinase-Dependent Immune Cell Cross-talk Drives Pancreas Cancer. Cancer Discov *6*, 270-285.

Halbrook, C. J., Pontious, C., Kovalenko, I., Lapienyte, L., Dreyer, S., Lee, H. J., Thurston, G., Zhang, Y., Lazarus, J., Sajjakulnukit, P.*, et al.* (2019). Macrophage-Released Pyrimidines Inhibit Gemcitabine Therapy in Pancreatic Cancer. Cell Metab *29*, 1390-1399 e1396.

Hang, J., Wu, L., Zhu, L., Sun, Z., Wang, G., Pan, J., Zheng, S., Xu, K., Du, J., and Jiang, H. (2018). Prediction of overall survival for metastatic pancreatic cancer: Development and validation of a prognostic nomogram with data from open clinical trial and real-world study. Cancer Med.

Hao, Z., and Rajewsky, K. (2001). Homeostasis of peripheral B cells in the absence of B cell influx from the bone marrow. J Exp Med *194*, 1151-1164.

Harbour, J. W., and Dean, D. C. (2000). The Rb/E2F pathway: expanding roles and emerging paradigms. Genes Dev *14*, 2393-2409.

Hargadon, K. M., Johnson, C. E., and Williams, C. J. (2018). Immune checkpoint blockade therapy for cancer: An overview of FDA-approved immune checkpoint inhibitors. Int Immunopharmacol *62*, 29-39.

He, S., Fei, M., Wu, Y., Zheng, D., Wan, D., Wang, L., and Li, D. (2011). Distribution and clinical significance of Th17 cells in the tumor microenvironment and peripheral blood of pancreatic cancer patients. Int J Mol Sci *12*, 7424-7437.

He, T. C., Sparks, A. B., Rago, C., Hermeking, H., Zawel, L., da Costa, L. T., Morin, P. J., Vogelstein, B., and Kinzler, K. W. (1998). Identification of c-MYC as a target of the APC pathway. Science *281*, 1509-1512.

Herranz, N., Pasini, D., Diaz, V. M., Franci, C., Gutierrez, A., Dave, N., Escriva, M., Hernandez-Munoz, I., Di Croce, L., Helin, K.*, et al.* (2008). Polycomb complex 2 is required for E-cadherin repression by the Snail1 transcription factor. Mol Cell Biol *28*, 4772-4781.

Herrmann, R., Bodoky, G., Ruhstaller, T., Glimelius, B., Bajetta, E., Schuller, J., Saletti, P., Bauer, J., Figer, A., Pestalozzi, B.*, et al.* (2007). Gemcitabine plus capecitabine compared with gemcitabine alone in advanced pancreatic cancer: a randomized, multicenter, phase III trial of the Swiss Group for Clinical Cancer Research and the Central European Cooperative Oncology Group. J Clin Oncol *25*, 2212-2217.

Hezel, A. F., Kimmelman, A. C., Stanger, B. Z., Bardeesy, N., and Depinho, R. A. (2006). Genetics and biology of pancreatic ductal adenocarcinoma. Genes & development *20*, 1218-1249.

Hingorani, S. R., Petricoin, E. F., Maitra, A., Rajapakse, V., King, C., Jacobetz, M. A., Ross, S., Conrads, T. P., Veenstra, T. D., Hitt, B. A.*, et al.* (2003). Preinvasive and invasive ductal pancreatic cancer and its early detection in the mouse. Cancer Cell *4*, 437-450.

Hingorani, S. R., Wang, L., Multani, A. S., Combs, C., Deramaudt, T. B., Hruban, R. H., Rustgi, A. K., Chang, S., and Tuveson, D. A. (2005). Trp53R172H and KrasG12D cooperate to promote chromosomal instability and widely metastatic pancreatic ductal adenocarcinoma in mice. Cancer Cell *7*, 469-483.

Hirooka, S., Yanagimoto, H., Satoi, S., Yamamoto, T., Toyokawa, H., Yamaki, S., Yui, R., Inoue, K., Michiura, T., and Kwon, A. H. (2011). The role of circulating dendritic cells in patients with unresectable pancreatic cancer. Anticancer Res *31*, 3827-3834.

Horvay, K., Jarde, T., Casagranda, F., Perreau, V. M., Haigh, K., Nefzger, C. M., Akhtar, R., Gridley, T., Berx, G., Haigh, J. J.*, et al.* (2015). Snai1 regulates cell lineage allocation and stem cell maintenance in the mouse intestinal epithelium. EMBO J *34*, 1319-1335.

Hotz, B., Arndt, M., Dullat, S., Bhargava, S., Buhr, H. J., and Hotz, H. G. (2007). Epithelial to mesenchymal transition: expression of the regulators snail, slug, and twist in pancreatic cancer. Clin Cancer Res *13*, 4769-4776.

Hou, Z., Peng, H., Ayyanathan, K., Yan, K. P., Langer, E. M., Longmore, G. D., and Rauscher, F. J., 3rd (2008). The LIM protein AJUBA recruits protein arginine methyltransferase 5 to mediate SNAIL-dependent transcriptional repression. Mol Cell Biol *28*, 3198-3207.

Hruban, R. H., Adsay, N. V., Albores-Saavedra, J., Compton, C., Garrett, E. S., Goodman, S. N., Kern, S. E., Klimstra, D. S., Kloppel, G., Longnecker, D. S.*, et al.* (2001). Pancreatic intraepithelial neoplasia: a new nomenclature and classification system for pancreatic duct lesions. Am J Surg Pathol *25*, 579-586.

Hruban, R. H., Goggins, M., Parsons, J., and Kern, S. E. (2000). Progression model for pancreatic cancer. Clin Cancer Res *6*, 2969-2972.

Hruban, R. H., Maitra, A., and Goggins, M. (2008). Update on pancreatic intraepithelial neoplasia. Int J Clin Exp Pathol *1*, 306-316.

Hruban, R. H., Maitra, A., Kern, S. E., and Goggins, M. (2007). Precursors to pancreatic cancer. Gastroenterol Clin North Am *36*, 831-849, vi.

Hsieh, C. H., Tai, S. K., and Yang, M. H. (2018). Snail-overexpressing Cancer Cells Promote M2-Like Polarization of Tumor-Associated Macrophages by Delivering MiR-21-Abundant Exosomes. Neoplasia *20*, 775-788.

Hsu, D. S., Wang, H. J., Tai, S. K., Chou, C. H., Hsieh, C. H., Chiu, P. H., Chen, N. J., and Yang, M. H. (2014). Acetylation of snail modulates the cytokinome of cancer cells to enhance the recruitment of macrophages. Cancer Cell *26*, 534-548.

Hu, H., Jiao, F., Han, T., and Wang, L. W. (2015). Functional significance of macrophages in pancreatic cancer biology. Tumour Biol *36*, 9119-9126.

Huang, B., Pan, P. Y., Li, Q., Sato, A. I., Levy, D. E., Bromberg, J., Divino, C. M., and Chen, S. H. (2006). Gr-1+CD115+ immature myeloid suppressor cells mediate the development of tumor-induced T regulatory cells and T-cell anergy in tumor-bearing host. Cancer Res *66*, 1123-1131.

Hurwitz, H., Fehrenbacher, L., Novotny, W., Cartwright, T., Hainsworth, J., Heim, W., Berlin, J., Baron, A., Griffing, S., Holmgren, E.*, et al.* (2004). Bevacizumab plus irinotecan, fluorouracil, and leucovorin for metastatic colorectal cancer. N Engl J Med *350*, 2335-2342.

Hwang, R. F., Moore, T., Arumugam, T., Ramachandran, V., Amos, K. D., Rivera, A., Ji, B., Evans, D. B., and Logsdon, C. D. (2008). Cancer-associated stromal fibroblasts promote pancreatic tumor progression. Cancer research *68*, 918-926.

Hwang, W. L., Yang, M. H., Tsai, M. L., Lan, H. Y., Su, S. H., Chang, S. C., Teng, H. W., Yang, S. H., Lan, Y. T., Chiou, S. H., and Wang, H. W. (2011). SNAIL regulates interleukin-8 expression, stem cell-like activity, and tumorigenicity of human colorectal carcinoma cells. Gastroenterology *141*, 279-291, 291 e271-275.

Ikenouchi, J., Matsuda, M., Furuse, M., and Tsukita, S. (2003). Regulation of tight junctions during the epithelium-mesenchyme transition: direct repression of the gene expression of claudins/occludin by Snail. J Cell Sci *116*, 1959-1967.

Ino, Y., Yamazaki-Itoh, R., Shimada, K., Iwasaki, M., Kosuge, T., Kanai, Y., and Hiraoka, N. (2013). Immune cell infiltration as an indicator of the immune microenvironment of pancreatic cancer. Br J Cancer *108*, 914-923.

Irizarry, R. A., Bolstad, B. M., Collin, F., Cope, L. M., Hobbs, B., and Speed, T. P. (2003). Summaries of Affymetrix GeneChip probe level data. Nucleic Acids Res *31*, e15.

Isaac, A., Cohn, M. J., Ashby, P., Ataliotis, P., Spicer, D. B., Cooke, J., and Tickle, C. (2000). FGF and genes encoding transcription factors in early limb specification. Mech Dev *93*, 41-48.

Izeradjene, K., Combs, C., Best, M., Gopinathan, A., Wagner, A., Grady, W. M., Deng, C. X., Hruban, R. H., Adsay, N. V., Tuveson, D. A., and Hingorani, S. R. (2007). Kras(G12D) and Smad4/Dpc4 haploinsufficiency cooperate to induce mucinous cystic neoplasms and invasive adenocarcinoma of the pancreas. Cancer Cell *11*, 229-243.

Jackson, E. L., Willis, N., Mercer, K., Bronson, R. T., Crowley, D., Montoya, R., Jacks, T., and Tuveson, D. A. (2001). Analysis of lung tumor initiation and progression using conditional expression of oncogenic K-ras. Genes Dev *15*, 3243-3248.

Jackstadt, R., and Sansom, O. J. (2016). Mouse models of intestinal cancer. J Pathol *238*, 141-151.

Jamora, C., Lee, P., Kocieniewski, P., Azhar, M., Hosokawa, R., Chai, Y., and Fuchs, E. (2005). A signaling pathway involving TGF-beta2 and snail in hair follicle morphogenesis. PLoS Biol *3*, e11.

Jang, J. E., Hajdu, C. H., Liot, C., Miller, G., Dustin, M. L., and Bar-Sagi, D. (2017). Crosstalk between Regulatory T Cells and Tumor-Associated Dendritic Cells Negates Anti-tumor Immunity in Pancreatic Cancer. Cell Rep *20*, 558-571.

Jass, J. R. (2007). Classification of colorectal cancer based on correlation of clinical, morphological and molecular features. Histopathology *50*, 113-130.

Jaster, R., Sparmann, G., Emmrich, J., and Liebe, S. (2002). Extracellular signal regulated kinases are key mediators of mitogenic signals in rat pancreatic stellate cells. Gut *51*, 579-584.

Jemal, A., Bray, F., Center, M. M., Ferlay, J., Ward, E., and Forman, D. (2011). Global cancer statistics. CA Cancer J Clin *61*, 69-90.

Jiang, R., Copeland, N. G., Gilbert, D. J., Jenkins, N. A., and Gridley, T. (1997). Genomic organization and chromosomal localization of the mouse snail (Sna) gene. Mamm Genome *8*, 686-688.

Jiang, R., Lan, Y., Norton, C. R., Sundberg, J. P., and Gridley, T. (1998). The Slug gene is not essential for mesoderm or neural crest development in mice. Dev Biol *198*, 277-285.

Jiang, Y., Zhao, X., Xiao, Q., Liu, Q., Ding, K., Yu, F., Zhang, R., Zhu, T., and Ge, G. (2014). Snail and Slug mediate tamoxifen resistance in breast cancer cells through activation of EGFR-ERK independent of epithelial-mesenchymal transition. J Mol Cell Biol *6*, 352-354.

Jin, H., Yu, Y., Zhang, T., Zhou, X., Zhou, J., Jia, L., Wu, Y., Zhou, B. P., and Feng, Y. (2010). Snail is critical for tumor growth and metastasis of ovarian carcinoma. Int J Cancer *126*, 2102-2111.

Johnson, C. M., Wei, C., Ensor, J. E., Smolenski, D. J., Amos, C. I., Levin, B., and Berry, D. A. (2013). Meta-analyses of colorectal cancer risk factors. Cancer Causes Control *24*, 1207-1222.

Jouppila-Matto, A., Narkio-Makela, M., Soini, Y., Pukkila, M., Sironen, R., Tuhkanen, H., Mannermaa, A., and Kosma, V. M. (2011). Twist and snai1 expression in pharyngeal squamous cell carcinoma stroma is related to cancer progression. BMC Cancer *11*, 350.

Kalluri, R., and Weinberg, R. A. (2009). The basics of epithelial-mesenchymal transition. J Clin Invest *119*, 1420-1428.

Kanda, M., Matthaei, H., Wu, J., Hong, S. M., Yu, J., Borges, M., Hruban, R. H., Maitra, A., Kinzler, K., Vogelstein, B., and Goggins, M. (2012). Presence of somatic mutations in most early-stage pancreatic intraepithelial neoplasia. Gastroenterology *142*, 730-733 e739.

Kang, R., Loux, T., Tang, D., Schapiro, N. E., Vernon, P., Livesey, K. M., Krasinskas, A., Lotze, M. T., and Zeh, H. J., 3rd (2012). The expression of the receptor for advanced glycation endproducts (RAGE) is permissive for early pancreatic neoplasia. Proc Natl Acad Sci U S A *109*, 7031-7036.

Karamitopoulou, E. (2019). Tumour microenvironment of pancreatic cancer: immune landscape is dictated by molecular and histopathological features. Br J Cancer *121*, 5-14.

Kataoka, H., Murayama, T., Yokode, M., Mori, S., Sano, H., Ozaki, H., Yokota, Y., Nishikawa, S., and Kita, T. (2000). A novel snail-related transcription factor Smuc regulates basic helix-loop-helix transcription factor activities via specific E-box motifs. Nucleic Acids Res *28*, 626-633.

Kenkel, J. A., Tseng, W. W., Davidson, M. G., Tolentino, L. L., Choi, O., Bhattacharya, N., Seeley, E. S., Winer, D. A., Reticker-Flynn, N. E., and Engleman, E. G. (2017). An Immunosuppressive Dendritic Cell Subset Accumulates at Secondary Sites and Promotes Metastasis in Pancreatic Cancer. Cancer Res *77*, 4158-4170.

Kikuta, K., Masamune, A., Watanabe, T., Ariga, H., Itoh, H., Hamada, S., Satoh, K., Egawa, S., Unno, M., and Shimosegawa, T. (2010). Pancreatic stellate cells promote epithelial-mesenchymal transition in pancreatic cancer cells. Biochem Biophys Res Commun *403*, 380-384.

Kiss, K., Baghy, K., Spisak, S., Szanyi, S., Tulassay, Z., Zalatnai, A., Lohr, J. M., Jesenofsky, R., Kovalszky, I., and Firneisz, G. (2015). Chronic hyperglycemia induces trans-differentiation of human pancreatic stellate cells and enhances the malignant molecular communication with human pancreatic cancer cells. PLoS One *10*, e0128059.

Knab, L. M., Ebine, K., Chow, C. R., Raza, S. S., Sahai, V., Patel, A. P., Kumar, K., Bentrem, D. J., Grippo, P. J., and Munshi, H. G. (2014). Snail cooperates with Kras G12D in vivo to increase stem cell factor and enhance mast cell infiltration. Mol Cancer Res *12*, 1440-1448.

Knight, R. D., and Shimeld, S. M. (2001). Identification of conserved C2H2 zinc-finger gene families in the Bilateria. Genome Biol *2*, RESEARCH0016.

Kopp, J. L., von Figura, G., Mayes, E., Liu, F. F., Dubois, C. L., Morris, J. P. t., Pan, F. C., Akiyama, H., Wright, C. V., Jensen, K.*, et al.* (2012). Identification of Sox9-dependent acinar-to-ductal reprogramming as the principal mechanism for initiation of pancreatic ductal adenocarcinoma. Cancer Cell *22*, 737-750.

Korinek, V., Barker, N., Morin, P. J., van Wichen, D., de Weger, R., Kinzler, K. W., Vogelstein, B., and Clevers, H. (1997). Constitutive transcriptional activation by a beta-catenin-Tcf complex in APC-/- colon carcinoma. Science *275*, 1784-1787.

Kosinski, C., Li, V. S., Chan, A. S., Zhang, J., Ho, C., Tsui, W. Y., Chan, T. L., Mifflin, R. C., Powell, D. W., Yuen, S. T.*, et al.* (2007). Gene expression patterns of human colon tops and basal crypts and BMP antagonists as intestinal stem cell niche factors. Proc Natl Acad Sci U S A *104*, 15418-15423.

Krebs, A. M., Mitschke, J., Lasierra Losada, M., Schmalhofer, O., Boerries, M., Busch, H., Boettcher, M., Mougiakakos, D., Reichardt, W., Bronsert, P.*, et al.* (2017). The EMT-activator Zeb1 is a key factor for cell plasticity and promotes metastasis in pancreatic cancer. Nat Cell Biol *19*, 518-529.

Krimpenfort, P., Quon, K. C., Mooi, W. J., Loonstra, A., and Berns, A. (2001). Loss of p16Ink4a confers susceptibility to metastatic melanoma in mice. Nature *413*, 83-86.

Kudo-Saito, C., Shirako, H., Takeuchi, T., and Kawakami, Y. (2009). Cancer metastasis is accelerated through immunosuppression during Snail-induced EMT of cancer cells. Cancer Cell *15*, 195-206.

Kurahara, H., Shinchi, H., Mataki, Y., Maemura, K., Noma, H., Kubo, F., Sakoda, M., Ueno, S., Natsugoe, S., and Takao, S. (2011). Significance of M2-polarized tumor-associated macrophage in pancreatic cancer. J Surg Res *167*, e211-219.

Lander, R., Nasr, T., Ochoa, S. D., Nordin, K., Prasad, M. S., and Labonne, C. (2013). Interactions between Twist and other core epithelial-mesenchymal transition factors are controlled by GSK3-mediated phosphorylation. Nat Commun *4*, 1542.

Lee, K. E., Spata, M., Bayne, L. J., Buza, E. L., Durham, A. C., Allman, D., Vonderheide, R. H., and Simon, M. C. (2016). Hif1a Deletion Reveals Pro-Neoplastic Function of B Cells in Pancreatic Neoplasia. Cancer Discov *6*, 256-269.

Leptin, M., and Grunewald, B. (1990). Cell shape changes during gastrulation in Drosophila. Development *110*, 73-84.

Leroy, P., and Mostov, K. E. (2007). Slug is required for cell survival during partial epithelial-mesenchymal transition of HGF-induced tubulogenesis. Mol Biol Cell *18*, 1943-1952.

Lesina, M., Kurkowski, M. U., Ludes, K., Rose-John, S., Treiber, M., Kloppel, G., Yoshimura, A., Reindl, W., Sipos, B., Akira, S.*, et al.* (2011). Stat3/Socs3 activation by IL-6 transsignaling promotes progression of pancreatic intraepithelial neoplasia and development of pancreatic cancer. Cancer Cell *19*, 456-469.

Leystra, A. A., Deming, D. A., Zahm, C. D., Farhoud, M., Olson, T. J., Hadac, J. N., Nettekoven, L. A., Albrecht, D. M., Clipson, L., Sullivan, R.*, et al.* (2012). Mice expressing activated PI3K rapidly develop advanced colon cancer. Cancer Res *72*, 2931-2936.

Li, W. Q., Kawakami, K., Ruszkiewicz, A., Bennett, G., Moore, J., and Iacopetta, B. (2006). BRAF mutations are associated with distinctive clinical, pathological and molecular features of colorectal cancer independently of microsatellite instability status. Mol Cancer *5*, 2.

Li, X., Xiang, Y., Li, F., Yin, C., Li, B., and Ke, X. (2019). WNT/beta-Catenin Signaling Pathway Regulating T Cell-Inflammation in the Tumor Microenvironment. Front Immunol *10*, 2293.

Lievre, A., Bachet, J. B., Le Corre, D., Boige, V., Landi, B., Emile, J. F., Cote, J. F., Tomasic, G., Penna, C., Ducreux, M.*, et al.* (2006). KRAS mutation status is predictive of response to cetuximab therapy in colorectal cancer. Cancer Res *66*, 3992-3995.

Ligorio, M., Sil, S., Malagon-Lopez, J., Nieman, L. T., Misale, S., Di Pilato, M., Ebright, R. Y., Karabacak, M. N., Kulkarni, A. S., Liu, A.*, et al.* (2019). Stromal Microenvironment Shapes the Intratumoral Architecture of Pancreatic Cancer. Cell *178*, 160-175 e127.

Lin, Y., Wu, Y., Li, J., Dong, C., Ye, X., Chi, Y. I., Evers, B. M., and Zhou, B. P. (2010). The SNAG domain of Snail1 functions as a molecular hook for recruiting lysine-specific demethylase 1. EMBO J *29*, 1803-1816.

Liu, G., McDonnell, T. J., Montes de Oca Luna, R., Kapoor, M., Mims, B., El-Naggar, A. K., and Lozano, G. (2000). High metastatic potential in mice inheriting a targeted p53 missense mutation. Proc Natl Acad Sci U S A *97*, 4174-4179.

Liu, Y., Zhou, H., Zhu, R., Ding, F., Li, Y., Cao, X., and Liu, Z. (2018). SPSB3 targets SNAIL for degradation in GSK-3beta phosphorylation-dependent manner and regulates metastasis. Oncogene *37*, 768-776.

Livak, K. J., and Schmittgen, T. D. (2001). Analysis of relative gene expression data using real-time quantitative PCR and the 2(-Delta Delta C(T)) Method. Methods *25*, 402-408.

Livasy, C. A., Karaca, G., Nanda, R., Tretiakova, M. S., Olopade, O. I., Moore, D. T., and Perou, C. M. (2006). Phenotypic evaluation of the basal-like subtype of invasive breast carcinoma. Mod Pathol *19*, 264-271.

Lonardo, E., Frias-Aldeguer, J., Hermann, P. C., and Heeschen, C. (2012). Pancreatic stellate cells form a niche for cancer stem cells and promote their self-renewal and invasiveness. Cell Cycle *11*, 1282-1290.

Louvet, C., Labianca, R., Hammel, P., Lledo, G., Zampino, M. G., Andre, T., Zaniboni, A., Ducreux, M., Aitini, E., Taieb, J.*, et al.* (2005). Gemcitabine in combination with oxaliplatin compared with gemcitabine alone in locally advanced or metastatic pancreatic cancer: results of a GERCOR and GISCAD phase III trial. J Clin Oncol *23*, 3509-3516.

Lu, Z., Ghosh, S., Wang, Z., and Hunter, T. (2003). Downregulation of caveolin-1 function by EGF leads to the loss of E-cadherin, increased transcriptional activity of beta-catenin, and enhanced tumor cell invasion. Cancer Cell *4*, 499-515.

Lundgren, K., Nordenskjold, B., and Landberg, G. (2009). Hypoxia, Snail and incomplete epithelial-mesenchymal transition in breast cancer. Br J Cancer *101*, 1769-1781.

Madison, B. B., Dunbar, L., Qiao, X. T., Braunstein, K., Braunstein, E., and Gumucio, D. L. (2002). Cis elements of the villin gene control expression in restricted domains of the vertical (crypt) and horizontal (duodenum, cecum) axes of the intestine. J Biol Chem *277*, 33275-33283.

Makinen, M. J. (2007). Colorectal serrated adenocarcinoma. Histopathology *50*, 131-150.

Malka, D., Rotolo, F., and Boige, V. (2017). First-line treatment in metastatic colorectal cancer: Important or crucial? Eur J Cancer *84*, 363-366.

Malumbres, M., and Barbacid, M. (2003). RAS oncogenes: the first 30 years. Nat Rev Cancer *3*, 459-465.

Mani, S. A., Guo, W., Liao, M. J., Eaton, E. N., Ayyanan, A., Zhou, A. Y., Brooks, M., Reinhard, F., Zhang, C. C., Shipitsin, M.*, et al.* (2008). The epithelial-mesenchymal transition generates cells with properties of stem cells. Cell *133*, 704-715.

Mao, L., Merlo, A., Bedi, G., Shapiro, G. I., Edwards, C. D., Rollins, B. J., and Sidransky, D. (1995). A novel p16INK4A transcript. Cancer Res *55*, 2995-2997.

Markowitz, S., Wang, J., Myeroff, L., Parsons, R., Sun, L., Lutterbaugh, J., Fan, R. S., Zborowska, E., Kinzler, K. W., Vogelstein, B., and et al. (1995). Inactivation of the type II TGF-beta receptor in colon cancer cells with microsatellite instability. Science *268*, 1336-1338.

Martin, T. A., Goyal, A., Watkins, G., and Jiang, W. G. (2005). Expression of the transcription factors snail, slug, and twist and their clinical significance in human breast cancer. Ann Surg Oncol *12*, 488-496.

Masamune, A., Kikuta, K., Watanabe, T., Satoh, K., Hirota, M., Hamada, S., and Shimosegawa, T. (2009). Fibrinogen induces cytokine and collagen production in pancreatic stellate cells. Gut *58*, 550-559.

Masamune, A., Watanabe, T., Kikuta, K., Satoh, K., and Shimosegawa, T. (2008). NADPH oxidase plays a crucial role in the activation of pancreatic stellate cells. Am J Physiol Gastrointest Liver Physiol *294*, G99-G108.

Mauhin, V., Lutz, Y., Dennefeld, C., and Alberga, A. (1993). Definition of the DNA-binding site repertoire for the Drosophila transcription factor SNAIL. Nucleic Acids Res *21*, 3951-3957.

Mazur, P. K., Einwachter, H., Lee, M., Sipos, B., Nakhai, H., Rad, R., Zimber-Strobl, U., Strobl, L. J., Radtke, F., Kloppel, G.*, et al.* (2010). Notch2 is required for progression of pancreatic intraepithelial neoplasia and development of pancreatic ductal adenocarcinoma. Proc Natl Acad Sci U S A *107*, 13438-13443.

McGuigan, A., Kelly, P., Turkington, R. C., Jones, C., Coleman, H. G., and McCain, R. S. (2018). Pancreatic cancer: A review of clinical diagnosis, epidemiology, treatment and outcomes. World J Gastroenterol *24*, 4846-4861.

Medema, J. P., and Vermeulen, L. (2011). Microenvironmental regulation of stem cells in intestinal homeostasis and cancer. Nature *474*, 318-326.

Michaud, D. S., Giovannucci, E., Willett, W. C., Colditz, G. A., Stampfer, M. J., and Fuchs, C. S. (2001). Physical activity, obesity, height, and the risk of pancreatic cancer. JAMA *286*, 921-929.

Millanes-Romero, A., Herranz, N., Perrera, V., Iturbide, A., Loubat-Casanovas, J., Gil, J., Jenuwein, T., Garcia de Herreros, A., and Peiro, S. (2013). Regulation of heterochromatin transcription by Snail1/LOXL2 during epithelial-to-mesenchymal transition. Mol Cell *52*, 746-757.

Mitra, D., Fernandez, P., Bian, L., Song, N., Li, F., Han, G., and Wang, X. J. (2013). Smad4 loss in mouse keratinocytes leads to increased susceptibility to UV carcinogenesis with reduced Ercc1-mediated DNA repair. J Invest Dermatol *133*, 2609-2616.

Montero, J. A., Ganan, Y., Macias, D., Rodriguez-Leon, J., Sanz-Ezquerro, J. J., Merino, R., Chimal-Monroy, J., Nieto, M. A., and Hurle, J. M. (2001). Role of FGFs in the control of programmed cell death during limb development. Development *128*, 2075-2084.

Moody, S. E., Perez, D., Pan, T. C., Sarkisian, C. J., Portocarrero, C. P., Sterner, C. J., Notorfrancesco, K. L., Cardiff, R. D., and Chodosh, L. A. (2005). The transcriptional repressor Snail promotes mammary tumor recurrence. Cancer Cell *8*, 197-209.

Moparthi, L., and Koch, S. (2019). Wnt signaling in intestinal inflammation. Differentiation *108*, 24-32.

Morin, P. J., Sparks, A. B., Korinek, V., Barker, N., Clevers, H., Vogelstein, B., and Kinzler, K. W. (1997). Activation of beta-catenin-Tcf signaling in colon cancer by mutations in beta-catenin or APC. Science *275*, 1787-1790.

Morris, J. P. t., Wang, S. C., and Hebrok, M. (2010). KRAS, Hedgehog, Wnt and the twisted developmental biology of pancreatic ductal adenocarcinoma. Nat Rev Cancer *10*, 683-695.

Moser, A. R., Mattes, E. M., Dove, W. F., Lindstrom, M. J., Haag, J. D., and Gould, M. N. (1993). ApcMin, a mutation in the murine Apc gene, predisposes to mammary carcinomas and focal alveolar hyperplasias. Proc Natl Acad Sci U S A *90*, 8977-8981.

Moser, A. R., Pitot, H. C., and Dove, W. F. (1990). A dominant mutation that predisposes to multiple intestinal neoplasia in the mouse. Science *247*, 322-324.

Mueller, S., Engleitner, T., Maresch, R., Zukowska, M., Lange, S., Kaltenbacher, T., Konukiewitz, B., Ollinger, R., Zwiebel, M., Strong, A.*, et al.* (2018). Evolutionary routes and KRAS dosage define pancreatic cancer phenotypes. Nature *554*, 62-68.

Mummert, M. E., Mummert, D., Edelbaum, D., Hui, F., Matsue, H., and Takashima, A. (2002). Synthesis and surface expression of hyaluronan by dendritic cells and its potential role in antigen presentation. J Immunol *169*, 4322-4331.

Munoz-Bravo, J. L., Flores-Martinez, A., Herrero-Martin, G., Puri, S., Taketo, M. M., Rojas, A., Hebrok, M., and Cano, D. A. (2016). Loss of Pancreas upon Activated Wnt Signaling Is Concomitant with Emergence of Gastrointestinal Identity. PLoS One *11*, e0164714.

Murray, S. A., Carver, E. A., and Gridley, T. (2006). Generation of a Snail1 (Snai1) conditional null allele. Genesis *44*, 7-11.

Muzumdar, M. D., Tasic, B., Miyamichi, K., Li, L., and Luo, L. (2007). A global double-fluorescent Cre reporter mouse. Genesis *45*, 593-605.

Nakamura, R., Ishii, H., Endo, K., Hotta, A., Fujii, E., Miyazawa, K., and Saitoh, M. (2018). Reciprocal expression of Slug and Snail in human oral cancer cells. PLoS One *13*, e0199442.

Nakhai, H., Sel, S., Favor, J., Mendoza-Torres, L., Paulsen, F., Duncker, G. I., and Schmid, R. M. (2007). Ptf1a is essential for the differentiation of GABAergic and glycinergic amacrine cells and horizontal cells in the mouse retina. Development *134*, 1151-1160.

Newman, A. M., Liu, C. L., Green, M. R., Gentles, A. J., Feng, W., Xu, Y., Hoang, C. D., Diehn, M., and Alizadeh, A. A. (2015). Robust enumeration of cell subsets from tissue expression profiles. Nat Methods *12*, 453-457.

Newman, A. M., Steen, C. B., Liu, C. L., Gentles, A. J., Chaudhuri, A. A., Scherer, F., Khodadoust, M. S., Esfahani, M. S., Luca, B. A., Steiner, D.*, et al.* (2019). Determining cell type abundance and expression from bulk tissues with digital cytometry. Nat Biotechnol *37*, 773-782.

Ni, T., Li, X. Y., Lu, N., An, T., Liu, Z. P., Fu, R., Lv, W. C., Zhang, Y. W., Xu, X. J., Grant Rowe, R.*, et al.* (2016). Snail1-dependent p53 repression regulates expansion and activity of tumour-initiating cells in breast cancer. Nat Cell Biol *18*, 1221-1232.

Nielsen, S. R., Quaranta, V., Linford, A., Emeagi, P., Rainer, C., Santos, A., Ireland, L., Sakai, T., Sakai, K., Kim, Y. S.*, et al.* (2016). Macrophage-secreted granulin supports pancreatic cancer metastasis by inducing liver fibrosis. Nat Cell Biol *18*, 549-560.

Nieto, M. A. (2002). The snail superfamily of zinc-finger transcription factors. Nature reviews Molecular cell biology *3*, 155-166.

Nieto, M. A., Bennett, M. F., Sargent, M. G., and Wilkinson, D. G. (1992). Cloning and developmental expression of Sna, a murine homologue of the Drosophila snail gene. Development *116*, 227-237.

Nieto, M. A., Huang, R. Y., Jackson, R. A., and Thiery, J. P. (2016). Emt: 2016. Cell *166*, 21-45.

Nizri, E., Sternbach, N., Bar-David, S., Ben-Yehuda, A., Gerstenhaber, F., Ofir, T., Wolf, I., Weiner, G., Lahat, G., and Klausner, J. (2018). T-Helper 1 Immune Response in Metastatic Lymph Nodes of Pancreatic Ductal Adenocarcinoma: A Marker For Prolonged Survival. Ann Surg Oncol *25*, 475-481.

Novellasdemunt, L., Antas, P., and Li, V. S. (2015). Targeting Wnt signaling in colorectal cancer. A Review in the Theme: Cell Signaling: Proteins, Pathways and Mechanisms. Am J Physiol Cell Physiol *309*, C511-521.

Nusslein-Volhard, C., Wieschaus, E., and Kluding, H. (1984). Mutations affecting the pattern of the larval cuticle inDrosophila melanogaster : I. Zygotic loci on the second chromosome. Wilehm Roux Arch Dev Biol *193*, 267-282.

Nywening, T. M., Belt, B. A., Cullinan, D. R., Panni, R. Z., Han, B. J., Sanford, D. E., Jacobs, R. C., Ye, J., Patel, A. A., Gillanders, W. E.*, et al.* (2018). Targeting both tumour-associated CXCR2(+) neutrophils and CCR2(+) macrophages disrupts myeloid recruitment and improves chemotherapeutic responses in pancreatic ductal adenocarcinoma. Gut *67*, 1112-1123.

Oettinger, M. A., Schatz, D. G., Gorka, C., and Baltimore, D. (1990). RAG-1 and RAG-2, adjacent genes that synergistically activate V(D)J recombination. Science *248*, 1517-1523.

Ohlund, D., Handly-Santana, A., Biffi, G., Elyada, E., Almeida, A. S., Ponz-Sarvise, M., Corbo, V., Oni, T. E., Hearn, S. A., Lee, E. J.*, et al.* (2017). Distinct populations of inflammatory fibroblasts and myofibroblasts in pancreatic cancer. J Exp Med *214*, 579-596.

Olive, K. P., Jacobetz, M. A., Davidson, C. J., Gopinathan, A., McIntyre, D., Honess, D., Madhu, B., Goldgraben, M. A., Caldwell, M. E., Allard, D.*, et al.* (2009). Inhibition of Hedgehog signaling enhances delivery of chemotherapy in a mouse model of pancreatic cancer. Science *324*, 1457-1461.

Olive, K. P., Tuveson, D. A., Ruhe, Z. C., Yin, B., Willis, N. A., Bronson, R. T., Crowley, D., and Jacks, T. (2004). Mutant p53 gain of function in two mouse models of Li-Fraumeni syndrome. Cell *119*, 847-860.

Olmeda, D., Jorda, M., Peinado, H., Fabra, A., and Cano, A. (2007a). Snail silencing effectively suppresses tumour growth and invasiveness. Oncogene *26*, 1862-1874.

Olmeda, D., Moreno-Bueno, G., Flores, J. M., Fabra, A., Portillo, F., and Cano, A. (2007b). SNAI1 is required for tumor growth and lymph node metastasis of human breast carcinoma MDA-MB-231 cells. Cancer Res *67*, 11721-11731.

Omary, M. B., Lugea, A., Lowe, A. W., and Pandol, S. J. (2007). The pancreatic stellate cell: a star on the rise in pancreatic diseases. J Clin Invest *117*, 50-59.

Orban, P. C., Chui, D., and Marth, J. D. (1992). Tissue- and site-specific DNA recombination in transgenic mice. Proc Natl Acad Sci U S A *89*, 6861-6865.

Ozdemir, B. C., Pentcheva-Hoang, T., Carstens, J. L., Zheng, X., Wu, C. C., Simpson, T. R., Laklai, H., Sugimoto, H., Kahlert, C., Novitskiy, S. V.*, et al.* (2014). Depletion of carcinoma-associated fibroblasts and fibrosis induces immunosuppression and accelerates pancreas cancer with reduced survival. Cancer Cell *25*, 719-734.

Pages, G., Lenormand, P., L'Allemain, G., Chambard, J. C., Meloche, S., and Pouyssegur, J. (1993). Mitogen-activated protein kinases p42mapk and p44mapk are required for fibroblast proliferation. Proc Natl Acad Sci U S A *90*, 8319-8323.

Palmer, H. G., Larriba, M. J., Garcia, J. M., Ordonez-Moran, P., Pena, C., Peiro, S., Puig, I., Rodriguez, R., de la Fuente, R., Bernad, A.*, et al.* (2004). The transcription factor SNAIL represses vitamin D receptor expression and responsiveness in human colon cancer. Nat Med *10*, 917-919.

Park, S. M., Gaur, A. B., Lengyel, E., and Peter, M. E. (2008). The miR-200 family determines the epithelial phenotype of cancer cells by targeting the E-cadherin repressors ZEB1 and ZEB2. Genes Dev *22*, 894-907.

Paul, M. C. (2013) Functions of snail homolog 1 (Snail) in pancreatic cancer, Dissertation, Technische Universität München.

Paznekas, W. A., Okajima, K., Schertzer, M., Wood, S., and Jabs, E. W. (1999). Genomic organization, expression, and chromosome location of the human SNAIL gene (SNAI1) and a related processed pseudogene (SNAI1P). Genomics *62*, 42-49.

Pei, D., Shu, X., Gassama-Diagne, A., and Thiery, J. P. (2019). Mesenchymal-epithelial transition in development and reprogramming. Nat Cell Biol *21*, 44-53.

Peinado, H., Ballestar, E., Esteller, M., and Cano, A. (2004). Snail mediates E-cadherin repression by the recruitment of the Sin3A/histone deacetylase 1 (HDAC1)/HDAC2 complex. Mol Cell Biol *24*, 306-319.

Peinado, H., Del Carmen Iglesias-de la Cruz, M., Olmeda, D., Csiszar, K., Fong, K. S., Vega, S., Nieto, M. A., Cano, A., and Portillo, F. (2005). A molecular role for lysyl oxidase-like 2 enzyme in snail regulation and tumor progression. EMBO J *24*, 3446-3458.

Peinado, H., Olmeda, D., and Cano, A. (2007). Snail, Zeb and bHLH factors in tumour progression: an alliance against the epithelial phenotype? Nat Rev Cancer *7*, 415-428.

Peiro, S., Escriva, M., Puig, I., Barbera, M. J., Dave, N., Herranz, N., Larriba, M. J., Takkunen, M., Franci, C., Munoz, A.*, et al.* (2006). Snail1 transcriptional repressor binds to its own promoter and controls its expression. Nucleic Acids Res *34*, 2077-2084.

Pergamo, M., and Miller, G. (2017). Myeloid-derived suppressor cells and their role in pancreatic cancer. Cancer Gene Ther *24*, 100-105.

Phillips, P. A., McCarroll, J. A., Park, S., Wu, M. J., Pirola, R., Korsten, M., Wilson, J. S., and Apte, M. V. (2003). Rat pancreatic stellate cells secrete matrix metalloproteinases: implications for extracellular matrix turnover. Gut *52*, 275-282.

Pino, M. S., Kikuchi, H., Zeng, M., Herraiz, M. T., Sperduti, I., Berger, D., Park, D. Y., Iafrate, A. J., Zukerberg, L. R., and Chung, D. C. (2010). Epithelial to mesenchymal transition is impaired in colon cancer cells with microsatellite instability. Gastroenterology *138*, 1406-1417.

Pinto, D., Gregorieff, A., Begthel, H., and Clevers, H. (2003). Canonical Wnt signals are essential for homeostasis of the intestinal epithelium. Genes Dev *17*, 1709-1713.

Pinton, L., Solito, S., Damuzzo, V., Francescato, S., Pozzuoli, A., Berizzi, A., Mocellin, S., Rossi, C. R., Bronte, V., and Mandruzzato, S. (2016). Activated T cells sustain myeloid-derived suppressor cell-mediated immune suppression. Oncotarget *7*, 1168-1184.

Piro, G., Simionato, F., Carbone, C., Frizziero, M., Malleo, G., Zanini, S., Casolino, R., Santoro, R., Mina, M. M., Zecchetto, C.*, et al.* (2017). A circulating TH2 cytokines profile predicts survival in patients with resectable pancreatic adenocarcinoma. Oncoimmunology *6*, e1322242.

Pollard, P., Deheragoda, M., Segditsas, S., Lewis, A., Rowan, A., Howarth, K., Willis, L., Nye, E., McCart, A., Mandir, N.*, et al.* (2009). The Apc 1322T mouse develops severe polyposis associated with submaximal nuclear beta-catenin expression. Gastroenterology *136*, 2204-2213 e2201-2213.

Poplin, E., Feng, Y., Berlin, J., Rothenberg, M. L., Hochster, H., Mitchell, E., Alberts, S., O'Dwyer, P., Haller, D., Catalano, P.*, et al.* (2009). Phase III, randomized study of gemcitabine and oxaliplatin versus gemcitabine (fixed-dose rate infusion) compared with gemcitabine (30-minute infusion) in patients with pancreatic carcinoma E6201: a trial of the Eastern Cooperative Oncology Group. J Clin Oncol *27*, 3778-3785.

Porembka, M. R., Mitchem, J. B., Belt, B. A., Hsieh, C. S., Lee, H. M., Herndon, J., Gillanders, W. E., Linehan, D. C., and Goedegebuure, P. (2012). Pancreatic adenocarcinoma induces bone marrow mobilization of myeloid-derived suppressor cells which promote primary tumor growth. Cancer Immunol Immunother *61*, 1373-1385.

Pothula, S. P., Xu, Z., Goldstein, D., Biankin, A. V., Pirola, R. C., Wilson, J. S., and Apte, M. V. (2016). Hepatocyte growth factor inhibition: a novel therapeutic approach in pancreatic cancer. Br J Cancer *114*, 269-280.

Pylayeva-Gupta, Y., Das, S., Handler, J. S., Hajdu, C. H., Coffre, M., Koralov, S. B., and Bar-Sagi, D. (2016). IL35-Producing B Cells Promote the Development of Pancreatic Neoplasia. Cancer Discov *6*, 247-255.

Pylayeva-Gupta, Y., Lee, K. E., Hajdu, C. H., Miller, G., and Bar-Sagi, D. (2012). Oncogenic Kras-induced GM-CSF production promotes the development of pancreatic neoplasia. Cancer Cell *21*, 836-847.

Qian, B. Z., Li, J., Zhang, H., Kitamura, T., Zhang, J., Campion, L. R., Kaiser, E. A., Snyder, L. A., and Pollard, J. W. (2011). CCL2 recruits inflammatory monocytes to facilitate breast-tumour metastasis. Nature *475*, 222-225.

Quelle, D. E., Zindy, F., Ashmun, R. A., and Sherr, C. J. (1995). Alternative reading frames of the INK4a tumor suppressor gene encode two unrelated proteins capable of inducing cell cycle arrest. Cell *83*, 993-1000.

R Development Core Team (2014). R: A Language and Environment for Statistical Computing. R Foundation for Statistical Computing, Vienna, Austria, http://www.R-project.org/.

Rad, R., Cadinanos, J., Rad, L., Varela, I., Strong, A., Kriegl, L., Constantino-Casas, F., Eser, S., Hieber, M., Seidler, B.*, et al.* (2013). A genetic progression model of Braf(V600E)-induced intestinal tumorigenesis reveals targets for therapeutic intervention. Cancer Cell *24*, 15-29.

Rahib, L., Smith, B. D., Aizenberg, R., Rosenzweig, A. B., Fleshman, J. M., and Matrisian, L. M. (2014). Projecting cancer incidence and deaths to 2030: the unexpected burden of thyroid, liver, and pancreas cancers in the United States. Cancer Res *74*, 2913-2921.

Rembold, M., Ciglar, L., Yanez-Cuna, J. O., Zinzen, R. P., Girardot, C., Jain, A., Welte, M. A., Stark, A., Leptin, M., and Furlong, E. E. (2014). A conserved role for Snail as a potentiator of active transcription. Genes Dev *28*, 167-181.

Rhim, A. D., Oberstein, P. E., Thomas, D. H., Mirek, E. T., Palermo, C. F., Sastra, S. A., Dekleva, E. N., Saunders, T., Becerra, C. P., Tattersall, I. W.*, et al.* (2014). Stromal elements act to restrain, rather than support, pancreatic ductal adenocarcinoma. Cancer Cell *25*, 735-747.

Rhim, H., Savagner, P., Thibaudeau, G., Thiery, J. P., and Pavan, W. J. (1997). Localization of a neural crest transcription factor, Slug, to mouse chromosome 16 and human chromosome 8. Mamm Genome *8*, 872-873.

Richards, K. E., Zeleniak, A. E., Fishel, M. L., Wu, J., Littlepage, L. E., and Hill, R. (2017). Cancer-associated fibroblast exosomes regulate survival and proliferation of pancreatic cancer cells. Oncogene *36*, 1770-1778.

Roy, H. K., Smyrk, T. C., Koetsier, J., Victor, T. A., and Wali, R. K. (2005). The transcriptional repressor SNAIL is overexpressed in human colon cancer. Dig Dis Sci *50*, 42-46.

Saavedra, H. I., Fukasawa, K., Conn, C. W., and Stambrook, P. J. (1999). MAPK mediates RAS-induced chromosome instability. J Biol Chem *274*, 38083-38090.

Sack, L. M., Davoli, T., Li, M. Z., Li, Y., Xu, Q., Naxerova, K., Wooten, E. C., Bernardi, R. J., Martin, T. D., Chen, T.*, et al.* (2018). Profound Tissue Specificity in Proliferation Control Underlies Cancer Drivers and Aneuploidy Patterns. Cell *173*, 499-514 e423.

Salahshor, S., and Woodgett, J. R. (2005). The links between axin and carcinogenesis. J Clin Pathol *58*, 225-236.

Sale, M. J., Balmanno, K., Saxena, J., Ozono, E., Wojdyla, K., McIntyre, R. E., Gilley, R., Woroniuk, A., Howarth, K. D., Hughes, G.*, et al.* (2019). MEK1/2 inhibitor withdrawal reverses acquired resistance driven by BRAF(V600E) amplification whereas KRAS(G13D) amplification promotes EMT-chemoresistance. Nat Commun *10*, 2030.

Samuels, Y., Wang, Z., Bardelli, A., Silliman, N., Ptak, J., Szabo, S., Yan, H., Gazdar, A., Powell, S. M., Riggins, G. J.*, et al.* (2004). High frequency of mutations of the PIK3CA gene in human cancers. Science *304*, 554.

Sansom, O. J., Meniel, V., Wilkins, J. A., Cole, A. M., Oien, K. A., Marsh, V., Jamieson, T. J., Guerra, C., Ashton, G. H., Barbacid, M., and Clarke, A. R. (2006). Loss of Apc allows phenotypic manifestation of the transforming properties of an endogenous K-ras oncogene in vivo. Proc Natl Acad Sci U S A *103*, 14122-14127.

Sansom, O. J., Meniel, V. S., Muncan, V., Phesse, T. J., Wilkins, J. A., Reed, K. R., Vass, J. K., Athineos, D., Clevers, H., and Clarke, A. R. (2007). Myc deletion rescues Apc deficiency in the small intestine. Nature *446*, 676-679.

Savagner, P., Yamada, K. M., and Thiery, J. P. (1997). The zinc-finger protein slug causes desmosome dissociation, an initial and necessary step for growth factor-induced epithelial-mesenchymal transition. J Cell Biol *137*, 1403-1419.

Scheffzek, K., Ahmadian, M. R., Kabsch, W., Wiesmuller, L., Lautwein, A., Schmitz, F., and Wittinghofer, A. (1997). The Ras-RasGAP complex: structural basis for GTPase activation and its loss in oncogenic Ras mutants. Science *277*, 333-338.

Schepers, A., and Clevers, H. (2012). Wnt signaling, stem cells, and cancer of the gastrointestinal tract. Cold Spring Harb Perspect Biol *4*, a007989.

Schmid-Kotsas, A., Gross, H. J., Menke, A., Weidenbach, H., Adler, G., Siech, M., Beger, H., Grunert, A., and Bachem, M. G. (1999). Lipopolysaccharide-activated macrophages stimulate the synthesis of collagen type I and C-fibronectin in cultured pancreatic stellate cells. Am J Pathol *155*, 1749-1758.

Schneider, G., Schmidt-Supprian, M., Rad, R., and Saur, D. (2017). Tissue-specific tumorigenesis: context matters. Nature reviews Cancer *17*, 239-253.

Schonhuber, N., Seidler, B., Schuck, K., Veltkamp, C., Schachtler, C., Zukowska, M., Eser, S., Feyerabend, T. B., Paul, M. C., Eser, P.*, et al.* (2014). A next-generation dual-recombinase system for time- and host-specific targeting of pancreatic cancer. Nat Med *20*, 1340-1347.

Schuck, K. (2018) Dual-recombination system for time- and host-specific targeting of pancreatic ductal adenocarcinoma, Dissertation, Technische Universität München.

Serrano, M., Hannon, G. J., and Beach, D. (1993). A new regulatory motif in cell-cycle control causing specific inhibition of cyclin D/CDK4. Nature *366*, 704-707.

Sharon, N., Vanderhooft, J., Straubhaar, J., Mueller, J., Chawla, R., Zhou, Q., Engquist, E. N., Trapnell, C., Gifford, D. K., and Melton, D. A. (2019). Wnt Signaling Separates the Progenitor and Endocrine Compartments during Pancreas Development. Cell Rep *27*, 2281-2291 e2285.

Sherr, C. J. (2006). Divorcing ARF and p53: an unsettled case. Nat Rev Cancer *6*, 663-673.

Shi, C., Washington, M. K., Chaturvedi, R., Drosos, Y., Revetta, F. L., Weaver, C. J., Buzhardt, E., Yull, F. E., Blackwell, T. S., Sosa-Pineda, B.*, et al.* (2014). Fibrogenesis in pancreatic cancer is a dynamic process regulated by macrophage-stellate cell interaction. Lab Invest *94*, 409-421.

Shields, M. A., Ebine, K., Sahai, V., Kumar, K., Siddiqui, K., Hwang, R. F., Grippo, P. J., and Munshi, H. G. (2013). Snail cooperates with KrasG12D to promote pancreatic fibrosis. Mol Cancer Res *11*, 1078-1087.

Shinkai, Y., Rathbun, G., Lam, K. P., Oltz, E. M., Stewart, V., Mendelsohn, M., Charron, J., Datta, M., Young, F., Stall, A. M., and et al. (1992). RAG-2-deficient mice lack mature lymphocytes owing to inability to initiate V(D)J rearrangement. Cell *68*, 855-867.

Shtutman, M., Zhurinsky, J., Simcha, I., Albanese, C., D'Amico, M., Pestell, R., and Ben-Ze'ev, A. (1999). The cyclin D1 gene is a target of the beta-catenin/LEF-1 pathway. Proc Natl Acad Sci U S A *96*, 5522-5527.

Shurin, G. V., Ma, Y., and Shurin, M. R. (2013). Immunosuppressive mechanisms of regulatory dendritic cells in cancer. Cancer Microenviron *6*, 159-167.

Sideras, K., Braat, H., Kwekkeboom, J., van Eijck, C. H., Peppelenbosch, M. P., Sleijfer, S., and Bruno, M. (2014). Role of the immune system in pancreatic cancer progression and immune modulating treatment strategies. Cancer Treat Rev *40*, 513-522.

Siegel, R., Ma, J., Zou, Z., and Jemal, A. (2014). Cancer statistics, 2014. CA Cancer J Clin *64*, 9-29.

Siegel, R. L., Miller, K. D., and Jemal, A. (2019). Cancer statistics, 2019. CA Cancer J Clin *69*, 7-34.

Siemens, H., Jackstadt, R., Hunten, S., Kaller, M., Menssen, A., Gotz, U., and Hermeking, H. (2011). miR-34 and SNAIL form a double-negative feedback loop to regulate epithelial-mesenchymal transitions. Cell Cycle *10*, 4256-4271.

Simoni, Y., Becht, E., Fehlings, M., Loh, C. Y., Koo, S. L., Teng, K. W. W., Yeong, J. P. S., Nahar, R., Zhang, T., Kared, H.*, et al.* (2018). Bystander CD8(+) T cells are abundant and phenotypically distinct in human tumour infiltrates. Nature *557*, 575-579.

Siveke, J. T., Einwachter, H., Sipos, B., Lubeseder-Martellato, C., Kloppel, G., and Schmid, R. M. (2007). Concomitant pancreatic activation of Kras(G12D) and Tgfa results in cystic papillary neoplasms reminiscent of human IPMN. Cancer Cell *12*, 266-279.

Smit, M. A., Geiger, T. R., Song, J. Y., Gitelman, I., and Peeper, D. S. (2009). A Twist-Snail axis critical for TrkB-induced epithelial-mesenchymal transition-like transformation, anoikis resistance, and metastasis. Mol Cell Biol *29*, 3722-3737.

Smith, D. E., Franco del Amo, F., and Gridley, T. (1992). Isolation of Sna, a mouse gene homologous to the Drosophila genes snail and escargot: its expression pattern suggests multiple roles during postimplantation development. Development *116*, 1033-1039.

Smyth, G. K. (2004). Linear models and empirical bayes methods for assessing differential expression in microarray experiments. Stat Appl Genet Mol Biol *3*, Article3.

Soncin, I., Sheng, J., Chen, Q., Foo, S., Duan, K., Lum, J., Poidinger, M., Zolezzi, F., Karjalainen, K., and Ruedl, C. (2018). The tumour microenvironment creates a niche for the self-renewal of tumour-promoting macrophages in colon adenoma. Nat Commun *9*, 582.

Spagnoli, F. M., Cicchini, C., Tripodi, M., and Weiss, M. C. (2000). Inhibition of MMH (Met murine hepatocyte) cell differentiation by TGF(beta) is abrogated by pre-treatment with the heritable differentiation effector FGF1. J Cell Sci *113 (Pt 20)*, 3639-3647.

Stanisavljevic, J., Loubat-Casanovas, J., Herrera, M., Luque, T., Pena, R., Lluch, A., Albanell, J., Bonilla, F., Rovira, A., Pena, C.*, et al.* (2015). Snail1-expressing fibroblasts in the tumor microenvironment display mechanical properties that support metastasis. Cancer Res *75*, 284-295.

Steele, C. W., Karim, S. A., Leach, J. D. G., Bailey, P., Upstill-Goddard, R., Rishi, L., Foth, M., Bryson, S., McDaid, K., Wilson, Z.*, et al.* (2016). CXCR2 Inhibition Profoundly Suppresses

Metastases and Augments Immunotherapy in Pancreatic Ductal Adenocarcinoma. Cancer Cell *29*, 832-845.

Stolzenberg-Solomon, R. Z., Graubard, B. I., Chari, S., Limburg, P., Taylor, P. R., Virtamo, J., and Albanes, D. (2005). Insulin, glucose, insulin resistance, and pancreatic cancer in male smokers. JAMA *294*, 2872-2878.

Stott, F. J., Bates, S., James, M. C., McConnell, B. B., Starborg, M., Brookes, S., Palmero, I., Ryan, K., Hara, E., Vousden, K. H., and Peters, G. (1998). The alternative product from the human CDKN2A locus, p14(ARF), participates in a regulatory feedback loop with p53 and MDM2. EMBO J *17*, 5001-5014.

Stromnes, I. M., Schmitt, T. M., Hulbert, A., Brockenbrough, J. S., Nguyen, H., Cuevas, C., Dotson, A. M., Tan, X., Hotes, J. L., Greenberg, P. D., and Hingorani, S. R. (2015). T Cells Engineered against a Native Antigen Can Surmount Immunologic and Physical Barriers to Treat Pancreatic Ductal Adenocarcinoma. Cancer Cell *28*, 638-652.

Subramanian, A., Tamayo, P., Mootha, V. K., Mukherjee, S., Ebert, B. L., Gillette, M. A., Paulovich, A., Pomeroy, S. L., Golub, T. R., Lander, E. S., and Mesirov, J. P. (2005). Gene set enrichment analysis: a knowledge-based approach for interpreting genome-wide expression profiles. Proc Natl Acad Sci U S A *102*, 15545-15550.

Taki, K., Ohmuraya, M., Tanji, E., Komatsu, H., Hashimoto, D., Semba, K., Araki, K., Kawaguchi, Y., Baba, H., and Furukawa, T. (2016). GNAS(R201H) and Kras(G12D) cooperate to promote murine pancreatic tumorigenesis recapitulating human intraductal papillary mucinous neoplasm. Oncogene *35*, 2407-2412.

Taki, M., Abiko, K., Baba, T., Hamanishi, J., Yamaguchi, K., Murakami, R., Yamanoi, K., Horikawa, N., Hosoe, Y., Nakamura, E.*, et al.* (2018). Snail promotes ovarian cancer progression by recruiting myeloid-derived suppressor cells via CXCR2 ligand upregulation. Nat Commun *9*, 1685.

Tan, C., Costello, P., Sanghera, J., Dominguez, D., Baulida, J., de Herreros, A. G., and Dedhar, S. (2001). Inhibition of integrin linked kinase (ILK) suppresses beta-catenin-Lef/Tcf-dependent transcription and expression of the E-cadherin repressor, snail, in APC-/- human colon carcinoma cells. Oncogene *20*, 133-140.

Tan, M. C., Goedegebuure, P. S., Belt, B. A., Flaherty, B., Sankpal, N., Gillanders, W. E., Eberlein, T. J., Hsieh, C. S., and Linehan, D. C. (2009). Disruption of CCR5-dependent homing of regulatory T cells inhibits tumor growth in a murine model of pancreatic cancer. J Immunol *182*, 1746-1755.

Tang, Y., Xu, X., Guo, S., Zhang, C., Tang, Y., Tian, Y., Ni, B., Lu, B., and Wang, H. (2014). An increased abundance of tumor-infiltrating regulatory T cells is correlated with the progression and prognosis of pancreatic ductal adenocarcinoma. PLoS One *9*, e91551.

Tassi, E., Gavazzi, F., Albarello, L., Senyukov, V., Longhi, R., Dellabona, P., Doglioni, C., Braga, M., Di Carlo, V., and Protti, M. P. (2008). Carcinoembryonic antigen-specific but not antiviral CD4+ T cell immunity is impaired in pancreatic carcinoma patients. J Immunol *181*, 6595-6603.

Tersmette, A. C., Petersen, G. M., Offerhaus, G. J., Falatko, F. C., Brune, K. A., Goggins, M., Rozenblum, E., Wilentz, R. E., Yeo, C. J., Cameron, J. L.*, et al.* (2001). Increased risk of incident pancreatic cancer among first-degree relatives of patients with familial pancreatic cancer. Clin Cancer Res *7*, 738-744.

Tetsu, O., and McCormick, F. (1999). Beta-catenin regulates expression of cyclin D1 in colon carcinoma cells. Nature *398*, 422-426.

Thayer, S. P., di Magliano, M. P., Heiser, P. W., Nielsen, C. M., Roberts, D. J., Lauwers, G. Y., Qi, Y. P., Gysin, S., Fernandez-del Castillo, C., Yajnik, V.*, et al.* (2003). Hedgehog is an early and late mediator of pancreatic cancer tumorigenesis. Nature *425*, 851-856.

Thiery, J. P., Acloque, H., Huang, R. Y., and Nieto, M. A. (2009). Epithelial-mesenchymal transitions in development and disease. Cell *139*, 871-890.

Thomas, D., and Radhakrishnan, P. (2019). Tumor-stromal crosstalk in pancreatic cancer and tissue fibrosis. Mol Cancer *18*, 14.

Thorsson, V., Gibbs, D. L., Brown, S. D., Wolf, D., Bortone, D. S., Ou Yang, T. H., Porta-Pardo, E., Gao, G. F., Plaisier, C. L., Eddy, J. A.*, et al.* (2018). The Immune Landscape of Cancer. Immunity *48*, 812-830 e814.

Thuault, S., Valcourt, U., Petersen, M., Manfioletti, G., Heldin, C. H., and Moustakas, A. (2006). Transforming growth factor-beta employs HMGA2 to elicit epithelial-mesenchymal transition. J Cell Biol *174*, 175-183.

Tian, L., Lu, Z. P., Cai, B. B., Zhao, L. T., Qian, D., Xu, Q. C., Wu, P. F., Zhu, Y., Zhang, J. J., Du, Q.*, et al.* (2016). Activation of pancreatic stellate cells involves an EMT-like process. Int J Oncol *48*, 783-792.

Tong, Z. T., Cai, M. Y., Wang, X. G., Kong, L. L., Mai, S. J., Liu, Y. H., Zhang, H. B., Liao, Y. J., Zheng, F., Zhu, W.*, et al.* (2012). EZH2 supports nasopharyngeal carcinoma cell aggressiveness by forming a co-repressor complex with HDAC1/HDAC2 and Snail to inhibit E-cadherin. Oncogene *31*, 583-594.

Trevino-Villarreal, J. H., Cotanche, D. A., Sepulveda, R., Bortoni, M. E., Manneberg, O., Udagawa, T., and Rogers, R. A. (2011). Host-derived pericytes and Sca-1+ cells predominate in the MART-1- stroma fraction of experimentally induced melanoma. J Histochem Cytochem *59*, 1060-1075.

Twigg, S. R., and Wilkie, A. O. (1999). Characterisation of the human snail (SNAI1) gene and exclusion as a major disease gene in craniosynostosis. Hum Genet *105*, 320-326.

Tymoszuk, P., Evens, H., Marzola, V., Wachowicz, K., Wasmer, M. H., Datta, S., Muller-Holzner, E., Fiegl, H., Bock, G., van Rooijen, N.*, et al.* (2014). In situ proliferation contributes to accumulation of tumor-associated macrophages in spontaneous mammary tumors. Eur J Immunol *44*, 2247-2262.

Usami, Y., Satake, S., Nakayama, F., Matsumoto, M., Ohnuma, K., Komori, T., Semba, S., Ito, A., and Yokozaki, H. (2008). Snail-associated epithelial-mesenchymal transition promotes oesophageal squamous cell carcinoma motility and progression. J Pathol *215*, 330-339.

Valdes, F., Alvarez, A. M., Locascio, A., Vega, S., Herrera, B., Fernandez, M., Benito, M., Nieto, M. A., and Fabregat, I. (2002). The epithelial mesenchymal transition confers resistance to the apoptotic effects of transforming growth factor Beta in fetal rat hepatocytes. Mol Cancer Res *1*, 68-78.

Van Cutsem, E., Kohne, C. H., Lang, I., Folprecht, G., Nowacki, M. P., Cascinu, S., Shchepotin, I., Maurel, J., Cunningham, D., Tejpar, S.*, et al.* (2011). Cetuximab plus irinotecan, fluorouracil, and leucovorin as first-line treatment for metastatic colorectal cancer: updated analysis of overall survival according to tumor KRAS and BRAF mutation status. J Clin Oncol *29*, 2011-2019.

van der Flier, L. G., and Clevers, H. (2009). Stem cells, self-renewal, and differentiation in the intestinal epithelium. Annu Rev Physiol *71*, 241-260.

Vega, S., Morales, A. V., Ocana, O. H., Valdes, F., Fabregat, I., and Nieto, M. A. (2004). Snail blocks the cell cycle and confers resistance to cell death. Genes Dev *18*, 1131-1143.

Veltmaat, J. M., Orelio, C. C., Ward-Van Oostwaard, D., Van Rooijen, M. A., Mummery, C. L., and Defize, L. H. (2000). Snail is an immediate early target gene of parathyroid hormone related peptide signaling in parietal endoderm formation. Int J Dev Biol *44*, 297-307.

Vennin, C., Murphy, K. J., Morton, J. P., Cox, T. R., Pajic, M., and Timpson, P. (2018). Reshaping the Tumor Stroma for Treatment of Pancreatic Cancer. Gastroenterology *154*, 820-838.

Vermeulen, L., De Sousa, E. M. F., van der Heijden, M., Cameron, K., de Jong, J. H., Borovski, T., Tuynman, J. B., Todaro, M., Merz, C., Rodermond, H.*, et al.* (2010). Wnt activity defines colon cancer stem cells and is regulated by the microenvironment. Nat Cell Biol *12*, 468-476.

Vinas-Castells, R., Beltran, M., Valls, G., Gomez, I., Garcia, J. M., Montserrat-Sentis, B., Baulida, J., Bonilla, F., de Herreros, A. G., and Diaz, V. M. (2010). The hypoxia-controlled FBXL14 ubiquitin ligase targets SNAIL1 for proteasome degradation. J Biol Chem *285*, 3794-3805.

Vincent, T., Neve, E. P., Johnson, J. R., Kukalev, A., Rojo, F., Albanell, J., Pietras, K., Virtanen, I., Philipson, L., Leopold, P. L.*, et al.* (2009). A SNAIL1-SMAD3/4 transcriptional repressor complex promotes TGF-beta mediated epithelial-mesenchymal transition. Nat Cell Biol *11*, 943-950.

Vizio, B., Novarino, A., Giacobino, A., Cristiano, C., Prati, A., Ciuffreda, L., Montrucchio, G., and Bellone, G. (2012). Potential plasticity of T regulatory cells in pancreatic carcinoma in relation to disease progression and outcome. Exp Ther Med *4*, 70-78.

Vogelmann, R., Ruf, D., Wagner, M., Adler, G., and Menke, A. (2001). Effects of fibrogenic mediators on the development of pancreatic fibrosis in a TGF-beta1 transgenic mouse model. Am J Physiol Gastrointest Liver Physiol *280*, G164-172.

Vogelstein, B., Fearon, E. R., Hamilton, S. R., Kern, S. E., Preisinger, A. C., Leppert, M., Nakamura, Y., White, R., Smits, A. M., and Bos, J. L. (1988). Genetic alterations during colorectal-tumor development. N Engl J Med *319*, 525-532.

von Burstin, J., Eser, S., Paul, M. C., Seidler, B., Brandl, M., Messer, M., von Werder, A., Schmidt, A., Mages, J., Pagel, P.*, et al.* (2009). E-cadherin regulates metastasis of pancreatic cancer in vivo and is suppressed by a SNAIL/HDAC1/HDAC2 repressor complex. Gastroenterology *137*, 361-371, 371 e361-365.

Von Hoff, D. D., Ervin, T., Arena, F. P., Chiorean, E. G., Infante, J., Moore, M., Seay, T., Tjulandin, S. A., Ma, W. W., Saleh, M. N.*, et al.* (2013). Increased survival in pancreatic cancer with nab-paclitaxel plus gemcitabine. N Engl J Med *369*, 1691-1703.

Wang, J., Ye, Q., Cao, Y., Guo, Y., Huang, X., Mi, W., Liu, S., Wang, C., Yang, H. S., Zhou, B. P.*, et al.* (2017a). Snail determines the therapeutic response to mTOR kinase inhibitors by transcriptional repression of 4E-BP1. Nat Commun *8*, 2207.

Wang, X., Lang, M., Zhao, T., Feng, X., Zheng, C., Huang, C., Hao, J., Dong, J., Luo, L., Li, X.*, et al.* (2017b). Cancer-FOXP3 directly activated CCL5 to recruit FOXP3(+)Treg cells in pancreatic ductal adenocarcinoma. Oncogene *36*, 3048-3058.

Wang, X., Park, J., Susztak, K., Zhang, N. R., and Li, M. (2019). Bulk tissue cell type deconvolution with multi-subject single-cell expression reference. Nat Commun *10*, 380.

Ward, J. H., Jr. (1963). Hierarchical grouping to optimize an objective function. Journal of the American Statistical Association *58*, 236–244.

Wei, D., Wang, L., Yan, Y., Jia, Z., Gagea, M., Li, Z., Zuo, X., Kong, X., Huang, S., and Xie, K. (2016). KLF4 Is Essential for Induction of Cellular Identity Change and Acinar-to-Ductal Reprogramming during Early Pancreatic Carcinogenesis. Cancer Cell *29*, 324-338.

Wei, K., Kucherlapati, R., and Edelmann, W. (2002). Mouse models for human DNA mismatch-repair gene defects. Trends Mol Med *8*, 346-353.

Willett, C. G., Boucher, Y., di Tomaso, E., Duda, D. G., Munn, L. L., Tong, R. T., Chung, D. C., Sahani, D. V., Kalva, S. P., Kozin, S. V.*, et al.* (2004). Direct evidence that the VEGF-specific antibody bevacizumab has antivascular effects in human rectal cancer. Nat Med *10*, 145-147.

Wormann, S. M., Diakopoulos, K. N., Lesina, M., and Algul, H. (2014). The immune network in pancreatic cancer development and progression. Oncogene *33*, 2956-2967.

Wu, J., Zhang, Y., Cheng, R., Gong, W., Ding, T., Zhai, Q., Wang, Y., Meng, B., and Sun, B. (2019). Expression of epithelial-mesenchymal transition regulators TWIST, SLUG and SNAIL in follicular thyroid tumours may relate to widely invasive, poorly differentiated and distant metastasis. Histopathology *74*, 780-791.

Wu, W. S., You, R. I., Cheng, C. C., Lee, M. C., Lin, T. Y., and Hu, C. T. (2017). Snail collaborates with EGR-1 and SP-1 to directly activate transcription of MMP 9 and ZEB1. Sci Rep *7*, 17753.

Xue, J., Sharma, V., Hsieh, M. H., Chawla, A., Murali, R., Pandol, S. J., and Habtezion, A. (2015). Alternatively activated macrophages promote pancreatic fibrosis in chronic pancreatitis. Nat Commun *6*, 7158.

Yam, C. H., Fung, T. K., and Poon, R. Y. (2002). Cyclin A in cell cycle control and cancer. Cell Mol Life Sci *59*, 1317-1326.

Yamamoto, T., Yanagimoto, H., Satoi, S., Toyokawa, H., Yamao, J., Kim, S., Terakawa, N., Takahashi, K., and Kwon, A. H. (2012). Circulating myeloid dendritic cells as prognostic factors in patients with pancreatic cancer who have undergone surgical resection. J Surg Res *173*, 299-308.

Yang, M. H., Chang, S. Y., Chiou, S. H., Liu, C. J., Chi, C. W., Chen, P. M., Teng, S. C., and Wu, K. J. (2007). Overexpression of NBS1 induces epithelial-mesenchymal transition and co-expression of NBS1 and Snail predicts metastasis of head and neck cancer. Oncogene *26*, 1459-1467.

Yang, Z., Rayala, S., Nguyen, D., Vadlamudi, R. K., Chen, S., and Kumar, R. (2005). Pak1 phosphorylation of snail, a master regulator of epithelial-to-mesenchyme transition, modulates snail's subcellular localization and functions. Cancer Res *65*, 3179-3184.

Yao, D., Dai, C., and Peng, S. (2011). Mechanism of the mesenchymal-epithelial transition and its relationship with metastatic tumor formation. Mol Cancer Res *9*, 1608-1620.

Ye, X., Tam, W. L., Shibue, T., Kaygusuz, Y., Reinhardt, F., Ng Eaton, E., and Weinberg, R. A. (2015). Distinct EMT programs control normal mammary stem cells and tumour-initiating cells. Nature *525*, 256-260.

Yin, T., Wang, C., Liu, T., Zhao, G., Zha, Y., and Yang, M. (2007). Expression of snail in pancreatic cancer promotes metastasis and chemoresistance. J Surg Res *141*, 196-203.

Yokoyama, K., Kamata, N., Fujimoto, R., Tsutsumi, S., Tomonari, M., Taki, M., Hosokawa, H., and Nagayama, M. (2003). Increased invasion and matrix metalloproteinase-2 expression by Snail-induced mesenchymal transition in squamous cell carcinomas. Int J Oncol *22*, 891-898.

Yook, J. I., Li, X. Y., Ota, I., Fearon, E. R., and Weiss, S. J. (2005). Wnt-dependent regulation of the E-cadherin repressor snail. J Biol Chem *280*, 11740-11748.

Yoshida, S., Yokota, T., Ujiki, M., Ding, X. Z., Pelham, C., Adrian, T. E., Talamonti, M. S., Bell, R. H., Jr., and Denham, W. (2004). Pancreatic cancer stimulates pancreatic stellate cell proliferation and TIMP-1 production through the MAP kinase pathway. Biochem Biophys Res Commun *323*, 1241-1245.

Yuen, S. T., Davies, H., Chan, T. L., Ho, J. W., Bignell, G. R., Cox, C., Stephens, P., Edkins, S., Tsui, W. W., Chan, A. S.*, et al.* (2002). Similarity of the phenotypic patterns associated with BRAF and KRAS mutations in colorectal neoplasia. Cancer Res *62*, 6451-6455.

Zadran, S., Arumugam, R., Herschman, H., Phelps, M. E., and Levine, R. D. (2014). Surprisal analysis characterizes the free energy time course of cancer cells undergoing epithelial-to-mesenchymal transition. Proc Natl Acad Sci U S A *111*, 13235-13240.

Zhang, A., Chen, G., Meng, L., Wang, Q., Hu, W., Xi, L., Gao, Q., Wang, S., Zhou, J., Xu, G.*, et al.* (2008). Antisense-Snail transfer inhibits tumor metastasis by inducing E-cadherin expression. Anticancer Res *28*, 621-628.

Zhang, F., Wang, H., Wang, X., Jiang, G., Liu, H., Zhang, G., Wang, H., Fang, R., Bu, X., Cai, S., and Du, J. (2016). TGF-beta induces M2-like macrophage polarization via SNAIL-mediated suppression of a pro-inflammatory phenotype. Oncotarget *7*, 52294-52306.

Zhang, Y., Morris, J. P. t., Yan, W., Schofield, H. K., Gurney, A., Simeone, D. M., Millar, S. E., Hoey, T., Hebrok, M., and Pasca di Magliano, M. (2013). Canonical wnt signaling is required for pancreatic carcinogenesis. Cancer Res *73*, 4909-4922.

Zhao, M., Mishra, L., and Deng, C. X. (2018). The role of TGF-beta/SMAD4 signaling in cancer. Int J Biol Sci *14*, 111-123.

Zheng, X., Carstens, J. L., Kim, J., Scheible, M., Kaye, J., Sugimoto, H., Wu, C. C., LeBleu, V. S., and Kalluri, R. (2015). Epithelial-to-mesenchymal transition is dispensable for metastasis but induces chemoresistance in pancreatic cancer. Nature *527*, 525-530.

Zhou, B. P., Deng, J., Xia, W., Xu, J., Li, Y. M., Gunduz, M., and Hung, M. C. (2004). Dual regulation of Snail by GSK-3beta-mediated phosphorylation in control of epithelial-mesenchymal transition. Nat Cell Biol *6*, 931-940.

Zhu, Y., Herndon, J. M., Sojka, D. K., Kim, K. W., Knolhoff, B. L., Zuo, C., Cullinan, D. R., Luo, J., Bearden, A. R., Lavine, K. J.*, et al.* (2017). Tissue-Resident Macrophages in Pancreatic Ductal Adenocarcinoma Originate from Embryonic Hematopoiesis and Promote Tumor Progression. Immunity *47*, 323-338 e326.

Zhu, Y., Knolhoff, B. L., Meyer, M. A., Nywening, T. M., West, B. L., Luo, J., Wang-Gillam, A., Goedegebuure, S. P., Linehan, D. C., and DeNardo, D. G. (2014). CSF1/CSF1R blockade reprograms tumor-infiltrating macrophages and improves response to T-cell checkpoint immunotherapy in pancreatic cancer models. Cancer Res *74*, 5057-5069.

Zhuge, X., Kataoka, H., Tanaka, M., Murayama, T., Kawamoto, T., Sano, H., Togi, K., Yamauchi, R., Ueda, Y., Xu, Y.*, et al.* (2005). Expression of the novel Snai-related zinc-finger transcription factor gene Smuc during mouse development. Int J Mol Med *15*, 945-948.